



**Democratic and Popular Republic of Algeria**  
MINISTRY OF HIGHER EDUCATION AND SCIENTIFIC  
RESEARCH  
UNIVERSITY MOHAMED KHIDER OF BISKRA



FACULTY OF EXACT SCIENCES AND SCIENCE OF NATURE AND LIFE

Department of Material Sciences

THESIS

Presented by:

**CHARROUF Hadjer**

Presented to obtain the degree of:

**DOCTORATE**

Entitled:

**Characterization by ab initio calculations on the  
physical properties of Yttrium based compounds for  
thermoelectric applications.**

**Board of Examiners:**

<b>Rahmane Saad</b>	<b>Professor</b>	<b>University of Biskra</b>	<b>President</b>
<b>LAKEL Said</b>	<b>Professor</b>	<b>University of Biskra</b>	<b>Supervisor</b>
<b>Ibrir Miloud</b>	<b>Professor</b>	<b>University of M'sila</b>	<b>Examiner</b>
<b>Tibermacine Toufik</b>	<b>Professor</b>	<b>University of Biskra</b>	<b>Examiner</b>



**République Algérienne Démocratique Et Populaire**  
MINISTRE DE L'ENSEIGNEMENT SUPERIEUR ET DE LA  
RECHERCHE SCIENTIFIQUE  
UNIVERSITE MOHAMED KHIDER BISKRA



FACULTE DES SCIENCES EXACTES DES SCIENCES DE LA NATURE ET DE LA VIE

Département des Sciences de la  
matière

**THESE**

Présentée par:

**CHARROUF Hadjer**

En vue de l'obtention du

diplôme de :

**DOCTORAT**

**Intitulée**

**Caractérisation par calculs ab initio des propriétés physiques  
des composés à base d'Yttrium pour applications  
thermoélectriques.**

Devant la commission d'Examen:

<b>Rahmane Saad</b>	Professeur	Université de <b>Biskra</b>	Président
<b>LAKEL Said</b>	Professeur	Université de <b>Biskra</b>	Encadreur
<b>Ibrir Miloud</b>	Professeur	Université de <b>M'sila</b>	Examineur
<b>Tibermacine Toufik</b>	Professeur	Université de <b>Biskra</b>	Examineur

***dedication***

*I dedicate this work*

*To my dear parents*

*To my husband, his family, and my son **WAEEL***

*To my brothers and sisters*

*To all who helped me from near or far*

## ***ACKNOWLEDGEMENT***

*I thank Allah for giving me the will and the courage to complete this thesis. And the construction of this humble work would not have been possible without the support and guidance of many people.*

*I would like to express my sincere gratitude to my supervisor **LAKEL Said**, for his advice, his availability, and his support which were invaluable, his encouragement enabled me to carry out this work in the best conditions. I am deeply thankful to Dr. **Kenza ALMI** for her scientific advice and valuable support. I would like to extend my warm acknowledgments to the respected board of examiners. My thanks also go to my teachers in the Department of Material Sciences.*

*I also thank all my colleagues and my friends for the beautiful moments.*

## Abstract

The physics of solids plays an important role in current technology. Among these materials are the semiconductors  $\text{III}^{\text{B}}\text{-N}$  (ScN, YN, LaN) and their alloys  $\text{III}^{\text{B}}\text{-III}^{\text{B}}\text{-N}^{\text{A}}$  and  $\text{III}^{\text{B}}\text{-N-V}^{\text{A}}$ , which are based on Yttrium. These materials are more significant for efficiency when used in the development of new technologies.

Nowadays, ab initio methods are increasingly proving to be a tool of choice for the microscopic interpretation of observations. The physical properties of the compounds  $\text{III}^{\text{B}}\text{-N}$  (ScN, YN, LaN) and their alloys,  $\text{III}^{\text{B}}\text{-III}^{\text{B}}\text{-N}^{\text{A}}$  and  $\text{III}^{\text{B}}\text{-N-V}^{\text{A}}$ , are calculated by the theory of density function (DFT) and the method of pseudo potentials coupled with plane waves (PP-PW) using the CASTEP program. We calculated the structural and elastic properties (elastic constants  $C_{ij}$  and  $S_{ij}$ , and modulus of elasticity: compression module B, shear module G, Young module E, Poisson module  $\nu$ , and Young module, Poisson module and propagation velocities of longitudinal and transverse elastic waves in different crystal directions, Debye temperature calculation for  $\text{Y}_{1-x}\text{M}_x\text{N}$  (Sc = M, La) and  $\text{YN}_{1-x}\text{B}_x$  (Sb, As, P = B), electronic properties (energy bands, DOS total density and TDOS partial states), optical properties (real dielectric coefficient  $\epsilon_1$  and imaginary  $\epsilon_2$ , refractive index  $n$ , extinction coefficient  $k$ , absorption coefficient, reflectivity) and phonon (the dissipation curve of phonons and the density of phonon states).

The results obtained are in good agreement with the available experimental results and the theoretical calculations, and on the other hand, these are reliable predictions as a reference.

**Key words:** Calculation ab-initio, DFT, pseudo-potential, compounds  $\text{III}^{\text{B}}\text{-N}$ ,  $\text{III}^{\text{B}}\text{-III}^{\text{B}}\text{-N}^{\text{A}}$  et  $\text{III}^{\text{B}}\text{-N-V}^{\text{A}}$ , structural, elastic, electronic, optical and phonon properties.

## Résumé :

La physique des solides joue un rôle important dans la technologie actuelle. Parmi ces matériaux, les semi-conducteurs  $\text{III}^{\text{B}}\text{-N}$  (ScN, YN, LaN) et leurs mélanges  $\text{III}^{\text{B}}\text{-III}^{\text{B}}\text{-N}^{\text{A}}$  et  $\text{III}^{\text{B}}\text{-N-V}^{\text{A}}$  qui sont basés sur d'Yttrium, ces matériaux ont une efficacité très importante lorsqu'ils sont utilisés dans le développement de nouvelles technologies.

De nos jours, les méthodes de types ab initio se révèlent de plus en plus comme étant un outil de choix pour interpréter à l'échelle microscopique les observations. Les propriétés physiques des composés  $\text{III}^{\text{B}}\text{-N}$  (ScN, YN, LaN) et leurs mélanges  $\text{III}^{\text{B}}\text{-III}^{\text{B}}\text{-N}^{\text{A}}$  et  $\text{III}^{\text{B}}\text{-N-V}^{\text{A}}$  sont calculées par la théorie de la fonctionnelle de la densité (DFT) et la méthode des pseudo potentiels couplés avec les ondes planes (PP-PW) à l'aide du programme CASTEP.

Nous avons calculé les propriétés structurales et élastiques (constantes élastiques  $C_{ij}$  et  $S_{ij}$ , et module d'élasticité : module de compression B, module de cisaillement G, module d'Young E, module de Poisson  $\nu$ , ainsi que module d'Young, module de Poisson et vitesses de propagation des élastiques longitudinales et transversales ondes selon différentes directions cristallographiques, Calcul de la température de Debye pour  $\text{Y}_{1-x}\text{M}_x\text{N}$  (Sc = M, La) et  $\text{YN}_{1-x}\text{B}_x$  (Sb, As, P = B), propriétés électroniques (bandes d'énergie, densité d'états total DOS et états partiels TDOS), propriétés optiques (coefficient diélectrique réel  $\epsilon_1$  et imaginaire  $\epsilon_2$ , indice de réfraction  $n$ , coefficient d'extinction  $k$ , coefficient d'absorption, réflectivité) et phonon (la courbe de dissipation des phonons et la densité d'états des phonons).

Les résultats obtenus sont en bon accord avec les résultats expérimentaux disponibles et les calculs théoriques et d'autre part ce sont des prédictions fiables comme référence.

**Mots clés :** Calcul ab-initio, DFT, pseudo-potentiels, les composés  $\text{III}^{\text{B}}\text{-N}$ ,  $\text{III}^{\text{B}}\text{-III}^{\text{B}}\text{-N}^{\text{A}}$  et  $\text{III}^{\text{B}}\text{-N-V}^{\text{A}}$ , les propriétés structurales, élastiques, électroniques, optiques et phonon.

## ملخص :

تلعب فيزياء المواد الصلبة دورًا مهمًا في التكنولوجيا الحالية. من بين هذه المواد أنصاف النواقل  $III^B-N$  (ScN, YN, LaN) وخالئتها  $III^B-III^B-N^A$  و  $III^B-N-V^A$  والتي أساسها Yttrium. هذه المواد لها فعالية جد مهمة عند استخدامها في تطوير التكنولوجيات الجديدة. في الوقت الحاضر، تعد طرق الحساب من البدا من أهم الطرق التي تساعد على تقديم تفسيرات دقيقة للملاحظات التجريبية. يتم حساب الخصائص الفيزيائية لمركبات  $III^B-N$  (ScN, YN, LaN) و خلائتها  $III^B-III^B-N^A$  و  $III^B-N-V^A$  من خلال نظرية الكثافة الوظيفية (DFT) وطريقة الكمون الوهمي والموجات المستوية (PP-PW) باستعمال برنامج CASTEP.

قمنا بحساب الخصائص البنيوية والمرنة (الثوابت المرنة  $C_{ij}$  و  $S_{ij}$ ، ومعاملات المرونة : معامل الانضغاط B، معامل القص G، معامل يونغ E، معامل بواسون  $\nu$  . وكذا معامل يونغ، معامل بواسون و سرعات انتشار الموجات المرنة الطولية والمستعرضة وفقًا لاتجاهات بلورية مختلفة، و كذلك تم حساب درجة حرارة ديباي لكل من  $Y_{1-x}M_xN$  (La, Sc = M) و  $YN_{1-x}B_x$  (Sb, As, P = B)، وكما تم إيجاد الخصائص الإلكترونية (عصابات الطاقة كثافة الحالات الكلية DOS و الجزئية TDOS)، الخصائص الضوئية (معامل العزل الحقيقي  $\epsilon_1$  والتخليبي  $\epsilon_2$ ، ومعامل الانكسار n ومعامل الخمود k ومعامل الامتصاص، والانعكاسية) و الفونونية (منحنى تبديد الفونونات و كثافة الحالات للفونونات).

النتائج التي تم الحصول عليها تتفق بشكل جيد مع النتائج التجريبية والحسابات النظرية المتاحة ومن جهة أخرى هي عبارة عن تنبؤات يمكن الاعتماد عليها كمرجع.

**الكلمات المفتاحية :** الحساب من البدا، نظرية الكثافة الوظيفية DFT، وطريقة الكمون الوهمي-PP-PW، المركبات  $III^B-N$  (  $III^B-III^B-N^A$  و  $III^B-N-V^A$  ). الخصائص البنيوية، المرنة، الإلكترونية، الضوئية، الفونونية.

## List of tables

### Chapter I

Table (I-1): Gives the experimental and calculated mesh parameters for these elements.....	6
Table (I-2): Below shows the electronic structure for Sc, Y, La, N, P, As, Sb atoms.....	8
Table (I-3): Below shows the elastic structure for Sc, Y, La, N, P, As, Sb atoms.....	10
Table (I-4): Thermal and electrical properties of certain elements. ....	13

### Chapter III

Table (III-1): Calculated lattice parameter $a(\text{\AA})$ and bulk modulus $B(\text{GPa})$ along with the experimental and other theoretical values $Y_{1-x}Sc_xN$ for $x = 0, 0.25, 0.5, 0.75$ and $1$ .....	68
Table (III-2): Calculated and experimental equilibrium structural parameters: lattice constants $a$ and bulk modulus $B(\text{GPa})$ for $Y_{1-x}La_xN$ ( $x = 0, 0.25, 0.50, 0.75$ ) alloys in B1 structure.....	69
Table (III-3): Calculated lattice parameter $a(\text{\AA})$ and bulk modulus $B(\text{GPa})$ of $YN_{1-x}B_x$ ( $B : P, As$ and $Sb$ ), ( $x = 0, 0.25, 0.50, 0.75$ and $1$ ) along with the experimental and other theoretical values... ..	70
Table (III-4):The calculated elastic constants for $Y_{1-x}Sc_xN$ ( $x= 0, 0.25, 0.5, 0.75, 1$ ) compared with both theoretical and experimental data.....	71
Table (III-5): The calculated bulk modulus ( $B$ ), shear modulus ( $G$ ), Young's modulus ( $E$ ), Poisson's ratio $\nu$ , Pugh's ratio( $B/G$ ), longitudinal ( $V_l$ ), shear ( $V_t$ ), average ( $V_m$ ) elastic wave velocities and Debye temperature ( $\theta_D$ ) for $Y_{1-x}Sc_xN$ ( $x= 0, 0.25, 0.5, 0.75, 1$ ) in rock salt phase.....	73
Table (III-6): Compliances $S_{11}, S_{12}, S_{44}$ and calculated anisotropy parameter $\Delta$ (in units of $\text{TPa}^{-1}$ ), Zener's factor $A$ , the percentage (in %) of anisotropy in the compression and shear ( $A_B$ and $A_G$ ), and the universal anisotropic index ( $A^U$ ) of $Y_{1-x}Sc_xN$ ( $x = 0, 0.25, 0.5, 0.75, 1$ ) alloys. ....	74
Table (III-7): The values of Zener's elastic anisotropy ratio $A$ , anisotropy parameter $\Delta$ , Extreme values of the Young's modulus $E$ , Maximum and minimum values of shear modulus $G$ , Extreme values of Poisson's ratio for particular orientations $\nu[100],[001], \nu[001],[110]$ ,	

and $v(111), [111]$ for $Y_{1-x}Sc_xN$ ( $x = 0, 0.25, 0.5, 0.75$ and $1$ ) alloys. ....	<b>75</b>
Table (III-8): The elastic wave velocities (in m/s) for different propagation directions for $Y_{1-x}Sc_xN$ ( $x = 0, 0.25, 0.5, 0.75, 1$ ) in rocksalt phase.....	<b>76</b>
Table (III-9): The calculated elastic constants for $Y_{1-x}La_xN$ ( $x = 0, 0.25, 0.5, 0.75, 1$ ) compared with both theoretical and experimental data.....	<b>76</b>
Table (III-10):The calculated bulk modulus (B), shear modulus (G), Young's modulus (E), Poisson's ratio $\nu$ , Pugh's ratio( G/B), longitudinal ( $V_l$ ), shear ( $V_t$ ), average ( $V_m$ ) elastic wave velocities and Debye temperature ( $\theta_D$ ) for $Y_{1-x}La_xN$ ( $x = 0, 0.25, 0.5, 0.75, 1$ ) in rocksalt phase.....	<b>78</b>
Table (III-11): Parameter values: $S_{ij}$ , calculated universal elastic anisotropy index $A^U$ and Zener's factor A.....	<b>79</b>
Table (III-12): anisotropy parameter $\Delta$ , Extreme values of the Young's modulus E, thermodynamic constraints $\Pi$ and $\delta$ , Extreme values of Poisson's ratio for particular orientations, maximum and minimum values of shear modulus G for $Y_{1-x}La_xN$ ( $x = 0, 0.25, 0.5, 0.75$ and $1$ ) alloys.....	<b>79</b>
Table (III-13): The elastic wave velocities (in m/s) for different propagation directions for $Y_{1-x}La_xN$ ( $x = 0, 0.25, 0.5, 0.75, 1$ ) in rocksalt phase. ....	<b>80</b>
Table (III-14): The calculated elastic constants for $YN_{1-x}B_x$ ( $x = 0, 0.25, 0.5, 0.75, 1$ ) compared with both theoretical and experimental data.....	<b>81</b>
Table (III-15):The calculated bulk modulus (B), shear modulus (G), Young's modulus (E), Poisson's ratio $\nu$ , Pugh's ratio( G/B), longitudinal ( $V_l$ ), shear ( $V_t$ ), average ( $V_m$ ) elastic wave velocities and Debye temperature ( $\theta_D$ ) for $YN_{1-x}B_x$ (B = P ,As and Sb), ( $x = 0, 0.25, 0.5, 0.75, 1$ ) in rocksalt phase.....	<b>82</b>
Table (III-16): Parameter values: $S_{ij}$ , calculated universal elastic anisotropy index $A^U$ and Zener's factor A of $YN_{1-x}P_x$ ( $x = 0, 0.25, 0.5, 0.75, 1$ ) alloys.....	<b>83</b>
Table (III-17): Parameter values: $S_{ij}$ , calculated universal elastic anisotropy index $A^U$ and Zener's factor A of $YN_{1-x}As_x$ ( $x = 0, 0.25, 0.5, 0.75, 1$ ) alloys.....	<b>84</b>
Table (III-18): Parameter values: $S_{ij}$ , calculated universal elastic anisotropy index $A^U$ and Zener's factor A of $YN_{1-x}Sb_x$ ( $x = 0, 0.25, 0.5, 0.75, 1$ ) alloys.....	<b>84</b>
Table (III-19): Anisotropy parameter $\Delta$ , Extreme values of the Young's modulus E, thermodynamic constraints $\Pi$ and $\delta$ , Extreme values of Poisson's ratio for particular orientations, maximum and minimum values of shear modulus G for $YN_{1-x}P_x$ ( $x = 0, 0.25, 0.5, 0.75$ and $1$ ) alloys.....	<b>85</b>

Table (III-20): Anisotropy parameter $\Delta$ , Extreme values of the Young's modulus $E$ , thermodynamic constraints $\Pi$ and $\delta$ , Extreme values of Poisson's ratio for particular orientations, maximum and minimum values of shear modulus $G$ for $YN_{1-x}As_x$ ( $x= 0, 0.25, 0.5, 0.75$ and $1$ ) alloys.....	<b>85</b>
Table (III-21): Anisotropy parameter $\Delta$ , Extreme values of the Young's modulus $E$ , thermodynamic constraints $\Pi$ and $\delta$ , Extreme values of Poisson's ratio for particular orientations, maximum and minimum values of shear modulus $G$ for $YN_{1-x}Sb_x$ ( $x= 0, 0.25, 0.5, 0.75$ and $1$ ) alloys. ....	<b>86</b>
Table (III-22): The elastic wave velocities (in m/s) for different propagation directions for $YN_{1-x}P_x$ ( $0. 0.25, 0.5, 0.75, 1$ ) in rock salt phase.....	<b>87</b>
Table (III-23): The elastic wave velocities (in m/s) for different propagation directions for $YN_{1-x}As_x$ ( $0. 0.25, 0.5, 0.75, 1$ ) in rocksalt phase.....	<b>87</b>
Table (III-24): The elastic wave velocities (in m/s) for different propagation directions for $YN_{1-x}Sb_x$ ( $0. 0.25, 0.5, 0.75, 1$ ) in rocksalt phase.....	<b>88</b>
Table (III-25): Experimental and calculated energy band of $Y_{1-x}Sc_xN$ ( $x=0, 0.25, 0.5, 0.75$ , and $1$ ) with different approximations GGA, and HSE06.....	<b>89</b>
Table (III-26): Experimental and calculated energy band of $Y_{1-x}La_xN$ ( $x=0, 0.25, 0.5, 0.75$ , and $1$ ) with different approximations GGA, and HSE06. ....	<b>92</b>
Table (III-27): Experimental and calculated energy band of $YN_{1-x}P_x$ ( $x=0, 0.25, 0.5, 0.75$ , and $1$ ) with different approximations GGA, and HSE06. ....	<b>95</b>
Table (III-28): Experimental and calculated energy band of $YN_{1-x}As_x$ ( $x=0, 0.25, 0.5, 0.75$ , and $1$ ) with different approximations GGA, and HSE06. ....	<b>100</b>
Table (III-29): Experimental and calculated energy band of $YN_{1-x}Sb_x$ ( $x=0, 0.25, 0.5, 0.75$ , and $1$ ) with different approximations GGA, and HSE06. ....	<b>104</b>
Table (III-30): dielectric function $\epsilon_1(0)$ of $YN_{1-x}B_x$ ( $B = P, As$ and $Sb$ ) in approximation HSE06. ....	<b>114</b>

# Liste of figure

## Chapter I

FIGURE (I-1): Periodic table.....	4
FIGURE (I-2): The structure of a sodium chloride crystal. Legend: Blue: Na <sup>+</sup> , Green: Cl <sup>-</sup> .....	5
FIGURE (I-3): Unit cell definition using <u>parallelepiped</u> with lengths $a, b, c$ and angles between the sides given by $\alpha, \beta, \gamma$ . .....	6
FIGURE (I-4): First Brillouin zone of the rock-salt structure with the representation of points and lines of high symmetry. ....	7
FIGURE (I-5): Direct Gap Energy Band Structure. ....	9
FIGURE (I-6): figure of merit for type N materials .....	12
FIGURE (I-7): Evolution of merit factor for different compounds as temperature function..	14
FIGURE (I-8): Evolution of the merit factor of the compound Ag <sub>x-1</sub> Nb <sub>x</sub> BiSe <sub>2</sub> as a temperature function.....	15
FIGURE (I-9): Vehicle Integration with Thermoelectric : FORD, GM and BMW Prototype integration pursued under DOE/industry sponsorship.....	16
FIGURE (I-10): Some applications of thermoelectric generators.....	17
FIGURE (I-11): Some applications of thermoelectric cooling.....	18
FIGURE (I-12): An image representing the computer's optimal cooling system (CP Cooler) .....	19

## Chapter II

FIGURE (II-1): Representation of pseudo potential and pseudo function of wave.....	33
FIGURE (II-2): Illustration of an experiment to measure the shear modulus. ....	42
FIGURE (II-3): Illustration of an experiment for measuring the Young's modulus.....	43
FIGURE (II-4): Initial and final geometric dimension of the specimen in a simple tensile test.....	44

FIGURE (II-5): propagation directions of [100], [110] and [111] in a cubic crystal solid.....	48
FIGURE (II-6): Monatomic one-dimensional crystal. Atomic positions in equilibrium and instantaneous displacements. ....	52
FIGURE (II-7): Dispersion curve for a mono atomic chain with only interactions between the closest neighbors. ....	54
FIGURE (II-8): Diatomic one-dimensional crystal. (a) Equilibrium positions; (b) instantaneous displacements.....	55
FIGURE (II-9): Optical and acoustic branches for a diatomic linear chain.....	56
FIGURE (II-10): Diagram illustrating the Seebeck, Peltier and Thomson effects.....	58

### *Chapter III*

FIGURE ( III-1): Crystal structure of $Y_{1-x}M_xN$ ( $M = Sc$ and $La$ ), $YN_{1-x}B_x$ ( $B = P, As$ and $Sb$ ) in the rock-salt structure.....	67
FIGURE ( III-2): Composition dependence of the calculated Lattice constant and Bulk modulus of $Y_{(1-x)}Sc_{(x)}N$ .....	68
FIGURE ( III-3): Composition dependence of the calculated Lattice constant and Bulk modulus of $Y_{(1-x)}La_{(x)}N$ alloys.....	69
FIGURE ( III-4): Composition dependence of the calculated Lattice constant and Bulk modulus of $YN_{1-x}P_x$ , $YN_{1-x}As_x$ and $YN_{1-x}Sb_x$ alloys.....	71
FIGURE ( III-5): Curves representing the shear module $G$ , the Young $E$ module and the compressibility module $B$ , longitudinal ( $V_l$ ), shear ( $V_t$ ), average ( $V_m$ ) elastic wave velocities and Debye temperature ( $\theta_D$ ) for $Y_{1-x}Sc_xN$ ( $x = 0, 0.25, 0.5, 0.75, 1$ ) in rocksalt phase.....	73
FIGURE ( III-6): Curves representing the shear module $G$ , the Young $E$ module and the compressibility module $B$ , longitudinal ( $V_l$ ), shear ( $V_t$ ), average ( $V_m$ ) elastic wave velocities and Debye temperature ( $\theta_D$ ) for $Y_{1-x}La_xN$ ( $x = 0, 0.25, 0.5, 0.75, 1$ ) in rocksalt phase.....	78
FIGURE ( III-7): shows the scale structures calculated along the high symmetry waves of $Y_{1-x}Sc_xN$ alloys with different $x$ concentration.....	90
FIGURE ( III-8): Total and partial density of states (TDOS and PDOS) for $Y_{1-x}Sc_xN$ alloys with the approximation «HSE06». ....	91
FIGURE ( III-9): Calculated electronic band structure of $Y_{1-x}La_xN$ alloys with different $x$ concentration with the approximation «HSE06». ....	93

FIGURE ( III-10): Calculated total and partial density of states of $Y_{1-x}La_xN$ alloys with different x concentration with the approximation «HSE06».....	<b>94</b>
FIGURE ( III-11) : Energy band structure of YN compound using the approximation «GGA and HSE06».....	<b>95</b>
FIGURE ( III-12) : Energy band structure of $YN_{0.75}P_{0.25}$ compound using the approximation «GGA and HSE06».....	<b>96</b>
FIGURE ( III-13) : Energy band structure of $YN_{0.5}P_{0.5}$ compound using the approximation «GGA and HSE06».....	<b>96</b>
FIGURE ( III-14) : Energy band structure of $YN_{0.25}P_{0.75}$ compound using the approximation «GGA and HSE06».....	<b>97</b>
FIGURE ( III-15) : Energy band structure of YP compound using the approximation «GGA and HSE06».....	<b>97</b>
FIGURE ( III-16) : The total and partial state density (DOS) of $YN_{1-x}P_x$ ( $x = 0.25, 0.50, 0.75$ and $1$ ) with the approximation «HSE06».....	<b>99</b>
FIGURE ( III-17) : Energy band structure of $YN_{0.75}As_{0.25}$ compound using the approximation «GGA and HSE06».....	<b>100</b>
FIGURE ( III-18): Energy band structures of the compounds $YN_{0.5}As_{0.5}$ calculated in GGA and HSE06 approximation. ....	<b>101</b>
FIGURE ( III-19): Energy band structures of the compounds $YN_{0.25}As_{0.75}$ calculated in GGA and HSE06 approximation.....	<b>101</b>
FIGURE ( III-20): Energy band structures of the compounds YAs calculated in GGA and HSE06 approximation.....	<b>102</b>
FIGURE ( III-21): The total and partial state density (DOS) of $YN_{1-x}As_x$ ( $x = 0.25, 0.50, 0.75$ and $1$ ) with the approximation «HSE06».....	<b>103</b>
FIGURE ( III-22): Calculated electronic band structure of the $YN_{1-x}Sb_x$ alloy in the B1 phase for $x = 0.25$ , using the approximation GGA and HSE06.....	<b>104</b>
FIGURE ( III-23): Calculated electronic band structure of the $YN_{1-x}Sb_x$ alloy in the B1 phase for $x = 0.5$ , using the approximation GGA and HSE06.....	<b>105</b>
FIGURE ( III-24): Calculated electronic band structure of the $YN_{1-x}Sb_x$ alloy in the B1 phase for $x = 0.75$ , using the approximation GGA and HSE06.....	<b>105</b>
FIGURE ( III-25): Calculated electronic band structure of the $YN_{1-x}Sb_x$ alloy in the B1 phase for $x = 1$ , using the approximation GGA and HSE06.....	<b>106</b>
FIGURE ( III-26): The total and partial state density (DOS) of $YN_{1-x}Sb_x$ ( $x = 0.25, 0.50, 0.75$ and $1$ ) with the approximation «HSE06».....	<b>107</b>

FIGURE ( III-27). Calculated imaginary parts and The real parts of the dielectric function for $Y_{1-x}Sc_xN$ alloys. ....	<b>109</b>
FIGURE ( III-28): Refractive index and extinction coefficient for $Y_{1-x}Sc_xN$ corresponding to different values of x. ....	<b>109</b>
FIGURE ( III-29): Absorption coefficient for $Y_{1-x}Sc_xN$ alloys.....	<b>110</b>
FIGURE ( III-30): Calculated imaginary parts and real parts of the dielectric function for $Y_{1-x}La_xN$ alloys. ....	<b>111</b>
FIGURE ( III-31): Refractive index and extinction coefficient for $Y_{1-x}La_xN$ corresponding to different values of x. ....	<b>112</b>
FIGURE ( III-32): Reflectivity for $Y_{1-x}La_xN$ alloys. ....	<b>112</b>
FIGURE ( III-33): Absorption coefficient for $Y_{1-x}La_xN$ alloys. ....	<b>113</b>
FIGURE ( III-34): Calculated imaginary parts and real parts of the dielectric function for $YN_{1-x}P_x$ alloys. ....	<b>115</b>
FIGURE ( III-35): Calculated imaginary parts and real parts of the dielectric function for $YN_{1-x}As_x$ alloys.....	<b>115</b>
FIGURE ( III-36): Calculated imaginary parts and real parts of the dielectric function for $YN_{1-x}Sb_x$ alloys.....	<b>116</b>
FIGURE (III-37): Variation of refractive index and extinction coefficients for $YN_{1-x}P_x$ alloys. ....	<b>117</b>
FIGURE (III-38): Variation of refractive index and extinction coefficients for $YN_{1-x}As_x$ alloys. ....	<b>117</b>
FIGURE (III-39): Variation of refractive index and extinction coefficients for $YN_{1-x}Sb_x$ alloys.....	<b>118</b>
FIGURE (III-40): Reflectivity variation for $YN_{1-x}P_x$ , $YN_{1-x}As_x$ and $YN_{1-x}Sb_x$ compounds in the HSE06 approximation.....	<b>119</b>
FIGURE (III-41): Optical absorption coefficients of the $YN_{1-x}P_x$ , $YN_{1-x}As_x$ and $YN_{1-x}Sb_x$ alloys calculated using the functional HSE06.....	<b>119</b>
FIGURE (III-42) : Calculated phonon dispersion curves and phonon DOS for a $Y_{1-x}Sc_xN$ ( $x = 0, 0.25, 0.50, 0.75$ and $1$ ) alloys along several high symmetry lines in the Brillouin zone..	<b>122</b>
FIGURE (III-43) :Calculated phonon dispersion curves and phonon DOS for $Y_{1-x}La_xN$ ( $x = 0, 0.25, 0.50, 0.75$ and $1$ ) alloys along several high symmetry lines in the Brillouin zone.....	<b>124</b>
FIGURE (III-44) : Calculated phonon dispersion curves and phonon DOS for $YN_{0.75}P_{0.25}$ and $YP$ alloys along several high symmetry lines in the Brillouin zone.....	<b>125</b>
FIGURE (III-45) : Calculated phonon dispersion curves and phonon DOS for $YN_{0.75}As_{0.25}$ and	

YAs alloys along several high symmetry lines in the Brillouin zone.....**126**  
FIGURE (III-46) : Calculated phonon dispersion curves and phonon DOS for YSb alloys  
along several high symmetry lines in the Brillouin.....**127**

## Table of Contents

General Introduction:	1
-----------------------	---

### ***CHAPTER I: Physical properties of III<sup>B</sup>-V<sup>A</sup> and Thermoelectric applications***

I-1- Introduction	4
I-2- Physical properties of binary materials: XN ( X = Sc, Y, La ) and YM (M = P, As, Sb )	4
I-2-1. Definitions of III <sup>B</sup> -V <sup>A</sup> materials	4
I-3. Structural Properties	5
I-3-1. Structure - Rock Salt (NaCl)	5
I-3-2. Lattice constant of Rocksalt type (NaCl)	6
I-3-3. Lattice constant of binary materials	6
I-4. First Brillouin zone	6
I-5. Electronic properties	8
I-5-1. Electronic structure	8
I-5-2. Band Structure	8
I-5-3. Direct gap and indirect gap	9
I-6. Elastic properties	9
I-7. Properties of ternary compounds (Sc <sub>x</sub> Y <sub>1-x</sub> N)	10
I-8. Application of III <sup>B</sup> -V <sup>A</sup> materials:	11
I-9. Thermoelectric materials	11
I-9-1. Introduction	11
I-9-2. Traditional materials	12
I-9-2-1. Bismuth Telluride (Bi <sub>2</sub> Te <sub>3</sub> )	12
I-9-2-2. Lead Telluride and its derivatives (Pb, Te)	13
I-9-2-3. Silicon and Germanium	13
I-9-3. Physical properties some thermoelectric materials	13
I-10-4. New thermoelectric materials	14
I-10. Applications	15
I-10-1. For thermoelectric generators (direct conversion of heat to electricity)	15

<b>I-10-2. Thermoelectric cooling</b>	<b>17</b>
<b>I-10-3. Electronic Device Cooler</b>	<b>18</b>
<b>I-10-4. Other Applications</b>	<b>19</b>
<b>Bibliographies</b>	<b>20</b>

## **CHAPTER II:**

## ***Theoretical Framework***

### ***Part A: Density functional theory (DFT)***

<b>II-A-1. Introduction</b>	<b>23</b>
<b>II-A-2 . Problem at N body with approximations</b>	<b>23</b>
<b>II-A-2-1. The Born-Oppenheimer approximation</b>	<b>24</b>
<b>II-A-2-3.Hartree-Fock approximation</b>	<b>25</b>
<b>II-A-4-Functional Density Theory (DFT)</b>	<b>26</b>
<b>II-A-4-1. Approximation of Kohn and Sham</b>	<b>27</b>
<b>II-A-4-2.Functional exchange and correlation</b>	<b>28</b>
<b>a - Local Density Approximation (LDA)</b>	<b>28</b>
<b>b - Generalized Gradient Approximation (GGA)</b>	<b>29</b>
<b>5- Pseudo potential method and plane waves</b>	<b>29</b>
<b>II-A-5-1- Introduction</b>	<b>29</b>
<b>II-A-5-2-2. Sampling of the Brillouin zone</b>	<b>30</b>
<b>II-A-5-2-3. Flat waves</b>	<b>30</b>
<b>II-A-5-2-3. Cut-off energy</b>	<b>30</b>
<b>II-A-5-2-4. Bloch theorem</b>	<b>31</b>
<b>II-A-6. Approach to pseudo potential</b>	<b>31</b>
<b>II-A-6-1. Frozen core approximation</b>	<b>31</b>
<b>II-A-6-2. Pseudo-potential method</b>	<b>32</b>
<b>II-A-7-The code of CASTEP</b>	<b>33</b>
<b>Bibliographies</b>	<b>34</b>

**Part B: Elastic ,optical , phonon and thermoelectric properties with DFT**

<b>II-B-1. Elastic properties</b>	<b>37</b>
<b>II-B-1-1. Tensors of the elastic constants</b>	<b>37</b>
<b>II-B-1-2. Energy and the elastic constants</b>	<b>38</b>
<b>II-1-2-1. Case of a crystal with cubic symmetry</b>	<b>39</b>
<b>II-B-1-2-2.Calculation Method</b>	<b>40</b>
<b>II-B-1-3. Mechanical Properties</b>	<b>41</b>
<b>II-B-1-3-1. Mechanical stability criteria of the crystal</b>	<b>41</b>
<b>II-B-1-3.2. Bulk modulu</b>	<b>41</b>
<b>II-B-1-3-3. Shear modulu</b>	<b>42</b>
<b>II-B-1-3-4. Pugh's index (<math>B/G</math>)</b>	<b>43</b>
<b>II-B-1-3-5. Young's modulus</b>	<b>43</b>
<b>II-B-1-3-6. The axial modulus</b>	<b>44</b>
<b>II-B-1-3-7. The Debye temperature</b>	<b>45</b>
<b>II-B-1-4. Elastic anisotropy</b>	<b>46</b>
<b>II-B-1-5. Elastic wave propagation velocities</b>	<b>46</b>
<b>II-B-2. Optical Properties</b>	<b>47</b>
➤ <b>The complex refractive index</b>	<b>50</b>
➤ <b>Reflectivity</b>	<b>50</b>
➤ <b>Absorption coefficient <math>\alpha(\omega)</math></b>	<b>50</b>
<b>II-B-3. Phonons Properties</b>	<b>50</b>
<b>II-B-3-1. Phonon Density of States</b>	<b>50</b>
<b>II-B-3-2. Acoustic and optical phonons</b>	<b>51</b>
➤ <b>Acoustic phonons</b>	<b>51</b>
➤ <b>Optical phonons</b>	<b>52</b>
<b>II-B-3-3. Classical harmonic crystal theory</b>	<b>52</b>
<b>II-B-3-3-1. Vibrations of a monatomic chain</b>	<b>52</b>
<b>II-B-3-3-1-1. Dispersion relationship</b>	<b>53</b>
<b>II-B-3-3-2. Vibrations of a diatomic chain</b>	<b>55</b>
<b>II-B-3-3-3. Three-dimensional lattice</b>	<b>57</b>
<b>II-B-4. Thermoelectricity</b>	<b>57</b>

II-B-4-1. Thermoelectric effects	57
II-B-4-2. Thermoelectric coefficients	59
II-B-4-3. ZT merit factor	60
Bibliographies	62

### **CHAPTER III:**

### ***Results and discussion***

III-1. Introduction	66
III-2. Method of calculations	66
III-3. Structural Properties $Y_{1-x}M_xN$ ( $M = Sc$ and $La$ ), $YN_{1-x}B_x$ ( $B = P$ , $As$ and $Sb$ )	67
III-3 -1. Structural Properties of $Y_{1-x}M_xN$ ( $M = Sc$ and $La$ )	67
III-3-1-1. The compounds $Y_{1-x}Sc_xN$ for ( $x = 0, 0.25, 0.50, 0.75$ and $1$ )	67
III-3-1-2. The compounds $Y_{1-x}La_xN$ for ( $x = 0, 0.25, 0.50, 0.75$ and $1$ )	68
III-3-2. Structural Properties of $YN_{1-x}B_x$ ( $B : P$ , $As$ and $Sb$ ) , ( $x = 0, 0.25, 0.50, 0.75$ and $1$ )	69
III-4. Elastic properties and mechanical stability $Y_{1-x}M_xN$ ( $M = Sc$ and $La$ ) and $YN_{1-x}B_x$ ( $B = P$ , $As$ and $Sb$ )	71
III-4-1. Elastic properties and mechanical stability of $Y_{1-x}M_xN$ ( $M = Sc$ and $La$ )	71
III-4-1-1. The compounds $Y_{1-x}Sc_xN$ for ( $x = 0, 0.25, 0.50, 0.75$ and $1$ )	71
A) Elastic constants and elasticity modules	71
B) Anisotropy of elastic moduli	74
1. Isotropic factor	74
2. Young modulus , Poisson coefficient and shear modulus	74
3. Elastic wave propagation velocities	75
III-4-1-1. The compounds $Y_{1-x}La_xN$ for ( $x = 0, 0.25, 0.50, 0.75$ and $1$ )	76
A ) Elastic constants and elasticity modules	76
B) Anisotropy of Elastic Moduli	79
1. Isotropic factor	79
2. Young modulus , Poisson coefficient and shear modulus	97

<b>3. Elastic wave propagation velocities</b>	<b>80</b>
<b>III-4-2. Elastic properties and mechanical stability of <math>YN_{1-x}B_x</math> (B = P ,As and Sb)</b>	<b>80</b>
<b>A) Elastic constants and elasticity modules</b>	<b>80</b>
<b>B) Anisotropy of Elastic Moduli</b>	<b>83</b>
<b>1. Isotropic factor</b>	<b>83</b>
<b>2. Young modulus , Poisson coefficient and shear modulus</b>	<b>85</b>
<b>3. Elastic wave propagation velocities</b>	<b>86</b>
<b>III-5- Electronic structure of <math>Y_{1-x}M_xN</math> ( M = Sc and La), <math>YN_{1-x}B_x</math> (B = P ,As and Sb) alloys</b>	<b>88</b>
<b>III-5.1 . Band structures and T-DOS and P-DOS of <math>Y_{1-x}M_xN</math> ( M = Sc and La)</b>	<b>88</b>
<b>III-5-1-1.The compounds <math>Y_{1-x}Sc_xN</math> for (x = 0, 0.25, 0.50, 0.75 and 1 )</b>	<b>88</b>
<b>III-5-1-2.The compounds <math>Y_{1-x}La_xN</math> for (x = 0, 0.25, 0.50, 0.75 and 1 )</b>	<b>92</b>
<b>III-5-2 . Band structures and T-DOS and P-DOS of <math>YN_{1-x}B_x</math> (B = P ,As and Sb) alloys</b>	<b>95</b>
<b>III-5-2-2. The compounds <math>YN_{1-x}P_x</math> (x = 0, 0.25, 0.50, 0.75 and 1 )</b>	<b>95</b>
<b>III-5-2-3. The compounds <math>YN_{1-x}As_x</math> (x = 0, 0.25, 0.50, 0.75 and 1 )</b>	<b>100</b>
<b>III-5-2-4. The compounds <math>YN_{1-x}Sb_x</math> (x = 0, 0.25, 0.50, 0.75 and 1 )</b>	<b>103</b>
<b>III-6. The optical properties of <math>Y_{1-x}M_xN</math> ( M = Sc and La), <math>YN_{1-x}B_x</math> (B = P ,As and Sb) alloys</b>	<b>108</b>
<b>III-6-1. The optical properties of <math>Y_{1-x}M_xN</math> ( M = Sc and La)</b>	<b>108</b>
<b>III-6-1-1.The compounds <math>Y_{1-x}Sc_xN</math> for (x = 0, 0.25, 0.50, 0.75 and 1 )</b>	<b>108</b>
<b>III-6-1-2.The compounds <math>Y_{1-x}La_xN</math> for (x = 0, 0.25, 0.50, 0.75 and 1 )</b>	<b>110</b>
<b>III-6-2. The optical properties of <math>YN_{1-x}B_x</math> (B = P ,As and Sb) alloys</b>	<b>113</b>
<b>III-7. Phonon properties of <math>Y_{1-x}M_xN</math> ( M = Sc and La), <math>YN_{1-x}B_x</math> (B = P ,As and Sb) alloys</b>	<b>120</b>
<b>III-7-1. Phonon properties of <math>Y_{1-x}M_xN</math> ( M = Sc and La) alloys</b>	<b>120</b>
<b>7-2. Phonon properties of <math>YN_{1-x}B_x</math> (B = P ,As and Sb) alloys</b>	<b>124</b>
<b>Bibliographies</b>	<b>128</b>
<b>General conclusion</b>	<b>131</b>

**General Introduction:**

Semiconductor technology has come a long way in recent years in many applications in electronics and optoelectronics. The field of the realization of materials has largely extended thanks to the use of elements of the periodic table to form binary compounds, alloys, or super-networks.

The industry increasingly uses metals with specific qualities, allowing high-performance applications. Rare metals constitute a rich palette of about fifty elements from which today metallurgists draw to develop new materials, among the rare metals Yttrium.

The latter, Yttrium, is a chemical element, symbol Y and atomic number 39. It is a transition element of metallic appearance, which possessed a chemical behavior close to that of lanthanides and historically ranked among rare earth, with Scandium and Lanthanides.

The study of transition metal nitride, Yttrium (YN), Scandium nitride (ScN), and lanthanum nitride (LaN) has attracted extensive interest for basic research as well as for technology because of its wide technological applications resulting from properties physicals (hardness, chemical inertness, electrical and thermal conductivity).

The techniques of calculation in the electronic structure developed in recent decades are numerous. The ab-initio methods have become an indispensable tool in calculating the structural properties, The most complex systems, and their physical properties [1].

They are also a tool of choice for prediction. Of new materials, and they have sometimes been able to replace very expensive or even impossible laboratory experiments.

This simulation was performed by the code CASTEP [2] (Cambridge serial total Energie Package). This program is based on the theory of functional density (DFT) and uses a technique of coupling between «PW» and the approach of plane waves «PP» pseudo-potentials [3]. This program makes it possible to obtain the total energy in the fundamental state of the system.

The purpose of this work is to calculate the structural, elastic, electronic and optical, and phononic properties of the  $Y_{1-x}M_xN$  ( $x = 0, 0.25, 0.5, 0.75, 1$ ). Where  $M = Sc$  and  $La$ .

$YN_{1-x}B_x$  ( $x = 0, 0.25, 0.5, 0.75, 1$ ). Where  $B = P, As, \text{ and } Sb$ .

The manuscript is composed of three chapters:

In the first chapter, we define the Physical properties of nitrides III-V and Thermoelectric materials and Thermoelectric applications.

The second chapter's theoretical aspect has two parts:

Part A: We recall the principle of the functional density of theory (DFT) we recall the

principle of the Functional density of Theory (DFT) [3]. which regards electronic density as a fundamental variable and all physical properties, in particular, the total energy of the electron system can be expressed, as a function of it, the density can be obtained by solving the Kohn and Sham equations [4] for a mono-electronic Schrödinger equation system by approximations LDA, GGA [5], and HSE06 [6].

Part B: we will present the relative formulas for elastic, optical, phononic, and thermoelectric properties.

The third chapter was devoted to a presentation of the results of our calculations with a parallel discussion and comparison of these with the results of other experimental and theoretical works available.

Finally, we conclude with a general conclusion that brings together all the main results of this work.

**Bibliographies**

- [1] A. Saliha, Thèse de doctorat ;Université D'Oran, 24/02/2014.
- [2] M. D. Segall, P. J. D. Lindan, M. J. Probert, C. J. Pickard; P.J. Hasnip S. J.Clark,M.C.Payne, "First principles simulation: ideas, illustrations and the . CASTEP code" , J Phys. Condens. Matter, 14, 2717 -2743 (2002).
- [3] D. Vanderbilt "Soft self –consistent pseudopotential in a generalized eigenvalue formalism " Phys. Rev. B 41:7892-7895, 1990.
- [4] P. Hohenberg, and W. Kohn, "Inhomogeneous electron gas", Phys. Rev. B.136:864,1964.
- [5] J.P.Perdew, K.Burke, and M.Ernzerhof, Phys. Rev. Lett. 77, 3865 (1996).
- [6] J. Heyd, G. E. Scuseria, M. Ernzerhof, Hybrid Functionals Based on a Screened Coulomb Potential, J. Chem. Phys. 118 (2003) 8207-8215.

I-1. Introduction:

Yttrium is an element of the III column of the table of Mendeleïev (of symbol Y and atomic number 39) [1], in the group of transition metals of metallic appearance classified in the family of rare earth with Scandium and Lanthanides. Reduced to powder or shavings, Yttrium is unstable in air and can ignite spontaneously if the temperature exceeds 400° C. The most applied use of Yttrium is the manufacture of phosphors, such as those used in cathode ray tube televisions or LEDs [2]. Its other applications include the production of electrodes, electrolytes, electronic filters, lasers and superconducting materials, and various medical applications. So, from a technological and fundamental point of view. Compounds Y-V and III-N have recently received considerable interest in solid state and materials science due to their diverse mechanical, electronic, and dynamical properties and for potential application in spintronics.

I-2. Physical properties of binary materials: XN ( X = Sc, Y, La, Cr ) and YM (M = P, As, Sb ).

I-2-1.Definitions of III<sup>B</sup>-V<sup>A</sup> materials:

IIIB-VA are compound materials formed from an element of the third (3rd) column, which represents the following elements: Scandium (Sc), Yttrium (Y), Lanthanum (La), and the elements of the fifth (5th ) column of the periodic table, which represents the following elements, Azot (N), Phosphorus (P), Arsenic (As), Antimony (Sb), Bismuth (Bi), (FIGURE (I-1)). They serve as the object of significant research, mainly because of the applications of electronic and optoelectronic devices.

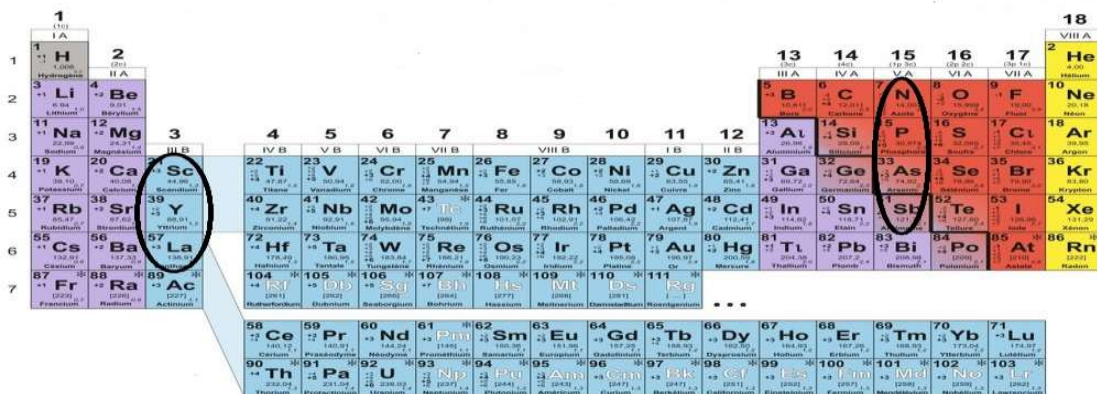


FIGURE (I-1): Periodic table of the III<sup>B</sup>-V<sup>A</sup> materials .

**I-3. Structural Properties:****I-3-1. Structure - Rock Salt (NaCl):**

Sodium chloride is an ion chemical compound of the NaCl formula. It is more commonly called food salt or kitchen salt, or simply salt in the common language. The structure of NaCl is formed by repeating the face-centred cubic unit cell. The compounds with the sodium chloride structure include alkali halides and metal oxides, and transition-metal compounds. And the role in many applications is the structure and dynamics of water. Some applications contain the crystallisation of proteins and the conformational behaviour of peptides and nucleic acids [3]. A mesh of Salt is a cube that contains the following:

- one chlorine atom at each of the 8 cell vertices (each top shared by 8 adjoining cells, this contributes one atom per cell).
- one chlorine atom in the center of each of the 6 sides of the mesh (each side divided between 2 adjoining cells, this makes 3 atoms per cell).
- one sodium atom in the center of the cell; one atom per cell.
- one sodium atom on the middle of each of the 12 edges of the mesh (each edge shared between 4 neighbouring cells, this makes 3 atoms per cell).

So, overall, each cell contributes 4 chlorine atoms and 4 sodium atoms.

- Na<sup>+</sup> :  $1_{center} + 12_{edge} \times \frac{1}{4} = 4$  sodium ions total per cell.
- Cl<sup>-</sup> :  $4_{face} \times \frac{1}{2} + 8_{corner} \times \frac{1}{8} = 4$  chloride ions total per cell.

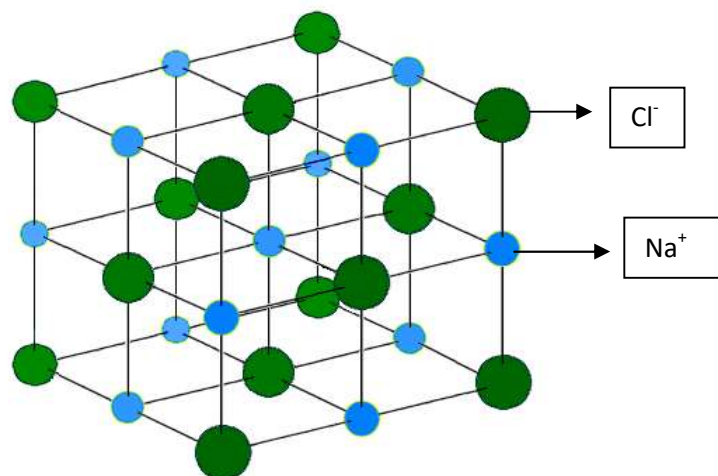


**FIGURE (I-2):** The structure of a sodium chloride crystal. Legend: Blue: Na<sup>+</sup>, Green: Cl<sup>-</sup>.

**I-3-2. Lattice constant of Rock-salt type (NaCl):**

The crystalline parameters (lattice parameters) are quantities used to describe the lattice of a crystal. One distinguishes three lengths  $a, b, c$  ( $a=b=c$ ) and three angles  $\alpha, \beta, \gamma$  ( $\alpha = \beta = \gamma$ ), which ultimately determines the parallelepiped, which is the mesh, elementary, or multiple.

Are shown in FIGURE (I-3).

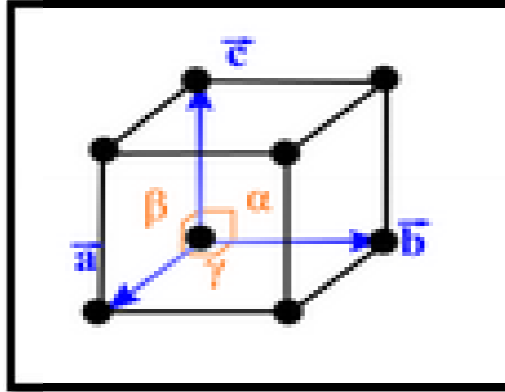


**FIGURE (I-3):** Unit cell definition using parallelepiped with lengths  $a, b, c$  and angles between the sides given by  $\alpha, \beta, \gamma$ .

**I-3-2. Lattice constant of binary materials:**

The structural types of transition metals XN ( $X = Sc, Y, La, Cr$ ) and YM ( $M = P, As, Sb$ ) crystallize in the face-centred cubic (fcc) system of the NaCl type [3-4]. Its space group is  $Fm\bar{3}m$  (225), whose base comprises a Na atom (0,0,0) and a Cl atom (1/2,1/2,1/2) separated by a half diagonal of the cube [5] (FIGURE (I-3)).

**Table (I-1):** The experimental and calculated mesh parameters for these elements.

		ScN	YN	LaN	YP	YAs	YSb
a(A°)	Expt.	4.50 <sup>a</sup>	4.87 <sup>c</sup>	5.30 <sup>e</sup>	5.65 <sup>i</sup>	5.78 <sup>i</sup>	6.15 <sup>k</sup>
	Calc.	4.51 <sup>b</sup>	4.91 <sup>d</sup>	5.32 <sup>f</sup>	5.68 <sup>j</sup>	5.81 <sup>j</sup>	6.20 <sup>t</sup>

Ref<sup>a</sup> [ 6], Ref<sup>b</sup> [7], Ref<sup>c</sup> [8], Ref<sup>d</sup> [9], Ref<sup>e</sup> [10], Ref<sup>f</sup> [11], Ref<sup>i</sup> [12], Ref<sup>j</sup> [13], Ref<sup>k</sup> [14].

**I-4. First Brillouin zone:**

All the physical properties of compounds in the first Brillouin Zone for a NaCl structure will be investigated. The first Brillouin zone has the shape of a truncated octahedron (FIGURE (I-4)). This reduced space of the reciprocal lattice is characterised by high symmetry points [15].

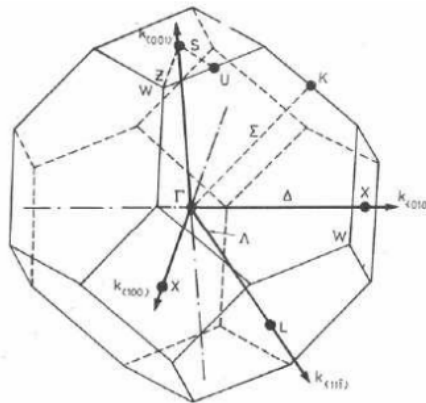


**FIGURE (I-4):** First Brillouin zone of the rock-salt structure with the representation of points and lines of high symmetry.

With:

➤ **Points of high symmetry:**

Γ: This point is the centre of the first Brillouin zone with the coordinates  $k_{\Gamma} = (0,0,0)$ .

X: This point is the centre of a square face of the octahedron which belongs to one of the axes.

❖  $k_x, k_y,$  or  $k_z$  with one of the square faces. So we have:

$$k_x = \frac{2\pi}{a} (\pm 1, 0, 0), k_y = \frac{2\pi}{a} (0, \pm 1, 0), k_z = \frac{2\pi}{a} (0, 0, \pm 1)$$

L : This point is the centre of a hexagonal face of the octahedron whose coordinates are:

$$k_l = \frac{2\pi}{a} (1, 1, 1)$$

W : Point lies on one of the vertices of the square faces. The contact details are:

$$k_w = \frac{2\pi}{a} (0, 1/2, 1)$$

Z : This point is located on the line that joins the centre of a square face to one of the corners of the octahedron with the coordinates:

$$k_z = \frac{2\pi}{a} (1, 1/2, 1)$$

❖ **Lines of high symmetry:**

Δ: This line represents the  $\langle 100 \rangle$  direction. It connects the centre Γ to point X.

Σ: It is a point belonging to the plane of symmetry  $k_x = k_y$  or  $k_y = k_z$  or  $k_x = k_z$ .

Λ: This line is the direction  $\langle 100 \rangle$ . It connects the centre of the zone (Γ) to the centre of a face

hexagonal which is the point L of the octahedron.

**I-5- Electronic properties:**

**I-5-1. Electronic structure:**

In particle physics, as in quantum chemistry, the electronic configuration, also called electronic structure or electronic formula, describes the distribution of electrons in an atom. The electrons are distributed around the atom’s nucleus and distributed in different layers. In the quantum model, the electrons are not characterised by their trajectories but by their energies.

**Table (I-2):** Below shows the electronic structure for Sc, Y, La, N, P, As, Sb atoms.

atomes	Electronic Structure
Scandium (Sc)	Sc:[ Ar]3d <sup>1</sup> 4s <sup>2</sup>
Yttrium (Y)	Y : [ Kr] 4d <sup>1</sup> 5s <sup>2</sup>
Lanthanium (La)	La: [Xe]5d <sup>1</sup> 6s <sup>2</sup>
Azot (N)	N :  He] 2s <sup>2</sup> 2p <sup>3</sup>
Phosphore (P)	P : [Ne] 3s <sup>2</sup> 3p <sup>3</sup>
Arsenic (As)	As : [Ar] 4s <sup>2</sup> 4p <sup>3</sup>
Antimoine (Sb)	Sb : [ Kr] 5s <sup>2</sup> 5p <sup>3</sup>

**I-5-2. Band Structure:**

The electrons of a single atom have well-defined allowable energy levels, but their behaviour in a periodic crystal lattice is different. If the distance between the neighbouring atoms generates a kind of interference between the allowed level of an atom, this results in a quasi-continuous multitude of states around each permitted level of the individual atoms; this set of states very close between them is considered as a band of allowed energy with an associated density of states. The energy levels of the valence electrons and the ionization energy level thus generate two particularly interesting, allowed energy bands. The valence band and the conduction band are separated. By a band devoid of permitted level, called the forbidden band. The particular of these are the permitted conduction bands because the electrons can circulate freely throughout the crystal lattice and thus generate currents of electrical conduction. [16] The ScN, YN, and LaN semiconductors are indirectly gapped. The maximum of the valence band at point  $\Gamma$  and the minimum of the conduction band at point X

are both located in the centre of the Brillouin zone [17-4]. While the other compounds (YP, YAs, YSb) in this series have a semi-metallic nature with a negative band gap which increases by changing the anion from top to bottom of the periodic table[3-4].

### I-5-3. Direct gap and indirect gap:

The term gap appears in the context of the physics of semiconductors when considering the valence band and the conduction band thereof. The energy gap is the distance between the valence band and the conduction band (band gap), an energy value that allows the electron to jump from the valence band to the conduction band. [18] FIGURE (I-5) shows types of energy gaps, direct gap and the other indirect. The difference between the two gaps is the wave vector  $K^{\rightarrow}$ .

#### Direct gap case:

The minimum of the conduction band and the maximum of the valence band are for the same point  $k$  of the Brillouin zone, point  $\Gamma$ . The semiconductor is said to have a direct gap.

As for the indirect gap: the maximum and the minimum correspond to different values of  $K^{\rightarrow}$ . The semiconductor is said to have an indirect gap.[19]

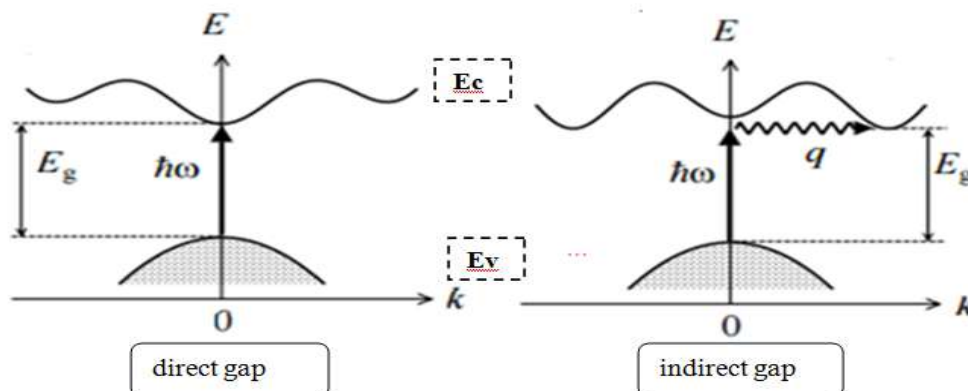


FIGURE (I-5): Direct Gap Energy Band Structure.

### I-6. Elastic properties:

Elastic properties define the properties of materials, when they undergo stress, deform and return to their original shape after the stress ceases. These properties play an important role in providing valuable information about the bonding characteristics between adjacent atomic plane, structural stability, specific heat, thermal expansion, Debye temperature . [20] Regarding the elastic properties of these binary compounds AB (A = Sc, Y, La; B = N, P, As,

Sb, Bi), have been widely studied, and it was the experimental and theoretical results are in relative convergence. Therefore, only three independent elastic constants  $C_{11}$ ,  $C_{12}$  and  $C_{44}$  are necessary to characterise their elastic nature. These constants are important to provide valuable information about the stability and stiffness of materials. They were calculated from the first numerical principal calculations by calculating the tensile stress components of small deformations using the WIEN2K code.

**Table (I-3):** Below shows the elastic structure for Sc, Y, La, N, P, As, Sb atoms.

Compounds	$C_{11}$	$C_{12}$	$C_{44}$	E	G	V	A	B/G
ScN	384.55 <sup>a</sup>	94.1 <sup>a</sup>	156.07 <sup>a</sup>	368.57 <sup>a</sup>	151.7 <sup>a</sup>	0.24 <sup>a</sup>	1.07 <sup>a</sup>	1.42 <sup>a</sup>
YN	133 <sup>b</sup>	45.9 <sup>b</sup>	79.2 <sup>b</sup>	291 <sup>c</sup>	102 <sup>c</sup>	0.20 <sup>d</sup>	1.08 <sup>d</sup>	1.19 <sup>e</sup>
LaN	249.15 <sup>a</sup>	72.14 <sup>a</sup>	67.44 <sup>a</sup>	210.5 <sup>a</sup>	85.56 <sup>a</sup>	0.23 <sup>a</sup>	0.76 <sup>a</sup>	1.51 <sup>a</sup>
YP	116 <sup>a</sup>	31.0 <sup>a</sup>	86.28 <sup>a</sup>	133 <sup>e</sup>	60 <sup>c</sup>	0.22 <sup>d</sup>	0.25 <sup>e</sup>	1.46 <sup>a</sup>
YAs	192 <sup>e</sup>	41 <sup>e</sup>	21 <sup>e</sup>	123 <sup>e</sup>	53 <sup>e</sup>	0.23 <sup>d</sup>	0.49 <sup>d</sup>	0.88 <sup>a</sup>
YSb	116 <sup>e</sup>	35 <sup>e</sup>	23 <sup>e</sup>	92 <sup>c</sup>	45 <sup>c</sup>	0.25 <sup>c</sup>	0.38 <sup>c</sup>	1.8 <sup>a</sup>

[3]<sup>a</sup>, [21]<sup>b</sup>, [22]<sup>c</sup>, [23]<sup>d</sup>, [24]<sup>e</sup>.

**I-7- Properties of ternary compounds ( $Sc_xY_{1-x}N$ ):**

Alloys can be produced by the partial substitution of one of the elements with another element from the same column. For example, the ternary crystal  $AxB1-xC$  is known to be composed of AC molecules with a molar fraction of x and BC molecules with a fraction (1-x) [21].

To determine the lattice constant (often denoted a) by applying a linear relationship between the lattice parameter of a ternary material as a function of its composition between its two extreme binary compounds, furthermore, a dependence of the band gap is presented as a function of the composition x of a ternary alloy. Vegard's law[22]:

$$a(x) = xa_{AC} + (1-x)a_{BC}$$

Where:

a (x): The lattice constant of the alloy.  $a_{AC}$  and  $a_{BC}$  the lattice constants of the binary compounds AC and BC respectively. And:

$$Eg(x) = xEg(AC) + (1-x)Eg(BC) + bx(1-x)$$

With:

Eg (AC): is the gap of compound AC.

Eg (BC): is the gap of compound BC.

b: Being the curvature parameter (bowing), which is often proven by experience. The origin of the bowing is due to the structural aspect and the compositional disorder, which are very dominant in the fluctuations of the ternary alloy.[22]

### **I-8. Application of III<sup>B</sup>-V<sup>A</sup> materials:**

Optoelectronics is the communication between optics and electronics which includes the study, design and manufacture of a hardware device that converts electrical energy into light and light into energy through semiconductors. Optoelectronics device is basically an electronic device involving light. This device can be found in many optoelectronics applications like military services, telecommunications, automatic access control systems and medical equipments.

This academic field covers a wide range of devices including LEDs and elements, image pick up devices, information displays, optical communication systems, optical storages and remote sensing systems, etc. Examples of optoelectronic devices include telecommunication laser, blue laser, optical fiber, LED traffic lights, photo diodes and solar cells. Majority of the optoelectronic devices (direct conversion between electrons and photons) are LEDs, laser diodes, photo diodes and solar cells.

### **I-9- Thermoelectric materials:**

#### **I-9-1.Introduction:**

Before 1950, a large-scale research campaign had begun that would lead to the discovery of new materials containing high ZT agents. There were no new theoretical approaches until the early 1990s to activate this field of research. However, this alleged material remains an active part of commercial units. These are low-gap semiconductors, most of which have the required characteristics contained in Chapter 2. Significant efforts have been made worldwide to discover new families of materials that have validated new concepts. In addition, the emergence of nanotechnology contributed to research and development in small-scale structures based on conventional materials. These systems now attract considerable interest in both empirical and theoretical terms as a result of work that has shown that they may have higher ZT values than solid matter. However, in recent years, many publications have emerged about research and the discovery of new families of potentially attractive materials for thermal electricity.

So we can distinguish between so-called conventional materials and those that have been

studied since the beginning of thermal energy. On the other hand, new materials have emerged over the years due to discovering new approaches to improving performance. [23].

### I-9-2. Traditional materials :

Conventional thermoelectric materials are classified into three main groups corresponding to temperature bands in which their worthiness factor is optimal and are as follows:

- ❖ The first is bismuth-based telluride substances.
- ❖ The second is lead telluride-based material.
- ❖ The third is silicon germanium-type substances.

These groups are determined according to the optimal temperature range as shown in FIGURE (I-6).

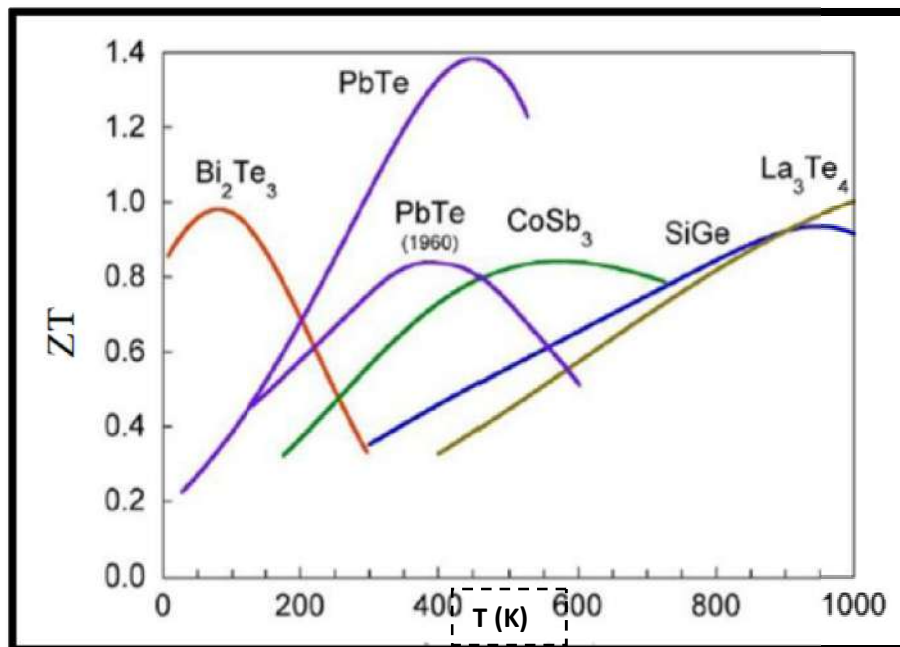


FIGURE (I-6): Factor of merit for type N materials [23].

#### I-9-2.1. Bismuth Telluride ( $\text{Bi}_2\text{Te}_3$ ):

Bismuth Telluride ( $\text{Bi}_2\text{Te}_3$ ) is the first material incorporated into thermoelectric components, thanks to its low-temperature performance (from ambient to  $\sim 450\text{K}$ ). Thus, the majority of the thermoelectric devices developed so far still rely on this alloy. Better performance is obtained when combined with  $\text{Sb}_2\text{Te}_3$  or  $\text{Bi}_2\text{Te}_3$ . Ioffe proposed this combination and his colleagues in 1956 [24], Bismuth Telluride ( $\text{Bi}_2\text{Te}_3$ ) is the first material incorporated into thermoelectric components, thanks to its low-temperature performance (from ambient to  $\sim 450\text{K}$ ). Thus, the majority of the thermoelectric devices developed so far still rely on this alloy. Better performance is obtained when combined with  $\text{Sb}_2\text{Te}_3$  or  $\text{Bi}_2\text{Te}_3$ .

Proposed selecting an element with a higher atomic number. Therefore, higher atomic mass creates local mass fluctuations to deploy phonons and obtain as little thermal conductivity as possible. It will get better the ZT thermoelectric worthiness factor. factor. Thus, optimal combinations are obtained Bi<sub>0.5</sub>Sb<sub>1.5</sub>Te<sub>3</sub> and Bi<sub>2</sub>Te<sub>2.7</sub>Se<sub>0.3</sub>, corresponding to types p and n, respectively. The best ZT merit factor obtained is 1.1 to 50 K around ambient temperature, with Seebeck  $S \sim 225 \mu\text{VK}^{-1}$  coefficient, electrical conductivity  $\sigma \sim 105 \Omega^{-1} \cdot \text{m}^{-1}$ , and thermal conductivity  $\sim 1.5 \text{ W/m.K}$  [25]. After 450 K, Bi<sub>2</sub>Te<sub>3</sub>-based compounds are no longer chemically stable.

### I-9-2.2. Lead Telluride and its derivatives (Pb, Te):

Lead telluride is a low-gap semiconductor, the most commonly used compound for power generation at medium temperatures [500 K - 800 K]. Type n or p can be obtained either by changing the chemical composition compared to measuring stoichiometry or by using steroids with items such as Na or Ti for type p or Zn, Bi for type n. and so, as with Bi<sub>2</sub>Te<sub>3</sub>, PbTe can integrate with PbSe and SnTe. In this way, thermal conductivity reduced, The thermal conductivity is lower in Pb<sub>1-X</sub>Sn<sub>X</sub>Te compounds than in PbTeXSe<sub>1-X</sub> compound. [ 26]

### I-9-2-3. Silicon and Germanium:

Silicon-based alloys and germanium have good thermoelectric properties at high temperatures (above 1000 K) and are designed for space electricity generation applications.

### I-9-3. Physical properties of some thermoelectric materials:

For example, a table summarises the thermal and electrical properties of certain elements belonging to different families of thermoelectric materials.

**Table (I-4):** thermal and electrical properties of certain elements.

compounds	T(K)	$k$ (W/m.K)	$\sigma$ ( $\Omega^{-1} \cdot \text{m}^{-1}$ )	$S(\mu\text{VK}^{-1})$	ZT
<b><i>Bi<sub>2</sub>Ti<sub>3</sub></i></b>	$\sim 298^{\text{a}}$	$\sim 1.4^{\text{a}}$	$\sim 2500^{\text{a}}$	$\sim -240^{\text{a}}$	$\sim 0.6^{\text{a}}$
<b><i>Pb<sub>0.5</sub>Sn<sub>0.5</sub>Te</i></b>	$\sim 550^{\text{b}}$	$\sim 1.15^{\text{b}}$	$\sim 360^{\text{b}}$	$\sim 170^{\text{b}}$	$\sim 0.5^{\text{b}}$
<b><i>Si<sub>0.8</sub>Ge<sub>0.2</sub></i></b>	$\sim 1150^{\text{c}}$	$\sim 3.6^{\text{c}}$	$\sim 588^{\text{c}}$	$\sim 235^{\text{c}}$	$\sim 1.03^{\text{c}}$
<b><i>Yb<sub>14</sub>MnSb<sub>11</sub></i></b>	$\sim 1200^{\text{d}}$	$\sim 0.7^{\text{d}}$	$\sim 185^{\text{d}}$	$\sim 185^{\text{d}}$	$\sim 1^{\text{d}}$
<b><i>Mg<sub>2</sub>Si</i></b>	$\sim 823^{\text{e}}$	$\sim$	$\sim 833^{\text{e}}$	$\sim 200^{\text{e}}$	$\sim 1^{\text{e}}$

Ref <sup>a</sup> [27]. Ref <sup>b</sup> [28], Ref <sup>c</sup> [29], Ref <sup>d</sup> [30], Ref <sup>e</sup> [31].

**I-9-4. New thermoelectric materials:**

The most promising families with high luminescence properties are those of the BiCuSeO compound. The structure of these materials, previously studied for optical electronics applications, is the same as the superconductor structure of the LaFeAsO family. The BiCuSeO parent compound is a large gap semiconductor with a low holder concentration. With appropriate steroids, can be combined strong thermoelectric power with moderate electrical resistance. However, electrical properties remain much lower than those of the best thermoelectric materials. what makes these materials so interesting is thermal conductivity which is inherently very low, much less than most other thermoelectric materials. As a result, these compounds contain high-temperature thermoelectric worthiness factors, as shown in the following FIGURE (I-7). These values are currently among the highest ever, obtained in large p-type polycrystalline materials that contain neither lead nor tellurium, two elements we seek to avoid, in the (400-650 ° C) Temperature range.[32.33]

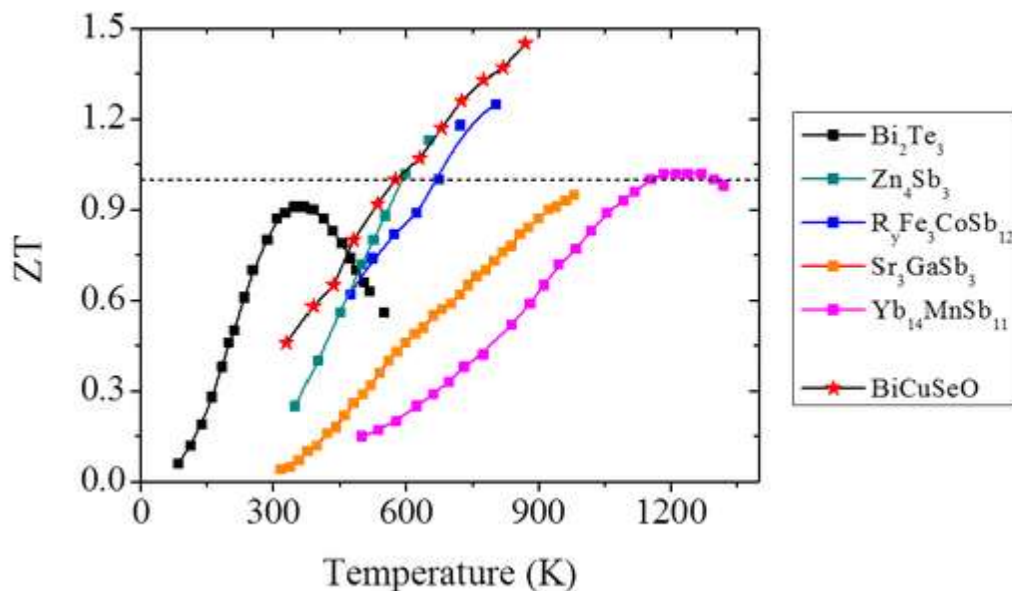


**FIGURE (I-7):** Evolution of merit factor for different compounds as temperature function.

Other families of materials whose properties have been a highlight in our group in recent years include:

Chalcogeners (I-V-VI) of parent compound AgBiSe<sub>2</sub>: Although I-V-VI has been studied for a

long time for thermoelectric applications, those based on AgBiSe<sub>2</sub> have only study very little. Unlike most other materials in this family are type p, AgBiSe<sub>2</sub> I-V-VI can be type p or n depending on the doping, the best properties being observed in type n materials. As in the case of BiCuSeO, these are materials with somewhat poor electrical properties compared to the best thermoelectric materials, but which are compensated by an inherently very low thermal conductivity, promising performance in the 450-550°C temperature range (Figure below, left). In addition, these materials are also interesting from the point of view of materials chemistry because they present structural transitions that can be modified by substitutions and that significantly influence the electrical and thermal transport properties (figure below, right) [ 34].

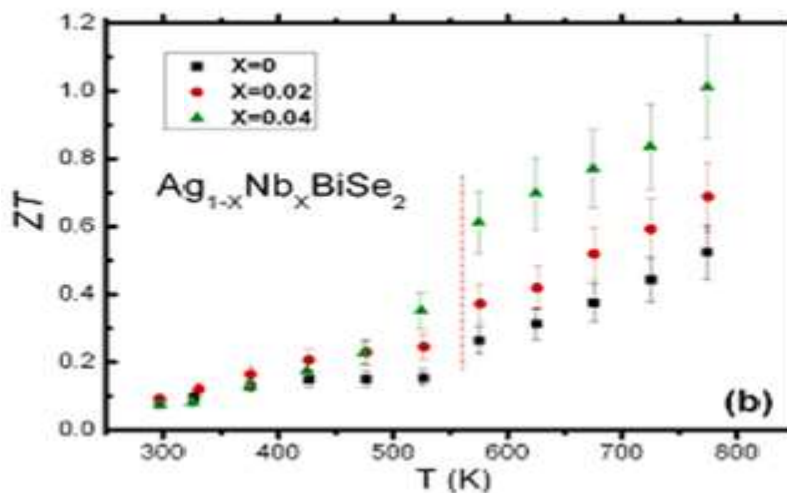


**FIGURE (I-8):** Evolution of the merit factor of the compound  $\text{Ag}_{x-1}\text{Nb}_x\text{BiSe}_2$  as a temperature function.

## I-10- Applications:

### I-9-1. For thermoelectric generators (direct conversion of heat to electricity):

The Seebeck effect can be fully exploited to turn heat into electric energy. In many sectors, in particular industrial or even local, thanks to thermoelectric generators, a large amount of heat (energy produced) is lost, for example: in automobiles. The efforts are increasing worldwide to enable the recovery of lost thermal energy [35]. About two-thirds of the energy generated during fuel combustion is released as heat in the car's hotspots, such as exhaust pipes, motor, etc. Heat generators can be competitive for use with heat sources. For example, can restore rejected thermal energy and provide electric power for battery recharge. This

will undo or even remove the generator. It is why the German manufacturer BMW aims to provide the exhaust line with a generator or set of thermoelectric generators capable of generating enough electricity when driving).



**FIGURE (I-9):**Vehicle Integration with Thermoelectric : FORD, GM and BMW Prototype integration pursued under DOE/industry sponsorship.

On the other hand, energy in high-flame temperature fuels, such as natural gas, is often used for heating with low  $\Delta T$  temperature differences (household heating, water heating, etc...). Thus, thermoelectric conversion can be exploited for rational use of primary energy, thus reducing the total energy produced. For domestic co-generation applications, the absence of vibrations and small dimensions (a few centimetres) prefer thermoelectric generators.

Low power generation (in watt order) finds its applications in the portable electronics sector (small computers, telephone, etc.) but also for the operation of miniature mechanical systems (micro-robots, exploration robots, aircraft, etc.). Megawatt generation is mainly for microelectronic components (detectors, transmitters, etc.).

Finally, thermoelectric generation found its first applications in space. Radio electric isotope

generators used radioisotopes as a heat source to power many electrical instruments in Galileo and Ulysses space probes.

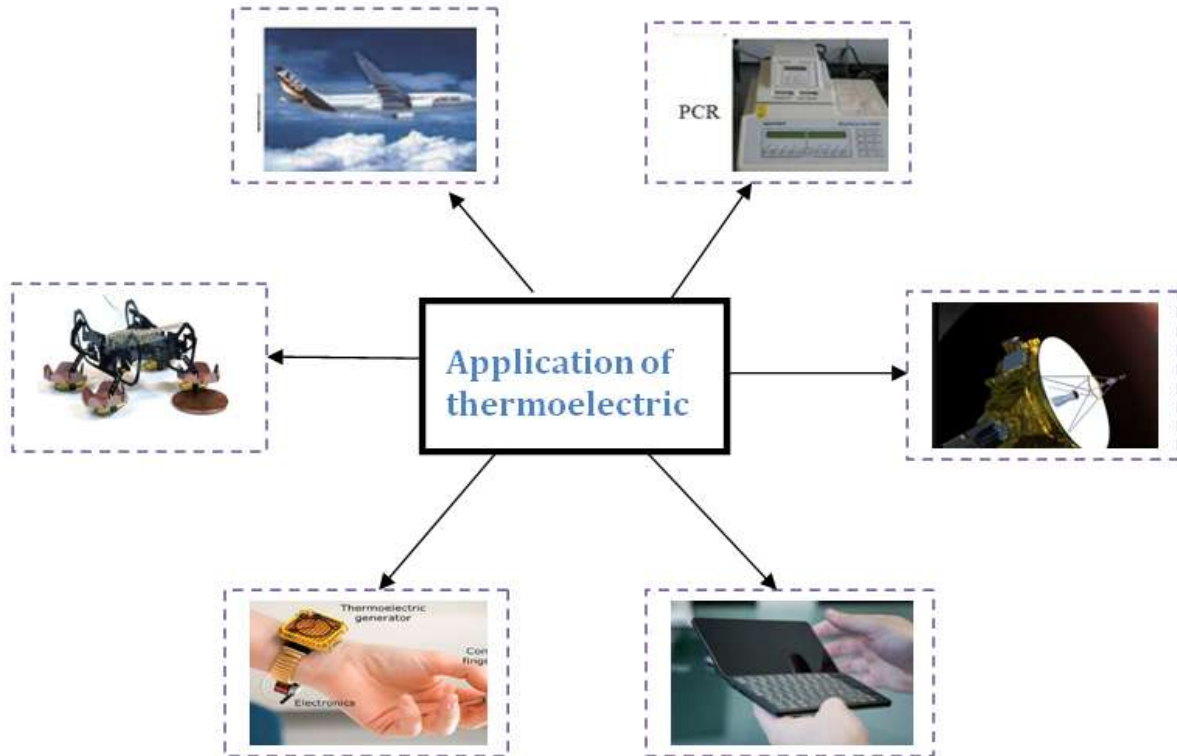


**FIGURE (I-10):**Some applications of thermoelectric generators.

**I-10-2. Thermoelectric cooling:**

Peltier's effective influence in thermoelectric cooling has benefited since 1960. using the semiconductors which he discovered. Among the most applications of thermoelectric cooling [ 36]:

-In the medical field: Optical electronic detectors are also used in portable devices, for example: in maintaining the cooling of packaging used to transport blood plasma, vaccination, and transmission (TE refrigerator), and some scientific and laboratory equipment such as magnetic resonance devices, microscopes...

In the military field, include field devices to adjust the temperature of infrared or laser detector cells and power transistors.

- Daily applications such as thermoelectric refrigerants.

- ICT sector: telecommunications.

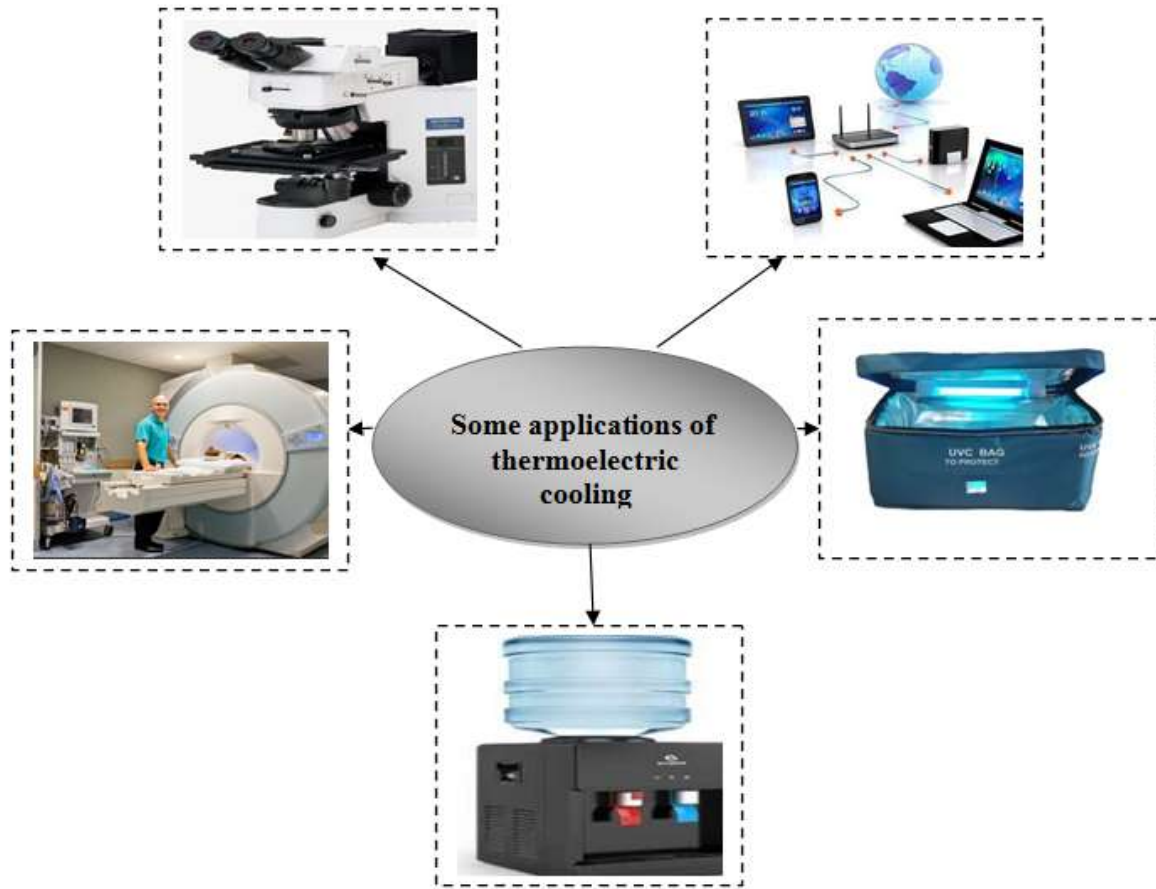


**FIGURE (I-11):** Some applications of thermoelectric cooling.

**I-9-3. Electronic Device Cooler:**

Microprocessors, power amplifiers, and computers used in servers work constantly and provide service to customers, electronic devices produce a large amount of heat within the system and therefore need refrigerants to avoid device failure and ensure their safety. The most prominent of these refrigerants are TE refrigerant which has several advantages over conventional cooling systems, such as being vibration-free because there is no moving part, compact size, running using a DC supply, less maintenance, etc. To cool the CPU, both Liu and al. provide a small thermal electric chiller (TEC) combined with a micro-thermoelectric siphon cooling system, FIGURE (I-12). Sun and al [37] improved and developed a TEC system integrated with a gravity auxiliary heat tube (GAHP) for electronic devices to enhance heat dissipation from the hot side of the TE unit and improve cooling capacity by 73.54 %, reducing electricity consumption by 42.20% to produce the same amount of electronic device

cooling.

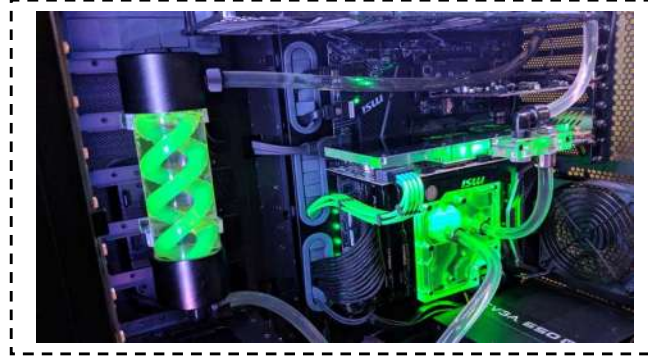


**FIGURE (I-12):** An image representing the computer's optimal cooling system (CP Cooler).

#### **I-9-4. Other Applications:**

Thermo-electrics many other applications, such as TE's various medical applications, such as electromagnetic imaging (EMG), wearable sensors for EEG, ECG, etc., are transplantable organs), the pacemaker, defibrillator, neurological stimulation, etc.) was reported [38]. A hybrid air chiller (thermal energy and evaporative cooling), is manufactured and experimentally found to lead to a 10 percent increase in hybrid air chiller from a simple evaporative air chiller [39]. Thermoelectric power can be used as a dehumidifier by connecting photovoltaic units in the matrix [40].

---

---

**Bibliographies**

- [1] Connelly N G; Damhus T; Hartshorn R M; Hutton A T, eds. (2005). Nomenclature of Inorganic Chemistry: IUPAC Recommendations 2005 (PDF). RSC Publishing. p. 51. ISBN 978-0-85404-438-2. Archived (PDF) from the original on 2009-03-04. Retrieved 2007-12-17.
- [2] Cotton, Simon A.). "Scandium, Yttrium & the Lanthanides: Inorganic & Coordination Chemistry". Encyclopedia of Inorganic Chemistry. (2006-03-15 doi:10.1002/0470862106.ia211. ISBN 978-0-470-86078-6.
- [3] M.Shoeib , G. Murtaza, M. Frooq, Roshan Ali, Computational. Materials Science.79 (2013) 239-246.
- [4] A. Saliha, Thèse de doctorat ;Université D'Oran, 24/02/2014.
- [5] A.I. Gusev, A. A. Rempel, A. J. Magerl, Disorder and Order in Strongly Nonstoichiometric Compounds, Transition Metal Carbides, Nitrides and Oxides, Springer (2001).
- [6] I. Shirovani, K. Yamanashi, J. Hayashi, N. Ishimatsu, O. Shimomura, T. Kikegawa, Solid State Commun. 127 (2003) 573.
- [7] S. Duman, S. Bağcı, H.M. Tutuncu, G. Uğur, G.P. Srivastava, Diam. Relat. Mater. 15 (2006) 1175.
- [8] D.G. Pettifor, Mater. Sci. Technol. 8 (1992) 345.
- [9] S.F. Pugh, Philos. Mag. 45 (1954) 823.
- [10] B. Amrani, F. El Haj Hassan, Comput. Mater. Sci. 39 (2007) 563.
- [11] C. Stampfl, W. Mannstadt, R. Asahi, A.J. Freeman, Phys. Rev. B 63 (2001) 155106.
- [12] A. Hao, X. Yang, X. Wang, R. Yu, X. Liu, W. Xin, R. Liu, Comput. Mater. Sci. 48(2010) 59.
- [13] F. Soyalp, S. Uğur, J. Phys. Chem. Solids 69 (2008) 791.
- [14] W.D.L. Cruz, J.A. Duaz, L. Mancera, N. Takeuchi, G. Soto, J. Phys. Chem. Solids 64 (2003) 2273.
- [15] J.S. Blakemore. Semiconducting and other major properties of gallium arsenide. J. Appl. Phys. 53 (10) .October (1982).
- [16] ] A. BECHRI, « effets de désordre et du substrat sur la structure électronique dans les

- alliages semi-conducteurs III-V », Thèse de Doctorat, Université de Constantine, 2006.
- [17] Wenhui Xue a, You Yu a, Yuna Zhao a, HuiLei Han b, Tao Gao a,\* . Computational Materials Science 45 (2009) 1025–1030.
- [18] M. LABIDI " Etude des propriétés structurales, électroniques des quaternaires" Thèse de Doctorat, UNIVERSITE BADJI MOKHTAR, (2011).
- [19] H. Mathieu, physique des semi-conducteurs et des composant électroniques, édition Dunod .Paris (2009).
- [20] Yujie Chen, Xiaozhou Liao, in Semiconductors and Semimetals, 2016
- [21] J. E. Bernard and A. Zunger, Phys. Rev. B36, 3199, (1987).
- [22] L. Vegard, Z.Phys. 5, 17 (1921).
- [23] Sun X., Cronin S.B., Liu J., Wang K.L., Koga T., Dresselhauss M.S., Chen G., Proceeding of the 18th International Conference on Thermoelectrics, Baltimore, USA, 652 (1999).
- [24] P.Bellanger « Etude de l'influence des paramètres nano et microstructuraux sur les propriétés thermoélectriques des siliciures de magnésium ( $Mg_2(Si,Sn)$  de type -n », Thèse de Doctorat, Université de Bordeaux, 2014.
- [25] H.Le-Quoc, « Matériaux thermoélectriques du type  $Mg_2Si-Mg_2Sn$  élaborés en couches minces par co-pulvérisation assistée par plasma », Thèse de Doctorat, Université de Grenoble,2006.
- [26] D.Boudemagh « Synthèse et Etude de Matériaux Thermoélectriques du Système  $Mg_2Si_{1-x}Sn_x$  », Thèse de Doctorat, Université de Grenoble, 2010.
- [27] Liu, W. et al. Studies on the  $Bi_2Tl_3-Bi_2S_3-Bi_2S_3$  system for mid-temperature thermoelectric energy conversion. Energy Environ. Sci. 6, 552–560 (2013).
- [28] LaLonde, A. D. & Moran, P. D. Synthesis and Characterization of p-Type  $Pb_{0.5}Sn_{0.5}Te$  Thermoelectric Power Generation Elements by Mechanical Alloying. Journal of Electronic Materials 39, 8–14. issn : 1543-186X (2010).
- [29] Fleurial, J. P. Design and Discovery of Highly Efficient Thermoelectric Materials. International Union of Materials Research Society, Florence, Italy (1998).
- [30] Fleurial, J. P. Design and Discovery of Highly Efficient Thermoelectric Materials. International Union of Materials Research Society, Florence, Italy (1998).
- [31] Aixala, L. RENOTER Project. 3rd Thermoelectric Applications Workshop Baltimore

- (2012).
- [32] L. D. Zhao, D. Berardan, Y. L. Pei, C. Bly, L. Pinsard-Gaudart, and N. Dragoe, *Applied Physics Letters* 97, 092118 (2010).
- [33] Jing Li, Jiehe Sui, Yanling Pei, Celine Barreteau, David Berardan. *Energy & Environmental Science* 5, 8543 (2012).
- [34] Lin Pan\*, David Bérardan\*, and Nita Dragoe. *Journal of the American Chemical Society* 135, 4914 (2013).
- [33] Sun X., Cronin S.B., Liu J., Wang K.L., Koga T., Dresselhaus M.S., Chen G., *Proceeding of the 18th International Conference on Thermoelectrics, Baltimore, USA*, 652 (1999).
- [36] Taylor, R.A.; Solbrekken, G.L. (2008). "Comprehensive system-level optimization of thermoelectric devices for electronic cooling applications". *IEEE Transactions on Components and Packaging Technologies*. 31: 23–31. doi:10.1109/TCAPT.2007.906333
- [37] Venkatasubramanian R., Siivola E., Colpitts T., O'Quinn B., *Nature*, 413, 597 (2001).
- [38] Terasaki I., Murayama N., *Research Signpost, Trivandrum, India* (2002).
- [39] Bobroff J., Hébert S., Lang G., Mendels P., Pelloquin D., Maignan A., *Phys. Rev. B*, 76,100407R (2007).
- [40] Rowe D.M., *Thermoelectrics Handbook, Macro to Nano*, CRC Press (2006).

**Part A:****Density functional theory (DFT)****II-A-1. Introduction:**

Today, DFT is one of the most commonly used methods for quantitative calculations of the electronic structure of solids, based on quantum mechanical laws that allow us to calculate and predict the different physical and chemical properties of atomic and molecular systems. These laws are grouped under the name First Principles for physics, hence the name ab initio, which is called the account based on these principles. In the case of a multi-object system, it is possible to solve Schrodinger's equation without introducing modified parameters by experiment. This chapter discusses the different approximations needed to solve Schrödinger's equation ( $\mathbf{H}\Psi = \mathbf{E}\Psi$ ). The approximate estimates used in the calculation of energy and the interconnectedness of the exchange are also provided [1]. The main objective of the functional density theory is to replace the multi-electron wave function with an electronic density as the core amount in the calculations [2].

**II-A-2 . Problem at N body with approximations:**

Hamilton writes for a system with N electrons moving under the influence of an external effort created by a set of M nuclei in the following :[3]

$$\mathbf{H} = T_e + T_n + U_{e-e} + U_{n-n} + U_{e-n} \quad (\text{II-1})$$

So that:

❖ **The total kinetic energy of electrons:**

$$T_e = \sum_{i=1}^{Ne} T_i = \sum_{i=1}^{Ne} \left( \frac{-\hbar^2 \nabla_i^2}{2m} \right) \quad (\text{II-2})$$

- With  $m$  the mass of the electron.

❖ **The total kinetic energy of the nuclei:**

$$T_n = \sum_{\alpha=1}^{N\alpha} T_\alpha = \sum_{\alpha=1}^{N\alpha} \left( \frac{-\hbar^2 \nabla_\alpha^2}{2M} \right) \quad (\text{II-3})$$

- With  $M$  the core mass.

❖ **The energy of interaction of electrons between them:**

$$U_{e-e} = \frac{1}{2} \sum_{i \neq j} \frac{e^2}{|r_i - r_j|} = \frac{1}{2} \sum_{i \neq j} U_{ij} \quad (\text{II-4})$$

- Where  $|r_i - r_j|$  is the distance between the two electrons  $i$  and  $j$ .

❖ **The energy of interaction between nuclei:**

$$U_{n-n} = \frac{1}{2} \sum_{\alpha \neq \beta} \frac{Z_{\alpha} Z_{\beta} e^2}{|R_{\alpha} - R_{\beta}|} = \frac{1}{2} \sum_{\alpha \neq \beta} U_{\alpha\beta} \quad (\text{II-5})$$

- Where :  $Z_{\alpha}$  and  $Z_{\beta}$  are the core load  $\alpha$  and  $\beta$ . and  $|R_{\alpha} - R_{\beta}|$  is the distance between the  $\alpha$  kernel and the  $\beta$  kernel.

❖ **Nucleus-electron interaction energy:**

$$U_{e-n} = - \sum_{i=1}^{N_e} \sum_{\alpha=1}^{N_{\alpha}} \frac{Z_{\alpha} e^2}{|r_i - R_{\alpha}|} = \sum_{i=1}^{N_e} \sum_{\alpha=1}^{N_{\alpha}} U_{i\alpha} \quad (\text{II-6})$$

- Where :  $|r_i - R_{\alpha}|$  is the distance between the nucleus  $\alpha$  and the electron  $i$ .

The Schrödinger equation can therefore be represented as:

$$(T_e + T_n + U_{e-e} + U_{n-n} + U_{e-n})\Psi = E \Psi \quad (\text{II-7})$$

For a system with M atoms and N electrons, the problem we are dealing with involves (N+M) particles in Colombian interaction. We cite as an example: a solid has  $25^{10}$  valence electrons that are mutually interacting and moving in the Colombian field, and  $24^{10}$  ion-core electrons are interacting with each other. In this form, the analytical resolution of the Schrödinger equation is too complex. Therefore, different approximations considered for the analytical resolution.

- The first level of approximation: is the Born-Oppenheimer approximation.
- The second level of approximation: Hartree Fock approximation or formalism of density functional theory.
- The third level approximation: The approximations inherent in solving equations.

### II-A-2-1. The Born-Oppenheimer approximation:

This approximation is based on the movement of nuclei from the movement of electrons because the nucleus's mass is much larger than an electron's. Therefore, the motion of nuclei can be neglected relative to electrons, and the nuclei are regarded as constant [ 4]. So the movement of electrons can be considered separate from the movement Hamiltonian becomes as follows:[ 5]

$$H = T_e + U_{e-e} + U_{e-n} \quad (\text{II-8})$$

The solution of the Schrödinger equation involving the electronic Hamiltonian:

$$H_e \Psi_e = E_e \Psi_e \quad (\text{II-9})$$

Because of the electron-electron interaction, the resolution of the Schrödinger equation remains complex to several bodies, so other additional approximations are used.

**II-A-2-2.Hartree approximation:**

In 1928, Hartrey [6] simplified the N-body problem into a single-particle problem. In this approximation, we consider electrons independent, with each electron moving alone in the medium field resulting from nuclei and other electrons. So, the problem travels from the larger number of electrons to one electron. Hamiltonians can write as a total of Hamiltonians describing a single electron:[ 7]

$$H_i\phi_i(\vec{r}) = \epsilon_i\phi_i(\vec{r}) \tag{II-10}$$

The equation from Schrödinger to N electrons comes down to N equations from Schrödinger to an electron:

$$\left(-\frac{\hbar^2}{2m}\Delta_i + \mathbf{Vext}(\vec{r}) + V_H(\vec{r})\right)\phi_i(\vec{r}) = \epsilon_i\phi_i(\vec{r}) \tag{II-11}$$

with:

$\phi_i(\vec{r})$ : mono-electronic wave functions

$\mathbf{Vext}(\vec{r})$  : explains the attractive coulombian interaction between electron and nuclei.

$V_H(\vec{r})$  : represents Hartree's potential.

**II-A-2-3.Hartree-Fock approximation:**

Fock [8] showed in 1930 that Hartrey Hamleton's [9] solutions violated the principle of Pauley's exclusion because they were not asymmetric compared to the exchange of two electrons. The anti-electronic wave function symmetries are written by switching two electrons, for example:

$$\phi(\vec{r}) (\vec{r}_1, \vec{r}_2, \dots, \vec{r}_j, \dots, \vec{r}_{Ne}) = -\phi(\vec{r}) (\vec{r}_1, \vec{r}_2, \dots, \vec{r}_j, \dots, \vec{r}_{Ne}) \tag{II-12}$$

To account for the asymmetry principle requiring the wave function to change the signal during the switch of two electrons, Hartrey and Fock circulated this concept by showing that the Pauli principle is respected if the wave function writes as a "slater determinant" [10].

$$\phi_i(\vec{r}) (\vec{r}_1\vec{\sigma}_1, \dots, \vec{r}_{Ne}\vec{\sigma}_{Ne}) = \frac{1}{N!} \begin{vmatrix} \varphi_1(\vec{r}_1\vec{\sigma}_1) & \varphi_1(\vec{r}_2\vec{\sigma}_2) & \dots & \varphi_1(\vec{r}_{Ne}\vec{\sigma}_{Ne}) \\ \varphi_2(\vec{r}_1\vec{\sigma}_1) & \varphi_2(\vec{r}_2\vec{\sigma}_2) & \dots & \varphi_2(\vec{r}_{Ne}\vec{\sigma}_{Ne}) \\ \dots & \dots & \dots & \dots \\ \varphi_{Ne}(\vec{r}_1\vec{\sigma}_1) & \varphi_{Ne}(\vec{r}_2\vec{\sigma}_2) & \dots & \varphi_{Ne}(\vec{r}_{Ne}\vec{\sigma}_{Ne}) \end{vmatrix} \tag{II-13}$$

- Where :  $\sigma$  represents the spin.

$\frac{1}{N!}$  : the normalization constant.

The function given by equation (III-12) leads to the Hartree-Fock equations For a single-

particle system:

$$\left( -\frac{\hbar^2}{2m} \Delta_i + V_{ext}(\vec{r}) + \sum_{\substack{j=1 \\ j \neq i}}^{N_e} \int \frac{|\phi_j(\vec{r}')|^2}{|\vec{r}-\vec{r}'|} d^3\vec{r}' \sum_{\substack{j=1 \\ j \neq i}}^{N_e} \delta_{\sigma_i \sigma_j} \int \frac{|\phi_j^*(\vec{r}') \cdot \phi_i(\vec{r}')|^2}{|\vec{r}-\vec{r}'|} d^3\vec{r}' \right) \phi_i(\vec{r}) = \epsilon_i \phi_i(\vec{r}) \quad (\text{II-14})$$

These Hartree-Fock equations are difficult to solve when the studied system has a large number of electrons.

Electron-electron interactions produce additional energy terms in addition to those of the Hartree approximation, called Wigner correlation energy terms [11].

Slater [11] approximates the exchange term assuming it has a local character, unlike the AHF, This potential for exchange written in the form [12]:

$$\hat{V}_x(\vec{r}) = -6\alpha \left( \frac{3\rho(\vec{r})}{4\pi} \right) \quad (\text{II-15})$$

Where:

$\alpha$ : is a dimensionless parameter, and  $\rho(r)$  the charge density.

In its calculations, Slater lays ( $\alpha = 1$ ) corresponds to a homogeneous gas without interaction. This Slater method raises two essential points: firstly, the simplicity of this potential about the AHF (because it is local); secondly, it gives a simple form of the term exchange-correlation. However, the choice of this practically intuitive potential leads to not always satisfactory results.

One can only hope for the upper bound of the ground state energy. However, it does show that we are gradually approaching the ground state by writing  $\phi$  as a sum of Slater's determinants. This makes the computation very cumbersome in numerical terms, which is why the density functional method is used because it simplifies the computations in a surprisingly large way.

#### II-A-4. Functional Density Theory (DFT):

To solve the Schrödinger equation with electrons. Approximate methods must be used accurately reproduce the physical quantities that contain the most information. A more modern and perhaps the best method is the functional density theory (DFT). Functional density theory (DFT) describes the system by considering  $\rho$  density ( $r$ ) as a basic quantity. It bases on two essential theories developed by Hohenberg and Kuhn in 1964 [13].

The total power of the core case E is a unique function of particle density for external potential given.

**Proof 2:** The total energy functional for any multi-particle system has a minimum corresponding to the ground state and the ground state particle density:

$$E = \min.$$

The consequences of these two fundamental DFT theorems are that variation in external potential implies variation in density. The energy equation for unary electronic functions describes by the following expression:

$$E(\rho) = F_{HK}[\rho] + \int \rho(r) V_{ext}(r) dr \quad (\text{II-16})$$

The functional  $F_{HK}$  is universal for any system with several electrons. If the function F is known, then it is relatively easy to use the principle of variation to determine the total energy and electron density of a ground state for a given external potential. Unfortunately, the theorem of Hohenberg and Kohn does not indicate the form of  $F_{HK}$ .

**II-A-4-1. Approximation of Kohn and Sham:**

Kohn and Sham (KS) [12] wrote the exact energy of the fundamental state of an interacting system in a ( $v_{ext}$ ) external potential in the form of a function dependent only on the electron density [ $\rho(\vec{r})$ ] in the form:

$$E[\rho(\vec{r})] = F[\rho(\vec{r})] + V_{ext}[\rho(\vec{r})] \quad (\text{II-17})$$

with:

$$F[\rho(\vec{r})] = T_0[\rho(\vec{r})] + V_H[\rho(\vec{r})] + E_{XC}[\rho(\vec{r})] \quad (\text{II-18})$$

So:

$$E[\rho(\vec{r})] = T_0[\rho(\vec{r})] + V_H[\rho(\vec{r})] + E_{XC}[\rho(\vec{r})] + V_{ext}[\rho(\vec{r})] \quad (\text{II-19})$$

with:

$T_0[\rho(\vec{r})]$  : is the kinetic energy of a density electron gas without interaction.

$V_H[\rho(\vec{r})]$ : represents the classical coulomb interaction between electrons (the term Hartree).

$E_{XC}[\rho(\vec{r})]$  : is the energy of exchange and correlation, is an additional function, and describes inter-electronic interaction.

$V_{ext}[\rho(\vec{r})]$  Colombian interactions of electrons with nuclei and those of nuclei between them:  $V_{ext}[\rho(\vec{r})] = \int \rho(r) V_{ext}(r) dr$

Schrödinger's equation in Kohn and Sham's approach is of form:

$$\left(-\frac{\hbar^2}{2m}\nabla^2 + V_{eff}(\mathbf{r})\right) \varphi_i(\vec{r}) = \varepsilon_i \varphi_i(\vec{r}) \quad (\text{II-20})$$

With:

$$V_{eff}(\mathbf{r}) = V_H(\mathbf{r}) + V_{ext}(\mathbf{r}) + V_{xc}(\mathbf{r}) \quad (\text{II-21})$$

where  $V_{xc}(\mathbf{r})$  is the exchange-correlation potential:

$$V_{xc}(\mathbf{r}) = \frac{\delta E_{xc}[\rho(\vec{r})]}{\delta \rho(\vec{r})} \quad (\text{II-22})$$

And the density is given by a sum over all occupied orbitals [14]:  $\rho(\vec{r}) = \sum_{j=1}^{N_e} |\phi_j(\vec{r})|^2$

In the wording of **Kohn** and **Sham**, all energy terms and associated potential can be evaluated, except for the problem of interchange association.

Therefore, the solution of the imaginary equations is impossible because the potential  $V_{xc}(\mathbf{r})$  has no clear form. In all cases, the calculation of energy and exchange potential depends on several approximations, which we will discuss later.

#### II-A-4-2. Functional exchange and correlation .

##### a - Local Density Approximation (LDA):

The rounding of local density (LDA) depends on the assumption that the terms of the district link consist solely of the local value of  $\rho(r)$ . The electronic density is treated locally as a standardized electronic gas [15].

In this approximation, each micro dimension of the system contributes to an energy exchange correlation equal to that due to the contribution of a homogeneous gas that occupies the same micro distance and has the same total load density as the original material of this size. The calculation of the cohesion energy of the solids and network parameters minimizes by LDA but can become important when sharing Vander Waals-type links [16]. Exchange functional bonding assumes that the total energy exchange bonding fraction of the ground state of the system under this approach is written in the form:

$$E_{xc}^{LDA}[\rho(\vec{r})] = \int \rho(\vec{r}) \varepsilon_{xc}^{LDA}[\rho(\vec{r})] d^3\vec{r} \quad (\text{II-23})$$

In which  $\varepsilon_{xc}^{LDA}[\rho(\vec{r})]$  represents the electron exchange and correlation energy in an electron gas whose distribution is assumed to be uniform.

The function of exchange and correlation has two terms:

$$\epsilon_{xc}^{LDA} [\rho (\vec{r})] = \epsilon_x^{LDA} [\rho (\vec{r})] + \epsilon_c^{LDA} [\rho (\vec{r})] \quad (\text{II-24})$$

with:

$\epsilon_x^{LDA} [\rho (\vec{r})]$  : is the exchange function.

$\epsilon_c^{LDA} [\rho (\vec{r})]$  : is the correlation function.

Dirac's exchange function is given by [17]:

$$\epsilon_c^{LDA} [\rho (\vec{r})] = -\frac{3}{3} \left( \frac{3}{\pi} \rho(\vec{r}) \right)^{1/3} \quad (\text{II-25})$$

From  $\epsilon_{xc}^{LDA} [\rho (\vec{r})]$ , the exchange-correlation potential  $V_{xc}^{LDA}(\vec{r})$  can be obtained in a variational way according to equation [18]:

$$V_{xc}^{LDA}(\vec{r}) = \frac{\delta(\rho(\vec{r})\epsilon_{xc}^{LDA}[\rho(\vec{r})])}{\delta\rho(\vec{r})} \quad (\text{II-26})$$

### b - Generalized Gradient Approximation (GGA):

Generalized Gradual Approximation (GGA) is an improvement of LDA convergence (because the latter provided discrepancies with experimental results in some cases). It consists of making  $E_{xc}^{LDA}$  functional based on the electronic density of its graduation [19]. This modification in functional  $E_{xc}^{LDA}$  reflects the non-uniform nature of electron gas. So we write the interchange-correlation energy in the form:

$$E_{xc}^{GGA} [\rho(\vec{r})] = \int \rho(\vec{r}) \epsilon_{xc}[\rho(\vec{r}), |\nabla\rho(\vec{r})|] d^3\vec{r} \quad (\text{II-27})$$

Or :  $\epsilon_{xc}[\rho(\vec{r})]$  represents the exchange-correlation energy per electron in a electron system in mutual interaction of non-uniform density.

## II-A-5- Pseudo potential method and plane waves:

### II-A-5-1. Introduction:

The accuracy of Kohn-Sham equations under DFT requires selection. Of their applications used to describe the capabilities and orbits of Kohn-Sham [20, 21]. The bases of wavelengths are called the first principle methods, including three ways to solve the Schrodinger equation based on the DFT theory:

- Linearized augmented-plane-wave method (LAPW ).
- Plan waves (PW ).

In this chapter, we are interested in describing the two approaches implemented in the CASTEP calculation code, citing the wave function level waves. It is called the Pseudo potential voltage method [22]. This method is the specific point technology in the mutual

space of the wave function. The electrons that obey the Schrodinger equation are called Bloch electrons.

**II-A-5-2. Bloch's Theorem and Plane Waves:**

**II-A-5-2-2. A sampling of the Brillouin zone:**

The number of waveguides allowed in the first Brillouin zone represents the number of sites in the crystal. In the study of solids, it is necessary to calculate the average single periodic function of  $k$  (wave vector) in the Brillouin region (ZB). These calculations are often long and complex because they require the principle of knowing the function values at any point of ZB and due to the infinite number of electrons, there are countless  $k$  points in this area. In practice, knowing the job values for a reduced set of  $k$  points in ZB is enough to get the average value of these functions via ZB. For high accuracy of calculations, it is generally necessary to know the values of the functions of a sufficiently large set of points [23].

**II- A-5-2-3. Flat waves:**

The plane wave base is suitable for periodic and independent systems of atomic positions. This base uses in the determination of the electronic structure to improve the convergence of calculations by increasing their dimensions. When systems have one or more infinite dimensions, the number of electrons in the system is also unlimited, and solving the problem is difficult numerically. Therefore, we return to the periodic systems where ions arrange regularly. The crystalline potential acting on the electrons has the frequency of the network:

$$U_{\vec{k}}(\vec{r}) = U_{\vec{k}}(\vec{r} + \vec{R}) \tag{II-28}$$

The effective potential of Kohn-Sham and the electronic density are thus periodic and have a vector of translation  $R$ :

$$U_{eff}(\vec{r}) = U_{eff}(\vec{r} + \vec{R}) \tag{II-29}$$

$$\rho(\vec{r}) = \rho(\vec{r} + \vec{R}) \tag{II-30}$$

**II- A-5-2-3. Cut-off energy:**

Representing a wave function requires the use of a large number of plane waves.

$C_{K+G}$  coefficients of plane waves with low kinetic energy  $\left(\frac{\hbar^2}{2m}\right) |K + G|^2$  are more important than those associated with plane waves with high kinetic energy. We will limit ourselves to plane waves whose kinetic energy is less than a confirmed value called cut-off energy  $E_{cut}$  :

$$\left(\frac{\hbar^2}{2m}\right) |\mathbf{K} + \mathbf{G}|^2 \leq E_{cut} \quad (\text{II-31})$$

The selection of plane waves consists of a sphere of  $G_{max}$  radius centered at the origin of the reciprocal space by imposing the  $|\mathbf{K} + \mathbf{G}| \leq G_{max}$  condition. The number of plane waves contained in this sphere is given by the following expression:

$$N_{pw} = N_K \frac{1}{2\pi^2} \alpha E_{cut}^{3/2} \quad (\text{II-32})$$

$N_K$  and  $\alpha$  are respectively the number of vectors  $\mathbf{k}$   $\mathbf{r}$  sampled in the first Brillouin zone and the volume of the simulation cell. The limitation of the plane wave base induces errors in the calculation of the total energy. A suitable choice of  $E_{cut}$  can lead to a good convergence of the total energy, and it determines the degree of accuracy of the calculation of the different properties [24].

#### II-A-5-2-4. Bloch theorem :

The material contains a very large number of atoms and electrons, so we find ourselves in a problem impossible to solve because of the too large number of degrees of freedom. But for a crystalline structure, the periodicity leads to important simplification. Indeed, for a periodic potential, the Bloch theorem [25] makes it possible to write the electron wave function as a product of a plane wave  $e^{i(\vec{k}\vec{r})}$  and a function  $U_{\vec{k}}(\vec{r})$  having the periodicity of the Bravais network, that is to say. We can write:

$$\Psi_{\vec{k}}(\vec{r}) = u_{\vec{k}}(\vec{r}) e^{i(\vec{k}\vec{r})} \quad (\text{II-33})$$

With:

$$U_{\vec{k}}(\vec{r}) = U_{\vec{k}}(\vec{r} + \vec{R}) \quad (\text{II-34})$$

With  $\vec{k}$  crystal reciprocal network vector and  $U_{\vec{k}}(\vec{r})$  is a periodic function, of the same crystal periodicity.

The Bloch theorem shows us that, from one cell of the direct network to another, the wave function is the same as the phase factor of the reciprocal network. In addition to  $\vec{k}$ , the functions  $u_{\vec{k}}(\vec{r})$  and  $u_{\vec{k}}(\vec{r} + \vec{R})$  are equivalent. The Bloch theorem thus allows us to limit the study of wave functions to the crystal unit cell, that is to say to a finite part of the reciprocal network.

### II-A-6. Approach to pseudo potential:

#### II-A-6- 1. Frozen core approximation :

As in the case of chemistry and atomic and molecular physics, the physical properties are

mainly due to the valence electrons: that is, electrons that operate the outer layers of atoms in the Burr planetary model. The deepest electrons in the heart are slightly affected, do not contribute practically to chemical bonds, and are therefore equivalent to those in isolated corn. This phenomenon is almost called a frozen heart [26]. But this does not mean that these electrons are not important in the atomic and molecular physics of the solids. They identify the cases and energies of those called parity. These cardiac electrons intervene in the Hamiltonian to describe the number of electronic components of atoms, molecules, and solids. [27, 24].

**II-A-6-2. Pseudo-potential method:**

The faulty voltage method [28] is an approximate process that develops level wave functions on the lower waves. The aim is to replace the Colombian reaction voltage of the nucleus and the effects of cardiac electrons strongly associated with effective potentials that only interact with equivalent electrons. We, therefore, seek to replace the voltage of the electron nucleus with less potential, which translates to the crushing of the nucleus by base electrons, and this greatly reduces the size of the calculations performed, especially in systems with heavy atoms, where calculations on all electrons become costly in time or machines. The idea presented by Fermi in 1934 [29, 30] consists of rationalizing calculations of electronic structure by eliminating the cardiac conditions that cause strong oscillations. Using the pseudo-potential approach allows us to circumvent this problem by reducing the level of the required wavelength base in the calculations, as it explicitly concerns only the electrons of equivalence. In practice, pseudo-potentials are constructed in a way that exceeds the radius of a particular section by determining the ball in which the nucleus electrons are present, the false potential, and the functions of the pseudo-wave. The parity must correspond to the true potential and wave directions of the imposed true parity outside the range  $r$  (see Figure (II-1)).

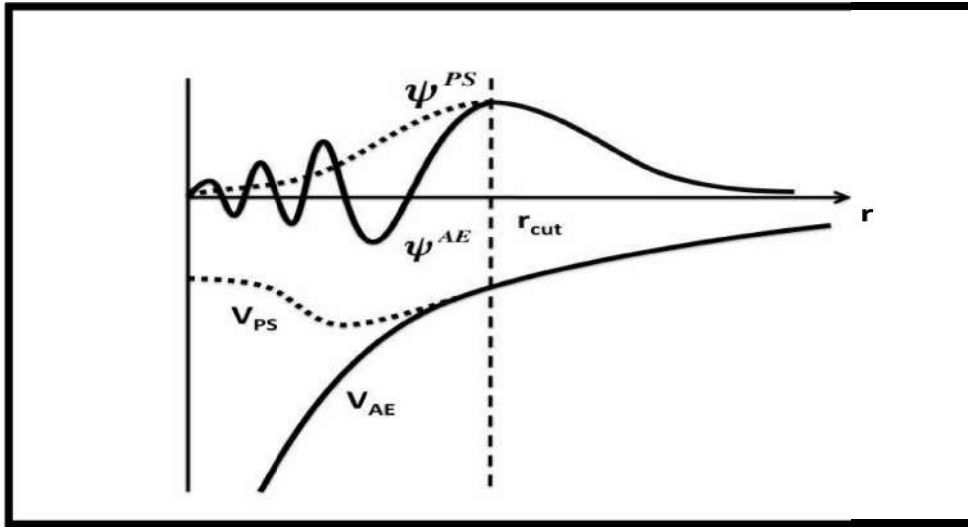


FIGURE (II-1): Representation of pseudo potential and pseudo function of wave [32]

### II-A-7. The code of CASTEP:

The codes of calculation in all fields and especially the state of matter, liquid-solid or gas have been put into operation for the last two or three decades. It has become more and more sophisticated to describe more precisely the interaction of the phases. These codes use ab initio methods or the first principle, using atomic constants to solve the Schrödinger equation. The DFT (functional density theory) implanted in these codes imposes the best method for the quantum calculation of the electronic structure of matter.

The use of computer simulation techniques is increasingly important in understanding the physical properties of materials. The calculations are made from the first principles with plane waves (Plane Wave Pseudo Potential: PWPP). The method is implemented in the simulation program CASTEP (Cambridge Serial Total Energy Package) [33].

This software was developed by Professor M.C.Payne [34] and marketed by Accelerys. CASTEP, developed in the Condensed Matter Theory group at the University of Cambridge, UK, is a program that uses functional density theory (DFT) to simulate the properties of solids and can predict the properties, including elastic constants, structural properties, band structures, state density, load densities, and optical properties. This code is used to simulate the total energy by using the special integration of the K points in the first Brillouin zone with a plane wave base for the expansion of wave functions and the summation in this zone is carried out on the wave vectors produced by the Monkhorst method and Pack

[35]. CASTEP runs on Windows and Unix. The user interface is compliant with Microsoft standards, allowing us to interact with 3D graphical models and analyze calculations through simple dialog boxes that will seem familiar to any Windows user.

CASTEP is software that provides some of the world's most advanced materials simulation and modeling technologies. It leverages the power of your Microsoft Windows and Linux servers to perform advanced calculations and deliver results directly to your computer. This software combines quantum mechanics, molecular mechanics, modeling, and simulation as analytical instruments and statistical correlations in an easy-to-use modeling environment. It makes it simple to communicate ideas related to the structure of materials and properties and to solve critical problems in the chemical and materials industries. With us, we can create better materials by their design. CASTEP can be used effectively to study the properties of point defects (gaps, interstitials, and surrogate impurities) and extended defects (for grain joints, for example, and dislocations) in semiconductors and other materials [36].

---

## Bibliographies

- [1] D. R. Hartree, Proc. Cambridge Phil. Soc. 89, 111, 42624 (1928).
- [2] P.A.M Schrödinger, Rev. 28.1049,(1926).
- [3] Guilherme Vilhena,École doctorale de Physique et d'Astrophysique (PHAST),Université de Lyon' A thesis submitted for the degree of Doctor of Philosophy'19/ September / 2011
- [4] ] S. Cottenier, Density Functional Theory and the family of (L)APW-methods: a step-by step introduction (Instituut voor Kern-en Stralingsfysica, K. U. Leuven, Belgium), 2002, ISBN 90-807215-1-4.
- [5] M. Born, J.R. Oppenhiemer, Zur Quanten theorie der Molekel, Annalen der Physik, 87 (1927) 457-484.
- [6] D. R. Hartree, Proc. Combridge Philos. Soc. 24, 89 (1928).
- [7] J. P. Perdew and Y. Wang, Phys. Rev. B. **33**, 8800 (1986).
- [8] W. Thomson, Proc. Roy. Soc. Edinburgh, 91, (1851).
- [9] A. F. Ioffe, Semiconductor Thermoelements and Thermoelectric Cooling, Infosearch, London, (1957).
- [10] D. M. Ceperlry and B. J. Alder, Phys. Rev. Lett. **45**, 566 (1980).
- [11] D. M. Rowe, CRC Handbook of Thermoelectrics, CRC Press, Boca Raton, FL, (1995).
- [12] E. Altenkirch, Phis. Z., 10, (1909) 560.
- [13] P. Hohenberg, W. Kohn, Inhomogeneous electron gas, Physical Review B 136 (1964) 864-870.
- [14] Peter Y.YU,Manuel Cardona. Fundamentals of semiconductors Physics and materials properties. Springer (2001).
- [15] C.Nassima, thèse de doctorat; Université Badji Mokhtari Anaba, 2014.
- [16] C.Tayeb, Thèse de doctorat; Université Ferhat Abbas -Sétif UFAS (ALGERIE).
- [17] P. A. M. Dirac, "Note on exchange phenomena in the Thomas -Fermi atom" Proc. Cambridge Phil. Roy. Soc. 26, 376 (1930).
- [18] A.ROUABHIA, Thèse de Magister " Étude ab initio des propriétés structurales et Magnétiques des antipérovskites Fe<sub>3</sub>MC (M= Zn,Al,Ga,et Sn)". Université des Sciences et de la Technologie d'Oran- Mohamed Boudiaf, (2010).
- [19] J. P. Perdew and A. Zunger, Phys. Rev. B 23, 5048 (1981).
- [20] E. Betranhandy, Thèse de doctorat, Université de Bordeaux (France), 2005.

- [21] C. Frayret, Thèse de doctorat, Université de Bordeaux (France), 2004.
- [22] M. C. Payne, M. C. Teter, M. P. Allan, D. C. Arias, T. A. Joannopoulos, J. D. "Iterative Minimization Techniques for Ab Initio Total Energy Calculations: Molecular Dynamics and Conjugate Gradients", *Rev. Mod. Phys.*, **64**, 1045-1097 (1992).
- [23] D. Khadidja, Thèse de doctorat; Université Farhat Abbas-sétif, 1503/2013.
- [24] M. A. Ghebouli, Thèse de doctorat; Université Bordj Bou Arréridj (2015).
- [25] V. G Dmitriev., G. G, Gurzadyhan., and D. N, Nikogosyan. [Handbook of Nonlinear Optical crystal] Springer, New York, (1999).
- [26] V. Barth, C.D. Gelatt, "Validity of the frozen-core approximation and pseudopotential theory for cohesive energy calculations", *Phys. Rev. B* 21, (1980) 2222.
- [27] N. Lebga, Thèse de Doctorat, Université Ferhat Abbas-Sétif (2011).
- [28] C. Escure, Thèse de doctorat, Université Toulouse III, 2010.
- [29] A. Bedjaoui, Thèse de doctorat, Université Sétif, 2011.
- [30] E. Fermi, *Il Nuovo Cimento* 11, 157, 1934.
- [31] K. Haddadi, Thèse de doctorat, université Sétif, 2013.
- [32] ] M C Payne, M P Teter, D C Allan, TA Arias, and ad JD Joannopoulos, (1992), Iterative minimization techniques for ab initio total-energy calculations : molecular dynamics and conjugate gradients, *Reviews of modern physics*, 64(4) : 1045.
- [33] D. Vanderbilt, *Phys. Rev. B.* 41 (1990) 7892.
- [34] M. C . payen, M. P. Teler, D. C. Allan, T. A. Arias, J. D. Joannopoulos, "Iterative Minimization Techniques for Ab-Initio Total Energy Calculations: Molecular Dynamics and Conjugate Gradients", *Rev. Mod. Phys.*, 64, 1045-1097 (1992).
- [35] H. J. Monkhorst, J. D. Pack, "Special points for Brillouin-zone integrations" *phys. Rev. B* 16, 1748-1749 (1977).
- [36] First principles methods using CASTEP, *Zeitschrift fuer Kristallographie*, S. J. Clark, M. D. Segall, C. J. Pickard, P. J. Hasnip, M. J. Probert, K. Refson, M. C. Payne, 220(5-6) pp. 567-570 (2005).

**Part B:** *Elastic ,optical , phonon and thermoelectric properties  
with DFT*

**II-B-1. Elastic properties:**

The elastic properties of materials provide important information because they relate to various fundamental solid-state properties such as understanding the mechanisms of bonds between atoms, equation of state (EOS), the structural stability, and the stiffness of materials (bulk modulus, shear modulus, Young's modulus, and Poisson's ratio), the anisotropic character of the bonding, and Debye temperature, melting point, and many others. These properties can be studied, by calculating the elastic constants and also provide important information about the response of materials to external forces.

In the following, we will prepare a theoretical method for calculating the elastic constants from the total energy of the crystal.

**II-B-1-1. Tensors of the elastic constants:**

Solid bodies deform under the action of external forces. In order to describe the evolution of this substance, it is necessary to define a set of parameters that make it possible to know. The stress  $\sigma$  and the strain  $\epsilon$  allow us to characterize the evolution of the material. The simplest behavior model associated with stress is the linear elastic model, limited to small deformations for its applicability to the material. The elastic behavior was characterized by a linear relationship between stresses  $\sigma$  and strains  $\epsilon$  (Hooke's law). The strain tensor of a crystal can be related to the stress tensor by the following law:

$$\sigma_{ij} = \sum_{k,l} C_{ijkl} \epsilon_{kl} \text{ or } \epsilon_{ij} = \sum_{k,l} S_{ijkl} \sigma_{kl} \quad (\text{II-35})$$

with:

$C_{ijkl}$  : are called moduli of elasticity and have the dimensions of a [force]/[area] or of an [energy]/[volume]. They have inverse dimensions.

$S_{ijkl}$  : the quantities S coefficients of deformability or constants of elasticity.

the stresses [ $\sigma$ ] and the deformations undergone by the crystal [ $\epsilon$ ] are represented by the following tensors:

$$\sigma = \begin{bmatrix} \sigma_{11} & \sigma_{12} & \sigma_{13} \\ \sigma_{12} & \sigma_{22} & \sigma_{23} \\ \sigma_{13} & \sigma_{23} & \sigma_{33} \end{bmatrix}, \quad \epsilon = \begin{bmatrix} \epsilon_{11} & \epsilon_{12} & \epsilon_{13} \\ \epsilon_{12} & \epsilon_{22} & \epsilon_{23} \\ \epsilon_{13} & \epsilon_{23} & \epsilon_{33} \end{bmatrix} \quad (\text{II-36})$$

$C_{ijkl}$  is a tensor of order 4, called elastic stiffness tensor, and defines the elastic constants of the material. The number of possible combinations of four  $ijkl$  indices is  $3^4 = 81$  elements. In the most general case and because of symmetry of  $\sigma_{ij}$ ,  $\epsilon_{kl}$  and by applying Maxwell's relation  $C_{ijkl} = C_{klij}$  [1], the elements  $C_{ijkl}$  are reduced to 21 elements independent. Furthermore, the symmetry of the crystalline solid significantly reduces this number.

The constants are therefore denoted by a new notation (Voigt notation), namely  $C_{IJkl}$  [2], such that the indices  $ij$  or  $kl$  are abbreviated by replacing each pair of initially quadrupled indices with a single index I or J. Thus, the abbreviations will be as follows:

11  $\rightarrow$  1, 22  $\rightarrow$  2, 33  $\rightarrow$  3, 32 ou 23  $\rightarrow$  4, 31 ou 13  $\rightarrow$  5, 21 ou 12  $\rightarrow$  6

Hooke's law is then expressed [3]:

$$\sigma_I = \sum_{I,J=1}^6 C_{IJ} \epsilon_J \quad (\text{II-37})$$

With: I,J = 1,2,...6

The generalized Hooke's law can be written in matrix form:

$$\begin{pmatrix} \sigma_1 \\ \sigma_2 \\ \sigma_3 \\ \sigma_4 \\ \sigma_5 \\ \sigma_6 \end{pmatrix} = \begin{pmatrix} C_{11} & C_{12} & C_{13} & C_{14} & C_{15} & C_{16} \\ C_{21} & C_{22} & C_{23} & C_{24} & C_{25} & C_{26} \\ C_{31} & C_{32} & C_{33} & C_{34} & C_{35} & C_{36} \\ C_{41} & C_{42} & C_{43} & C_{44} & C_{45} & C_{46} \\ C_{51} & C_{52} & C_{53} & C_{54} & C_{55} & C_{56} \\ C_{61} & C_{62} & C_{63} & C_{64} & C_{65} & C_{66} \end{pmatrix} \begin{pmatrix} \epsilon_1 \\ \epsilon_2 \\ \epsilon_3 \\ \epsilon_4 \\ \epsilon_5 \\ \epsilon_6 \end{pmatrix} \quad (\text{II-38})$$

we define the deformation  $\epsilon$  as follows:

let be  $(x_1, x_2, x_3)$  where the coordinates before the deformation along any axes and  $X_1=x_1+u_1$ ,  $X_2=x_2+u_2$ ,  $X_3=x_3+u_3$  the coordinates after deformation. Then the tensor of deformation is defined by:

$$\epsilon_{ij} = \frac{1}{2} \left( \frac{\partial u_i}{\partial x_j} + \frac{\partial u_j}{\partial x_i} \right) \quad (\text{II-39})$$

### II-B-1-2. Energy and the elastic constants:

The elastic constants  $C_{ij}$  are obtained by calculating the total energy as a function of the conservation of the deformations by the Mehl method [4-5]. The elastic moduli require the knowledge of the energy derivative as a function of lattice deformation. The energy  $E$  and the volume  $V_0$  equilibrium in the absence of system constraints. If we carry out a quadratic development of the energy concerning variable  $\epsilon_{ij}$ , we obtain:

$$\frac{E}{V_0} = \frac{E_0}{V_0} + \sum_{ij} C_{ij} \epsilon_{ij} + \frac{1}{2} \sum_{ijkl} C_{ijkl} \epsilon_{ij} \epsilon_{kl} \quad (\text{II-40})$$

with:

$$C_{ij} = \frac{1}{V_0} \left( \frac{\partial^2 E_0}{\partial \varepsilon_{ij} \partial \varepsilon_{kl}} \right)_{\varepsilon=0}, \quad C_{ij} = \frac{1}{V_0} \left( \frac{\partial^2 E_0}{\partial \varepsilon_{ij}} \right)_{\varepsilon=0}$$

We are close to a point of equilibrium, that is to

$$\text{say a minimum of energy therefore: } C_{ij} = \frac{1}{V_0} \left( \frac{\partial^2 E_0}{\partial \varepsilon_{ij}} \right)_{\varepsilon=0} = \mathbf{0}$$

Schwartz's theorem allows us to write the equality of cross derivatives:

$$\frac{\partial^2 E_0}{\partial \varepsilon_{ij} \partial \varepsilon_{kl}} = \frac{\partial^2 E_0}{\partial \varepsilon_{kl} \partial \varepsilon_{ij}}, \quad C_{ijkl} = C_{klij} \quad (\text{II-41})$$

### II-B-1-2-1 . Case of a crystal with cubic symmetry:

Any symmetry present in the structure can make some constants equal, and others can be equal to zero. In the case of a cubic system, there are only three independent elastic constants,  $C_{11}$ ,  $C_{12}$  and  $C_{44}$  each representing three elastic constants [6]. ( $C_{11} = C_{22} = C_{33}$ ,  $C_{12} = C_{23} = C_{31}$ , and  $C_{44} = C_{55} = C_{66}$ ) and all other constants are zero. Which means that three types of deformation should be applied to the starting crystals.

The tensor of the elastic constants is simplified and the matrix  $[C]$  is written in this case:

$$C_{ij} = \begin{pmatrix} C_{11} & C_{12} & C_{12} & 0 & 0 & 0 \\ C_{12} & C_{11} & C_{12} & 0 & 0 & 0 \\ C_{12} & C_{12} & C_{11} & 0 & 0 & 0 \\ 0 & 0 & 0 & C_{44} & 0 & 0 \\ 0 & 0 & 0 & 0 & C_{44} & 0 \\ 0 & 0 & 0 & 0 & 0 & C_{44} \end{pmatrix} \quad (\text{II-42})$$

The matrix of elastic compliances  $[S]$  which has the same form of  $[C]$ , is reciprocally linked to the matrix  $[C]$  by Hooke's relation. And is therefore written in this form [7]:

$$S_{ij} = \begin{pmatrix} S_{11} & S_{12} & S_{12} & 0 & 0 & 0 \\ S_{12} & S_{11} & S_{12} & 0 & 0 & 0 \\ S_{12} & S_{12} & S_{11} & 0 & 0 & 0 \\ 0 & 0 & 0 & S_{44} & 0 & 0 \\ 0 & 0 & 0 & 0 & S_{44} & 0 \\ 0 & 0 & 0 & 0 & 0 & S_{44} \end{pmatrix} \quad (\text{II-43})$$

The components  $C_{ij}$  and  $S_{ij}$  are interconnected by the following relations [8-9]:

$$C_{11} = \frac{(S_{11} + S_{12})}{(S_{11} - S_{12})(S_{11} + 2S_{12})}, \quad C_{12} = \frac{-S_{12}}{(S_{11} - S_{12})(S_{11} + 2S_{12})}, \quad C_{44} = \frac{1}{S_{44}}$$

$$S_{11} = \frac{(C_{11} + C_{12})}{(C_{11} - C_{12})(C_{11} + 2C_{12})}, \quad S_{12} = \frac{-C_{12}}{(C_{11} - C_{12})(C_{11} + 2C_{12})}, \quad S_{44} = \frac{1}{C_{44}} \quad (\text{II-44})$$

**II-B-1-2-2.Calculation Method:**

For calculation of the modulus  $C_{11} - C_{12}$ , used the volume-conserving orthorhombic strain tensor. When applied strain changes the total energy from its unstrained value to:

$$\boldsymbol{\varepsilon} = \begin{pmatrix} \gamma & 0 & 0 \\ 0 & -\gamma & 0 \\ 0 & 0 & \frac{1}{1-\gamma} - 1 \end{pmatrix} \quad (\text{II-45})$$

When this strain is applied, the total energy will change from its unrestricted value to:

$$E = E_0 + P(V - V_0) + \phi_{elast} \quad (\text{II-46})$$

With:

$$P = - \left( \frac{\partial E_0}{\partial V} \right) (V_0) \quad \text{And} \quad \phi_{elast} = \frac{V}{2} C_{ij} \varepsilon_i \varepsilon_j$$

For cubic samples [ 10]:

$$B(V_0) = \frac{1}{3} (C_{11} + 2C_{12}) = V_0 \left( \frac{\partial^2 E}{\partial V^2} \right) (V_0) \quad (\text{II-47})$$

Equation (II-46) becomes as follows:

$$E(\gamma) = E(-\gamma) = E_0 + \frac{1}{2} (C_{11} + C_{12}) V \gamma^2 + O[\gamma^4] \quad (\text{II-48})$$

Where V is the volume of the unit cell and  $E_0$  the energy of the unrestrained lattice at volume V. For the elastic modulus  $C_{44}$ , we used the volume-conserving trigonal strain tensor:

$$\boldsymbol{\varepsilon} = \begin{pmatrix} 0 & \frac{\gamma}{2} & \frac{\gamma}{2} \\ \frac{\gamma}{2} & 0 & \frac{\gamma}{2} \\ \frac{\gamma}{2} & \frac{\gamma}{2} & 0 \end{pmatrix} \quad (\text{II-49})$$

Which changes the total energy to:

$$E(\gamma) = E(-\gamma) = E_0 + \frac{3}{2} (C_{44}) V \gamma^2 + O[\gamma^4] \quad (\text{II-50})$$

From equations (II-46) and (II-47) we calculate  $C_{11}, C_{12}$  From equation (II-50) we calculate  $C_{44}$ .

**II-B-1-3. Mechanical Properties:**

The modulus of elasticity is an intrinsic quantity of material and characterizes a material's response to experimental stress. We want to discuss all the elastic moduli, namely the bulk modulus, Young moduli, shear moduli, and Poisson ratio.

**II-B-1-3-1. Mechanical stability criteria of the crystal:**

M. Born et K. Huang [11, 12] formulated the mechanical stability conditions for the crystal lattice and showed that by developing the internal energy of a crystal in powers in the imposed constraint and by stressing the convexity of energy, it is possible to obtain stability criteria in terms of conditions on the constants elastics. Thus a necessary condition for mechanical stability is that the matrix of constants elastics is positively defined (Born's criteria). A matrix is positively defined if the determinants of the successive-order matrices that compose it are all positive. Thus, for cubic symmetry the traditional mechanical stability conditions elastic constants in cubic crystals are known to be:

$$C_{11} - C_{12} > 0 \quad , \quad C_{11} > 0 \quad , \quad C_{44} > 0 \quad , \quad C_{11} + 2C_{12} > 0 \quad , \quad C_{12} < B < C_{11} \quad (\text{II-51})$$

**II-B-1-3-1. Bulk modulus:**

The mass modulus  $B$  (also called the modulus of compressive stiffness) is defined as the ratio of the hydrostatic pressure to the partial change in volume produced by this pressure [13]. Characterizes volumetric deformation at applying stress isotropic (hydrostatic pressure) without changing shape. In other words, the moduli of compressibility measures the resistance to volume change in solids and thus gives an estimate of the elastic response of a material to external hydrodynamic pressure.

$$B = -V \frac{dP}{dV} \quad (\text{II-52})$$

Where:  $V$  is the volume of the body at an applied pressure  $P$ .

The more  $B$  increases less compressible the material (the modulus of rigidity is considerable when the inter-atomic distance becomes smaller). The modulus of compressibility, therefore, measures the resistance to a change in volume in solids and thus gives an estimate of the elastic response of a material to external hydrodynamic pressure.

For the cubic system, the modulus of rigidity  $B$  can be expressed as a linear combination of the two elastic constants [14, 15]:

$$B = \frac{(C_{11} + 2C_{12})}{3} \quad (\text{II-53})$$

The compressibility  $K$  is the inverse of the modulus of compressibility  $B$ , in physics, speaks of a compressible object whose volume can reduce under the action of pressure. Solids having long weak bonds generally have higher compressibility than those with short strong bonds. Compounds with long weak bonds are compressed more easily.

$$k = \frac{1}{B} = - \frac{1}{V} \frac{dV}{dP} \quad (\text{II-54})$$

**II-B-1-3-3. Shear modulus:**

In materials science, The shear modulus (also called slip modulus) denoted by  $G$  is a physical quantity specific to each material and which intervenes in the characterization of the deformations produced by shear stress (see FIGURE (II-2)). In other words, it is the resistance to shape change at constant volume (a measure of the elastic shear stiffness of a material). The shear stress  $\tau$  is related to the strain angle  $\theta$  by the shear modulus through the following relationship:

$$\tau = G \cdot \text{tag}(\theta) \approx 2 \cdot G \cdot \gamma \quad (\text{II-55})$$

**With:**  $G$  is the shear modulus in  $GPa$ ,  $\theta$ : The deformation angle,  $\gamma$ : Deformation by distortion (slip), ( see FIGURE (II-2):)

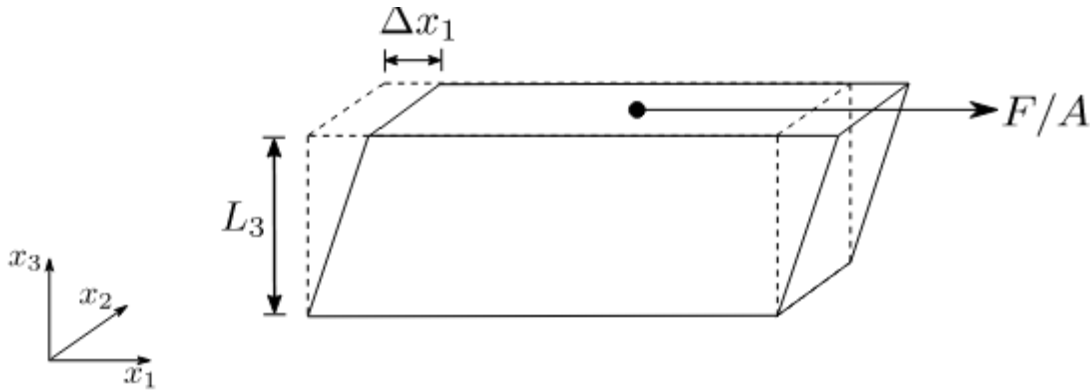


FIGURE (II-2): Illustration of an experiment to measure the shear modulus.

For the cubic system (mono-crystalline solids), the shear modulus  $G$  is also can be expressed as a linear combination of the elastic constants  $C_{11}$  and  $C_{12}$  [16, 9]:

$$G = \frac{1}{2}(C_{11} - C_{12}) \quad (\text{II-56})$$

But generally, this formula does not give good results for polycrystalline solids, from where one passes to another formula, defined by Voigt in 1928 [17] and Reuss in 1929 [18], which

gives better results [19]. Voigt's method corresponds to the application of a uniform stress ( $\sigma$ ) on the mesh and gives the shear modulus as a function of the elastic constants. But the Reuss method corresponds to the application of a uniform deformation ( $\epsilon$ ) of the mesh and gives the shear modulus as a function of the elastic constants [ 20-21]. In our case, where we have the cubic system is presented in the following form [ 22-19]:

$$G = \frac{1}{2} (G_v + G_R) \tag{II-57}$$

$G_v$  is called Voigt's modulus and  $G_R$  is called Reuss' modulus .

With:

$$G_v = \frac{1}{5} (C_{11} - C_{12} + 3C_{44}) \quad \text{and} \quad C_R = \frac{5(C_{11}-C_{12})C_{44}}{4C_{44}+3(C_{11}-C_{12})} \tag{II-58}$$

**II-B-1-3-4. Pugh's index (B/G):**

To determine if a material is brittle or ductile. Pugh [23, proposed the empirical relation ( $B/G = 1.75$  ) linking the compressibility modulus B to the shear modulus. For ( $B/G > 1.75$  ), the material is ductile, otherwise for ( $B/G < 1.75$  ), the material is brittle [24].

**II-B-1-3-5. Young's modulus:**

Young modulus or constant (longitudinal) modulus of elasticity is a property that describes the hardness of a material and is one of the most important properties of solid materials. Young modulus measures the change in length along the  $x_1$  axis when uniaxial stress (or stress) is applied by  $\sigma_{11}$  in the same direction. (FIGURE (II-3)) shows an example where in the  $x_1$ , direction tensile stress is applied. This results in an expansion stress of  $\epsilon_{11}$ . Then Young's modulus along the  $x_1$  direction is defined as:

$$E = \frac{F/A}{\Delta L/L} = \frac{\sigma_{11}}{\epsilon_{11}} \tag{II-59}$$

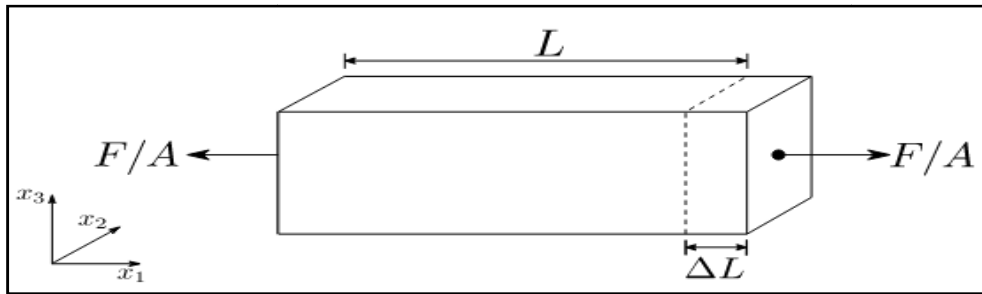


FIGURE (II-3): Illustration of an experiment for measuring the Young's modulus.

Young modulus depends on [25 ]:

- The energy of the bonds between atoms.
- The nature of the elastic restoring forces.
- The structure of the material (amorphous, crystalline, polycrystalline).

From Hook’s law, the modulus of elasticity is defined as the ratio of the stress to the strain:[ 26]

$$E = \frac{\sigma}{\epsilon} \tag{II-60}$$

where:

$\sigma$  : is stress [ MPa ]

$E$  : modulus of elasticity [MPa]

$\epsilon$  : strain [unitless or %]

**II-B-1-3-6. The axial modulus :**

The axial modulus is also known as the Poisson ratio because it is related to the Poisson effect (relating to Denis Poisson's French mathematician (1781-1840). This effect describes the behavior of many materials. When a material undergoes axial elongation (or shortening), it simultaneously undergoes transverse contraction (dilation). This ratio, called the Poisson ratio, makes it possible to characterize the contraction of the material perpendicular to the direction of the force applied ( $\nu$  = unit transverse contraction/unit axial elongation) (see FIGURE (II-4)).

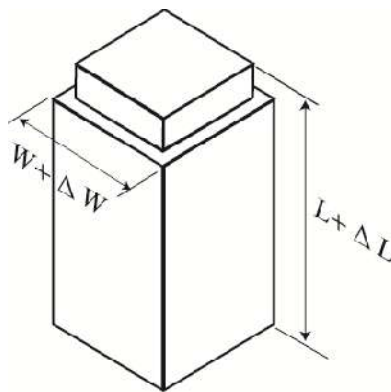


**FIGURE (II-4):** Initial and final geometric dimension of the specimen in a simple tensile test.

The radial unit strain  $\epsilon_w = \frac{\Delta w}{w_0}$  (with the radial elongation  $\Delta w = w - w_0$ ), and the resulting longitudinal unit strain  $\epsilon_L = \frac{\Delta L}{L_0}$  (with the longitudinal elongation  $\Delta L = L - L_0$ ), the Poisson's ratio ( $\nu$ ) is therefore expressed as follows:

$$\nu = -\frac{\varepsilon_w}{\varepsilon_L} = -\frac{(w - w_0)/w_0}{(L - L_0)/L_0}$$

Poisson's ratio is one of the elastic constants. It is theoretically equal to 0.25 for a perfectly isotropic material. It is always less than or equal to 0.5. If it is equal to 0.5, the material is perfectly incompressible.

The constants E,  $\nu$ , G, and B are therefore not independent but can all be expressed as a function of two of them thanks to the relations: [27]

$$\begin{aligned} G &= \frac{E}{2(1 + \nu)} \\ B &= \frac{E}{3(1 - 2\nu)} \Rightarrow \nu = \frac{3B - E}{6B} \\ G &= \frac{3}{2} B \frac{(1 - 2\nu)}{(1 + \nu)} \\ E &= \frac{9BG}{G + 3B} \end{aligned} \tag{II-61}$$

**II-B-1-3-7. The Debye temperature :**

The Debye temperature  $\theta_D$  is an important physical parameter of solids. It is found in equations describing properties that arise from atomic vibrations and in theories that study phonons. One of the standard methods of calculating the Debye temperature is from the constant data since  $\theta_D$  is proportional to the sound velocity (averaged)  $V_m$ , by the equation [28] :

$$\theta_D = \frac{h}{k_B} \left[ \frac{3n}{4\pi} \left( \frac{N_A \rho}{M} \right) \right]^{1/3} V_m \tag{II-62}$$

where  $h$  is Planck's constant,  $k$  is Boltzmann's constant,  $N_A$  is Avogadro's number,  $n$  is the number of atoms per formula unit,  $M$  is the molecular mass per formula unit,  $\rho=(M/V)$  is the density. The average speed of sound  $V_m$  can be obtained by using the following equation (where  $V_t$  and  $V_l$  are the shear and longitudinal sound velocities, respectively, and obtained by the following formula) [29]:

$$V_m = \left[ \frac{1}{3} \left( \frac{2}{V_t^3} + \frac{1}{V_l^3} \right) \right]^{-1/3} \quad (\text{II-63})$$

$$V_l = \sqrt{\frac{3B+4G}{3\rho}}, \quad V_t = \sqrt{\frac{G}{\rho}} \quad (\text{II-64})$$

**II-B-1-4. Elastic anisotropy:**

An isotropic body means its properties depend on the crystallographic orientation, unlike an isotropic body. The elastic anisotropy represents the elastics response of a material in such a crystal structure to the stress direction, which gives a measure of the anisotropy of the elastic wave velocity in cubic crystals. For cubic systems, the elastics anisotropy factor are given by the relation:

$$A = \frac{2C_{44} + C_{12}}{C_{11}} - 1 \quad (\text{II-65})$$

From the  $B$  and  $G$  of Voigt and Reuss is obtained universal elastic anisotropy index ( $A^U$ ) [30] as follows:

$$A^U = 5 \frac{G_V}{G_R} + \frac{B_V}{B_R} - 6 \quad (\text{II-66})$$

Where. refers  $B_V$ ,  $B_R$ ,  $G_V$ , and  $G_R$  are the Voigt and Reuss bounds [31,32] of the bulk modulus ( $B$ ) and shear modulus ( $G$ ), respectively.

$$G_V = \frac{1}{5} (C_{11} - C_{12} + 3C_{44}) \quad \text{and} \quad C_R = \frac{5(C_{11} - C_{12})C_{44}}{4C_{44} + 3(C_{11} - C_{12})} \quad (\text{II-67})$$

These parameters  $A^U$  can be expressed as a function of the elastic constants  $C_{ij}$ . They give each other:

$$A^U = \frac{C_{11} - C_{12} - 2C_{44}}{C_{11} - C_{44}} \quad (\text{II-68})$$

Generally, in an elastically isotropic crystal, we find that  $C_{11} - C_{12} = 2C_{44}$ , then  $A^U = 0$  and  $A = 1$ . On the other hand for an anisotropic crystal, the values are usually  $A^U \neq 0$  and  $A \neq 1$ . If  $A < 1$ , the crystal is more rigid along the axes  $\langle 100 \rangle$  of the cube, and when  $A > 1$ , it is more rigid along the diagonals  $\langle 111 \rangle$  of the cube.

Both Young and Poisson's modulus depend on two Eulerian angles  $(\varphi, \theta)$  and angular variables [ 33-34].

$$\frac{1}{e} = 1 - \frac{\delta}{2} M(\varphi, \theta) \quad , \quad \frac{\nu}{e} = -\frac{\delta}{2} [N(\varphi, \theta, \psi) - \Pi] \quad , \quad e = E S_{11} \quad (\text{II-69})$$

$$0 \leq M(\varphi, \theta) = \sin^2 2\theta + \sin^4 \theta \sin^2 2\varphi \leq \frac{4}{3}$$

$$0 \leq N(\varphi, \theta, \psi) = 3 \sin^2 \theta \cos^2 \theta \cos^2 \psi + (\cos \theta \cos 2\varphi \cos \psi - \sin \psi)^2 \sin^2 \theta \leq 1. \quad (\text{II-70})$$

$$\Pi = \frac{2S_{11}}{\Delta}, \quad \delta = \frac{\Delta}{S_{11}} \quad (\text{II-71})$$

The dimensional combination of the compliance coefficients ( $\Delta = S_{11} - S_{12} - 0.5S_{44}$ ) is known as the anisotropy parameter of the cubic crystals. The requirement for positive determination of elastic energy imposes the following constraints on compliance parameters:

$$S_{11} > 0, S_{44} > 0, S_{11} > S_{12} > -0.5S_{44} \quad (\text{II-72})$$

Which can be written in terms of dimensionless assemblers in the model :

$$\Pi\delta > 2\delta - 2, 1 > \delta\Pi > -2, 1.5 > \delta \quad (\text{II-73})$$

From Eqs. (II-71) it is also clear that for complete auxetics,  $\delta > 0, 0 > \Pi$  or  $0 > \delta, \Pi > 1$ . (of importance are the opposite signs of two dimensionless complexes and the value of  $\Pi$ ), and for non-auxetics,  $0 > \Pi, 0 > \delta$  or  $\delta > 0, 1 > \Pi$ . [ 35]

Appreciate the Poisson's ratio for cubic crystals among the following crystallographic directions:[35]

$$\nu_{[100],[001]} = -\frac{S_{12}}{S_{11}} = \frac{\Pi\delta}{2}, \quad \nu_{[001],[110]} = \frac{S_{12}}{S_{11} - \Delta} = \frac{\Pi\delta}{2 - \delta} \quad (\text{II-74})$$

$$\nu_{[1-11],[110]} = \frac{2S_{12} + \Delta}{2S_{11} - \Delta} = \frac{(\Pi - 1)\delta}{2 - \delta}, \quad \nu_{[111]} = \frac{3S_{12} + \Delta}{3S_{11} - 2\Delta} = \frac{\delta(1.5\Pi - 1)}{3 - 2\delta} \quad (\text{II-75})$$

The last three indices (II-75) in brackets refer to the directions of stretching, and the first three (II-74) numbers indicate the transverse direction.

On the other hand, the maximum and minimum values of the shear modulus G are obtained using the formula [ 36] :

$$G = \frac{1}{S_{44} + 2\Delta N(\varphi, \theta, \psi)} \quad (\text{II-76})$$

Analysis of this phrase gives [ 37]:

$$G_1 = \frac{1}{S_{11}} \quad G_2 = \frac{1}{2(S_{11} - S_{12})} \quad (\text{II-77})$$

The values of Young's modulus in different crystalline orientations depend on the coefficient of anisotropy  $\Delta$ . From the relationship ( $\Delta = S_{11} - S_{12} - 0.5S_{44}$ ) we can see that the anisotropy  $\Delta$  takes positive or negative values. For the positive anisotropy ( $\Delta > 0$ ), we have  $E[111] > E[110] > E[100]$ . In the case of negative anisotropy, we have ( $\Delta < 0$ ), and we have  $E[100] > E[110] > E[111]$ .

**II-B-1-5. Elastic wave propagation velocities :**

In a cubic crystalline solid, the elastic wave propagation speeds as a function of the elastic constants  $C_{ij}$  for certain crystallographic orientations are given in the following equations :[38]

- Along the direction: [100]

$$V_l = \left(\frac{C_{11}}{\rho}\right)^{1/2}, V_{t1,2} = \left(\frac{C_{44}}{\rho}\right)^{1/2} \tag{II-78}$$

- Along the direction: [110]

$$V_l = \left(\frac{C_{11}+C_{12}+2C_{44}}{\rho}\right)^{1/2}, V_{t,1} = \left(\frac{C_{44}}{\rho}\right)^{1/2} \text{ and } V_{t,2} = \left(\frac{C_{11}-C_{12}}{\rho}\right)^{1/2} \tag{II-79}$$

- Along the direction: [111]

$$V_l = \left(\frac{C_{11}+2C_{12}+4C_{44}}{\rho}\right)^{1/2}, V_{t1,2} = \left(\frac{C_{11}-C_{12}+C_{44}}{\rho}\right)^{1/2} \tag{II-80}$$

FIGURE (II-5) shows the three main directions of propagation [100], [110] and [111], in a cubic crystalline solid. The wave vector  $k$  is coincident on the main axes of propagation, the vectors of the propagation speeds of the longitudinal waves are parallel to the vector  $k$ , and the vectors of the propagation speeds of the transverse waves are perpendicular to the wave vector  $k$ .

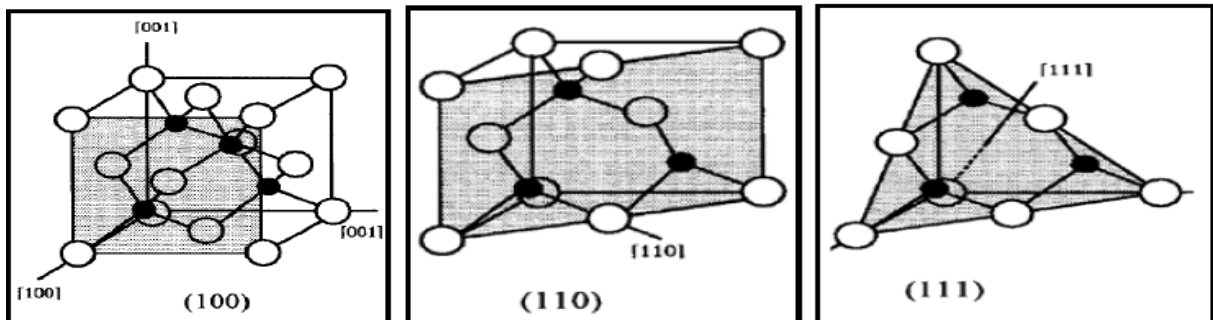


FIGURE (II-5): propagation directions of [100], [110] and [111] in a cubic crystal solid.

### II-B-2- Optical Properties:

The optical properties of a material are generally described by certain physical parameters such as dielectric function,  $\alpha$  absorption coefficient, refractive index, reflectivity coefficient, and so on. All these optical parameters can be theoretically calculated from the frequency-dependent dielectric function [39,40 ]:

$$\boldsymbol{\varepsilon}(\boldsymbol{\omega}) = \boldsymbol{\varepsilon}'(\boldsymbol{\omega}) + i\boldsymbol{\varepsilon}''(\boldsymbol{\omega}) \quad (\text{II-81})$$

where  $\boldsymbol{\varepsilon}'(\boldsymbol{\omega})$  and  $\boldsymbol{\varepsilon}''(\boldsymbol{\omega})$  are the real and imaginary components of the dielectric function, respectively. The imaginary part  $\boldsymbol{\varepsilon}''(\boldsymbol{\omega}) = \text{Im}(\boldsymbol{\varepsilon}(\boldsymbol{\omega}))$  of the dielectric function  $\boldsymbol{\varepsilon}(\boldsymbol{\omega})$  is calculated numerically by a direct evaluation of the matrix elements between the occupied and unoccupied electronic states [41], is given by:

$$\boldsymbol{\varepsilon}''(\boldsymbol{\omega}) = \frac{\hbar e^2}{3\pi m^2 \omega^2} \int d^3 \mathbf{k} |M_{cv}(\mathbf{k})|^2 \delta(E_c - E_v - \hbar\omega) \quad (\text{II-82})$$

The integral is over the first Brillouin zone. The momentum dipole elements:  $M_{cv}(\mathbf{k}) = \langle \mathbf{u}_{c\mathbf{k}} | \boldsymbol{\delta} \cdot \nabla | \mathbf{u}_{v\mathbf{k}} \rangle$ . where  $\boldsymbol{\delta}$  is the potential vector defining the electric field, are matrix elements for direct transitions with the wave vector  $\mathbf{k}$  between valence ( $\mathbf{u}_{v\mathbf{k}}$ ) and conduction band ( $\mathbf{u}_{c\mathbf{k}}$ ) states.  $\boldsymbol{\omega}$  is the angular frequency of light,  $\mathbf{c}$  and  $\mathbf{v}$  denote the conduction and valence band, respectively,  $e$  and  $m$  are the charge and mass of the electron.

The real part of the dielectric function  $\boldsymbol{\varepsilon}'(\boldsymbol{\omega})$  can be derived from the imaginary part using the Kramers-Kronig relations[42 ] :

$$\boldsymbol{\varepsilon}'(\boldsymbol{\omega}) = \mathbf{1} + \frac{2}{\pi} N \int_0^\infty \frac{\omega' \boldsymbol{\varepsilon}''(\omega')}{\omega'^2 - \omega^2} d\omega' \quad (\text{II-83})$$

where, N implies the principal value of the integral.

The knowledge of both the real and imaginary parts of the dielectric function allows the calculation of important optical functions such as refractive index  $n(\omega)$ , extinction coefficient  $k(\omega)$ , reflectivity  $R(\omega)$  and absorption coefficient  $\alpha(\omega)$ . These different amounts can be presented as follows:

➤ **The complex refractive index:**

In optics, light propagation in absorbing materials can be described using a complex-valued refractive index [43]. has two parts, real ( $n$ ) and imaginary ( $k$ ), with the imaginary part handles the attenuation, while the real part accounts for refraction. the complex refractive index linked to the dielectric function ( $\boldsymbol{\varepsilon}(\boldsymbol{\omega})$ ) by the relation :

$$\begin{cases} \epsilon = N^2 \\ N = n + ik \end{cases} \rightarrow \epsilon'(\omega) = n^2 - k^2 \quad \text{and} \quad \epsilon''(\omega) = 2nk \quad (\text{II-84})$$

The refractive index  $n(\omega)$  and extinction coefficient  $k(\omega)$ , equation is given by:

$$n(\omega) = \frac{\left[ \sqrt{\epsilon'^2(\omega) + \epsilon''^2(\omega) + \epsilon'(\omega)} \right]^{1/2}}{\sqrt{2}}, \quad k(\omega) = \frac{\left[ \sqrt{\epsilon'^2(\omega) + \epsilon''^2(\omega) - \epsilon'(\omega)} \right]^{1/2}}{\sqrt{2}} \quad (\text{II-85})$$

➤ **Reflectivity  $R(\omega)$ :**

The reflectance of the surface of a material is its effectiveness in reflecting radiant energy, is the response of the electronic structure of the material to the electromagnetic field of light and is in general a function of the frequency, or wavelength, of the light its polarization, and the angle of incidence. Reflection occurs when light moves from a medium with one index of refraction into a second medium with a different index of refraction. The refractive index  $n(\omega)$  and the extinction coefficient  $k(\omega)$  are related to the reflection  $R(\omega)$  under normal incidence by the relation [29] :

$$R(\omega) = \frac{(n-1)^2 + k^2}{(n+1)^2 + k^2} \quad (\text{II-86})$$

➤ **Absorption coefficient  $\alpha(\omega)$ :**

The absorption coefficient indicates how far light of a specific energy or wavelength can penetrate the material before being absorbed and depends on the material and on the wavelength of the absorbed light. Since the light that has the energy below the band gap does not have sufficient energy to excite an electron into the conduction band from the valence band, therefore, this light is not absorbed by the absorption coefficient, which is defined by the following relationship:

$$\alpha(\omega) = \frac{\pi 2\sqrt{2}}{\lambda} \left[ \sqrt{\epsilon'^2(\omega) + \epsilon''^2(\omega) - \epsilon'(\omega)} \right]^{1/2} \quad (\text{II-87})$$

Where :  $\omega = \frac{2\pi}{\lambda}$  ( $\lambda$  is the wavelength).

**II-B-3- Phonons properties:**

The atoms in a solid are bound by strong restoring forces elastic waves will be able to propagate in such a medium. However, just like the energy of an electromagnetic wave in a cavity, the energy of an elastic wave in a solid is quantified: the associated energy quantum is a phonon.

The term "phonon" designates a quasi-particle associated with a progressive sinusoidal elastic wave. One can imagine the phonons resulting from the collective vibrations of the atoms in a

crystalline solid. The crystalline solid is the only medium in which phonons can exist. Thus, when a vibrating crystal loses or gains energy, it does so in packets whose value is proportional to the frequency of vibration. These packets of energy are called phonons. In condensed matter physics, the phonon plays a crucial role. It is indeed involved in many physical properties of solids such as thermal or electrical conductivity, the propagation of sound waves, or the ability to store heat [45].

**II-B-3-1. Phonon Density of States:**

In solid-state physics and condensed matter physics, the density of states (DOS) of the system describes the proportion of states that are to be occupied by the system at each energy. The state density function plays a significant role in most of the physical phenomena involving lattice vibration.

The total density of states basically counts the number of states in the frequency range  $[\omega, \omega + d\omega]$ . The density of states related to volume  $V$  of the primitive cell and  $N$  countable energy levels is defined as:[ 46]

$$g(\omega) = \sum_q \sum_{i=1}^N \delta(\omega - \omega_i(q)) = \frac{V}{(2\pi)^3} \sum_{i=1}^N \int \delta(\omega - \omega_i(q)) dq \quad \text{(II-88)}$$

The integral is over the entire first Brillouin region, and the sum extends over all phonon  $N$  branches. By leaving assembly on the domains, one gets the partial DOS of the individual phonon branches.

**II-B-3-2. Acoustic and optical phonons:**

In a real solid with more than one atom in the smallest unit cell exhibit two types of phonons: "acoustic" and "optical" phonons.

- **Acoustic phonons** are coordinated movements of atoms of the lattice out of their equilibrium positions. If the displacement is in the direction of propagation, then in some areas the atoms will be closer, in others farther apart, as in a sound wave in the air (hence the name acoustic). Displacement perpendicular to the propagation direction is comparable to waves on a string. If the wavelength of acoustic phonons goes to infinity, this corresponds to a simple displacement of the whole crystal and this costs zero deformation energy. Acoustic phonons exhibit a linear relationship between frequency and phonon wave vectors for long wavelengths. The frequencies of acoustic phonons tend to zero with a longer wavelength. Longitudinal and

transverse acoustic phonons are often abbreviated as LA and TA phonons, respectively.

- **Optical phonons** are out-of-phase movements of the atoms in the lattice, with one atom moving to the left, and its neighbor to the right. They are called "optical" because in crystals they are very easily excited by light waves. This is because they correspond to vibration modes for which the positive and negative ions located on adjacent sites of the network get closer and further away from each other by creating an electric dipolar moment oscillating with time. Optical phonons that interact in this way with light are said to be active in the infrared. Optical phonons are active in Raman spectrometry and can interact with light through Raman diffusion. Longitudinal and transverse optical phonons are often written in abbreviated LO and TO, respectively.[ 47]

**II-B-3-3. Classical harmonic crystal theory:**

**II-B-3-3-1. Vibrations of a monatomic chain:**

Let us consider a linear chain of network parameter  $a$  with atoms of mass  $M$ . We assume that an elastic  $K$ -wave vector wave propagates in such a direction that the polarizations are purely or longitudinally (colinear displacement at  $K$  ) or transversely (perpendicular displacement at  $K$  ). Atoms, their equilibrium positions, and instant displacements are shown in FIGURE (II-6).

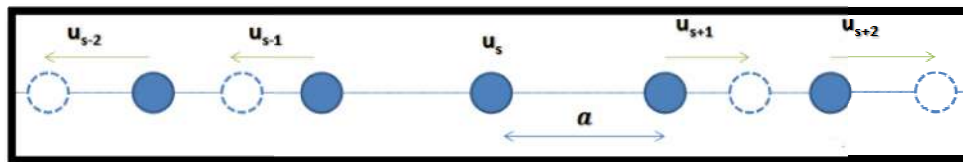


**FIGURE (II-6):** Monatomic one-dimensional crystal. Atomic positions in equilibrium and instantaneous displacements.

with:

$u_s$  : The displacement of the atom of rank  $s$  with respect to its equilibrium point.

$u_{s+1}$  : with respect to its point of equilibrium  $s+1$  with respect to its equilibrium point.

$u_{s-1}$  : with respect to its point of equilibrium  $s-1$  with respect to its equilibrium point.

**II-B-3-3-1-1. Dispersion relationship:**

Let  $C_t$  be the spring constant between the atom  $s$  and the atom  $s + t$ ,  $s$  is subject to the action of all the atoms  $t$ ,  $t \neq s$ . The resultant force exerted on the atom of index  $s$  is written:

$$F_s = \sum_{s \neq t} C_t (u_{s+t} - u_s) \quad (\text{II-90})$$

$$F_s = C_t (u_{s+1} + u_s) + C_t (u_{s-1} - u_s) \quad (\text{II-91})$$

The second law of newton [ 46 ] gives:

$$F_s = M \frac{d^2 u_s}{dt^2} \quad (\text{II-92})$$

By identifying the two relationships ((II-91) and (II-92)) we obtain:

$$M \frac{d^2 u_s}{dt^2} = C_t (u_{s+1} + u_s) - C_t (u_{s-1} - u_s) \quad (\text{II-93})$$



$$M u_s = C_t (u_{s+1} + u_{s-1} - 2u_s) \quad (\text{II-94})$$

It is a linear differential equation of the second order. We seek a solution to this differential equation in the form of a monochromatic plane wave of amplitude  $u_0$  and  $\vec{k}$  wave vector.

$$\begin{aligned} u_s &= u_0 \exp i(ska - \omega t) \\ u_{s+1} &= u_0 \exp i((s+1)ka - \omega t) \\ u_{s-1} &= u_0 \exp i((s-1)ka - \omega t) \end{aligned} \quad (\text{II-95})$$

$$\frac{d^2 u_s}{dt^2} = -u_s \omega^2 \exp i(ska - \omega t)$$

with:

- **exp** is the exponential function.
- $\omega$  the pulsation of the monochromatic wave.

We replace the expressions of the relation ( 3-14) in ((3-12)) which gives :

$$\begin{aligned} -M u_s \omega^2 &= C_t (u_{s+1} + u_{s-1} - 2u_s) \\ -M \omega^2 u_0 \exp i(ska) &= C_t u_0 (\exp i((s+1)ka) + \exp i((s-1)ka) - 2 \exp i(ska)) \end{aligned}$$

Then this relationship becomes:

$$M \omega^2 u_0 = -C_t u_0 (\exp ika + \exp -i(ka) - 2 \exp i(ka)) \quad (\text{II-96})$$

We know that:  $2 \cos ka = \exp ika + \exp -i(ka)$

The relationship (II-96) can be written as follows:

$$M \omega^2 = -2C_t (1 - \cos ka) \quad (\text{II-97})$$

so that:

$$\omega^2 = \frac{2C_t(1-\cos ka)}{M} \tag{II-98}$$

We know that:  $\cos 2ka = 1 - \sin^2(ka)$

So equation (II-97) becomes:

$$\omega = \sqrt{\frac{4C_t}{M}} \left| \sin \frac{ka}{2} \right| \tag{II-99}$$

This relation is called the relation of dispersion of phonons. We choose  $\omega$  positive for a stable network. FIGURE (II-7) gives the graphical representation of the relationship (II-99).

where the frequency  $\omega$  of the vibration is given according to the wave vector  $q$ , the function  $\omega$   $k$  is periodic and period  $2\pi a$ , it takes all possible values for:  $-\pi/a < k < +\pi/a$  a This value domain of  $k$  is confused with the first Brillions zone of the linear chain. The extreme values of  $k$  in this zone are:  $k_{mas} = \pm \pi/a$  where  $\omega = \pm \sqrt{\frac{C_t}{M}}$ .

Outside this zone the atom s are repeated in the same pattern (  $g$  : belonging to the reciprocal network ):  $u_s = u_0 \exp is(k - g)a = u_0 \exp iksa$

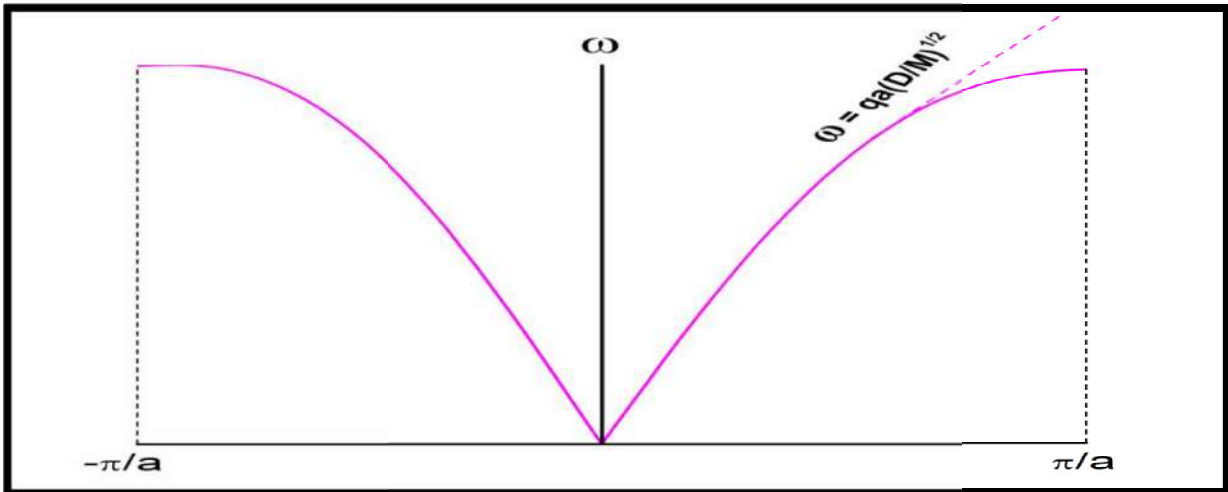
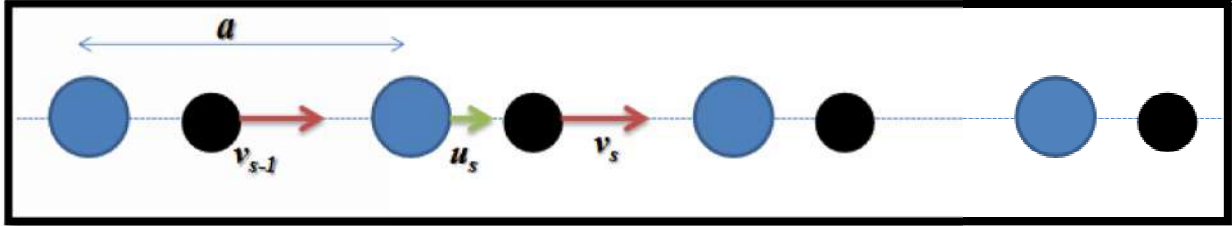


FIGURE (II-7): Dispersion curve for a mono atomic chain with only interactions between the closest neighbors.

The frequency is proportional to  $K$  in the system. However, becomes dispersive on the edges of the Brillions area within this limit, the neighboring atoms oscillate almost perfectly in phase and the movement corresponds to the oscillation of an elastic continuum, that is to say to the propagation of sound waves.

**II-B-3-2. Vibrations of a diatomic chain:**

Let us consider a diatomic chain, of network parameter  $a$ , with two atoms of respective masses  $m_1$  and  $m_2$  ( $m_1 > m_2$ ). It is assumed that each atom interacts with its close neighbours with the same  $C$  reminder constant, we note  $u$  the displacement of the  $m_1$  mass atom and  $\vartheta$  the displacement of the  $m_2$  mass atom. It is assumed that an elastic  $k$  wave vector wave propagates through the chain.



**FIGURE (II-8):** Diatomic one-dimensional crystal. (a) Equilibrium positions; (b) instantaneous displacements.

The motion equations of atoms are written:

$$\begin{cases} m_1 \frac{d^2 u_s}{dt^2} = C (\vartheta_s + \vartheta_{s-1} - 2u_s) \\ m_2 \frac{d^2 \vartheta_s}{dt^2} = C (u_{s+1} + u_s - 2\vartheta_s) \end{cases} \quad \text{(II-100)}$$

We are looking for solutions having the propagation wave form of amplitudes  $u$  and  $\vartheta$ . with a pulsation wave  $\omega$  and the  $k$ -wave detector:

$$\begin{cases} u_s = u_0 \exp i(ska - \omega t) \\ \vartheta_s = \vartheta_0 \exp i(ska - \omega t) \end{cases} \quad \text{(II-101)}$$

Substitute (II-100) in (II-101):

$$m_1 \omega^2 u_0 \exp iska = -C \vartheta_0 (\exp iska + \exp -ika(s-1) - 2u_0 \exp i(ska))$$

$$m_2 \omega^2 \vartheta_0 \exp iska = -C u_0 (\exp iska + \exp -ika(s+1) - 2\vartheta_0 \exp i(ska))$$

Where  $C$  constant hardness and  $s$  positive integers.

The determinant of the matrix of coefficients must be zero:

$$\begin{vmatrix} 2Cm_1\omega^2 & -C(1 - \exp i(ka)) \\ -C(1 + \exp i(ka)) & 2C - m_2\omega^2 \end{vmatrix} = 0$$

where :  $\cos ka = 1 + \exp i(ka)$

We then obtain an equation:

$$m_1 m_2 \omega^4 - 2C(m_1 + m_2) \omega^2 + 2C^2 (1 - \cos ka) = 0$$

It's a two-way equation in  $w$ .

We solve the equation by changing the variable:  $\delta = \omega^2$ .

$$\omega^2 = C \left( \frac{1}{m_1} + \frac{1}{m_2} \right) \pm \sqrt{\left( \frac{1}{m_1} + \frac{1}{m_2} \right)^2 - \frac{4}{m_1 m_2} \sin^2 \left( \frac{ka}{2} \right)} \quad (\text{II-102})$$

- The expression  $\omega^2$  with the ( - ) sign translates the dispersion relationship for the acoustic branch. In the vicinity of 0, the group speed is constant and equal to the speed of sound.
- The expression of  $\omega^2$  with the ( + ) sign reflects the dispersion relationship for the optical branch. The corresponding dispersion relationships are shown in the FIGURE (II-9).

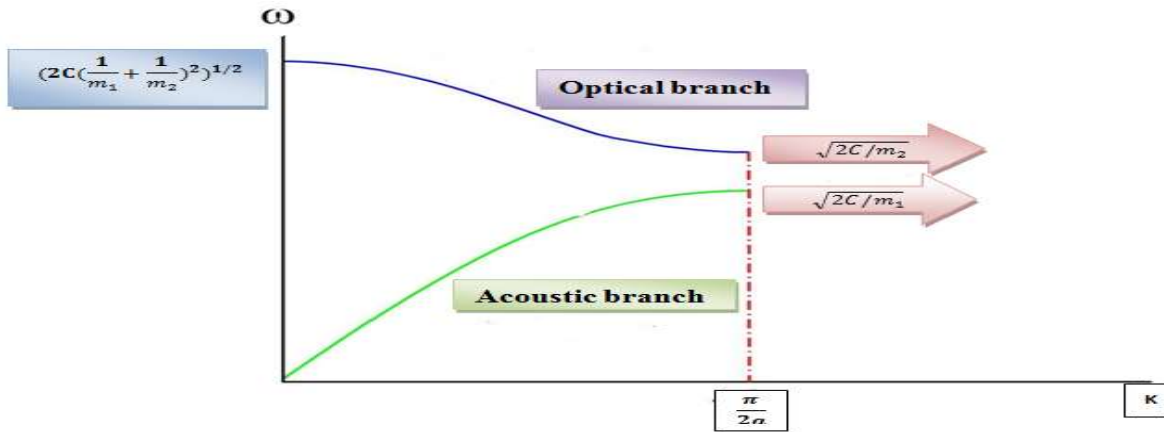


FIGURE (II-9): Optical and acoustic branches for a diatomic linear chain.

FIGURE (II-9) above shows that wave solutions do not exist for values of  $\omega$  such that:

$$\sqrt{\frac{2C}{m_1}} < \omega < \sqrt{\frac{2C}{m_2}}$$

This result is a characteristic of elastic waves in diatomic lattices. There is a band gap of frequencies at the boundary of the first Brillouin zone. If we look for solutions in this interval, the value of the wave vector  $\mathbf{K}$  will be complex, and the wave will be damped in space.

- For the optical branch at  $\mathbf{K} = \mathbf{0}$ , we have:

$$\frac{\mathbf{u}}{\vartheta} = - \frac{m_1}{m_2}$$

- The two atoms vibrate relative to each other, but their centers of gravity remain fixed. If the atoms have opposite charges, we can generate such vibration by the electric field of a light wave, which is why this branch is called the optical branch.[ 48]

- For  $\mathbf{K}$  small another possible solution is the ratio:  $\mathbf{u} = \vartheta$

Atoms vibrate together as in long wavelength acoustic vibrations hence the name acoustic branch.

**II-B-3-3. Three-dimensional lattice:**

The three-dimensional generalization of the previous one-dimensional model is easy (but rather heavy). The wave number is replaced by a three-dimensional vector. In addition,  $k$  is now associated, with three normal coordinates.

In the one-dimensional model, the atoms were limited to moving along the line, so the phonons corresponded to longitudinal waves. In three dimensions, vibration is not restricted to the direction of propagation and can also occur in perpendicular planes, like transverse waves. This gives rise to the additional normal coordinates, which, as the form of the Hamiltonian indicates, we may view as independent species of phonons.

It is generally shown that if the unit cell contains  $N$  atoms, the dispersion curves consist of  $3N$  branches, including 3 acoustic branches and  $3N - 3$  optical branches. In a crystal with  $N = 2$  different atoms the primitive cell exhibits three acoustic modes: one longitudinal acoustic mode and two transverse acoustic modes, and 3 optical branches.

**II-B-4. Thermoelectricity:**

The thermoelectric effect is a physical phenomenon characteristic of certain materials contributing to the conversion of energy. A thermoelectric material makes it possible to convert heat directly into electricity (generation of electricity) or to move calories by the application of an electric current (application of refrigeration).

In this section, we will present a historical introduction to thermoelectricity, the understanding of how heat energy and electrical current were interrelated, and the discovery of the phenomenon to the characterization of the performance of thermoelectric compounds.[49]

**II-B-4-1. Thermoelectric effects:**

In 1821, Seebeck discovered the first thermoelectric effect, it was observed as a potential difference when two metallic materials A and B are connected in a temperature - difference  $\Delta T$  exists between the two junctions. The charge carriers diffuse from the hot side to the cold side [ 50]. In this flow of charge a potential difference  $\Delta V$  appears between the two junctions. Thus, thermoelectricity was discovered. The main use of the Seebeck effect is to measure temperature with a thermocouple [ 51]. Through a coefficient  $S$ , according to the formula:

$$S_{AB} = S_B - S_A = \frac{V_2 - V_1}{T_2 - T_1} = \frac{\Delta V}{\Delta T} \quad (\text{II-103})$$

where  $S_{AB}$  is the Seebeck coefficient.  $S_{AB}$  is positive if the potential difference tends to create a current from junction 1 to junction 2. if  $T_1 > T_2$ ,  $S_{AB}$  will be negative in the opposing case.

We will see later that this can be understood by specifying which charge carriers are involved. The second thermoelectric effect discovers, by Jean Peltier [52], in 1834. Peltier concluded that the passage of an electric current imposed by an external generator in the circuit made of two materials a and b causes absorption of heat at one of the junctions while the other generates it. The coefficient of proportionality is called the Peltier coefficient  $\pi_{ab}$  measuring the magnitude of produced and absorbed heat at the junction when a current is applied:

$$Q = \pi_{ab} \cdot I \tag{II-104}$$

with:

$Q$  : being the produced or absorbed heat.

$I$  : being the electric current.

$\pi_{ab}$  : being the Peltier coefficient for the couple a and b.

The third thermoelectric phenomenon (the Thomson effect): This effect was discovered by the physicist William Thomson in 1851[53] and describes the generation or absorption of heat  $Q_T$  by the simultaneous application of a current  $\vec{j}$  and a temperature gradient  $\vec{\nabla}T$  through a single material and no junction is required, this makes the Thomson effect different from the Seebeck and Peltier effect. We can quantify the heat flux emitted or absorbed per unit volume with the following formula [54]:

$$Q_T = - \tau \cdot \vec{j} \cdot \vec{\nabla}T \tag{II-105}$$

with:

$\tau$ : the Thomson coefficient.

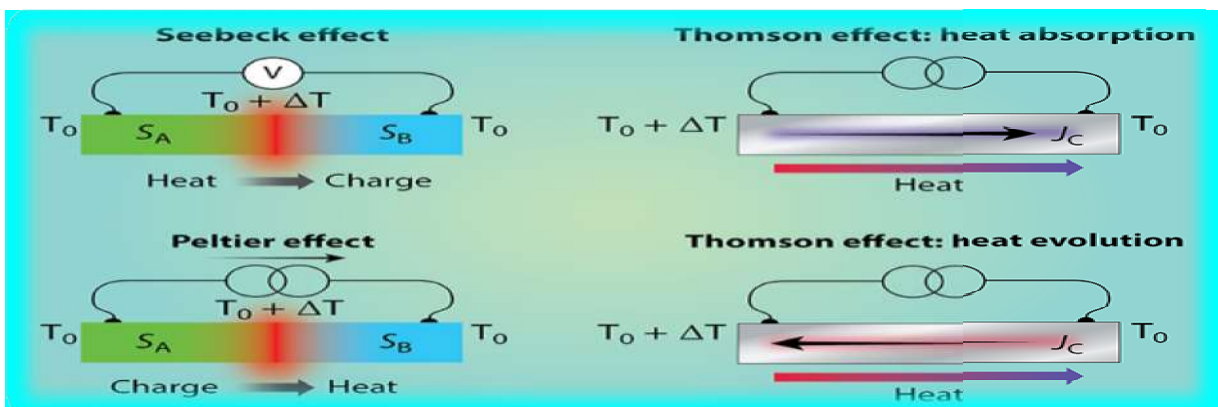


FIGURE (II-10) : Diagram illustrating the Sebeck, Peltier and Thomson effects.

Kelvin related all the thermoelectric coefficients (Seebeck, Peltier and Thomson) in the following relationship:

$$\pi_{ab} = S_{ab} \cdot T \quad (\text{II-106})$$

$$\tau_{ab} = T \frac{dS_{ab}}{dT} \quad (\text{II-107})$$

The first relation (II-106) links the Peltier coefficient and the Seebeck coefficient of a junction of two conductive materials (a and b). For a standard a / b junction. Kelvin's second relation (II-107) relates to the Seebeck and Thomson coefficients.

These relations show that the knowledge of any one of the three coefficients tells us the value of the two others. Most often the choice falls to the Seebeck coefficient  $S$  because it is the easiest to determine experimentally. More importantly, there is one physical mechanism behind the three effects which are sometimes grouped under the common name thermoelectric effects.

**II-B-4-2. Thermoelectric coefficients:**

Thermoelectric materials are characterized by three parameters ( Seebeck coefficient, electronic conductivity, and thermal conductivity ) we can obtain the electronic transport properties by calculating the total energies at different unit cell volumes and then fitting the obtained  $E(v)$  data into the Birch-Murnaghan [ 55 ] equation:

$$E(v) = E_0 + \frac{9V_0 B_0}{16} \left\{ \left[ \left( \frac{V_0}{V} \right)^{2/3} - 1 \right]^3 B_0 + \left[ \left[ \left( \frac{V_0}{V} \right)^{2/3} - 1 \right]^2 \right] \left[ 6 - 4 \left( \frac{V_0}{V} \right)^{2/3} \right] \right\} \quad (\text{II-108})$$

Then, the transport calculations in the present study are carried out using the code Boltztrap [56], which uses a Fourier expansion scheme to fit the band structures for transport property calculations. In the semi-classical transport theory, the Seebeck coefficient  $S(T,P)$  which depends on temperature doping and electrical conductivity, and electronic thermal conductivity transport, are given by:

$$S(T,P) = \frac{\int dE \sigma(E-\mu) df/dE}{\int dE \sigma(E) df/dE} \quad (\text{II-109})$$

$$\sigma_{\alpha\beta}(T, \mu) = \frac{1}{\Omega} \int \left[ -\frac{\partial f(T, \epsilon, \mu)}{\partial \epsilon} \right] d\epsilon \quad (\text{II-115})$$

$$K_{\alpha\beta}^{\circ} = \frac{1}{e^2 T \Omega} \int \sigma_{\alpha\beta}(\varepsilon) (\varepsilon - \mu)^2 \left[ -\frac{\partial f(T, \varepsilon, \mu)}{\partial \varepsilon} \right] d\varepsilon \quad (\text{II-110})$$

where  $f$  is the Fermi function,  $\mu$  is the chemical potential and  $\sigma(E)$  is the transport function by:

$$\sigma(E) = N(E) \vartheta^2(E) \tau(E) \quad (\text{II-111})$$

where  $N(E)$  is the density of states (DOS),  $\vartheta(E)$  is the band velocity and  $\tau(E)$  is the scattering time. Under the constant scattering time approximation  $\tau(E)$  is independent of energy [56,57]. To assess thermoelectric power factor  $S^2\sigma$ , the term  $\sigma(T)$  is required and is given by:

$$\sigma(T) = \int dE \sigma(E) df/dE \quad (\text{II-112})$$

### II-B-4-3. ZT merit factor:

Edmund Altenkirch (1909) was the first to establish a mathematical expression relating the efficiency of the thermoelectric generator to the physical properties of materials. The Altenkirch equation [58] includes parameters such as electromotive force, resistance, electrical and thermal conductivity, and other variables. and in 1949, Abram F. Loffe developed the modern theory of thermoelectricity by integrating these parameters into a quantity ( $Z$ ) and used this parameter to calculate the efficiency of a thermoelectric generator. The thermoelectric figure of merit  $ZT$  is a dimensionless number that combines the Seebeck coefficient with other key physical parameters to describe the energy conversion efficiency of a material.  $ZT$  is defined to be [12 ] :

$$ZT = \frac{S^2 \sigma T}{\kappa} \quad (\text{II-113})$$

with:

$ZT$ : is the thermoelectric figure of merit.

$\sigma$ : is the electrical conductivity of a material.

$S$ : is the Seebeck coefficient.

$T$ : is the temperature.

$\kappa = (\kappa_e + \kappa_l)$  is the thermal conductivity. In a solid, there are two contributions to thermal conductivity, one from the lattice through  $\kappa_l$  phonons and another directly through electrons  $\kappa_e$ .

For obtained to have a good thermoelectric material must have: An efficiency high and must have a good Seebeck coefficient ( $S$ ): to generate the expected effects.

A good electrical conductivity: to reduce the heat losses by the Joule effect to increase the current which crosses the load. And a low thermal conductivity to maintain an appreciable temperature gradient across the material. There are three problems linked to the optimization of **ZT** linked to the interdependence of the physical properties involved:

- First, there is a dependence between electrical conductivity and the contribution of electrons to thermal conductivity. We do not know of a way to decouple the contribution to the thermal conductivity of electrons from that of phonons. Experimentally, what is measured is total thermal conductivity. After measuring the total thermal conductivity, the contribution of phonons is deduced from the measurement of the electrical conductivity in combination with the Wiedemann-Franz law.
- Second, the inverse dependence of the Seebeck coefficient and electrical conductivity on the concentration of charge carrier. Indeed, to increase the electrical conductivity: it is necessary to increase the number of charge carriers  $n$  this is beneficial for the electrical conductivity, but it also decreases the Seebeck coefficient. The Seebeck coefficient can be written as:

$$S = \frac{8\pi^2 k_B^2}{3eh^2} m^* \left(\frac{\pi}{3n}\right)^{2/3} \quad \text{(II-114)}$$

- Finally, the inverse dependence between effective mass and mobility, from Equation (II-114), that a larger effective mass leads to a better Seebeck coefficient. However, this also implies that the charge carriers are heavier and move with reduced speeds, i.e. say smaller mobility. However, electrical conductivity is directly proportional to mobility.

These three problems leave little scope for optimization. The easiest way to optimize the **ZT** is therefore to reduce the thermal conductivity of the phonon because this is not supposed to influence the electronic properties, this nevertheless poses another problem of modifying the materials by playing only on the thermal conductivity of the phonon.

---

## Bibliographies

- [1] M. D. Segall, P. J. D. Lindan, M. J. Probert, C. J. Pickard; P.J. Hasnip S. J.Clark,M.C.Payne, "First principles simulation: ideas, illustrations and the . CASTEP code", *J Phys. Condens. Matter*, 14, 2717 -2743 (2002).
- [2] J.P.Perdew, K.Burke, and M.Ernzerhof, *Phys. Rev. Lett.* **77**, 3865 (1996).
- [3] P.Kireev, *La physique des semi-conducteurs*, 2<sup>e</sup> édition Mir. Moscou, (1975).
- [4] M.J. Mehl, *Physical Review B : Condensed Matter* 47 (1993) 2493- 2500
- [5] E.Schreiber, O.I.Anderson, N. Soga. *Elastic Constants and their Measurements*, McGraw-Hill, New York, 1973.
- [6] S.Saib, N.Bouarissa, *Solid State Electron.* 50 (2006) 763.
- [7] C. G. Broyden, *J of the Institute for Mathematics and Applications.* **6**, 222 (1970). See also summary in: D. F. Shanno, *J of Optimization Theory and Applications.* **46**(1), 87 (1985).
- [8] E. Schreiber, O. L. Anderson et N. Soga, *Elastic constants and their measurement* (McGraw- Hill, Inc, New York, (1974).
- [9] H. J. Monkhorst and J. D. Pack, *Phys. Rev. B.* **13**, 5189 (1976)
- [10] E.Schreiber, O.L.Anderson and N. Soga, << *Elastic Constants and their Measurement* >>. McGraw-Hill, New York, (1973).
- [11] M. H. Manghnani; in *Advanced Materials 98* (5 NIRIM International Symposium on Advanced Materials, Tsukuba, Japan 1998) p.73
- [12] M. Grimsditch and E. S. Zouboulis, *J. Appl. Phys.* **76**, 832 (1994).
- [13] J. R. Buschert, F. C. Peiris, N. Samarth, H. Luo, and J. K. Furdyna. *Phys. Rev. B* 49 (1994) 4619.
- [14] J. Perdew and Y. Wang, *Phys. Rev. B.* **45**, 13244 (1992).
- [15] C. G. Broyden, *J of the Institute for Mathematics and Applications.* **6**, 222 (1970). See also summary in: D. F. Shanno, *J of Optimization Theory and Applications.* **46**(1), 87 (1985).
- [16] Teter Pade, fitting of PW92 data: see the appendix of S. Goedecker, M. Teter, and J. Hutter, *Phys. Rev. B***54**, 1703 (1996), J. P. Perdew, K. Burke, and M. Ernzerhof, *Phys. Rev. Lett.* **77**, 3865 (1996)
- [17] P. Blaha, K. Schwarz and J. Luitz, *Wien97*, Viena University of Technology (1997).
- [18] P. Rodriguez-Hernandez, M. Gonzalez-Diaz and A. Munoz, *Phys. Rev. B.* **51**, 14705

- (1995).
- [19] J.R. Chelikowski, J. J. Wagener, J. H. Weaver and A. Jin, *Phys Rev. B.* **40**, 9644 (1989)
- [20] P. Blaha, K. Schwarz and J. Luitz, *Wien 97*, Viena University of Technology (1997)
- [21] P. Rodriguez-Hernandez, M. Gonzalez-Diaz and A. Munoz, *Phys. Rev. B.* **51**, 14705 (1995)
- [22] B. Hönerlage, C. Klingshirn and J. B. Grun, *Phys. Status Solidi B.* **78**, 599 (1976).
- [23] R. Hill, *Proc. Phys. Soc. Lond. A* **65** (1952) 349.
- [24] S.F. Pugh, *Philos. Mag.* **45** (1954) 823.
- [25] D. N. Nikogosyan. "Nonlinear Optical Crystals :A Complete Survey". Springer Science + Business Media.Inc.
- [26] J. P. Perdew, K. Burke, and Y . Wang, *Phys. Rev. B* **54** (1996) 16533.
- [27] B. Hönerlage, C. Klingshirn and J. B. Grun, *Phys. Status Solidi B.* **78**, 599 (1976).
- [28] r. de. l. Kronig, *j.opt.soc.am.* **12**, (1926) 547.
- [29] PANKOVE, J.L., *Optical processes in semiconductors*, Dover publications Inc. (1971).
- [30] S.I. Ranganathan, M. Ostoja-Starzewski, *Phys. Rev. Lett.* **101** (2008) 055504.
- [31] J.P. Watt, L. Peselnick, *J. Appl. Phys.* **51** (1980) 1525–1531.
- [32] J.P. Watt, *J. Appl. Phys.* **51** (1980) 1520–1524.
- [33] R. V. Goldstein, V. A. Gorodtsov, D. S. Lisovenko, and M. A. Volkov, "Negative Poisson's ratio for cubic crystals and nano/microtubes," *Phys. Mesomech.* **17** (2), 97–115 (2014).
- [34] R. V. Goldstein, V. A. Gorodtsov, and D. S. Lisovenko, "Classification of cubic auxetics," *Phys. Status Solidi B* **250** (10), 2038–2043 (2013).
- [35] V. A. Gorodtsov and D. S. Lisovenko, " Auxetics among Materials with Cubic Anisotropy," *Mech. Solids* **55**(4), 461–474 (2020).  
[doi.org/10.3103/S0025654420040044](https://doi.org/10.3103/S0025654420040044)
- [36] W.A. Brantley, " Calculated elastic constants for stress problems associated with semiconductor devices," *J. Appl. Phys.* **44**, 534 (1973). [doi.org/10.1063/1.1661935](https://doi.org/10.1063/1.1661935)
- [37] R.V. Goldstein, V.A. Gorodtsov, D.S. Lisovenko. Shear modulus of cubic crystals. *Lett. Mater.*, **2**(1) 21-24 (2012). [doi.org/10.22226/2410-3535-2012-1-21-24](https://doi.org/10.22226/2410-3535-2012-1-21-24)
- [38] A. Hachemia, A. Saoudi, L. Louail, D. Maouche and A. Bouguerra. *Phase Transitions* .Vol. 82, No. 1, January 2009, 87–97.

- [39] L. Makinistian, E.A. Albanesi, Phys. Rev. B 74 .045206 .(2006).
- [40] C.M.I. Okoye, J. Phys. Condens. Matter 15 .5945. (2003).
- [41] C. Amrosch-Draxl, J.O. Sofo, Comput. Phys. Commun. 175 .1. (2006).
- [42] H.I. Zhang, J. Callaway, Physical Review 181.1163–1172. (1969).
- [43] Attwood, David (1999). Soft X-rays and extreme ultraviolet radiation: principles and applications. p. 60. ISBN 978-0-521-02997-1.
- [44] Hieu T. Nguyen-Truong. Journal of Electron Spectroscopy and Related Phenomena. S0368-2048(14)00079-6. DOI: <http://dx.doi.org/doi:10.1016>
- [45] Girvin, Steven M.; Yang, Kun (2019). Modern Condensed Matter Physics. Cambridge University Press. pp. 78–96. ISBN 978-1-107-13739-4
- [46] G. Czycholl. Theoretische Festkörperphysik: Von den klassischen Modellen zu modernen Forschungsthemen. Springer-Lehrbuch. Springer Berlin Heidelberg, 2007
- [47] C. KITTEL, Physique de l'état solide (5ème édition), Dunod, Paris(1985) N.
- [48] P. Y. Yu and M. Cardona. Fundamentals of Semiconductors, Physics and Material, 3rd edition, Springer Verlag Berlin Heidelberg, New york (1996).
- [49] G.S. Nolas, J.Sharp, and H.J.Goldsmid. Thermoelectrics - Basic Principles and New Materials Developments. 2001.
- [50] T. Seebeck, "Ueber den magnetismus der galvenische kette. abh. k," Akad. Wiss., Berlin, vol. 289, 1821.
- [51] J. C. Peltier, Ann. Chem. LVI, 371-387 (1834).
- [52] J. Peltier, "Nouvelles expériences sur la caloricité des courants électriques," Annales de chimie, vol. 56, 371, 1834
- [53] W. Thomson, "On a mechanical theory of thermo-electric currents," Proceedings of the Royal Society of Edinburgh, 1851.
- [54] G. S. Nolas, J. Sharp, et H. J. Goldsmid, Thermoelectric: basic principles and new materials developments. Springer, 2001.
- [55] J. Mani, N. Rajeev Kumar, R. Radhakrishnan, and G. Anbalagan. Conference Proceedings 2265, 030390 (2020).
- [56] G.K.H. Madsen, D.J. Singh, Comput. Phys. Commun. 175 (2006) 67.

- [57] D.J. Singh, Phys. Rev. B 81 (2010) 195217.
- [58] Altenkirch E. Elektrothermische Kälteezeugung und reversible elektrische Heizung. Phys Zeitschrift 1911;10:560–580.

**III-1.Introduction:**

This chapter deals with the various results obtained concerning the Structural, electronic, optical, elastic and phononic properties of :

- $Y_{1-x}M_xN$  ( $x = 0, 0.25, 0.5, 0.75, 1$ ) . Where  $M = Sc$  and  $La$ .
- $YN_{1-x}B_x$  ( $x = 0, 0.25, 0.5, 0.75, 1$ ) . Where  $B = P, As,$  and  $Sb$ .

For this purpose, we used an ab-initio method based on Density Functional Theory (DFT).

This part will therefore be devoted to the interpretation of our results and their comparison with some theoretical works available in the literature.

**III-2. Method of calculations:**

In this work, we used the pseudo-potential method of the plane wave based on density functions (DFT) [1]. This method is applied using CASTEP [2] codes. In order to determine the exchange and correlation potential, we used the generalised gradient approximation (GGA) [ 3]. According to the convergence study, we got the value of the cut-off energy that determines the optimal size of the plane wave base to develop the wave functions, and the number of points  $k$  determines the electronic states in the first Brillouin area. The plane wave cut-off energy in reciprocal space takes as 850 eV. The BZ with Monkhorst – Pack scheme at special  $k$ -points [4] of  $8 \times 8 \times 8$ .

The Elastic constants at the equilibrium volumes are calculated using the stress–strain method [5]. The method implemented in CASTEP is setting homogeneous deformation (strain) to a finite value, optimizing any free parameters, and calculating the resulting stress. To overcome the well-known deficiency of standard DFT regarding the calculations of the electronic energy and optical properties modified form of HSE06 (Hybride) functional has been employed to investigate the electronic and optical properties as it is considered a more precise approach.

This work studies structural, elastic, electronic, optical, and phononic properties as an attempt to understand the effect of  $M$  replacement on  $Y$  atoms in the rock phase and the influence of  $B$  replacement on  $N$  atoms (FIGURE (III-1)) for the following compounds:

- $Y_{1-x}M_xN$  ( $x = 0, 0.25, 0.5, 0.75, 1$ ) . Where  $M = Sc$  and  $La$ .
- $YN_{1-x}B_x$  ( $x = 0, 0.25, 0.5, 0.75, 1$ ) . Where  $B = P, As,$  and  $Sb$ .

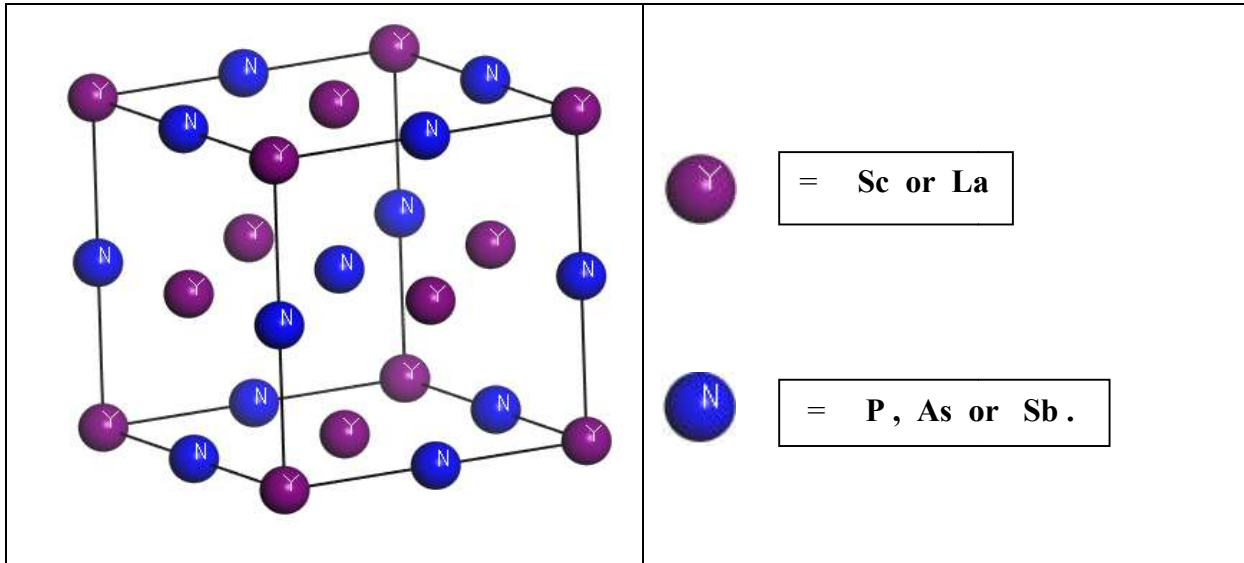


**FIGURE ( III-1):** Crystal structure of  $Y_{1-x}M_xN$  ( $M = Sc$  and  $La$ ),  $YN_{1-x}B_x$  ( $B = P$ ,  $As$  and  $Sb$ ) in the rock-salt structure.

### III-3. Structural Properties $Y_{1-x}M_xN$ ( $M = Sc$ and $La$ ), $YN_{1-x}B_x$ ( $B = P$ , $As$ and $Sb$ ):

To determine the structural parameters of the material's balance state, we adjusted the total energy varies according to the size of the primitive cell  $E(V)$  by the Mornagan case equation:

$$E(V) - E_0 = \frac{B_0 V}{B'_0(B'_0 - 1)} \left[ B'_0 \left( 1 - \frac{V_0}{V} \right) + \left( \frac{V_0}{V} \right)^{B'_0} - 1 \right]$$

when  $E_0$  and  $V_0$  are the equilibrium energy and volume and  $B$ ,  $B'$  are the compressibility module and its derivative from the pressure in the case of balance.  $B_0 = V \frac{\partial^2 E}{\partial^2 V}$ ,  $B' = \frac{\partial B_0}{\partial P}$ .

#### III-3 -1. Structural Properties of $Y_{1-x}M_xN$ ( $M = Sc$ and $La$ ):

##### III-3-1-1. The compounds $Y_{1-x}Sc_xN$ for ( $x = 0, 0.25, 0.50, 0.75$ and $1$ ) :

The structural properties of  $Y_{1-x}Sc_xN$  for  $x = 0, 0.25, 0.5, 0.75$ , and  $1$ , were studied in the B1 structure. The calculated bulk modulus and the lattice constants are listed in Table (III-1). These results are in good agreement with previous calculations and experimental data. [6]. On the other hand, there is no consistent experimental or theoretical research with alloys  $Y_{1-x}Sc_xN$  which  $x = 0.25, 0.5$ , and  $0.75$ . see FIGURE (III-2), which illustrates the relationship between the calculated lattice constants and the composition of  $Y_{1-x}Sc_xN$  alloys. It noted that the lattice constants **decrease** monotonically with the **increase of the Scandium (Sc)** component because the ionic radius of **Sc** is **smaller** than that of **Y**. Thus, the length of the bond between atoms decreases.

**Table (III-1):** Calculated lattice parameter  $a(\text{\AA})$  and bulk modulus  $B(\text{GPa})$  along with the experimental and other theoretical values  $Y_{1-x}Sc_xN$  for  $x = 0, 0.25, 0.5, 0.75,$  and  $1$ .

Composition x	a( $\text{\AA}$ )			B(GPa)		
	This work	Exp.	Other calculation	This work	Exp.	Other calculation
YN	5.04	4.877 <sup>a</sup> , 4.894 <sup>b</sup>	4.91 <sup>c</sup> , 5.20 <sup>d</sup> , 4.93 <sup>e</sup>	169.44	-	162 <sup>f</sup> , 164 <sup>c</sup> , 160 <sup>g</sup>
Y <sub>0.75</sub> Sc <sub>0.25</sub> N	4.95	-	-	171.66	-	-
Y <sub>0.5</sub> Sc <sub>0.5</sub> N	4.84	-	-	175.88	-	-
Y <sub>0.25</sub> Sc <sub>0.75</sub> N	4.69	-	-	186.82	-	-
ScN	4.51	4.501 <sup>h</sup> , 4.50 <sup>g</sup>	4.52 <sup>c</sup> , 4.51 <sup>i</sup> , 4.54 <sup>j</sup>	198.69	182 <sup>g</sup>	197 <sup>i</sup> , 221.6 <sup>k</sup> , 215.8 <sup>l</sup>

<sup>a</sup> Ref [7], <sup>b</sup> Ref [8], <sup>c</sup> Ref [9], <sup>d</sup> Ref [10], <sup>e</sup> Ref [11], <sup>f</sup> Ref [12], <sup>g</sup> Ref [13], <sup>h</sup> Ref [14], <sup>i</sup> Ref [15], <sup>j</sup> Ref [16], <sup>k</sup> Ref [17], <sup>l</sup> Ref [18].

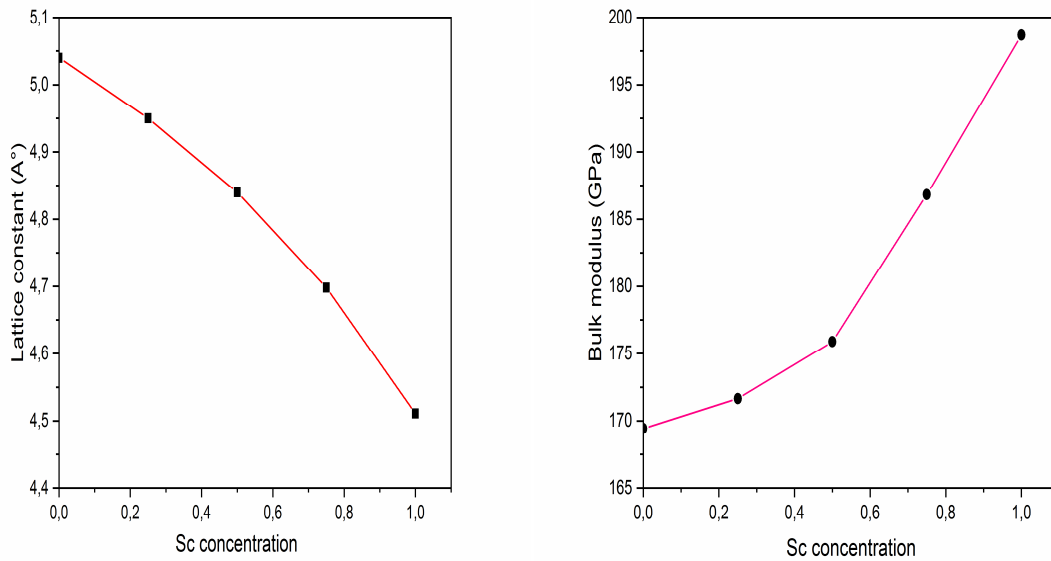


**FIGURE ( III-2):** Composition dependence of the calculated Lattice constant and Bulk modulus of  $Y_{1-x}Sc_xN$  alloys.

**III-3-1-2. The compounds  $Y_{1-x}La_xN$  ( $x = 0, 0.25, 0.50, 0.75$  and  $1$ ) :**

The crystal structures of  $Y_{1-x}La_xN$  ( $x = 0, 0.25, 0.50, 0.75$ ) that achieved the systematic substitution of atoms Y by La. the optimized lattice constants of  $Y_{1-x}La_xN$  alloys listed in Table (III-2). The lattice parameters of  $Y_{1-x}La_xN$  **increase** along with the **increase of La** ( see FIGURE ( III-3)) component because of the ionic radius of **La** that is relatively **big** than that of **Y**.

**Table (III-2):** Calculated and experimental equilibrium structural parameters: lattice constants  $a$  and bulk modulus  $B$ (GPa) for  $Y_{1-x}La_xN$  ( $x = 0, 0.25, 0.50, 0.75$ ) alloys in B1 structure.

Composition $x$	$a(\text{Å})$			$B(\text{GPa})$		
	This work	Exp.	Other calculation	This work	Exp.	Other calculation
0.00	5.040	4.877 <sup>a</sup> , 4.894 <sup>b</sup>	4.90 <sup>c</sup> , 5.20 <sup>d</sup>	169.44		162 <sup>e</sup> , 164 <sup>e</sup>
0.25	5.124	-	-	140.918		-
0.5	5.208	-	-	130.404		-
0.75	5.218	-	-	129.227		-
1	5.361	5.3 <sup>f</sup> , 5.295 <sup>d</sup>	5.32 <sup>e</sup> , 5.27 <sup>g</sup>	103.62	112 <sup>h</sup>	95.22 <sup>i</sup> , 116.947 <sup>j</sup>

<sup>a</sup> Ref [7] , <sup>b</sup> Ref [8] , <sup>c</sup> Ref [9] , <sup>d</sup> Ref [10] , <sup>e</sup> Ref [11] , Ref <sup>f</sup>[ 19 ] , Ref <sup>g</sup>[ 20 ] , Ref <sup>h</sup>[ 21 ] , Ref <sup>i</sup>[ 22 ] , Ref <sup>j</sup>[ 23 ] .

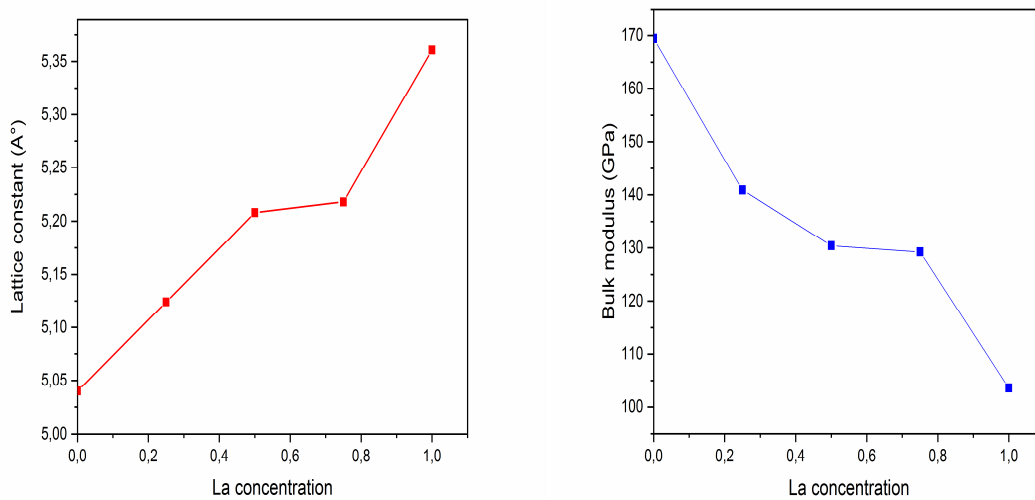


**FIGURE ( III-3):** Composition dependence of the calculated Lattice constant and Bulk modulus of  $Y_{1-x}La_xN$  alloys.

**III-3-2. Structural Properties of  $YN_{1-x}B_x$  ( $B : P, As$  and  $Sb$ ), ( $x = 0, 0.25, 0.50, 0.75$  and  $1$ ):**

Table ( III-3) also shows a good agreement between our results and those of previous calculations. The results obtained, the value of lattice parameter  $a(\text{Å})$  increases by increasing the atomic number of  $Z$ :  $a_{YNP} < a_{YNAs} < a_{YNSb}$ . We could explain this trend by the increase in the atom radius of the  $B$  in the  $YN_{1-x}B_x$  series ( $B : P, As$  and  $Sb$ ).

With an increase in the number of Z atomic:  $R ( P ) < R ( As ) < R ( Sb )$ . On the other hand, increase the lattice parameters of the component  $YN_{1-x}P_x$ ,  $YN_{1-x}As_x$ , and  $YN_{1-x}Sb_x$  along with the increase of P, As, and Sb elements, respectively.

**Table (III-3):** Calculated lattice parameter  $a(\text{\AA})$  and bulk modulus  $B(\text{GPa})$  of  $YN_{1-x}B_x$  ( $B : P, As$  and  $Sb$ ), ( $x = 0, 0.25, 0.50, 0.75$  and  $1$ ) along with the experimental and other theoretical values.

Composition x	a( $\text{\AA}$ )			B(GPa)		
	This work	Exp.	Other calculation	This work	Exp.	Other calculation
YN	5.040	4.877 <sup>a</sup> , 4.894 <sup>b</sup>	4.90 <sup>c</sup> , 5.20 <sup>d</sup>	169.44		162 <sup>e</sup> , 164 <sup>e</sup>
YN <sub>0.75</sub> P <sub>0.25</sub>	5.189	-	-	140.379		-
YN <sub>0.5</sub> P <sub>0.5</sub>	5.356	-	-	106.35		-
YN <sub>0.25</sub> P <sub>0.75</sub>	5.584	-	-	100.297		-
YP	5,683	5.652 <sup>f</sup>	5.683 <sup>d</sup> , 5.62 <sup>g</sup>	90.93	-	86.28 <sup>d</sup> , 89.51 <sup>h</sup>
YN <sub>0.75</sub> As <sub>0.25</sub>	5.289	-	-	123.101		-
YN <sub>0.5</sub> As <sub>0.5</sub>	5.400	-	-	94.225		-
YN <sub>0.25</sub> As <sub>0.75</sub>	5.704	-	-	78.631		-
YAs	5,875	5.78 <sup>f</sup>	5.835 <sup>d</sup> , 5.815 <sup>i</sup>	76.27	-	76.198 <sup>d</sup> , 76.8 <sup>i</sup>
YN <sub>0.75</sub> Sb <sub>0.25</sub>	5.425	-	-	107.562	-	-
YN <sub>0.5</sub> Sb <sub>0.5</sub>	5.535	-	-	80.617	-	-
YN <sub>0.25</sub> Sb <sub>0.75</sub>	6.018	-	-	70.271	-	-
YSb	6,155	6.155 <sup>j</sup>	6.205 <sup>d</sup> , 6.14 <sup>k</sup>	67.98	-	61 <sup>k</sup> , 62.3 <sup>l</sup>

<sup>a</sup> Ref [7], <sup>b</sup> Ref [8], <sup>c</sup> Ref [9], <sup>d</sup> Ref [10], <sup>e</sup> Ref [11], Ref <sup>f</sup>[ 23 ], Ref <sup>g</sup>[ 24], Ref <sup>h</sup>[ 15 ], Ref <sup>i</sup>[ 25 ], Ref <sup>j</sup>[ 26 ], Ref <sup>k</sup>[ 27 ], Ref <sup>l</sup>[ 28 ].

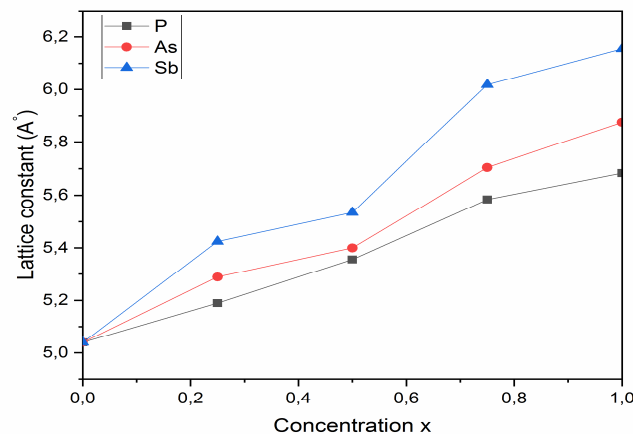


**FIGURE ( III-4):** Composition dependence of the calculated Lattice constant and Bulk modulus of  $YN_{1-x}P_x$ ,  $YN_{1-x}As_x$  and  $YN_{1-x}Sb_x$  alloys.

### III-4. Elastic properties and mechanical stability $Y_{1-x}M_xN$ ( $M = Sc$ and $La$ ) and $YN_{1-x}B_x$ ( $B = P, As$ and $Sb$ ) :

To ensure the credibility of the calculated values of elastic constants of  $Y_{1-x}M_xN$  ( $M = Sc$  and  $La$ ),  $YN_{1-x}B_x$  ( $B = P, As$ , and  $Sb$ ) compounds, we used a method to calculate them based on the stress relationship as applied in the CASTEP code [29]. CASTEP calculates the elastic properties of the first principles using limited pressure theory, which gives elastic constants as factors of proportionality that link the applied stress to calculated stress,  $\sigma_i = C_{ij}\epsilon$ . EXC interchange energy was processed using the GGA-PBE [30] version of the generalized gradual approximation because it gave the best value to the lattice parameter  $a(\text{\AA})$ .

#### III-4-1. Elastic properties and mechanical stability of $Y_{1-x}M_xN$ ( $M = Sc$ and $La$ ):

##### III-4-1-1. The compounds $Y_{1-x}Sc_xN$ for ( $x = 0, 0.25, 0.50, 0.75$ and $1$ ) :

###### A) Elastic constants and elasticity modules:

The calculated elastic constants  $C_{ij}$  for  $Y_{1-x}Sc_xN$  ( $x = 0, 0.25, 0.5, 0.75, 1$ ) in the salty rock phase are shown in Table (III-4). As we know, experimental and theoretical results have yet to deal with these constants. Consequently, the results obtained can be an indication of future investigations. Our results comply well with masculinity standards. from which we can conclude that the crystal  $Y_{1-x}Sc_xN$  ( $x = 0, 0.25, 0.5, 0.75, 1$ ) is mechanically stable.

**Table (III-4):** The calculated elastic constants for  $Y_{1-x}Sc_xN$  (  $x= 0, 0.25, 0.5, 0.75, 1$  ) compared with both theoretical and experimental data.

Composition x		$C_{11}$ (GPa)	$C_{12}$ (GPa)	$C_{44}$ (GPa)
YN	This work	348.96	79.68	112.78
	Calculations	314 <sup>a</sup> , 321 <sup>b</sup> , 325.70 <sup>c</sup>	80.7 <sup>d</sup> , 67.15 <sup>c</sup>	118.14 <sup>c</sup> , 124.4 <sup>d</sup>
$Y_{0.75}Sc_{0.25}N$	This work	355.75	79.61	114.23
	Calculations	-	-	-
$Y_{0.5}Sc_{0.5}N$	This work	346.32	96.16	125.66
	Calculations	-	-	-
$Y_{0.25}Sc_{0.75}N$	This work	376.83	91.82	141.00
	Calculations	-	-	-
ScN	This work	386.29	104.89	167.84
	Calculations	384.55 <sup>c</sup> , 380.9 <sup>e</sup>	94.1 <sup>c</sup> , 104.56 <sup>e</sup>	156.07 <sup>c</sup> , 167.18 <sup>e</sup>

<sup>a</sup> Ref [31], <sup>b</sup> Ref [32], <sup>c</sup> Ref [24], <sup>d</sup> Ref [33], <sup>e</sup> Ref [34].

The values of bulk and shear modulus B and G, Young's modulus E, Poisson's ratio  $\nu$ , ratio B/G, longitudinal ( $V_L$ ), shear ( $V_t$ ), average ( $V_m$ ) elastic wave velocities and Debye temperature ( $\theta_D$ ) for each x of  $Y_{1-x}Sc_xN$  alloys are given in Table (III-5). The conclusions can be presented as follows:

- ❖ It is noted that Young modulus E and Shear modulus G increase with the increasing concentration of Sc, as shown in FIGURE ( III-5). Because the size of the Sc atom is smaller than the size of the Y atom, this causes a reduction in the size of the composite cell unit, and thus the connections between the atoms become stronger.
- ❖ Poisson's ratio  $\nu$  is a significant property for industrial applications (Table (III-5)). Indicates that the Poisson's ratio decreases with the increasing concentration of Sc .
- ❖ From the point of view of ductility and brittleness, the ratio B/G for  $Y_{1-x}Sc_xN$  is generally below the critical value of 1.75 that separates ductile/ brittle (brittle  $< 1.75 <$  ductile) behaviors, which allows us to classify our compounds as fragile materials.
- ❖ The shear and longitudinal sound velocities  $V_t$ ,  $V_L$ , average wave velocities  $V_m$  and Debye temperatures  $\theta_D$  are determined and listed in Table (III-5). This later shows that the sound velocities  $V_t$ ,  $V_L$  and  $V_m$  increase with the increased concentration of Sc. According to our knowledge, no data is available in the literature concerning the shear, longitudinal sound velocities, and Debye temperatures  $\theta_D$  of the ternary alloy  $Y_{1-x}Sc_xN$  ( $x = 0.25, 0.5, \text{ and } 0.75$ ).

Our results are predictions and may serve as a reference for future experimental investigations.

**Table (III-5):** The calculated bulk modulus ( $B$ ), shear modulus ( $G$ ), Young's modulus ( $E$ ), Poisson's ratio  $\nu$ , Pugh's ratio( $B/G$ ), longitudinal ( $V_l$ ), shear ( $V_t$ ), average ( $V_m$ ) elastic wave velocities and Debye temperature ( $\theta_D$ ) for  $Y_{1-x}Sc_xN$  ( $x= 0, 0.25, 0.5, 0.75, 1$ ) in rocksalt phase.

Composition x		B(GPa)	G(GPa)	E(GPa)	$\nu$	B/G	$V_l$ (m/s)	$V_t$ (m/s)	$V_m$ (m/s)	$\theta_D$ (K)
YN	This work	169.44	121.52	294.22	0.210	1.39	7878.6	4770.38	5272.46	622.92
	Other calculation	162 <sup>a</sup> ,164 <sup>b</sup> , 160 <sup>b</sup>	122.59 <sup>c</sup> ,122 <sup>d</sup>	287.47 <sup>c</sup> , 291 <sup>d</sup>	0.20 <sup>c</sup>	1.19 <sup>c</sup>	7417 <sup>f</sup> , 7414 <sup>g</sup>	4558 <sup>f</sup> , 4550 <sup>g</sup>	5030 <sup>f</sup> , 5022 <sup>g</sup>	611 <sup>e</sup>
Y <sub>0.75</sub> Sc <sub>0.25</sub> N	This work	171.66	126.16	304.00	0.204	1.36	8211.89	5003.18	5526.29	665.11
	Other calculation	-	-	-	-	-	-	-	-	-
Y <sub>0.5</sub> Sc <sub>0.5</sub> N	This work	175.88	131.11	315.05	0.201	1.34	8592.39	5253.71	5800.91	714.16
	Other calculation	-	-	-	-	-	-	-	-	-
Y <sub>0.25</sub> Sc <sub>0.75</sub> N	This work	186.82	141.61	339.12	0.20	1.32	9156.71	5622.12	6205.03	786.42
	Other calculation	-	-	-	-	-	-	-	-	-
ScN	This work	198.69	156.98	372.77	0.19	1.27	9774.94	6063.28	6684.76	882.384
	Other calculation	197 <sup>h</sup> ,210.3 <sup>i</sup> , 215.8 <sup>f</sup>	151.7 <sup>c</sup>	368.57 <sup>c</sup>	0.24 <sup>c</sup>	1.42 <sup>c</sup>	9796.03 <sup>c</sup>	5903.56 <sup>c</sup>	6528.04 <sup>c</sup>	867.04 <sup>c</sup>

<sup>a</sup> Ref[33], <sup>b</sup> Ref[32], <sup>c</sup> Ref[24], <sup>d</sup> Ref[35], <sup>e</sup> Ref[36], <sup>f</sup> Ref[37], <sup>g</sup> Ref[38], <sup>h</sup> Ref[39], <sup>i</sup> Ref[40].

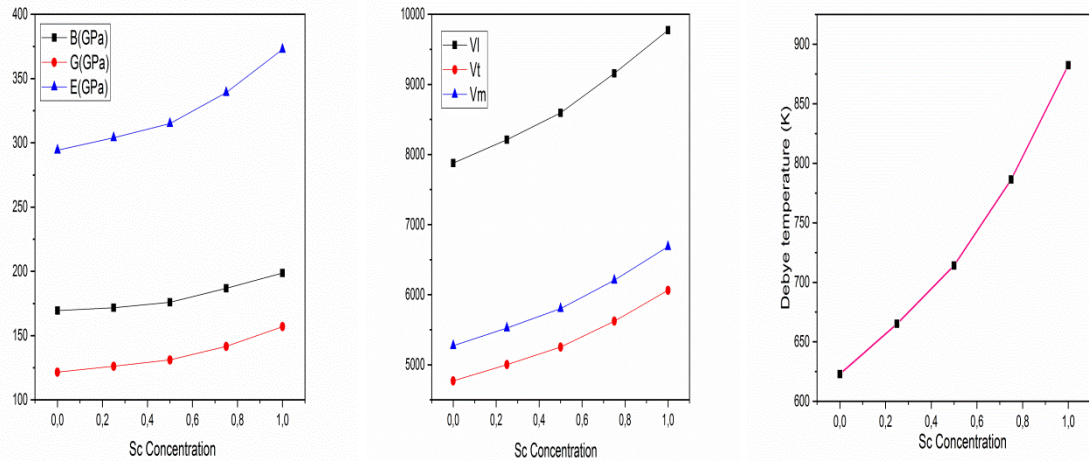


**FIGURE ( III-5):** Curves representing the shear module G, the Young E module and the compressibility module B, longitudinal ( $V_l$ ), shear ( $V_t$ ), average ( $V_m$ ) elastic wave velocities and Debye temperature ( $\theta_D$ ) for  $Y_{1-x}Sc_xN$  ( $x= 0, 0.25, 0.5, 0.75, 1$ ) in rocksalt phase.

**B) Anisotropy of elastic moduli:**

**1. Isotropic factor:**

To determine the anisotropy of  $Y_{1-x}Sc_xN$  alloys, the values  $A$ ,  $A^U$ ,  $A_B$  and  $A_G$  were calculated as a function of the elastic constants  $C_{ij}$ . the results are given in Table (III-6). The anisotropy factors differ from 1, indicating that these alloys are anisotropic. For Table (III-6), since the elastic anisotropy index ( $A^U$ ) is different from 0, all alloys are anisotropic.

**Table (III-6):** Compliances  $S_{11}$ ,  $S_{12}$ ,  $S_{44}$  and calculated anisotropy parameter  $\Delta$  (in units of  $TPa^{-1}$ ), Zener's factor  $A$ , the percentage (in %) of anisotropy in the compression and shear ( $A_B$  and  $A_G$ ), and the universal anisotropic index ( $A^U$ ) of  $Y_{1-x}Sc_xN$  ( $x = 0, 0.25, 0.5, 0.75, 1$ ) alloys.

<b>Material</b>	<b><math>S_{11}</math> (<math>TPa^{-1}</math>)</b>	<b><math>S_{12}</math> (<math>TPa^{-1}</math>)</b>	<b><math>S_{44}</math> (<math>TPa^{-1}</math>)</b>	<b>A</b>	<b><math>A_B</math></b>	<b><math>A_G</math></b>	<b><math>A^U</math></b>	<b><math>\Delta</math> (<math>TPa^{-1}</math>)</b>
<b>YN</b>	3.1315	0.5821	8.8661	0.83	0	0.39	3.93	-0.719
<b><math>Y_{0.75}Sc_{0.25}N</math></b>	3.0615	0.5599	8.4583	0.85	0	0.44	4.36	-0.607
<b><math>Y_{0.5}Sc_{0.5}N</math></b>	3.1543	0.6295	7.9019	0.95	0	0.28	2.85	-0.167
<b><math>Y_{0.25}Sc_{0.75}N</math></b>	2.9338	0.5628	7.0921	0.98	0	0.39	3.91	-0.049
<b>ScN</b>	2.9283	0.6254	5.9582	1	0	0.37	3.72	0.574

**2. Young modulus , Poisson coefficient and shear modulus:**

To better understand the anisotropic characteristics, Young's modulus of the  $Y_{1-x}Sc_xN$  single crystal in the normal direction of the three low-index crystal planes  $\{100\}$ ,  $\{110\}$ , and  $\{111\}$  were calculated. Young's modulus in all directions increases with the increase in the value of Zener's elastic anisotropy ratio  $A$  (see Table (III-7)). The extreme values of Young's modulus depending on the sign of the anisotropy parameter  $\Delta$ . For ScN ( $x = 1$ ) crystal with positive anisotropy,  $\Delta > 0$ , we have  $E[111] > E[110] > E[100]$  (see Table (III-7)). For negative anisotropy,  $\Delta < 0$ , the same relationships imply opposite inequalities  $E[100] > E[110] > E[111]$ . The bold font in Table (III-7) emphasizes the maximum values of Young's modulus. The Poisson's ratios for the  $Y_{1-x}Sc_xN$  alloy are determined and listed in Table (III-7). This later shows that Poisson's ratios  $\nu$  increase with an increase in Sc content. The values of Poisson's ratio for  $Y_{1-x}Sc_xN$  alloys monotonically increases with increasing scandium content from  $\nu[100], [001] = 0.1858$  (for  $x = 0$ ) to  $\nu[100], [001] = 0.1918$  ( $x = 1$ ) and from  $\nu[001], [110] = 0.1667$  ( $x = 0$ ) to  $\nu[001], [110] = 0.2368$  ( $x = 1$ ).

In orientations [1–10], [110] ,and [111] Poisson’s ratio for  $Y_{1-x}Sc_xN$  alloys decreases monotonically from 0.2697 ( $x = 0$ ) to 0.1280 ( $x = 1$ ) and from 0.2276 ( $x = 0$ ) to 0.1704 ( $x = 1$ ), respectively.

For  $Y_{1-x}Sc_xN$  alloys (with  $x = 0, 0.25, 0.5$  ,and 0.75), the shear modulus increases with increasing the value of Zener’s elastic anisotropy ratio  $A$  and with increasing Sc concentrations (see Table (III-7)).

For  $Y_{1-x}Sc_xN$  ( $x = 0, 0.25, 0.5$  and 0.75) alloys with negative anisotropy  $\Delta < 0$  (or  $0 < A < 1$ ) relationships (II-77) imply  $G_1 < G_2$  [46]. For ScN ( $x = 1$ ) with positive anisotropy  $\Delta > 0$  (or  $A > 1$ ), relationship (II-77) imply  $G_1 > G_2$ .

According to our knowledge, no data is available in the literature concerning the elastic constants, mechanical properties, and anisotropy of elastic moduli of the ternary alloy  $Y_{1-x}Sc_xN$ . Our results are predictions and a reference for future experimental investigations.

**Table (III-7):** The values of Zener’s elastic anisotropy ratio  $A$ , anisotropy parameter  $\Delta$ , Extreme values of Young’s modulus  $E$ , Maximum and minimum values of shear modulus  $G$ , Extreme values of Poisson’s ratio for particular orientations  $\nu$ [100],[001],  $\nu$ [001],[110], and  $\nu$ (111),[111]) for  $Y_{1-x}Sc_xN$  ( $x = 0, 0.25, 0.5, 0.75$  and 1) alloys.

Material	A	$E$ [100] GPa	$E$ [110] GPa	$E$ [111] GPa	$G_1$ GPa	$G_2$ GPa	$\nu$ [100], [001]	$\nu$ [001], [110]	$\nu$ [1-10] ,[110]	$\nu$ (111), [111]
YN	0.83	<b>319.33</b>	286.43	276.92	112.78	<b>134.64</b>	0.1858	0.1667	0.2697	0.2279
$Y_{0.75}Sc_{0.25}N$	0.85	<b>326.63</b>	297.14	288.46	118.22	<b>138.06</b>	0.1858	0.1663	0.2566	0.2199
$Y_{0.5}Sc_{0.5}N$	0.95	<b>328.02</b>	308.84	306.21	126.55	<b>132.14</b>	0.1828	0.1944	0.2202	0.2098
$Y_{0.25}Sc_{0.75}N$	0.98	<b>340.85</b>	338.01	337.07	141.00	<b>142.99</b>	0.1995	0.1902	0.1985	0.1952
ScN	1.19	341.49	378.64	<b>392.89</b>	<b>167.83</b>	140.69	0.1918	0.2368	0.1280	0.1704

**3. Elastic wave propagation velocities :**

Calculated results of the wave velocities ( longitudinal, transverse waves ) along [100],[110], and[111] directions for a  $Y_{1-x}Sc_xN$  in the rock-salt structure are shown in Table (III-8). From the results in Table (III-8), Note that the propagation velocities of the longitudinal waves and transverse waves are increasing with the increasing concentration of Sc in all directions, that  $V_l \approx 2V_t$ . On the other hand, we note that in the direction of [100], longitudinal waves are faster than in the other directions ( [110], [111] ) , which is that the directions of [100] are more rigid, which confirms the previous results. The transverse waves are slowest along [110] ( polarization [100] ( $V_{t1}$ ) ) and directions [100] (with a polarization plane following [001] ( $V_{t1,2}$ )).

**Table (III-8):** The elastic wave velocities (in m/s) for different propagation directions for  $Y_{1-x}Sc_xN$  (  $x= 0, 0.25, 0.5, 0.75, 1$  ) in rocksalt phase.

Compos- ition x	propagation direction		[100]		[110]			[111]	
	Polarization plane		[100]	[100]	[100]	[100]	[1-10]	[111]	[111]
	$\rho(\frac{g}{cm^3})$		$V_l(m/s)$	$V_{t1,2}(m/s)$	$V_l(m/s)$	$V_{t1}(m/s)$	$V_{t2}(m/s)$	$V_l(m/s)$	$V_{t1,2}(m/s)$
YN	This work	5340	8083.91	4595.82	7826.72	4595.82	5021.30	7738.87	4883.60
	Other calcul	-	-	-	-	-	-	-	-
X=0.25	This work	5040	8401.51	4760.74	8115.12	4760.74	5234.01	8017.38	5081.15
	Other calcul	-	-	-	-	-	-	-	-
X=0.5	This work	4750	8538.70	5143.42	8545.85	5143.42	5131.53	8548.23	5135.49
	Other calcul	-	-	-	-	-	-	-	-
X=0.75	This work	4480	9171.36	5610.09	9153.09	5610.09	5639.86	9146.98	5629.95
	Other calcul	-	-	-	-	-	-	-	-
X=1	This work	4270	9511.36	6269.51	9839.82	6269.51	5740.28	9946.89	5921.94
	Other calcul	-	-	-	-	-	-	-	-

**III-4-1-1. The compounds  $Y_{1-x}La_xN$  for (  $x = 0, 0.25, 0.50, 0.75$  and  $1$  ) :**

**A ) Elastic constants and elasticity modules:**

We display elastic constants  $C_{ij}$  tabulated in Table (III-9) along with the available experimental and theoretical results. The mechanical stability criteria for a cubic crystal of  $Y_{1-x}La_xN$  alloys with different x concentrations observed that our calculated elastic constants of all the phases are mechanically stable.

**Table (III-9):** The calculated elastic constants for  $Y_{1-x}La_xN$  (  $x= 0, 0.25, 0.5, 0.75, 1$  ) compared with both theoretical and experimental data.

Composition x		$C_{11}(GPa)$	$C_{12}(GPa)$	$C_{44}(GPa)$
YN	This work	348.96	79.68	112.78
	Calculations	325.70 <sup>a</sup>	80.7 <sup>a</sup>	118.14 <sup>b</sup>
$Y_{0.75}La_{0.25}N$	This work	287.98	70.38	102.27
	Calculations	-	-	-
$Y_{0.5}La_{0.5}N$	This work	279.59	70.61	93.589
	Calculations	-	-	-
$Y_{0.25}La_{0.75}N$	This work	248.255	69.714	84.822
	Calculations	-	-	-
LaN	This work	212.086	49.392	77.581
	Calculations	264.15 <sup>b</sup>	72.14 <sup>b</sup>	67.07 <sup>b</sup>

<sup>a</sup> Ref [41], <sup>b</sup> Ref [42].

---

The calculated values of the mentioned elastic  $Y_{1-x}La_xN$  ( $x= 0, 0.25, 0.5, 0.75, 1$ ) alloys are also quoted in Table (III-10).

- Young modulus  $E$  characterizes the stiffness of a material. When it is higher for a given material, the material seems stiffer. From the present results of the  $E$ ,  $G$ , and  $B$  modulus, we can say that the stiffness of these alloys decreases with an increase in  $x$  concentration. And we explain that when the concentration of  $La$  increases, the distance between atoms ( length of the bond) becomes longer, and the length of the association is known to be inversely commensurate with the association's strength and dismantling energy, and the shorter it is, the stronger the bonds between the atoms ( $YN$ ). (FIGURE ( III-6))
- Poisson's ratio is an essential elasticity-related characteristic property of the material, this ratio is confined between two values of 0.25 and 0.5, for they are two limits that show us the fragility of the material.
- In our case, this value is smaller than 0.25. So our materials have the property of brittleness. Pugh proposes the ratio  $B / G$  as a criterion of machining behavior [26]. A high ratio is associated with ductility, while a low value indicates the fragility of the compound. The critical value separating ductility from brittleness is about 1.75. The calculated values of the  $Y_{1-x}La_xN$  alloys have a ratio lower than 1.75, which explains their fragility. Based on the Pugh concept, our studied compounds may be appropriate for some technological applications.
- From this table, it can be seen that the values of the isotropic acoustic velocities ( $V_l$ ,  $V_t$  and  $V_m$ ) and the temperature of Debye  $\theta_D$  gradually decrease according to the increasing the increasing concentration of  $x$  (see FIGURE ( III-6)). We can also see that longitudinal acoustic velocities propagate faster than transverse acoustic velocities in these materials.

**Table (III-10):** The calculated bulk modulus ( $B$ ), shear modulus ( $G$ ), Young's modulus ( $E$ ), Poisson's ratio  $\nu$ , Pugh's ratio ( $G/B$ ), longitudinal ( $V_l$ ), shear ( $V_t$ ), average ( $V_m$ ) elastic wave velocities and Debye temperature ( $\theta_D$ ) for  $Y_{1-x}La_xN$  ( $x= 0, 0.25, 0.5, 0.75, 1$ ) in rocksalt phase.

Composition x		B(GPa)	G(GPa)	E(GPa)	$\nu$	B/G	$V_l$ (m/s)	$V_t$ (m/s)	$V_m$ (m/s)	$\theta_D$ (K)
YN	This work	169.44	121.52	294.22	0.210	1.39	7878.6	4770.38	5272.46	622.913
	Other calculation	164 <sup>a</sup> ,162 <sup>b</sup>	122.59 <sup>c</sup> ,122 <sup>d</sup>	287.47 <sup>e</sup> , 291 <sup>d</sup>	0.20 <sup>e</sup>	1.19 <sup>e</sup>	7417 <sup>f</sup>	4558 <sup>f</sup> , 4550 <sup>g</sup>	5030 <sup>f</sup> , 5022 <sup>g</sup>	611 <sup>g</sup>
Y <sub>0.75</sub> La <sub>0.25</sub> N	This work	142.91	104.83	252.70	0.205	1.01	7042.27	4288.49	4737.13	549.855
	Other calculation	-	-	-	-	-	-	-	-	-
Y <sub>0.5</sub> La <sub>0.5</sub> N	This work	140.21	97.79	238.03	0.217	1.43	6704.44	4030.40	4457.77	509.718
	Other calculation	-	-	-	-	-	-	-	-	-
Y <sub>0.25</sub> La <sub>0.75</sub> N	This work	129.227	86.601	212.364	0.226	1.49	6227.27	3704.64	4101.61	461.718
	Other calculation	-	-	-	-	-	-	-	-	-
LaN	This work	103.62	79.087	189.141	0.195	1.31	6275.50	3464.27	3860.27	428.83
	Other calculation	130.92 <sup>c</sup>	85.56 <sup>c</sup>	210.49 <sup>e</sup>	0.23 <sup>c</sup>	1.51 <sup>c</sup>	5532.161 <sup>h</sup>	3170.372 <sup>h</sup>	3521.986 <sup>h</sup>	395 <sup>a</sup> , 300 <sup>c</sup>

<sup>a</sup> Ref[33], <sup>b</sup> Ref[32], <sup>c</sup> Ref[24], <sup>d</sup> Ref[35], <sup>e</sup> Ref[36], <sup>f</sup> Ref[37], <sup>g</sup> Ref[38], <sup>h</sup> Ref[22].

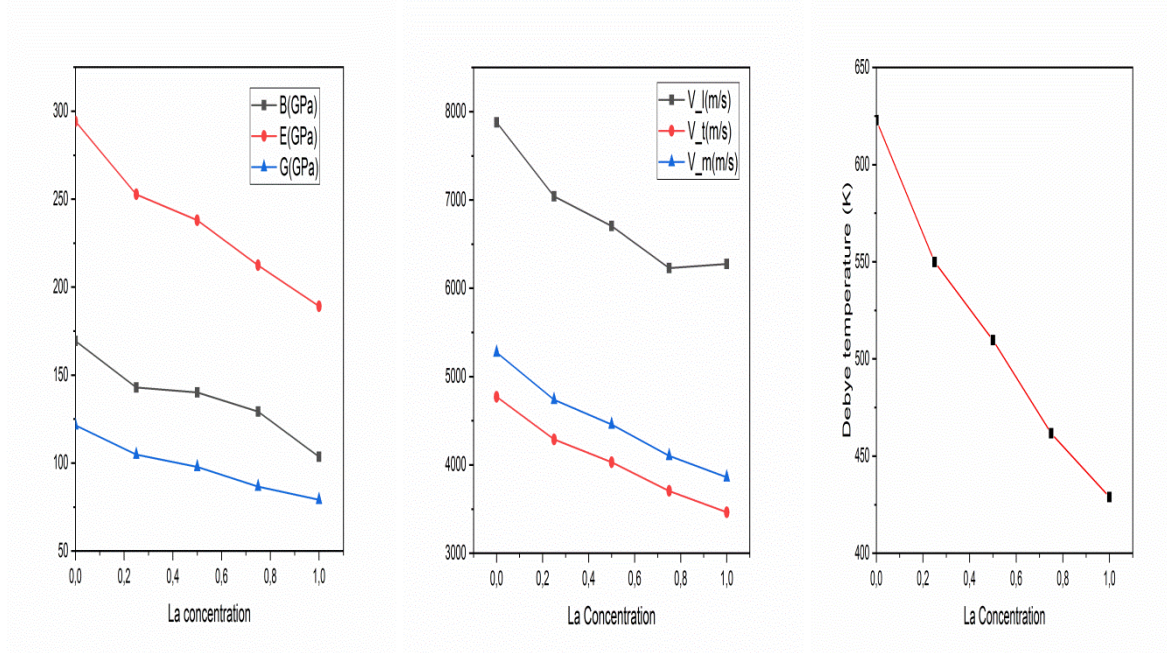


**FIGURE ( III-6):** Curves representing the shear module G, the Young E module and the compressibility module B, longitudinal ( $V_l$ ), shear ( $V_t$ ), average ( $V_m$ ) elastic wave velocities and Debye temperature ( $\theta_D$ ) for  $Y_{1-x}La_xN$  ( $x= 0, 0.25, 0.5, 0.75, 1$ ) in rocksalt phase.

**B) Anisotropy of Elastic Moduli:**

**1. Isotropic factor:**

To determine the anisotropy of  $Y_{1-x}La_xN$  ( $x= 0, 0.25, 0.5, 0.75, 1$ ), the Zener anisotropy factor  $A$  calculated as a function of the elastic constants  $C_{ij}$ , These results for the  $A$  and  $A^U$  are listed in Table (III-11). Concerning  $A$  and  $A^U$ , the values of contrast agents  $A$  and  $A^U$  appear to differ from zero, indicating that these alloys are anisotropic. It has been found that  $A \neq 1$ . Therefore, It could be concluded that it is an elastic anisotropy because ( $A < 1$ ). The latter confirms that in the diagonal directions  $\langle 100 \rangle$ , the material is more rigid

**Table (III-11).** Parameter values  $S_{ij}$ , calculated universal elastic anisotropy index  $A^U$  and Zener's factor  $A$ .

Materials	$S_{11}$	$S_{12}$	$S_{44}$	$A^U$	$A$
YN	0.0031315	-0.0005821	0.0088661	3.77	0.837
$Y_{0.75}La_{0.25}N$	0.0038412	-0.0007544	0.0097773	0.45	0.939
$Y_{0.5}La_{0.5}N$	0.0039944	-0.0008149	0.0105731	0.91	0.916
$Y_{0.25}La_{0.75}N$	0.0045938	-0.0010072	0.0117894	0.31	0.950
LaN	0.0051699	-0.0009766	0.0128897	0.26	0.953

**2. Young modulus , Poisson coefficient and shear modulus:**

The values of Young's modulus in different crystalline orientations depend on the coefficient of anisotropy  $\Delta$ . From the relationship ( $\Delta = S_{11} - S_{12} - 0.5S_{44}$ ), It could be observed that the anisotropy  $\Delta$  takes positive or negative values. For the positive anisotropy ( $\Delta > 0$ ), we have  $E[111] > E[110] > E[100]$ . In the case of negative anisotropy, and we have ( $\Delta < 0$ ), we have  $E[100] > E[110] > E[111]$ . Our results are shown in Table (III-12).

The maximum and minimum of the shear modulus, for  $Y_{1-x}La_xN$  ( $x = 0, 0.25, 0.5$  and  $0.75$ ) alloys with negative anisotropy  $\Delta < 0$  (or  $0 < A < 1$ ) imply  $G_1 < G_2$ .

**Table (III-12):** Anisotropy parameter  $\Delta$ , Extreme values of Young's modulus  $E$ , thermodynamic constraints  $\Pi$  and  $\delta$ , Extreme values of Poisson's ratio for particular orientations, maximum and minimum values of shear modulus  $G$  for  $Y_{1-x}La_xN$  ( $x= 0, 0.25, 0.5, 0.75$  and  $1$ ) alloys.

Materials	$\Delta$ TPa <sup>-1</sup>	$E[100]$ (GPa)	$E[110]$ (GPa)	$E[111]$ (GPa)	$\Pi$	$\delta$	$\nu[100]$	$\nu[110]$	$\nu[1-10]$ [110]	$\nu[111]$	$G_1$ (GPa)	$G_2$ (GPa)
YN	-0.719	319.33	286.43	276.92	-1.61	-0.22	0.185	0.166	0.269	0.227	112.79	134.64
$Y_{0.75}La_{0.25}N$	-0.293	260.33	250.77	247.73	-5.14	-0.07	0.196	0.189	0.226	0.221	102.28	108.79
$Y_{0.5}La_{0.5}N$	-0.474	250.35	236.31	231.96	-3.43	-0.11	0.204	0.193	0.248	0.225	94.62	103.96
$Y_{0.25}La_{0.75}N$	-0.291	217.68	211	208.86	-6.92	-0.06	0.219	0.213	0.243	0.231	84.86	89.27
LaN	-0.298	193.43	180	186.26	-6.54	-0.05	0.188	0.183	0.211	0.200	77.58	81.35

**3. Elastic wave propagation velocities :**

Calculated results of the wave velocities ( longitudinal, transverse waves ) along [100],[110], and[111] directions for a  $Y_{1-x}La_xN$  in the B1 structure. Based on the results in Table (III-13), it has been found that the propagation velocities of the longitudinal waves in the three propagation directions [100], [110], [111] are more significant than the propagation velocities of the transverse waves. And we can see longitudinal waves are fastest along [100]. This confirms the validity of our calculated results of the coefficient of variation that showed that E [100] is greater than E [110] and E [111], which means that the trend of [100] is more rigid. On the other hand, shear waves are slowest along[110] ( polarization [100] ( $V_{t1}$ )) and the directions [100] (with a polarization plane following [001] ( $V_{t1,2}$ )).

**Table (III-13):** The elastic wave velocities (in m/s) for different propagation directions for  $Y_{1-x}La_xN$  (  $x= 0, 0.25, 0.5, 0.75, 1$  ) in rock-salt phase.

Compos- ition x	propagation direction Polarization plane	$\rho(\frac{g}{cm^3})$	[100]		[110]			[111]	
			[100]	[100]	[100]	[100]	[1-10]	[111]	[111]
			$V_l(m/s)$	$V_{t1,2}(m/s)$	$V_l(m/s)$	$V_{t1}(m/s)$	$V_{t2}(m/s)$	$V_l(m/s)$	$V_{t1,2}(m/s)$
YN	This work	5340	8083.91	4595.82	7826.72	4595.82	5021.30	7738.87	4883.60
	Other calcul	-	-	-	-	-	-	-	-
X=0.25	This work	5700	7107.94	4235.81	7026.89	4235.81	4368.94	6999.66	4325.03
	Other calcul	-	-	-	-	-	-	-	-
X=0.5	This work	6020	6801.77	3965.17	6695.38	3965.17	4142.29	6659.53	4084.11
	Other calcul	-	-	-	-	-	-	-	-
X=0.75	This work	6310	6273.48	3666.39	6215.96	3666.39	3761.26	6197.00	3729.94
	Other calcul	-	-	-	-	-	-	-	-
X=1	This work	6590	5673.01	3431.11	5622.41	3431.11	3531.40	5606.45	3486.19
	Other calcul	-	-	-	-	-	-	-	-

**III-4-2. Elastic properties and mechanical stability of  $YN_{1-x}B_x$  (B = P ,As and Sb) :**

**A) Elastic constants and elasticity modules :**

The evaluated elastic constants ( $C_{ij}$ ) for  $YN_{1-x}B_x$  (B = P ,As and Sb) are given in Table (III-14). The elastic constants are positive check the mechanical stability criteria. The compressibility module also satisfies the condition  $C_{12} < B < C_{44}$ . Therefore our compounds are elastically stable and noted that the alloy is characterized by a value of  $C_{11}$  higher than  $C_{12}$  and  $C_{44}$ , meaning that it is more resistant to unidirectional compression than to shear deformations. The high value of the elastic constant  $C_{11}$  reflects the hardness of the covalent bond Y-N in the directions [100], [010], and [001].

**Table (III-14):** The calculated elastic constants for  $YN_{1-x}B_x$  (  $x= 0, 0.25, 0.5, 0.75, 1$  ) were compared with theoretical and experimental data.

Composition x		$C_{11}$ (GPa)	$C_{12}$ (GPa)	$C_{44}$ (GPa)
YN	This work	348.96	79.68	112.78
	Calculations	314 <sup>a</sup> , 321 <sup>b</sup> , 325.70 <sup>c</sup>	80.7 <sup>d</sup> , 67.15 <sup>c</sup>	118.14 <sup>c</sup> , 124.4 <sup>d</sup>
YN <sub>0.75</sub> P <sub>0.25</sub>	This work	316.971	90.610	52.084
	Calculations	-	-	-
YN <sub>0.5</sub> P <sub>0.5</sub>	This work	209.117	75.64	64.22
	Calculations	-	-	-
YN <sub>0.25</sub> P <sub>0.75</sub>	This work	240.044	30.493	55.493
	Calculations	-	-	-
YP	This work	224.04	24.38	43.94
	Calculations	204.6 <sup>c</sup> , 205 <sup>d</sup>	20.07 <sup>c</sup> , 28.7 <sup>d</sup>	40.46 <sup>c</sup> , 46.3 <sup>d</sup>
YN <sub>0.75</sub> As <sub>0.25</sub>	This work	266.644	51.3304	78.885
	Calculations			
YN <sub>0.5</sub> As <sub>0.5</sub>	This work	181.083	67.115	55.136
	Calculations			
YN <sub>0.25</sub> As <sub>0.75</sub>	This work	193.341	21.276	47.024
	Calculations			
YAs	This work	193.434	35.337	41.691
	Calculations	184.2 <sup>c</sup> , 192 <sup>d</sup>	30.75 <sup>c</sup> , 23 <sup>a</sup>	42.71 <sup>c</sup> , 39 <sup>a</sup>
YN <sub>0.75</sub> Sb <sub>0.25</sub>	This work	232.105	45.291	64.077
	Calculations			
YN <sub>0.5</sub> Sb <sub>0.5</sub>	This work	147.442	64.179	38.971
	Calculations			
YN <sub>0.25</sub> Sb <sub>0.75</sub>	This work	163.734	23.539	32.341
	Calculations			
YSb	This work	154	23.47	30.55
	Calculations	151 <sup>c</sup> , 149.5 <sup>d</sup>	21 <sup>c</sup> , 19.3 <sup>d</sup>	24 <sup>c</sup> , 24.6 <sup>d</sup>

<sup>a</sup> Ref [31], <sup>b</sup> Ref [32], <sup>c</sup> Ref [24], <sup>d</sup> Ref [33].

In addition, the study of the elastic modules for  $YN_{1-x}B_x$  (B = P, As, and Sb) and obtained the results shown in Table (III-15).

- For elastic modules,  $B$  and  $G$  decrease with increasing concentrations  $x$  for all compounds  $YN_{1-x}B_x$  (B = P, As, and Sb). As noted, these values go down from  $YN_{1-x}P_x$  to  $YN_{1-x}As_x$  to  $YN_{1-x}Sb_x$  in the direction of increasing the volume of the systems studied ( $YN_{1-x}P_x \rightarrow YN_{1-x}As_x \rightarrow YN_{1-x}Sb_x$ ).  $YN_{1-x}P_x$  is more resistive to compressibility and shear than  $YN_{1-x}As_x$  and  $YN_{1-x}Sb_x$  because  $B, G (YN_{1-x}P_x) > B, G (YN_{1-x}As_x) > B, G (YN_{1-x}Sb_x)$ .

- In the Young module  $E$ , defined as the ratio of stress to deformation in a uniaxial tensile or

compression experiment, we see that the young module of all alloys decreases with increased x concentration. So, decreases in these values from  $YN_{1-x}P_x$  to  $YN_{1-x}As_x$  to  $YN_{1-x}Sb_x$ , indicate a decrease in the stiffness of these systems in the same direction. where:  $E(YN_{1-x}P_x) > E(YN_{1-x}As_x) > E(YN_{1-x}Sb_x)$ .

- The Poisson coefficient measures the crystal's stability against the shear. For both  $YN_{1-x}P_x$ ,  $YN_{1-x}As_x$  and  $YN_{1-x}Sb_x$  materials, the ratio of Poisson is less than 0.25. The small values also reflect the mechanical stability of the cubic phase.

- The B/G ratio values are less than 1.75 for  $YN_{1-x}B_x$  (B = P, As, and Sb) compounds. Therefore, these systems must be classified as fragile materials.

- This table shows that longitudinal waves propagate faster than transverse waves (shear elastic waves). Elastic wave speeds decrease in value from  $YN_{1-x}P_x$  to  $YN_{1-x}As_x$  to  $YN_{1-x}Sb_x$ , and the more x concentration, these speeds decrease for each compound.

The Debye temperature  $\theta_D$  also decreases in ascending order of the primary cell volume:  $\theta_D(YN_{1-x}P_x) > \theta_D(YN_{1-x}As_x) > \theta_D(YN_{1-x}Sb_x)$ .

**Table (III-15):** The calculated bulk modulus (B), shear modulus (G), Young's modulus (E), Poisson's ratio  $\nu$ , Pugh's ratio( G/B), longitudinal ( $V_l$ ), shear ( $V_t$ ), average ( $V_m$ ) elastic wave velocities and Debye temperature ( $\theta_D$ ) for  $YN_{1-x}B_x$  (B = P, As and Sb), ( x= 0, 0.25, 0.5, 0.75, 1 ) in rocksalt phase.

Compositio n x		B(GPa)	G(GPa)	E(GPa)	$\nu$	B/G	$V_l$ (m/s)	$V_t$ (m/s)	$V_m$ (m/s)	$\theta_D$ (K)
YN	This work	169.44	121.52	294.22	0.210	1.39	7878.6	4770.38	5272.46	622.913
	Other calculation	164 <sup>a</sup> ,162 <sup>b</sup> ,	122.59 <sup>c</sup> ,122 <sup>d</sup>	287.47 <sup>c</sup> ,291 <sup>d</sup>	0.20 <sup>c</sup>	1.19 <sup>d</sup>	7417 <sup>f</sup>	4558 <sup>f</sup> ,4550 <sup>g</sup>	5030 <sup>f</sup> ,5022 <sup>g</sup>	611 <sup>g</sup>
YN <sub>0.75</sub> P <sub>0.25</sub>	This work	140.379	105.528	253,151	0.199	1.33	7431.213	4553.299	5026.463	576.755
	Other calculation	-	-	-	-	-	-	-	-	-
YN <sub>0.5</sub> P <sub>0.5</sub>	This work	106.35	83.233	198.037	0.190	1.28	6735.821	4168.519	4596.910	510.072
	Other calculation	-	-	-	-	-	-	-	-	-
YN <sub>0.25</sub> P <sub>0.75</sub>	This work	100.297	71.789	173.881	0.211	1.40	6563.563	3972.128	4390.416	472.969
	Other calculation	-	-	-	-	-	-	-	-	-
YP	This work	87.65	60.58	150.477	0.224	1.48	6230.877	3761.638	4158.792	436.742
	Other calculation	89.34 <sup>c</sup>	61.19 <sup>c</sup> ,60 <sup>h</sup>	151.28 <sup>c</sup> ,147 <sup>i</sup>	0.22 <sup>c</sup>	1.5 <sup>c</sup>	6111 <sup>h</sup>	3667 <sup>h</sup>	4056 <sup>h</sup>	427 <sup>h</sup>
YN <sub>0.75</sub> As <sub>0.25</sub>	This work	123.101	90.393	217,855	0.205	1.36	6779,895	4129,804	5272,464	479,059
	Other calculation	-	-	-	-	-	-	-	-	-
YN <sub>0.5</sub> As <sub>0.5</sub>	This work	94.225	71.457	171,115	0.197	1.32	5806,809	3565,777	5026,463	413,288

	Other calculation	-	-	-	-	-	-	-	-	-
YN <sub>0.25</sub> As <sub>0.75</sub>	This work	78.631	62.627	148,465	0.185	1.26	5525,725	3434,262	4596,910	397,540
	Other calculation	-	-	-	-	-	-	-	-	-
YAs	This work	78.48	53.304	104,5444	0.224	1.62	5464,702	3174,691	3522,573	369,931
	Other calculation	49.55 <sup>c</sup>	56.31 <sup>c</sup> 52 <sup>h</sup>	122.8 <sup>c</sup> 137 <sup>i</sup>	0.22 <sup>c</sup>	0.9 <sup>c</sup>	5041 <sup>h</sup>	2997 <sup>h</sup>	3318 <sup>h</sup>	342 <sup>h</sup>
YN <sub>0.75</sub> Sb <sub>0.25</sub>	This work	107.562	75.808	184,159	0.215	1.42	6215,859	3746,801	4142,992	435,086
	Other calculation	-	-	-	-	-	-	-	-	-
YN <sub>0.5</sub> Sb <sub>0.5</sub>	This work	80.617	53.199	130.822	0.230	1.52	4968.148	3623.516	3909.854	410.602
	Other calculation	-	-	-	-	-	-	-	-	-
YN <sub>0.25</sub> Sb <sub>0.75</sub>	This work	70.271	47.444	116,184	0.224	1.48	4883,091	2910.801	3221,976	338,363
	Other calculation	-	-	-	-	-	-	-	-	-
YSb	This work	67.98	42.03	104.544	0.244	1.68	4546,427	2646.696	2936,176	308,349
	Other calculation	60.65 <sup>c</sup>	35 <sup>c</sup>	104 <sup>c</sup>	0.27 <sup>c</sup>	1.8 <sup>c</sup>	4324 <sup>h</sup>	2481 <sup>h</sup>	2756 <sup>h</sup>	266 <sup>h</sup>

<sup>a</sup> Ref[33], <sup>b</sup> Ref[32], <sup>c</sup> Ref[24], <sup>d</sup> Ref[35], <sup>e</sup> Ref[36], <sup>f</sup> Ref[37], <sup>g</sup> Ref[38], <sup>h</sup> Ref[23], <sup>i</sup> Ref[25].

## B) Anisotropy of Elastic Moduli

### 1. Isotropic factor :

The Zener anisotropy factors  $A$  of the  $YN_{1-x}B_x$  ( $B = P, As$  and  $Sb$ ), ( $x = 0, 0.25, 0.5, 0.75, 1$ ), calculated in the rock salt structure. The values obtained for  $YN_{1-x}P_x$ ,  $YN_{1-x}As_x$ , and  $YN_{1-x}Sb_x$  compounds are shown in Tables (III-16), (III-17), and (III-18), respectively. Since the elastic anisotropy index ( $A^U$ ) is different from 0 and  $A \neq 1$ , all alloys are anisotropic.

**Table (III-16):** Parameter values:  $S_{ij}$ , calculated universal elastic anisotropy index  $A^U$ , and Zener's factor  $A$  of  $YN_{1-x}P_x$  ( $x = 0, 0.25, 0.5, 0.75, 1$ ) alloys.

Materials		$S_{11}$	$S_{12}$	$S_{44}$	$\Delta$ (TPa <sup>-1</sup> )	$A^U$	$A$
YN	This work	0.0031315	-0.0005821	0.0088661	-0.719	3.777	0.83
	Other work	-	-	-	-	-	0.91 <sup>a</sup> ,0.76 <sup>b</sup>
YN <sub>0.75</sub> P <sub>0.25</sub>	This work	0,0033083	-0,0004669	0,0110363	-1.743	39.55	0.567
	Other work	-	-	-	-	-	-
YN <sub>0.5</sub> P <sub>0.5</sub>	This work	0,0055415	-0,0019507	0,0155699	-0.292	27.64	0.621
	Other work	-	-	-	-	-	-
YN <sub>0.75</sub> P <sub>0.25</sub>	This work	0,0042882	-0,0004824	0,0180204	-4.239	50.12	0.529
	Other work	-	-	-	-	-	-

YP	This work	0,0045964	-0,0003853	0,0226065	-6.321	85.45	0.44
	Other work	-	-	-	-	-	0.44 <sup>a</sup> ,0.54 <sup>c</sup>

<sup>a</sup> Ref[24], <sup>b</sup> Ref[10], <sup>c</sup> Ref[33].

**Table (III-17):** Parameter values:  $S_{ij}$ , calculated universal elastic anisotropy index  $A^U$ , and Zener's factor A of  $YN_{1-x}As_x$  (  $x= 0, 0.25, 0.5, 0.75, 1$  ) alloys.

Materials		$S_{11}$	$S_{12}$	$S_{44}$	$\Delta$ (TPa <sup>-1</sup> )	$A^U$	A
YN	This work	0.0031315	-0.0005821	0.0088661	-0.719	3.77	0.837
	Other work	-	-	-	-	-	0.91 <sup>a</sup> ,0.76 <sup>b</sup>
YN <sub>0.75</sub> As <sub>0.25</sub>	This work	0,0039989	-0,0006455	0,0126766	-1.694	11.69	0.732
	Other work	-	-	-	-	-	-
YN <sub>0.5</sub> As <sub>0.5</sub>	This work	0,006485	-0,0022925	0,0181367	-0.29	0.13	0.967
	Other work	-	-	-	-	-	-
YN <sub>0.75</sub> As <sub>0.25</sub>	This work	0,0052876	-0,0005242	0,0212654	-4.820	45.21	0.546
	Other work	-	-	-	-	-	-
YAs	This work	0,0054789	-0,0008463	0,023986	-5.667	50.81	0.527
	Other work	-	-	-	-	-	0.56 <sup>a</sup> ,0.84 <sup>c</sup>

<sup>a</sup> Ref[24], <sup>b</sup> Ref[10], <sup>c</sup> Ref[26].

**Table (III-18):**Parameter values:  $S_{ij}$ , calculated universal elastic anisotropy index  $A^U$ , and Zener's factor A of  $YN_{1-x}Sb_x$  (  $x= 0, 0.25, 0.5, 0.75, 1$  ) alloys.

Materials		$S_{11}$	$S_{12}$	$S_{44}$	$\Delta$ (TPa <sup>-1</sup> )	$A^U$	A
YN	This work	0.0031315	-0.0005821	0.0088661	-0.719	3.77	0.837
	Other work	-	-	-	-	-	0.91 <sup>a</sup> ,0.76 <sup>b</sup>
YN <sub>0.75</sub> Sb <sub>0.25</sub>	This work	0,0046016	-0,0007513	0,0156062	-2.450	17.34	0.685
	Other work	-	-	-	-	-	-
YN <sub>0.5</sub> Sb <sub>0.5</sub>	This work	0,0084715	-0,0035387	0,0256601	-0.189	0.523	0.936
	Other work	-	-	-	-	-	-
YN <sub>0.25</sub> Sb <sub>0.75</sub>	This work	0,006336	-0,0007965	0,0309197	-8.326	75.45	0.461
	Other work	-	-	-	-	-	-
YSb	This work	0,0066268	-0,0008619	0,0327308	-10.60	67.96	0.479
	Other work	-	-	-	-	-	0.38 <sup>c</sup> ,0.36 <sup>d</sup>

<sup>a</sup> Ref[24], <sup>b</sup> Ref[10], <sup>c</sup> Ref[33], <sup>d</sup> Ref[26].

**2. Young modulus, Poisson coefficient, and shear modulus:**

The values of the Young module, the Poisson coefficient, and the shear modulus for certain specific crystallographic orientations were determined by applying the formulae (II-35) and (II-40, II-41). The values obtained for certain specific crystallographic orientations of these mechanical parameters, for their components  $YN_{1-x}P_x$ ,  $YN_{1-x}As_x$  and  $YN_{1-x}Sb_x$ , are given in Table (III-19), (III-20) and (III-21).

- For the values of Young's modulus in different crystalline orientations, we can see that the anisotropy  $\Delta$  takes negative values ( $\Delta < 0$ ), so we have  $E[100] > E[110] > E[111]$  for all alloys. On the other hand, the values of the Poisson's modulus of  $YN_{1-x}B_x$  ( $B = P, As$  and  $Sb$ ) alloys were determined in crystal directions, using thermodynamic constraints  $\Pi$  and  $\delta$ , shows that  $\Pi < 0$ ,  $\delta < 0$ , the term  $\nu[1-10],[110]$  takes maximum values and thus:  $\nu[1-10],[110] > \nu[111],[111] > \nu[100],[001] > \nu[001],[110]$ . About the maximum and minimum of the shear modulus, we can see  $G_1 < G_2$  for all  $YN_{1-x}B_x$  ( $B = P, As$ , and  $Sb$ ) alloys because of the value  $\Delta < 0$  (or  $0 < A < 1$ ).

**Table (III-19):** Anisotropy parameter  $\Delta$ , Extreme values of the Young's modulus  $E$ , thermodynamic constraints  $\Pi$  and  $\delta$ , Extreme values of Poisson's ratio for particular orientations, maximum and minimum values of shear modulus  $G$  for  $YN_{1-x}P_x$  ( $x= 0, 0.25, 0.5, 0.75$  and  $1$ ) alloys.

Materials	$\Delta$ TPa <sup>-1</sup>	E[100] (GPa)	E[110] (GPa)	E[111] (GPa)	$\Pi$	$\delta$	$\nu$ [100]	$\nu$ [110]	$\nu$ [1-10] [110]	$\nu$ [111]	$G_1$ (GPa)	$G_2$ (GPa)
YN	-0.719	319.33	286.43	276.92	-1.61	-0.22	0.185	0.166	0.269	0.227	112.79	134.64
YN <sub>0.75</sub> P <sub>0.25</sub>	-1.743	302.27	239.24	223.70	-0.53	-0.52	0.141	0.111	0.320	0.234	90.61	132.44
YN <sub>0.5</sub> P <sub>0.5</sub>	-0.292	180.45	175.81	174.31	-13.3	-0.05	0.352	0.342	0.368	0.357	64.22	66.73
YN <sub>0.75</sub> P <sub>0.25</sub>	-4.239	233.19	156.05	140.55	-0.22	-0.98	0.112	0.075	0.406	0.266	55.49	104.8
YP	-6.321	217.56	128.91	113.49	-0.12	-1.37	0.084	0.049	0.457	0.282	44.23	100.36

**Table (III-20):** Anisotropy parameter  $\Delta$ , Extreme values of the Young's modulus  $E$ , thermodynamic constraints  $\Pi$  and  $\delta$ , Extreme values of Poisson's ratio for particular orientations, maximum and minimum values of shear modulus  $G$  for  $YN_{1-x}As_x$  ( $x= 0, 0.25, 0.5, 0.75$  and  $1$ ) alloys.

Materials	$\Delta$ TPa <sup>-1</sup>	E[100] (GPa)	E[110] (GPa)	E[111] (GPa)	$\Pi$	$\delta$	$\nu$ [100]	$\nu$ [110]	$\nu$ [1-10] [110]	$\nu$ [111]	$G_1$ (GPa)	$G_2$ (GPa)
YN	-0.719	319.33	286.43	276.92	-1.61	-0.52	0.185	0.166	0.269	0.227	112.79	134.64
YN <sub>0.75</sub> As <sub>0.25</sub>	-1.694	250.06	106.36	195.00	-0.76	-0.42	0.161	0.133	0.307	0.235	78.88	107.65
YN <sub>0.5</sub> As <sub>0.5</sub>	-0.290	154.20	150.82	149.72	-15.7	-0.04	0.353	0.345	0.367	0.357	55.13	56.96
YN <sub>0.25</sub> As <sub>0.75</sub>	-4.820	189.12	219.90	117.62	-0.21	-0.91	0.099	0.068	0.381	0.250	47.02	86.03
YAs	-5.667	182.52	120.29	108.29	-0.29	-1.0	0.154	0.101	0.442	0.295	41.69	79.04

**Table (III-21):** Anisotropy parameter  $\Delta$ , Extreme values of the Young's modulus  $E$ , thermodynamic constraints  $\Pi$  and  $\delta$ , Extreme values of Poisson's ratio for particular orientations, maximum and minimum values of shear modulus  $G$  for  $YN_{1-x}Sb_x$  ( $x= 0, 0.25, 0.5, 0.75$  and  $1$ ) alloys.

Materials	$\Delta$ TPa <sup>-1</sup>	E[100] (GPa)	E[110] (GPa)	E[111] (GPa)	$\Pi$	$\delta$	$\nu$ [100]	$\nu$ [110]	$\nu$ [1-10] [110]	$\nu$ [111]	$G_1$ (GPa)	$G_2$ (GPa)
YN	-0.719	319.33	286.43	276.92	-1.61	-0.22	0.185	0.166	0.269	0.227	112.79	134.64
YN <sub>0.75</sub> Sb <sub>0.25</sub>	-2.450	217.31	171.62	160.38	-0.61	-0.53	0.163	0.128	0.339	0.251	64.07	93.40
YN <sub>0.5</sub> Sb <sub>0.5</sub>	-0.189	118.04	112.59	110.88	-8.63	-0.09	0.125	0.075	0.444	0.422	38.97	41.63
YN <sub>0.25</sub> Sb <sub>0.75</sub>	-8.326	157.81	95.24	84.12	-0.19	-1.31	0.125	0.075	0.472	0.300	32.34	70.09
YSb	-10.60	150.91	90.37	97.71	-0.16	-1.33	0.130	0.072	0.479	0.304	30.55	66.76

### 3. Elastic wave propagation velocities :

To determine the propagation velocities of longitudinal and transverse elastic waves in the  $YN_{1-x}B_x$  ( $B = P, As,$  and  $Sb$ ) alloys, the elastic wave velocity expressions are used for cubic crystals following the propagation directions [100], [110] and [111]. We use relations (II-78), (II-79), and (II-80) (Chapter II). The results obtained in this calculation are given in Tables (III-22), (III-23), and (III-24).

The results are in Tables (III-22), (III-23), and (III-24). It can be seen that the propagation velocities of the longitudinal waves in the three propagation directions are great than the propagation velocities of the transverse waves for the  $YN_{1-x}B_x$  ( $B = P, As,$  and  $Sb$ ) compounds.

On the other hand, we can observe the decrease of the acoustic wave velocities in the same trend as a decrease of the elastic constants when we go from P to As to Sb. this indicates that the speed at which sound waves propagate longitudinal or accidentally is faster in the  $YN_{1-x}P_x$  than followed by  $YN_{1-x}As_x$  than  $YN_{1-x}Sb_x$ .

We also note, show that longitudinal elastic waves ( $V_l$ ) (called compression waves) for  $YN_{1-x}B_x$  ( $B = P, As,$  and  $Sb$ ) compounds. Propagate faster in the directions [100] (which is considered the most compressible direction) and are relatively slow according to directions [110] and [111] (directions considered less compressible). This result confirms that the three compounds are stiffer along the diagonals [100] and the calculated results of the anisotropy factor ( $0 < A < 1$ ) for these compounds. Also, the transverse acoustic waves ( $V_t$ ) (also called the elastic shear waves) are faster according to directions [110] (with the plane of polarization at (1-10)), they are relatively slow in [110] (polarization [100] ( $V_{t,1}$ )) and [100] directions (with a polarization plane following [001] ( $V_{t1,2}$ )) and directions [111] (with a

polarization plane following [111]) for all YN  $1-xB_x$  (B = P, As and Sb) compounds.

**Table (III-22):** The elastic wave velocities (in m/s) for different propagation directions for YN  $1-xP_x$  (0. 0.25, 0.5, 0.75, 1 ) in rock salt phase.

Compos- ition x	propagation direction		[100]		[110]			[111]	
	Polarization plane		[100]	[100]	[100]	[100]	[1-10]	[111]	[111]
		$\rho(\frac{g}{cm^3})$	$V_l(m/s)$	$V_{t1,2}(m/s)$	$V_l(m/s)$	$V_{t1}(m/s)$	$V_{t2}(m/s)$	$V_l(m/s)$	$V_{t1,2}(m/s)$
YN	This work	5340	8083.91	4595.82	7826.54	4595.63	5021.30	7738.87	4883.53
	Other calcul	-	-	-	-	-	-	-	-
X=0.25	This work	5090	7891.34	3552.03	7256.53	3552.03	4715.18	7032.21	4362.06
	Other calcul	-	-	-	-	-	-	-	-
X=0.5	This work	4790	6606.19	3403.70	6048.88	3403.70	4317.16	5851.34	4035.71
	Other calcul	-	-	-	-	-	-	-	-
X=0.75	This work	4550	7263.39	3492.31	6474.99	3492.31	4798.70	6189.92	4406.48
	Other calcul	-	-	-	-	-	-	-	-
YP	This work	4370	7160,15	3170,94	6203.08	3170,94	4779.58	5849.36	4310.59
	Other calcul	-	-	-	-	-	-	-	-

**Table (III-23):** The elastic wave velocities (in m/s) for different propagation directions for YN  $1-xAs_x$  (0. 0.25, 0.5, 0.75, 1 ) in rocksalt phase.

Compos- ition x	propagation direction		[100]		[110]			[111]	
	Polarization plane		[100]	[100]	[100]	[100]	[1-10]	[111]	[111]
		$\rho(\frac{g}{cm^3})$	$V_l(m/s)$	$V_{t1,2}(m/s)$	$V_l(m/s)$	$V_{t1}(m/s)$	$V_{t2}(m/s)$	$V_l(m/s)$	$V_{t1,2}(m/s)$
YN	This work	5340	8083.83	4595.63	7826.53	4595.63	5021.30	7738.87	4883.53
	Other calcul	-	-	-	-	-	-	-	-
X=0.25	This work	5300	7092.96	3857.97	6699.36	3857.97	4506.95	6562.93	4301.52
	Other calcul	-	-	-	-	-	-	-	-
X=0.5	This work	5620	5679.37	3132.19	5647.33	3132.19	3184.26	5637.62	3167.00
	Other calcul	-	-	-	-	-	-	-	-
X=0.75	This work	5310	6035.58	2975.86	5361.96	2975.86	4026.26	5159.61	3709.32
	Other calcul	-	-	-	-	-	-	-	-
YAs	This work	5360	6007.36	2788.93	5396.18	2788.93	3840.29	5176.44	3524.85
	Other calcul	-	-	-	-	-	-	-	-

**Table (III-24):** The elastic wave velocities (in m/s) for different propagation directions for  $YN_{1-x}Sb_x$  (0, 0.25, 0.5, 0.75, 1) in rock salt phase.

Compo sition x	propagation direction		[100]		[110]			[111]	
	Polarization plane		[100]	[100]	[100]	[100]	[1-10]	[111]	[111]
		$\rho(\frac{g}{cm^3})$	$V_l(m/s)$	$V_{t1,2}(m/s)$	$V_l(m/s)$	$V_{t,1}(m/s)$	$V_{t,2}(m/s)$	$V_l(m/s)$	$V_{t1,2}(m/s)$
YN	This work	5340	8083.83	4595.63	7826.53	4595.63	5021.30	7738.87	4883.53
	Other calcul	-	-	-	-	-	-	-	-
X=0.25	This work	5400	6556.09	3442.84	6126.82	3442.84	4159.04	5976.88	3934.82
	Other calcul	-	-	-	-	-	-	-	-
X=0.5	This work	6140	4900.34	2519.34	4855.93	2519.34	2603.92	4841.03	2576.03
	Other calcul	-	-	-	-	-	-	-	-
X=0.75	This work	5600	5407.23	2403.16	4742.99	2403.16	3537.99	4499.84	3204.68
	Other calcul	-	-	-	-	-	-	-	-
YSb	This work	6000	5016.64	2256.47	4430.66	2256.47	3259.98	4217.29	2963.48
	Other calcul	-	-	-	-	-	-	-	-

### III-5. Electronic structure of $Y_{1-x}M_xN$ (M = Sc and La) and $YN_{1-x}B_x$ (B = P, As and Sb) alloys:

Understanding the electronic structure of a material requires the study of the electronic band structure and the partial and total state density PDOS and TDOS, which provide important information for the characterization of the electronic properties of a material, and the energy bands give the possible energies of an electron as a function of the wave vector. These bands are represented in the reciprocal space, and for convenience, the higher symmetrical directions in the first area of Brillouin are treated. We will present our results for  $Y_{1-x}M_xN$  (M = Sc and La) and  $YN_{1-x}B_x$  (B = P, As and Sb) compounds using two approximations, GGA PBE, and HSE06.

#### III-5-1 . Band structures and T-DOS and P-DOS of $Y_{1-x}M_xN$ (M = Sc and La):

##### III-5-1-1.The compounds $Y_{1-x}Sc_xN$ for (x = 0, 0.25, 0.50, 0.75 and 1)

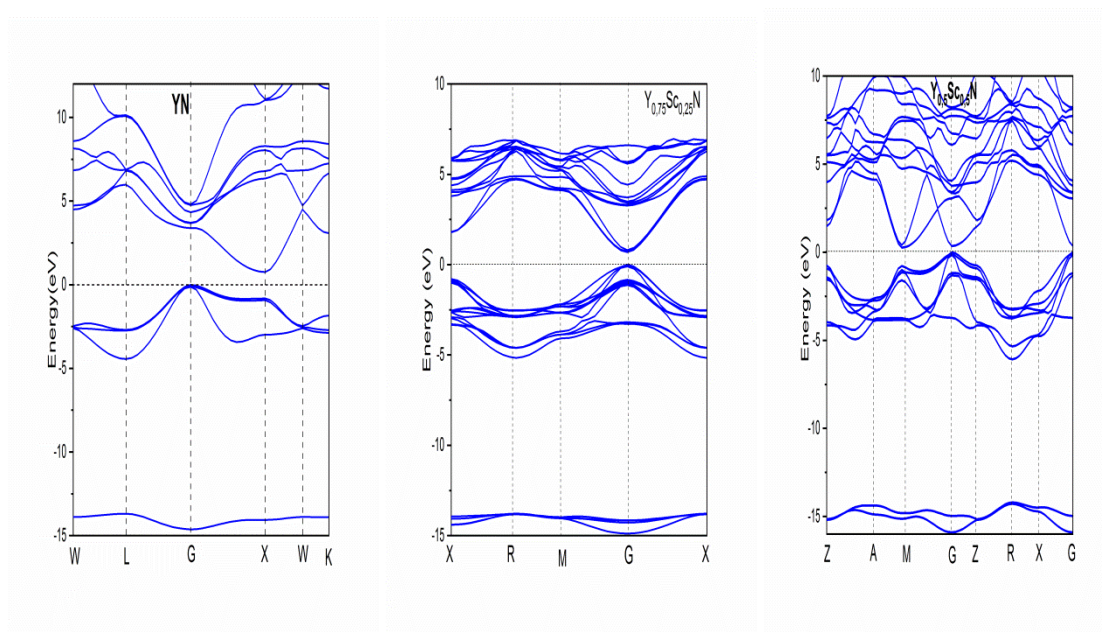
The electronic properties of  $Y_{1-x}Sc_xN$  compounds are obtained by calculating the band structures. The calculated band structures of the compounds along the high symmetry lines of the first Brillouin zone using HSE06. Schemes show in FIGURE ( III-7). For YN and ScN,

the maximum valence band lying at the G-point and the minimum of the conduction band lying at the X-point show it is an indirect band gap semiconductor. While comparing the electronic structures of  $Y_{1-x}Sc_xN$  ( $x = 0.25, 0.50, \text{ and } 0.75$ ) with ScN and YN, It is clear from FIGURE ( III-7), we find that the compounds  $Y_{1-x}Sc_xN$  ( $x = 0.25, 0.50, \text{ and } 0.75$ ) have a direct band gap (G–G) character. It shows in Table (III-25).

**Table (III-25):** Experimental and calculated energy band of  $Y_{1-x}Sc_xN$  ( $x=0, 0.25, 0.5, 0.75,$  and 1) with different approximations GGA, and HSE06.

Composition x	Eg (eV)			
	This work (GGA-PBE)	HSE06	Exp	Other calculation
YN	0	0.755	0.85 <sup>a</sup>	0.8 <sup>b</sup> , 1.0 <sup>a</sup> , 0.761 <sup>c</sup>
$Y_{0.75}Sc_{0.25}N$	0.01	0.692	-	-
$Y_{0.5}Sc_{0.5}N$	0.0	0.257	-	-
$Y_{0.25}Sc_{0.75}N$	0.045	0.723	-	-
ScN	0.0	0.860	0.9 <sup>d</sup>	0.99 <sup>e</sup> , 0.97 <sup>f</sup>

<sup>a</sup> Ref [32] , <sup>b</sup> Ref [33] , <sup>c</sup> Ref [34] , <sup>d</sup> Ref [35] , <sup>e</sup> Ref [36] , <sup>f</sup> Ref [37].



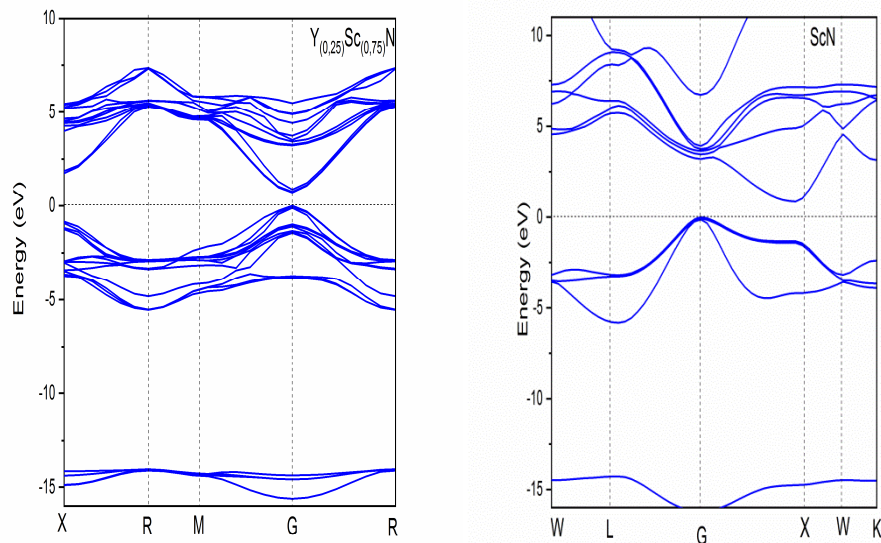


**FIGURE ( III-7):** shows the scale structures calculated along the high symmetry waves of  $Y_{1-x}Sc_xN$  alloys with different x concentration.

The density of states (PDOS and TDOS) is an important physical quantity to understand the nature of the electronic band structure of a material. Most electronic transport properties are determined based on knowledge of the density of states. It also makes it possible to know the nature of the chemical bonds in a material. FIGURE ( III-8) shows the density of states of  $Y_{1-x}Sc_xN$  alloys. For the YN, it notes that the states in the interval (-13.5, -11.5 eV) derive by the state participation N(2s). While intervals (-4.5eV, 0eV) present the contribution of the states N(p) with the association of states (5s, p, 4d) of the Y atom that interacts. The minimum of the conduction band is formed by the contribution of the states Y(5s, p, 4d) and a small contribution of the states N (2s, 2p). It is also evident that for ScN, the conduction band is occupied by N(2p) and Sc(3s,3d), whereas the valence band is occupied by N(2s) in the interval (-16.11,-13.33), and N(2p), Sc( 3s,3p,3d) in the field (-5.8, 0 eV). For the ternary alloys, Y(4d), Sc (3d), and N(2p) states are the primary contributors to the conduction bands, while the valence bands are mainly composed of two intervals: The first interval limit between (-16,-13 eV). It comes from a domination of the states of N(2s) for  $Y_{0.75}Sc_{0.25}N$ ,  $Y_{0.5}Sc_{0.5}N$  but N(2s) and Y(5s) for  $Y_{0.25}Sc_{0.75}N$  in interval ( -16,-13.5 eV) . The second interval is limited between (-4.45 , 0 eV). It comes from a domination of states N(2p) and a contribution of Y(5s , 4d) and Sc(3d) states for  $Y_{0.75}Sc_{0.25}N$ ,  $Y_{0.5}Sc_{0.5}N$  and Y(3p, 4d) for  $Y_{0.25}Sc_{0.75}N$ .

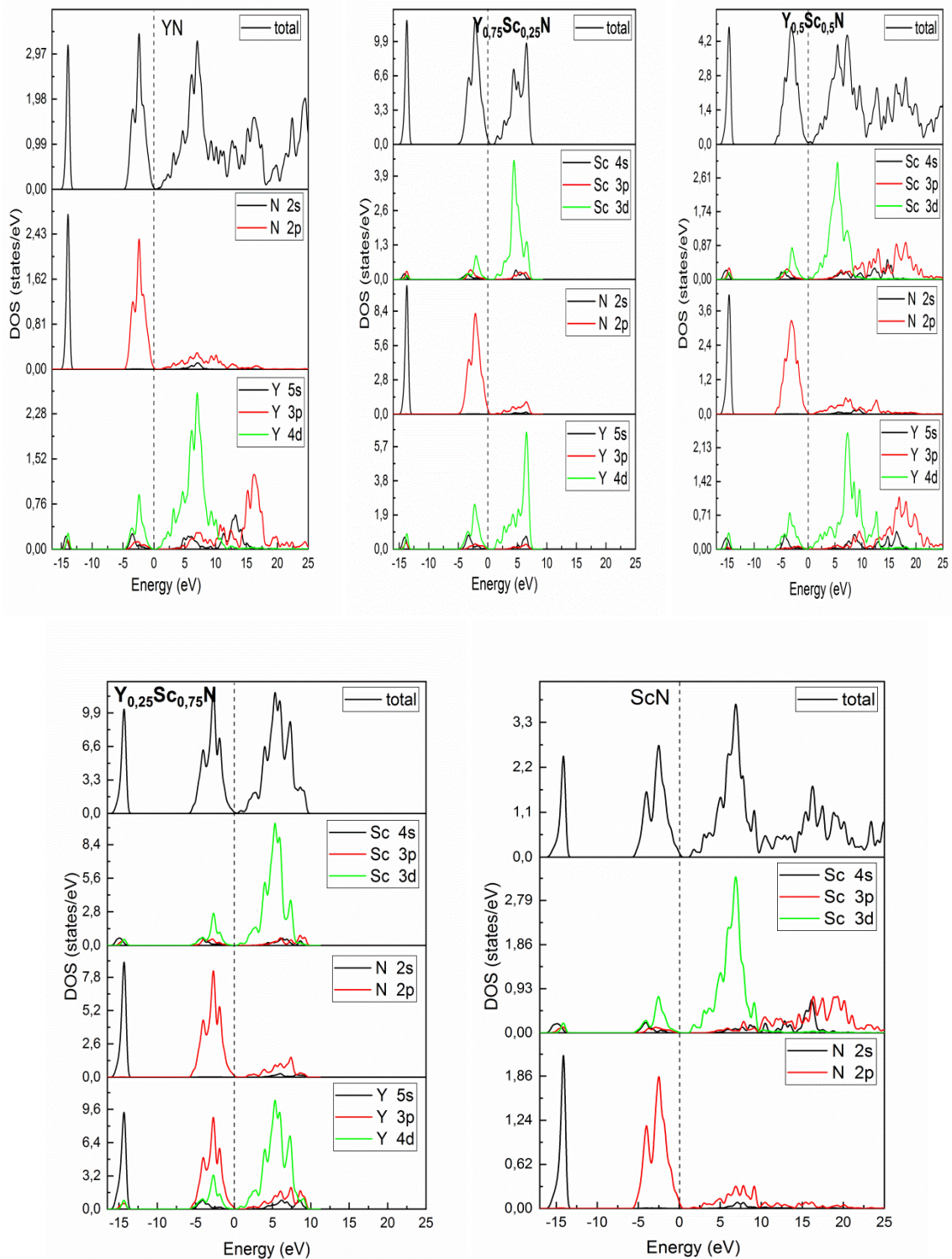


FIGURE ( III-8): Total and partial density of states (TDOS and PDOS) for  $Y_{1-x}Sc_xN$  alloys with the approximation  $\langle HSE06 \rangle$ .

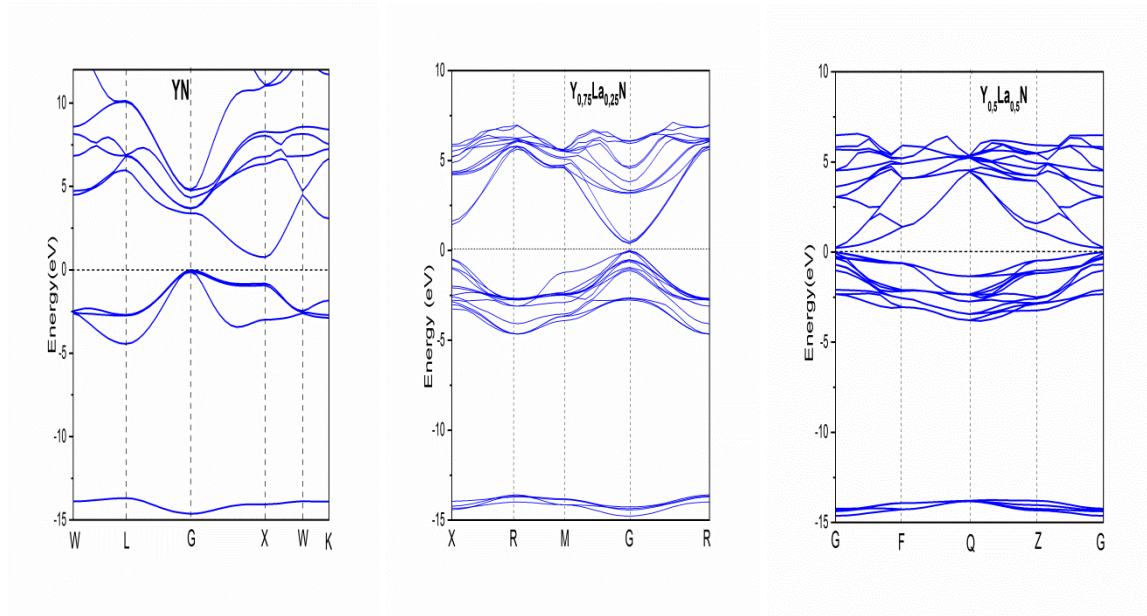
**III-5-1-2. The compounds  $Y_{1-x}La_xN$  for ( $x = 0, 0.25, 0.50, 0.75$  and  $1$ ) :**

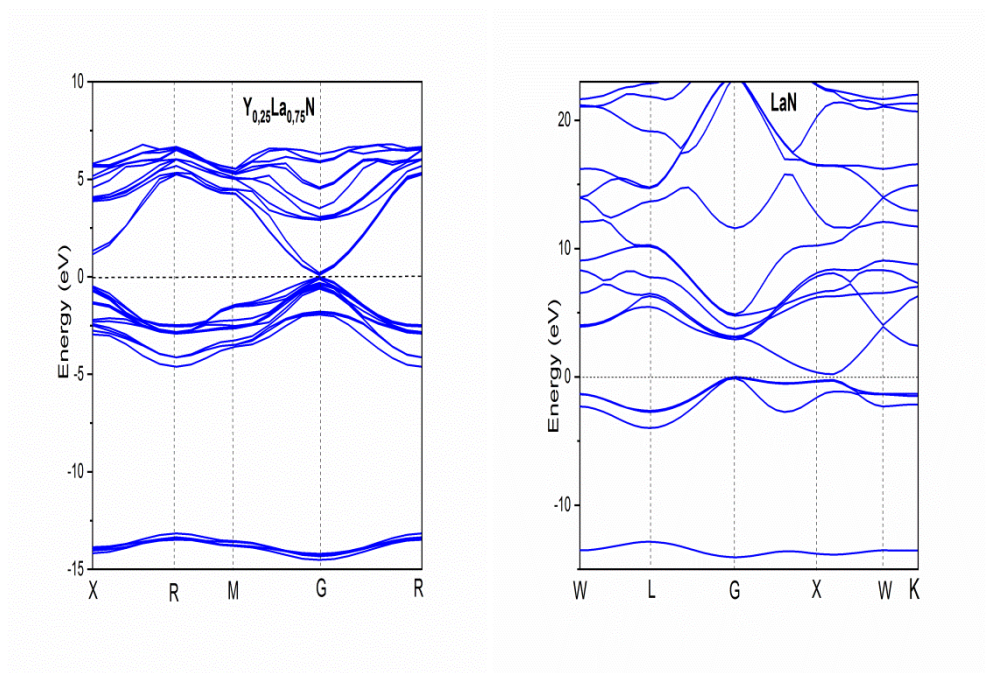
Studying the electronic properties is crucial to understanding the stability of the different structures of the  $Y_{1-x}La_xN$  alloys. We show results in FIGURE ( III-9). Starting, the electronic structure of YN and LaN shows that they have an indirect band gap, in which the maximum of the valence band locates at G point while the conduction band minimum locates at X. FIGURE ( III-9) shows for  $Y_{1-x}La_xN$  ( $x = 0.25, 0.50,$  and  $0.75$ ) the band gap is direct and occurs at G point (G-G), the  $Y_{1-x}La_xN$  alloys turn into a direct band gap semiconductor.

**Table (III-26):** Experimental and calculated energy band of  $Y_{1-x}La_xN$  ( $x=0, 0.25, 0.5, 0.75,$  and  $1$ ) with different approximations GGA, and HSE06.

Composition x	Eg (eV)			
	This work (HSE06)	GGA-PBE	Exp	Other calculation
YN	0.755	0	0.85 <sup>a</sup>	0.8 <sup>b</sup> , 1.0 <sup>a</sup> , 0.761 <sup>c</sup>
$Y_{0.75}La_{0.25}N$	0.378	0.043	-	-
$Y_{0.5}La_{0.5}N$	0.229	0	-	-
$Y_{0.25}La_{0.75}N$	0.173	0.023	-	-
LaN	0.201	0	0.45 <sup>a</sup>	0.3 <sup>c</sup>

<sup>a</sup> Ref [32] , <sup>b</sup> Ref [33] , <sup>c</sup> Ref [34].





**FIGURE( III-9):** Calculated electronic band structure of  $Y_{1-x}La_xN$  alloys with different  $x$  concentration with the approximation «HSE06».

The partial electronic state density gives information on the occupation of the electronic strips of material. FIGURE ( III-10) shows the partial and total state densities of  $Y_{1-x}La_xN$  alloys. For YN and LaN, the conduction band is mainly formed from Y-4d, and La-5d states, respectively. The valence band dominates by N-2p states. For the ternary alloys, Y-4d and La-5d states are the primary contributors to the conduction bands, while the valence bands are at most composed of N-2p states. It is seen that the distribution of the states appears similar for the ternary compounds for some differences in details.

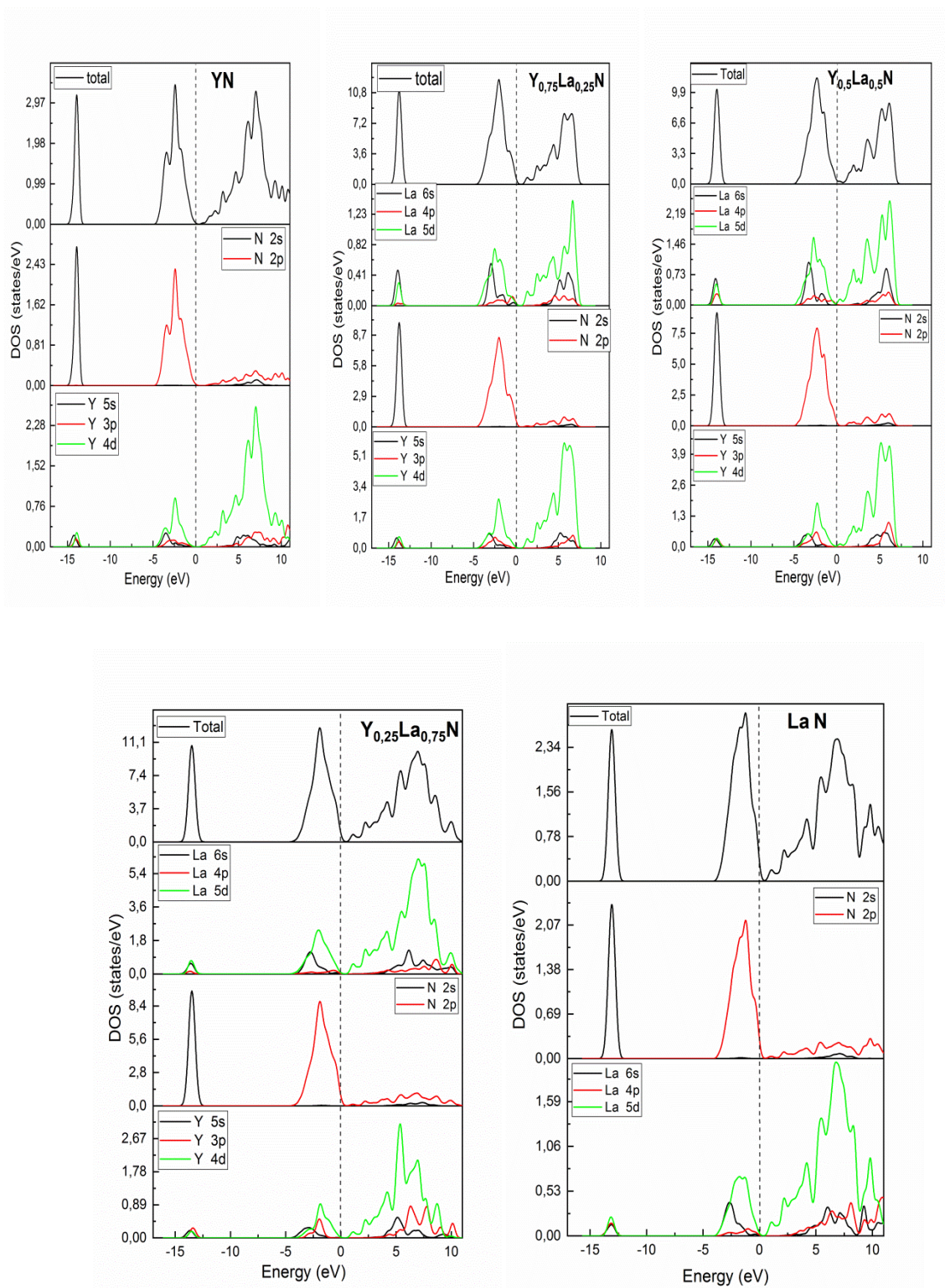


FIGURE ( III-10): Calculated total and partial density of states of  $Y_{1-x}La_xN$  alloys with different  $x$  concentrations with the approximation «HSE06».

III-5.2 - Band structures and T-DOS and P-DOS of  $YN_{1-x}B_x$  (B = P, As and Sb) alloys:

III-5-2-2. The compounds  $YN_{1-x}P_x$  (x = 0, 0.25, 0.50, 0.75 and 1):

The  $YN_{1-x}P_x$  alloy band structure calculations for each concentration (x=0, 0.25, 0.5, 0.75, and 1) were performed in the high symmetry directions in the first Brillouin area, using two approximations, GGA PBE and HSE06 (see FIGURE ( III-11) →III.15)). We note for the approximations GGA PBE that: YN, x=0.5 and YP: The valence and conduction bands overlap each other, this explains the semi-metallic character. But for x=0.25 and x=0.75, there has a direct gap  $E_g = 0.294$  eV and  $E_g = 0.092$  eV, respectively. For the approximations HSE06, we notice x= 0.5 and YP semi-metallic character. As regards YN, the maximum of the valence band at point G and the minimum of the conduction band at point X shows that the compound YN has an indirect gap ( $E_g = 0.755$  eV). for x=0.25 and x=0.75 have a direct band gap in the G direction, estimates  $E_g = 0.036$  eV and  $E_g = 0.34$  eV, respectively.

**Table (III-27):** Experimental and calculated energy band of  $YN_{1-x}P_x$  (x=0, 0.25, 0.5, 0.75, and 1) with different approximations GGA, and HSE06.

Composition x	Eg (eV)			
	This work GGA-PBE	HSE06	Exp	Other calculation
YN	0	0.755	0.85 <sup>a</sup>	0.8 <sup>b</sup> , 1.0 <sup>a</sup> , 0.761 <sup>c</sup>
YN <sub>0.75</sub> P <sub>0.25</sub>	0.294	0.036	-	-
YN <sub>0.5</sub> P <sub>0.5</sub>	0	0	-	-
YN <sub>0.25</sub> P <sub>0.75</sub>	0.092	0.34	-	-
YP	0	0	-	0 <sup>d</sup>

<sup>a</sup> Ref [32], <sup>b</sup> Ref [33], <sup>c</sup> Ref [34], <sup>d</sup> Ref [24].

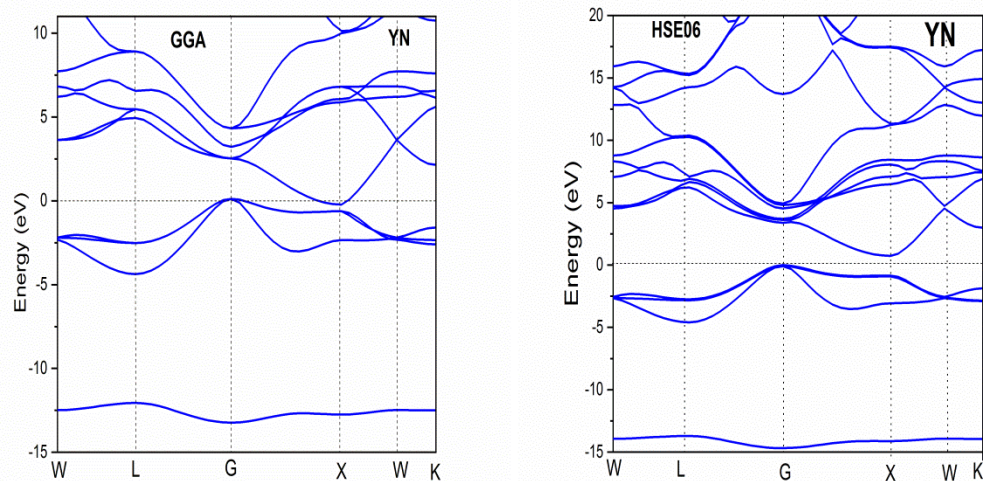


**FIGURE ( III-11) :** Energy band structure of YN compound using the approximation «GGA and HSE06».

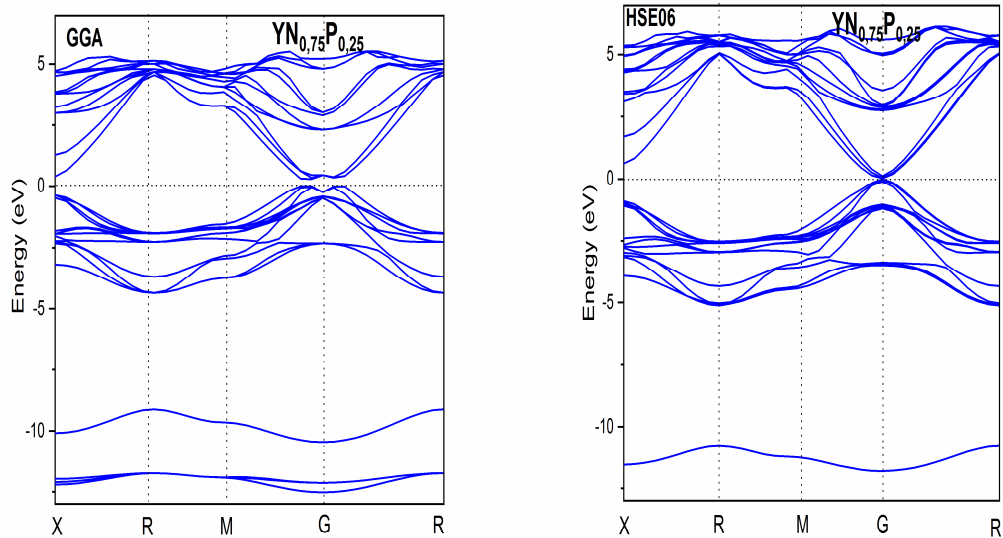


FIGURE ( III-12): Energy band structure of  $YN_{0.75}P_{0.25}$  compound using the approximation «GGA and HSE06».

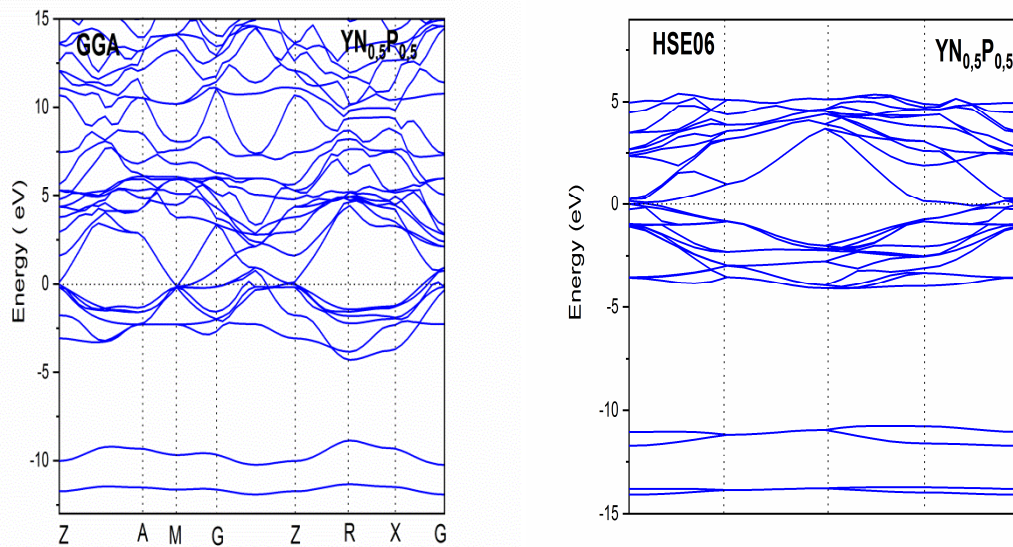


FIGURE ( III-13) :Energy band structure of  $YN_{0.5}P_{0.5}$  compound using the approximation «GGA and HSE06»

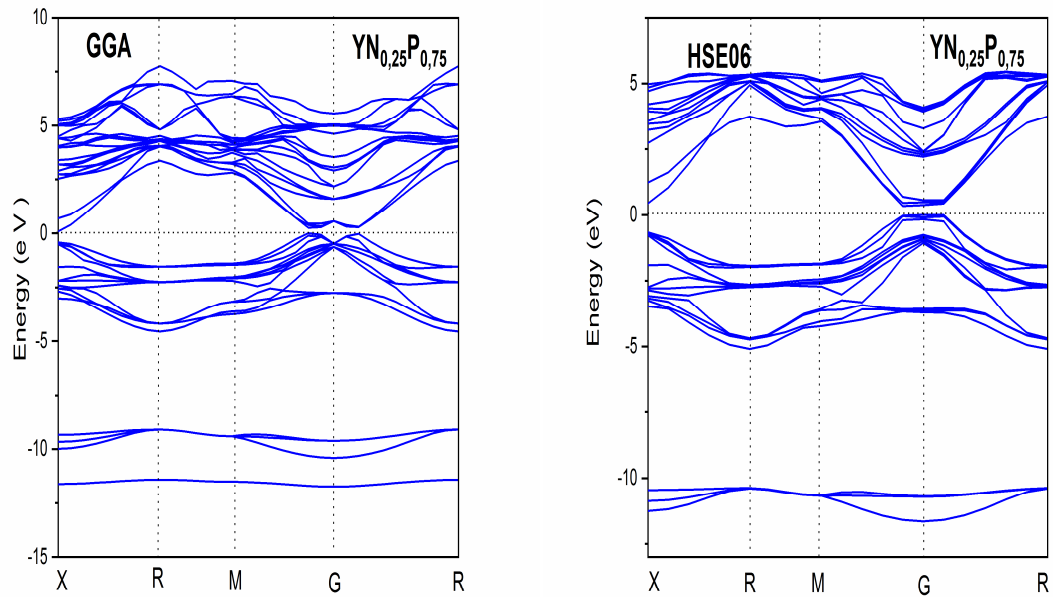


FIGURE ( III-14): Energy band structure of  $YN_{0.25}P_{0.75}$  compound using the approximation «GGA and HSE06».

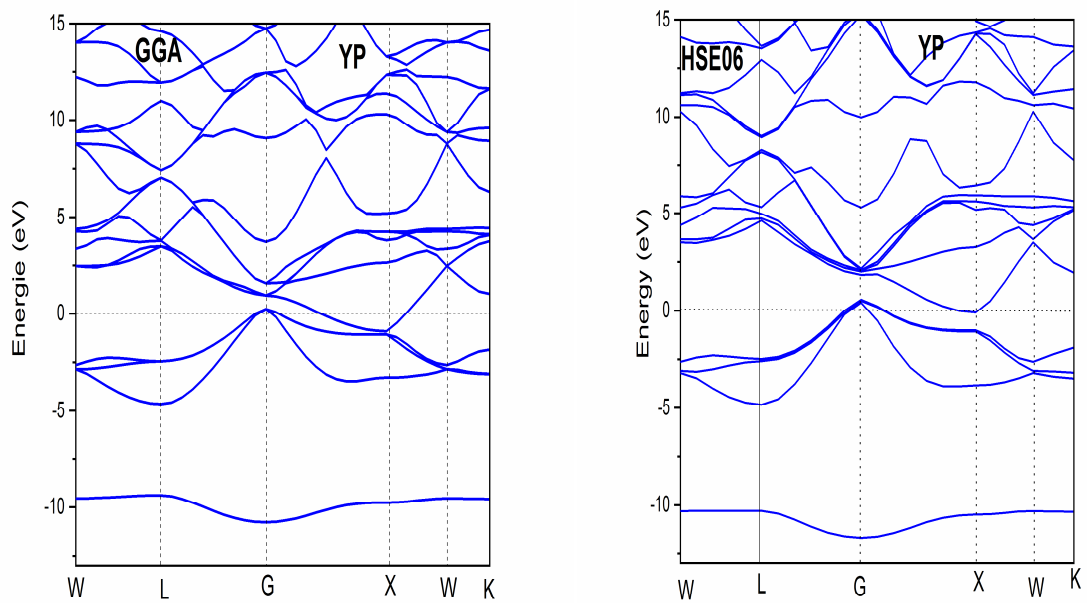


FIGURE ( III-15) : Energy band structure of YP compound using the approximation «GGA and HSE06».

To determine the distribution of electronic states according to the energy that makes up the energy bands of the compounds  $YN_{1-x}P_x$  ( $x = 0, 0.25, 0.5, 0.75, \text{ and } 1$ ). The diagrams of the densities of total and partial states (TDOS and PDOS) are calculated using HSE06 and shown in FIGURE ( III-16). The figure shows that the valence band of YN and YP consists of two groups named: VB1 and VB2, and those of  $YN_{0.75}P_{0.25}$ ,  $YN_{0.5}P_{0.5}$ ,  $YN_{0.25}P_{0.75}$  fall into three groups called VB1, VB2, and VB3.

**For YN and YP:**

- The first interval of valence bands (VB1) is limited between YN (-13.5 and -11.5eV) and YP (-10.97, 9 eV). They come from the domination of states N (2s) and P (3s).
- The second interval of valence bands (VB2) between YN (-4.5 and 0 eV) and YP (-5 and 0 eV), in which the N (2s) and P (3s) states dominates and a small contribution of the Y(5s, p, 4d) states.

**For  $YN_{0.75}P_{0.25}$ ,  $YN_{0.5}P_{0.5}$  and  $YN_{0.25}P_{0.75}$ :**

- The first interval of valence bands (VB1) is limited between  $YN_{0.75}P_{0.25}$  (-14.5, -12.8ev),  $YN_{0.5}P_{0.5}$  (-14.5, -13ev),  $YN_{0.25}P_{0.75}$  (-13.7, 12.3ev) are composed of electronic states N (2s).
- The second interval (VB2) between (-11.8, -10), (-12.1, -10.1) and (-11.7, -9.5) consists mainly of electronic states [ N (2s), P (3s) ], P (3s) and P (3s) for  $YN_{0.75}P_{0.25}$ ,  $YN_{0.5}P_{0.5}$  and  $YN_{0.25}P_{0.75}$  respectively.
- The third interval (VB3) between  $YN_{0.75}P_{0.25}$  (-4.9,0),  $YN_{0.5}P_{0.5}$  (-5.35,0) and  $YN_{0.25}P_{0.75}$  (-4.9,0) consists mainly of N (2s), P (3s), Y (4d) electronic states.

The BC conduction band consists of each compound of a mixture of several electronic states; YN: N (2s,2p) and Y (5s,3p,4d), YP :P (3s,3p) and Y (5s,3p,4d) et  $YN_{0.75}P_{0.25}$ ,  $YN_{0.5}P_{0.5}$  et  $YN_{0.25}P_{0.75}$ : Y (4d).

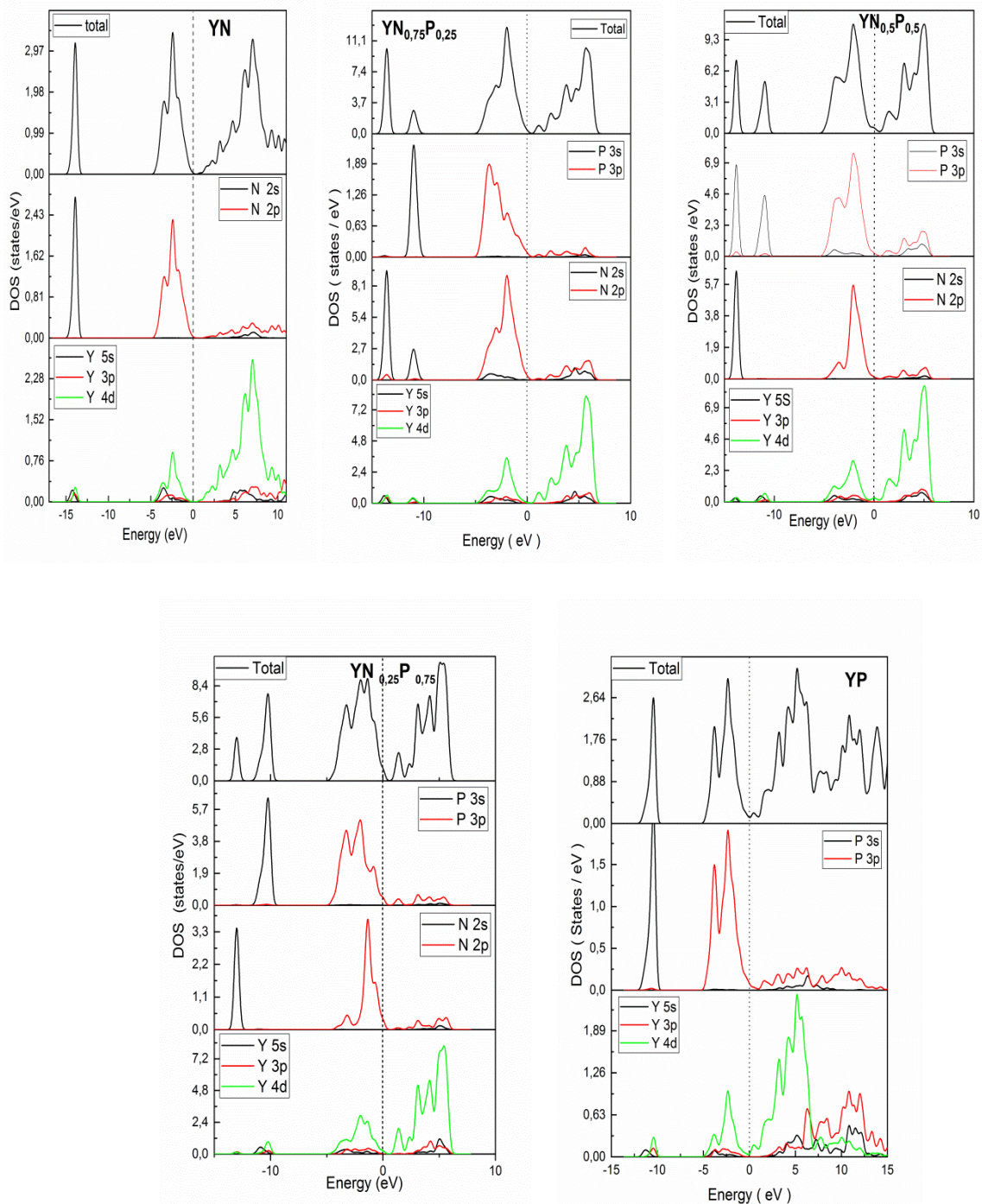


**FIGURE ( III-16):** The total and partial state density (DOS) of  $YN_{1-x}P_x$  ( $x = 0.25, 0.50, 0.75,$  and  $1$ ) with the approximation «HSE06».

III-5-2-2. The compounds  $YN_{1-x}As_x$  ( $x = 0, 0.25, 0.50, 0.75$  and  $1$ )

The energy band structures of  $YN_{1-x}As_x$  ( $x = 0, 0.25, 0.50, 0.75,$  and  $1$ ) calculated using the GGA and HSE06 approximation are shown in FIGURE ( III-17)→ ( III-20). From this Figure, we can note the following observations:

For  $YN_{0.75}As_{0.25}$  and  $YN_{0.25}As_{0.75}$ , the maximum of the valence band and the minimum of the conduction band are at the same point of high symmetry G, the alloys obtained are direct gap semiconductors, with an exception for YAs and alloy  $YN_{0.5}As_{0.5}$ , we note that there is an indirect overlap between the conduction band and the valence band that the system has a semi-metallic character, in Table (III-28), the values obtained from the energy gaps of the  $YN_{1-x}As_x$  alloy for different composition values (x).

**Table (III-28):** Experimental and calculated energy band of  $YN_{1-x}As_x$  ( $x=0, 0.25, 0.5, 0.75,$  and  $1$ ) with different approximations of GGA, and HSE06.

Composition x	Eg (eV)			
	This work (GGA)	HSE06	Exp	Other calculation
YN	0	0.755	0.85 <sup>a</sup>	0.8 <sup>b</sup> , 1.0 <sup>a</sup> , 0.761 <sup>c</sup>
$YN_{0.75}As_{0.25}$	0.236	0.052	-	-
$YN_{0.5}As_{0.5}$	0	0	-	-
$YN_{0.25}As_{0.75}$	0.068	0.018	-	-
YAs	0	0	0	0

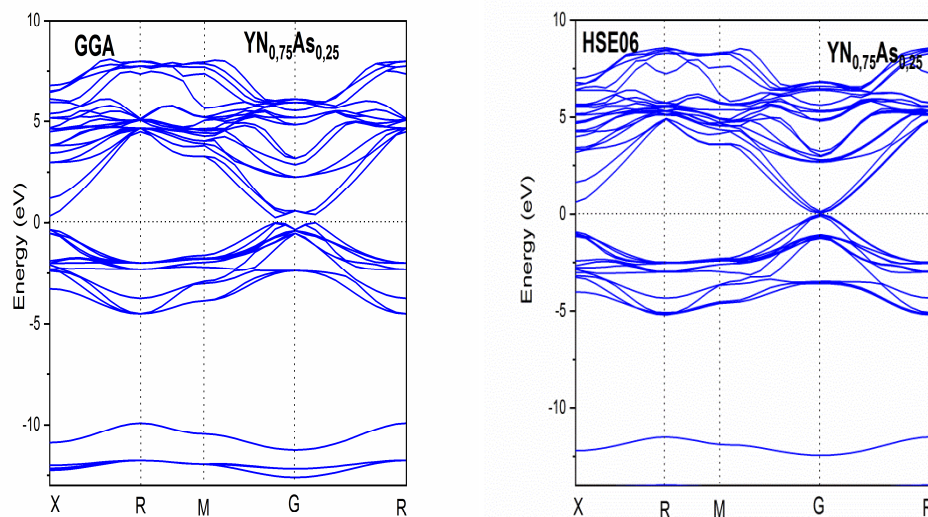


FIGURE ( III-17): Energy band structure of  $YN_{0.75}As_{0.25}$  compound using the approximation «GGA and HSE06».

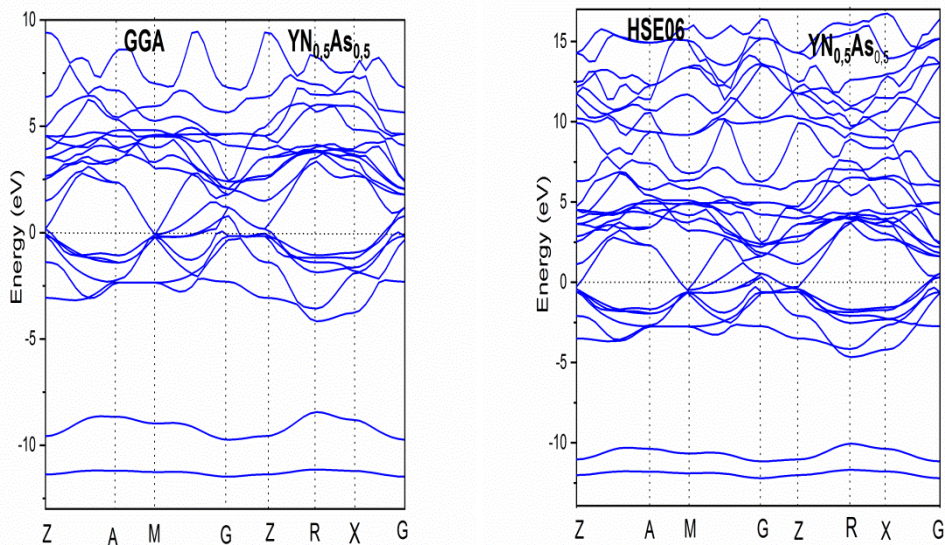


FIGURE ( III-18): Energy band structures of the compounds  $YN_{0.5}As_{0.5}$  calculated in GGA and HSE06 approximation.

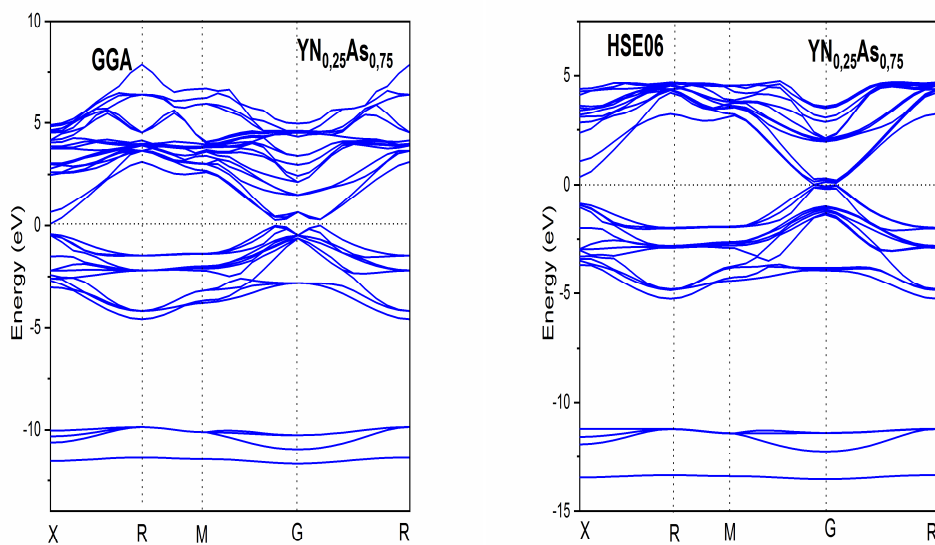


FIGURE ( III-19): Energy band structures of the compounds  $YN_{0.25}As_{0.75}$  calculated in GGA and HSE06 approximation.

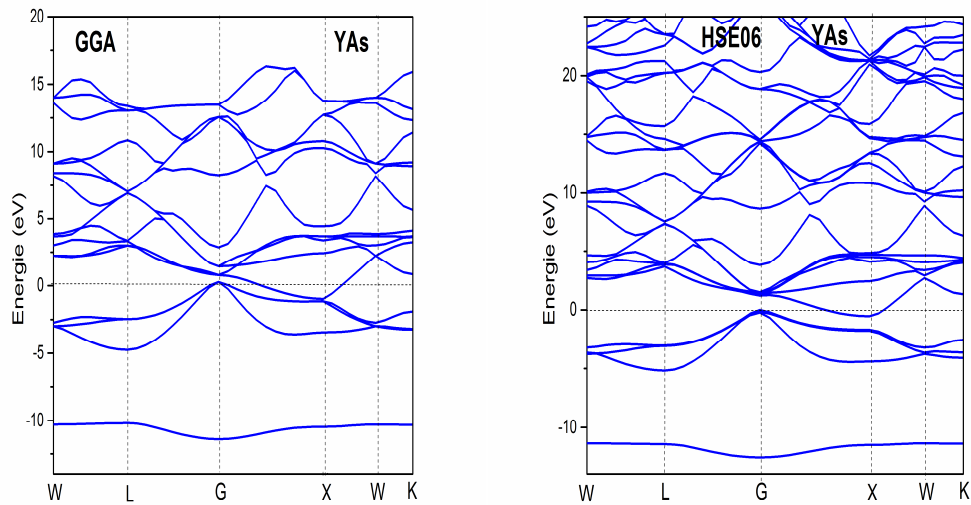
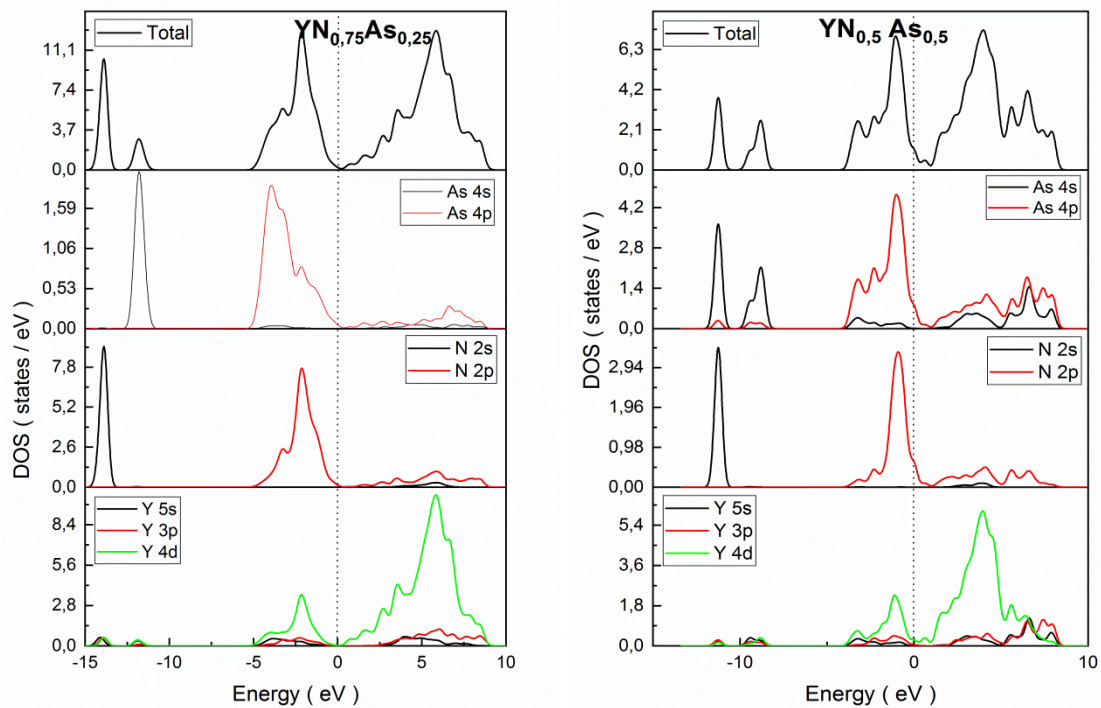
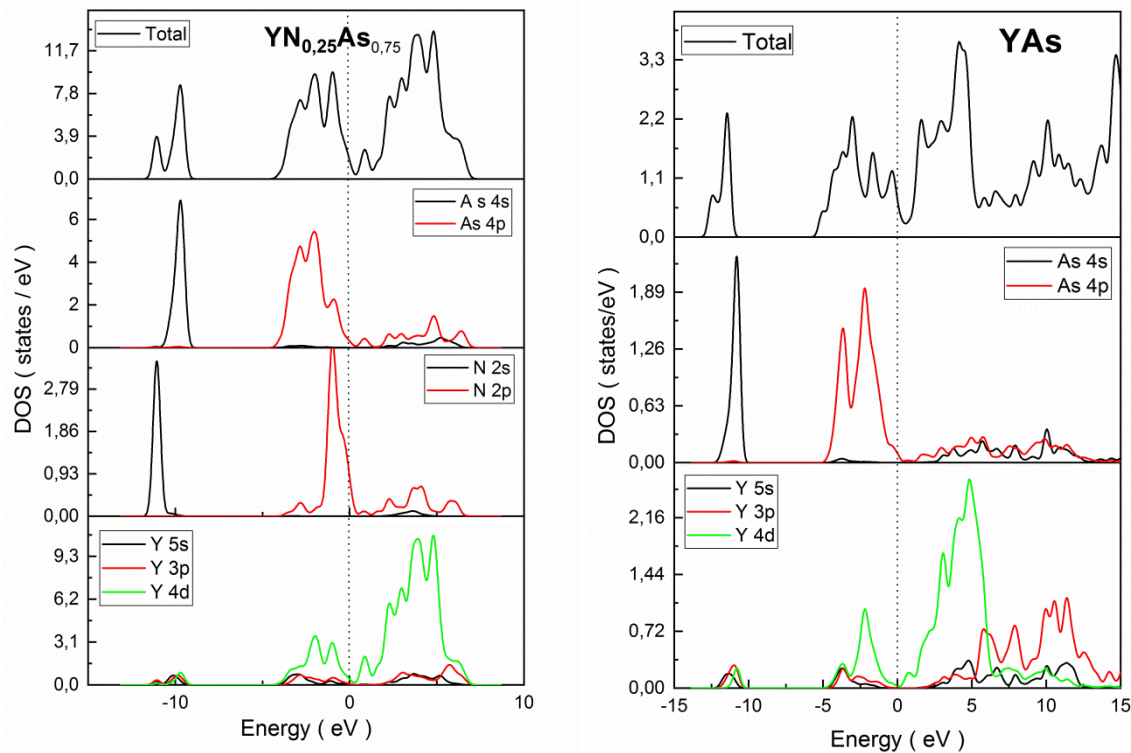


FIGURE ( III-20): Energy band structures of the compounds YAs calculated in GGA and HSE06 approximation.





**FIGURE ( III-21):** The total and partial state density (DOS) of  $YN_{1-x}As_x$  ( $x = 0.25, 0.50, 0.75$  and  $1$ ) with the approximation «HSE06».

Total and partial state densities (DOS) of  $YN_{1-x}As_x$  ( $x = 0.25, 0.50, 0.75,$  and  $1$ ) are calculated. FIGURE ( III-21) illustrates the densities of total and partial states obtained by HSE06 of these alloys. We can distinguish that the conduction band is mainly formed from the Y-4d state for alloys  $YN_{0.75}As_{0.25}$ ,  $YN_{0.5}As_{0.5}$ , and  $YN_{0.25}As_{0.75}$ , while YAs are dominated by Y-4d and 3p states. We come to the valence band, which we can note the following:

For alloys, we can see that the distribution of states seems similar for the  $YN_{0.75}As_{0.25}$ ,  $YN_{0.5}As_{0.5}$  and  $YN_{0.25}As_{0.75}$  compounds and are grouped into three groups. The first group is mainly composed of N(2s) -  $YN_{0.75}As_{0.25}$ , N(2s) -  $YN_{0.5}As_{0.5}$ , (4s) - As and N(2s) -  $YN_{0.25}As_{0.75}$ . Group II: is formed by the states (4s) -As for all alloys  $YN_{0.75}As_{0.25}$ ,  $YN_{0.5}As_{0.5}$ ,  $YN_{0.25}As_{0.75}$ .

Group III: is formed by the states Y (4d), N(2s) and As(4s) for all alloys  $YN_{0.75}As_{0.25}$ ,  $YN_{0.5}As_{0.5}$ ,  $YN_{0.25}As_{0.75}$ . But for YAs, the valence band consists of two bands: Group I: comes from the participation of the states (4s) of As. Group II: presents the contribution of states (4p) of the As atom with the association of states (5s, p, and 4d) of the Y atom.

III-5-2-3. The compounds  $YN_{1-x}Sb_x$  ( $x = 0, 0.25, 0.50, 0.75$  and  $1$ )

FIGURE ( III-22)  $\rightarrow$  (III-25) shows that for  $YN_{0.75}Sb_{0.25}$  and  $YN_{0.25}Sb_{0.75}$ , the maximum of the valence band and the minimum of the conduction band are at the same point of high symmetry G, so the alloys obtained are direct gap semiconductors, with an exception for YAs and alloy  $YN_{0.5}Sb_{0.5}$ , we note that there is an indirect overlap between the conduction band and the valence band. This means that the system has a semi-metallic character. in Table (III-29) the values obtained energy gaps of the  $YN_{1-x}Sb_x$  alloy for different composition values (x).

**Table (III-29):** Experimental and calculated energy band of  $YN_{1-x}Sb_x$  ( $x=0, 0.25, 0.5, 0.75,$  and  $1$ ) with different approximations GGA, and HSE06.

Composition x	Eg (eV)			
	This work (GGA)	HSE06	Exp	Other calculation
YN	0	0.755	0.85 <sup>a</sup>	0.8 <sup>b</sup> , 1.0 <sup>a</sup> , 0.761 <sup>c</sup>
$YN_{0.75}Sb_{0.25}$	0.109	0.072	-	-
$YN_{0.5}Sb_{0.5}$	0	0	-	-
$YN_{0.25}Sb_{0.75}$	0.042	0.077	-	-
YSb	0	0	0	0

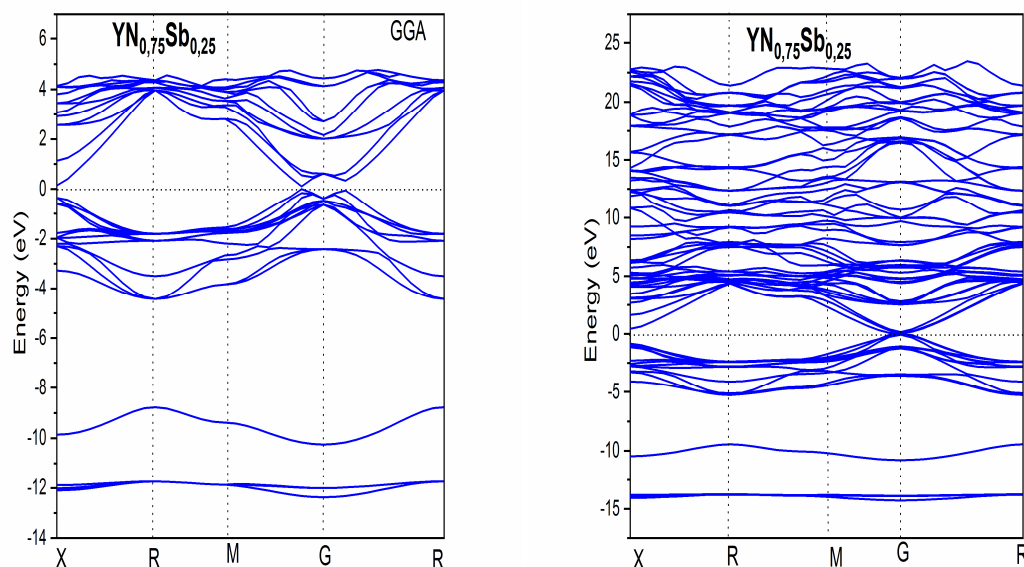


**FIGURE ( III-22):** Calculated electronic band structure of the  $YN_{1-x}Sb_x$  alloy in the B1 phase for  $x = 0.25$ , using the approximation GGA and HSE06.

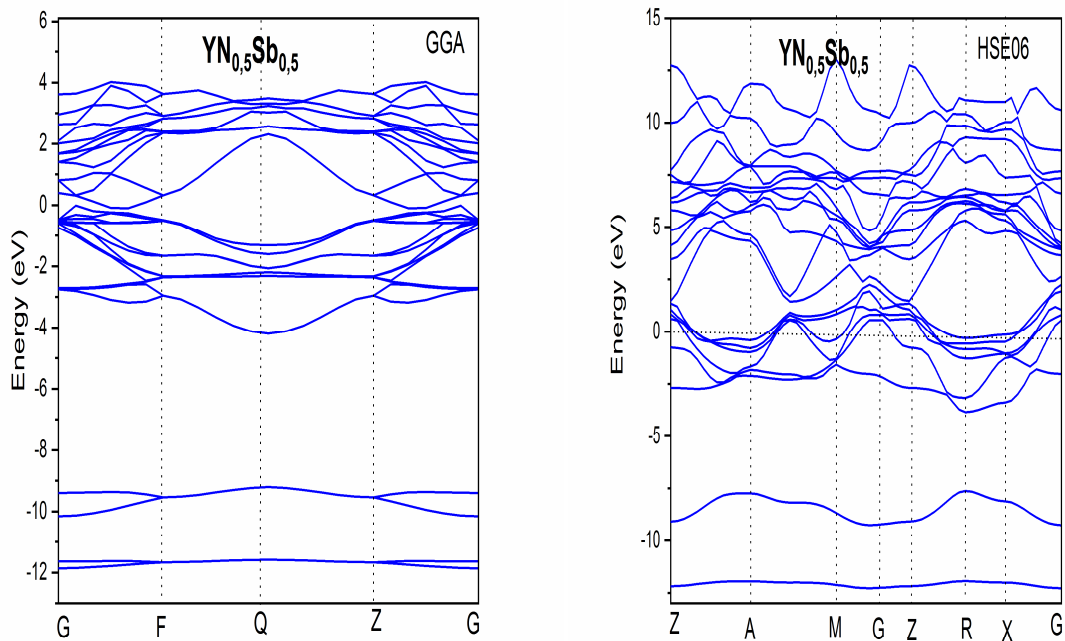


FIGURE ( III-23): Calculated electronic band structure of the  $YN_{1-x}Sb_x$  alloy in the B1 phase for  $x = 0.5$ , using the approximation GGA and HSE06.

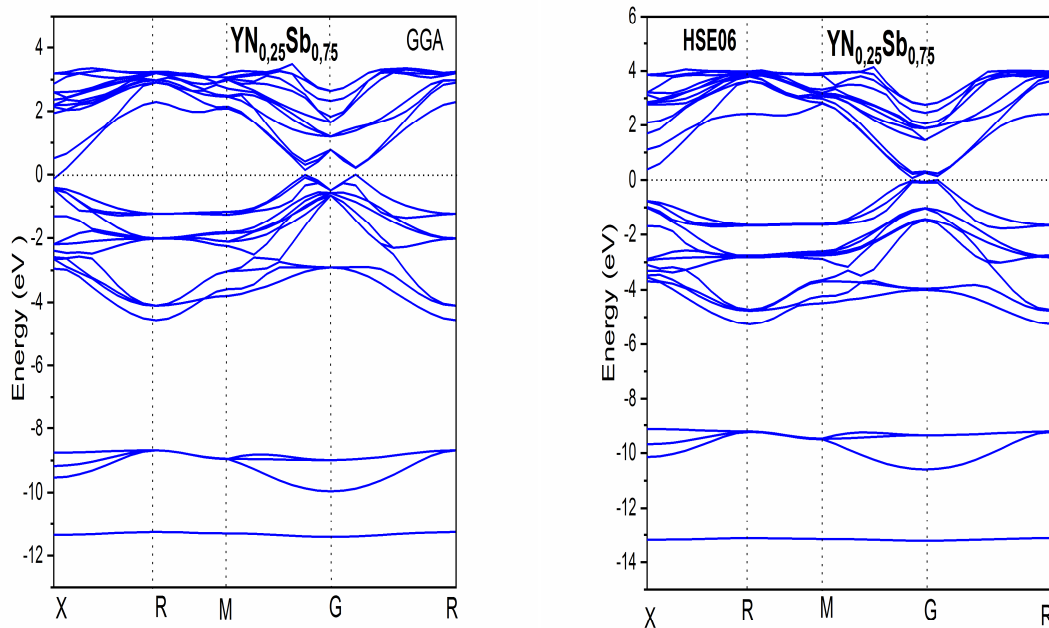


FIGURE ( III-24): Calculated electronic band structure of the  $YN_{1-x}Sb_x$  alloy in the B1 phase for  $x = 0.75$ , using the approximation GGA and HSE06.

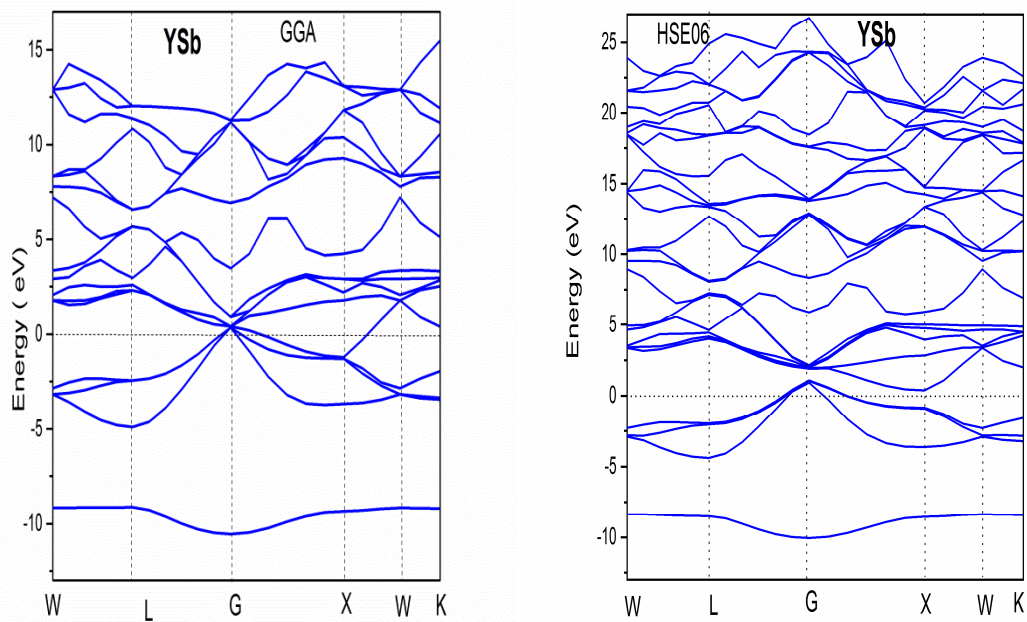
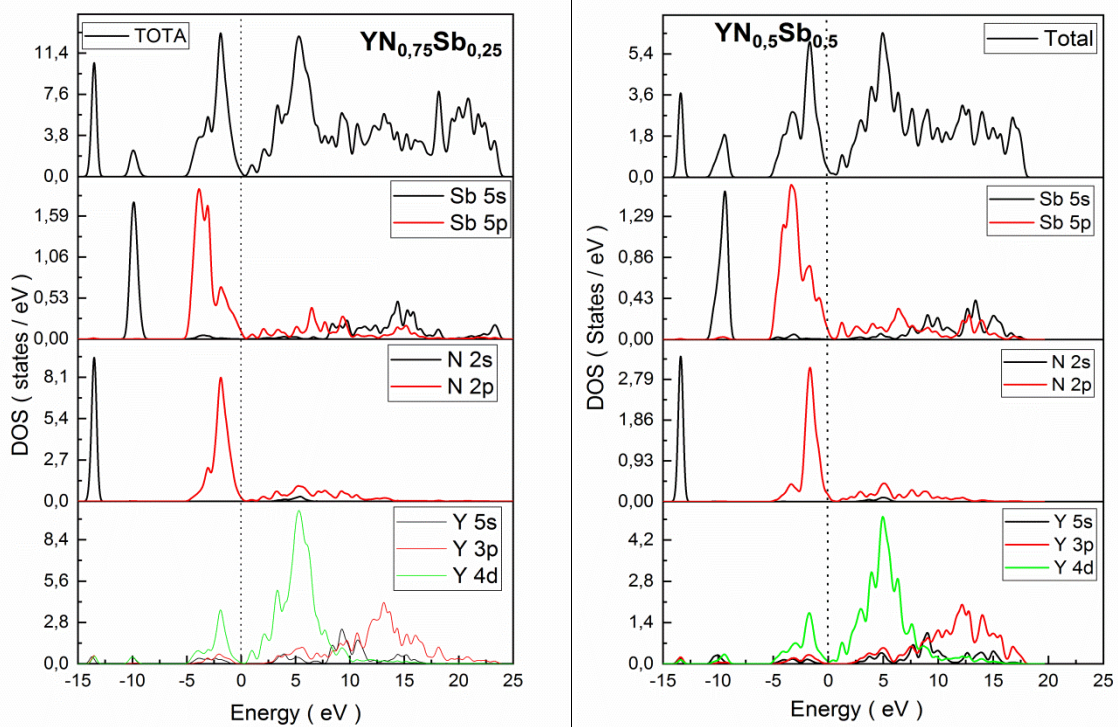
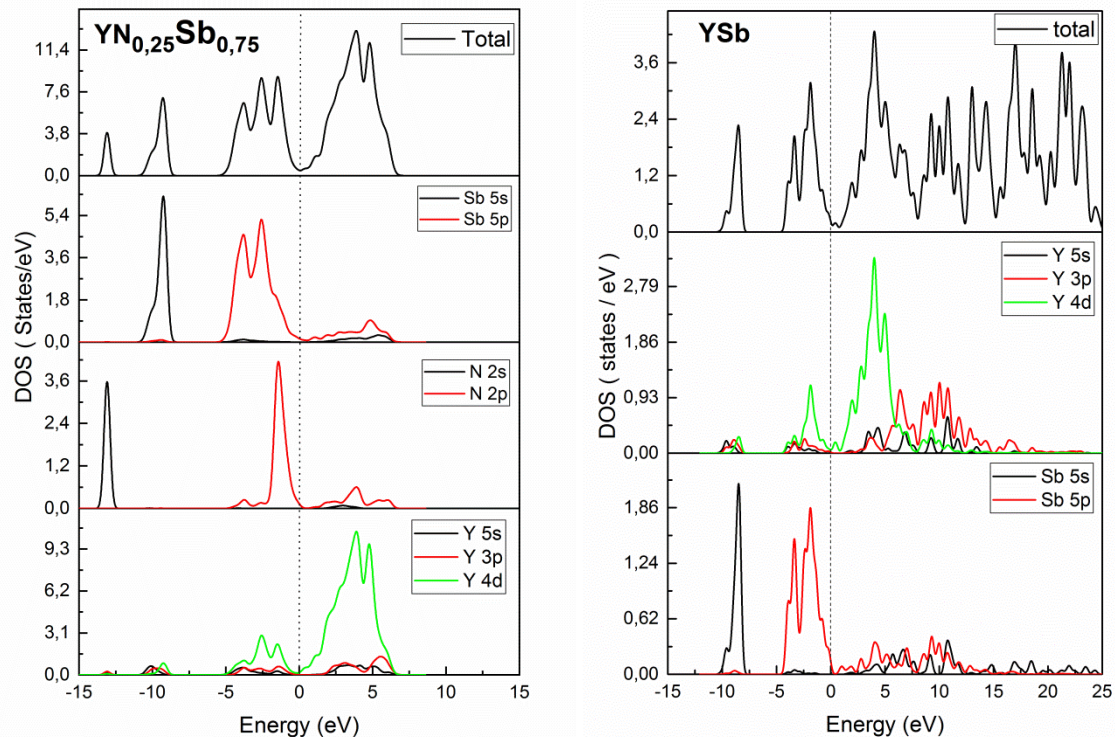


FIGURE (III-25): Calculated electronic band structure of the  $YN_{1-x}Sb_x$  alloy in the B1 phase for  $x = 1$ , using the approximation GGA and HSE06.





**FIGURE ( III-26):** The total and partial state density (DOS) of  $YN_{1-x}Sb_x$  ( $x = 0.25, 0.50, 0.75$  and  $1$ ) with the approximation «HSE06».

FIGURE ( III-26) represents the densities of total and partial states of  $YN_{1-x}Sb_x$  ( $x = 0.25, 0.50, 0.75$ , and  $1$ ) obtained by the HSE06 approximation.

For  $YN_{0.75}Sb_{0.25}$ ,  $YN_{0.5}Sb_{0.5}$ , and  $YN_{0.25}Sb_{0.75}$ : the first region consists mainly of the (2s) states of the N atom. The second region consists of the states (5s) of the Sb atom. The third region is composed of the (2p) state of the N atom with a small contribution of the state(4d) of the Y atom.

Finally, a conduction band consists mainly of (4d) states of Y atoms, with a small contribution of the (2p) state of the N atom and (5p) state of the Sb atoms. For YSb: The highest valence band is native to the state (5p) of the Sb atom. The second region is dominated by the states (5p) of Sb and (4d) of the Y atom. Finally, the conduction band is dominated mainly by the (3p,4d) states of atom Y and (5s,5p) states of atom Sb.

### III-6. The optical properties of $Y_{1-x}M_xN$ ( $M = Sc$ and $La$ ), $YN_{1-x}B_x$ ( $B = P, As$ and $Sb$ ) alloys:

The optical properties of the material determine how it interacts with light. It is of great interest to know the different ways in which light interacts with matter in solid-state physics, such as absorption, reflection, refractive, etc. The CASTEP code allows us to calculate using the approximation HSE06.

#### III-6-1. The optical properties of $Y_{1-x}M_xN$ ( $M = Sc$ and $La$ ):

##### III-6-1-1. The compounds $Y_{1-x}Sc_xN$ for ( $x = 0, 0.25, 0.50, 0.75$ and $1$ ):

The parts real of the dielectric function for the considered compounds are shown in FIGURE (III-27). It is well known that the zero frequency limits are an important quantity that represents the dielectric response to the static electric field. The static dielectric constants of the  $Y_{1-x}Sc_xN$  alloys at considered compositions are 5.77 , 6.58 , 6.51 , 4.78 , and 5.98 eV corresponding to  $x = 0.0, 0.25, 0.50, 0.75$  and  $1.0$  respectively.

FIGURE (III-28) shows the refractive index and extinction coefficient of  $Y_{1-x}Sc_xN$  with different  $x$  concentrations. From this Figure, we can see that the constant refractive index  $n(0)$  for  $x = 0.0, 0.25, 0.50, 0.75, 1$ . are found to be 2.40 , 2.38 , 2.55 , 2.19 , and 2.44 respectively. The absorption coefficient refers to the percentage of light attenuation of light during propagation during unit distance. FIGURE ( III-29) shows absorption coefficients for all studied compounds. The absorption region of the  $Y_{1-x}Sc_xN$  alloys is near-ultraviolet and shows less absorption in visible light, reflecting their highly transparent nature in the lower energy field.

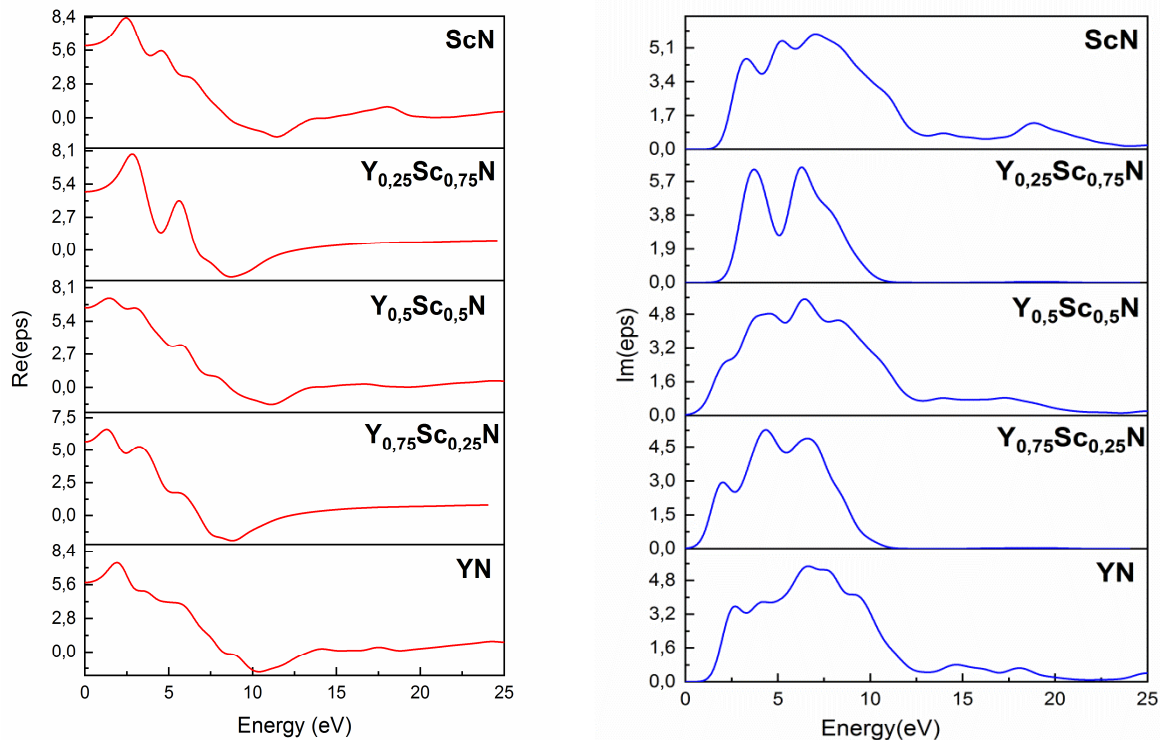


FIGURE ( III-27): Calculated imaginary parts and The real parts of the dielectric function for  $Y_{1-x}Sc_xN$  alloys.

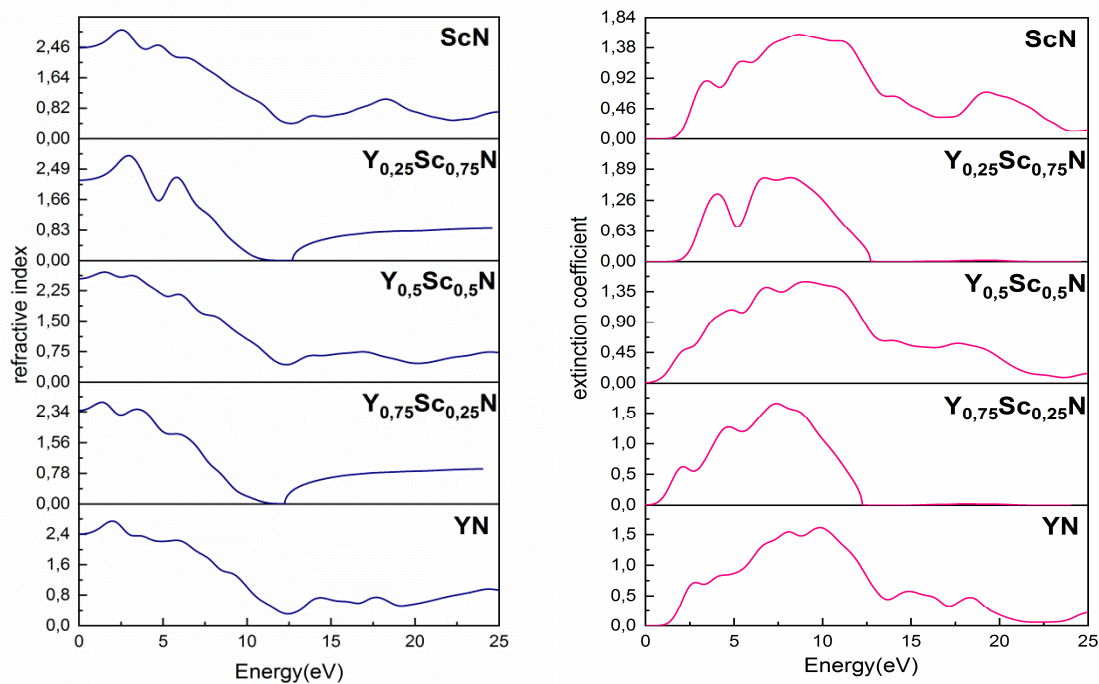


FIGURE ( III-28): Refractive index and extinction coefficient for  $Y_{1-x}Sc_xN$  corresponding to different values of  $x$ .

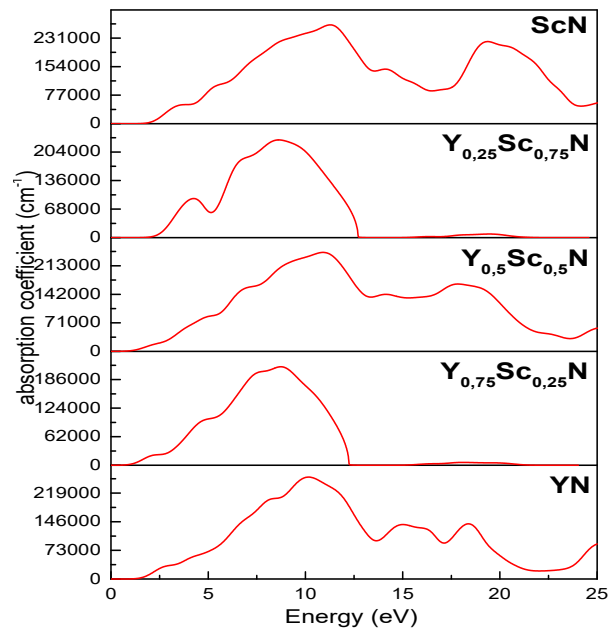


FIGURE ( III-29): Absorption coefficient for  $Y_{1-x}Sc_xN$  alloys.

### III-6-1-2. The compounds $Y_{1-x}La_xN$ for ( $x = 0, 0.25, 0.50, 0.75$ and $1$ )

It is convenient to evaluate the complex dielectric function when calculating the optical properties, the figure ( III-30) shows the variation of the dielectric function of  $Y_{1-x}La_xN$  alloys in the energy range up to 25eV.

The imaginary part of the dielectric function has a sharp peak at 2.5, 2.09, 0.86, 2.06, and 1.2 eV for the  $Y_{1-x}La_xN$  for ( $x = 0, 0.25, 0.5, 0.75$  and  $1$ ) alloys, respectively. The origin of these peaks is due to the inter band transition between the N-2p states and the Y-4d conduction bands (for compounds YN and  $Y_{0.75}La_{0.25}N$ ,  $Y_{0.5}La_{0.5}N$ ) and La-5d (for compounds LaN and  $Y_{0.25}La_{0.75}N$ ).

The real parts of the dielectric function for the considered compounds are displayed in FIGURE ( III-30). It is well known that the real parts of the dielectric constant describe a material's ability to interact with an electric field (store and remit energy) without absorbing energy. The static dielectric constants ( $\epsilon_1(0)$ ) of the  $Y_{1-x}La_xN$  alloys at considered compositions are 5.774 eV, 6.097 eV, 16.140 eV, 7.292 eV, and 11.648 eV corresponding to  $x = 0.0, 0.25, 0.50, 0.75$  and  $1.0$  respectively.

FIGURE( III-31). shows the refractive index and the extinction coefficient for the compounds studied. At zero frequency ( $\omega = 0$ ). The static dielectric constants  $\epsilon(0)$  [corresponding refractive indices  $n(0)$ ] calculated at the hydrostatic equilibrium of the mesh parameter for the

compounds  $Y_{1-x}La_xN$  are respectively 2.403, 2.472, 4.023, 2.70, and 3.414. The refractive index of  $Y_{1-x}La_xN$  reaches a maximum value of 2,769, 2,680, 4,056, 3.106, and 3.41 eV, respectively.

The variation of the optical reflectivity of the different compounds is shown as a function of photon energy in FIGURE (III-32). It is noted that the reflectivity increases in these compounds  $Y_{1-x}La_xN$  for ( $x = 0, 0.25, 0.5$  and  $1$ ) up to about 12.5 eV, but for the compound  $Y_{0.25}La_{0.75}N$ , the reflectivity increases up to at around 15 eV before decreasing.

The absorption spectrum is shown in FIGURE (III-33). The absorption threshold for  $Y_{1-x}La_xN$  for ( $x = 0, 0.25, 0.5, 0.75$  and  $1$ ) starts at approximately 1.44, 0.94, 0.36, 1.02, and 0.61 eV, respectively. This results from a transition of the N-2s electronic states (for the YN and LaN compounds) located at the top of the valence band to the empty electronic state Y-4d (for the compounds YN,  $Y_{0.75}La_{0.25}N$  and  $Y_{0.5}La_{0.5}N$ ) and La-5d (for compounds LaN and  $Y_{0.25}La_{0.75}N$ ), located at the bottom of the conduction band. The peak in the absorption spectrum occurs at about [5.8 to 12 eV].

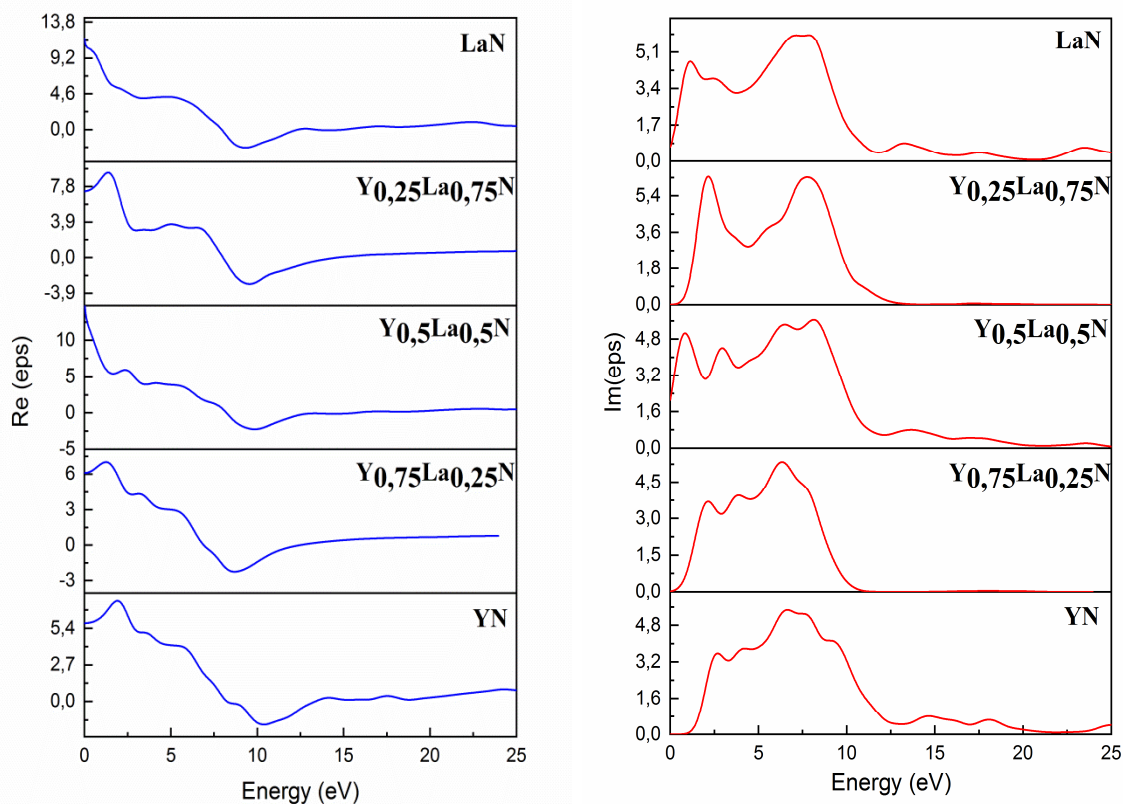


FIGURE (III-30): Calculated imaginary parts and real parts of the dielectric function for  $Y_{1-x}La_xN$  alloys.

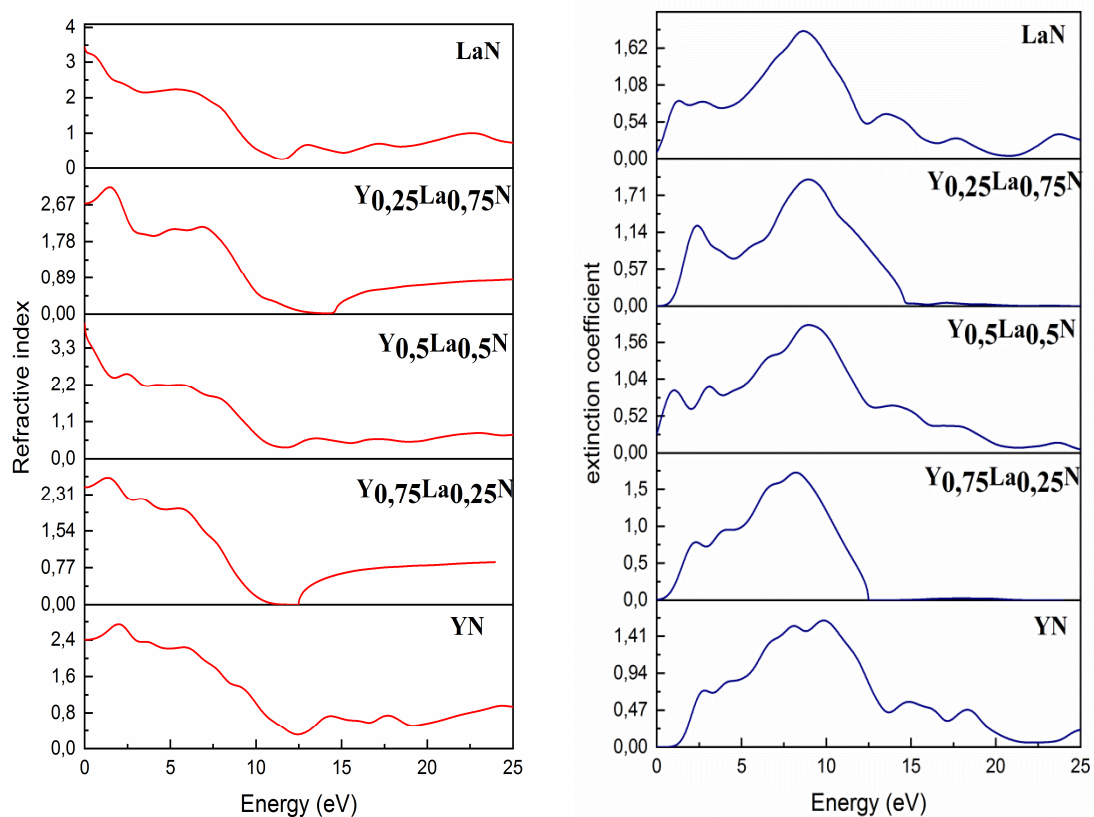


FIGURE ( III-31): Refractive index and extinction coefficient for  $Y_{1-x}La_xN$  corresponding to different values of  $x$ .

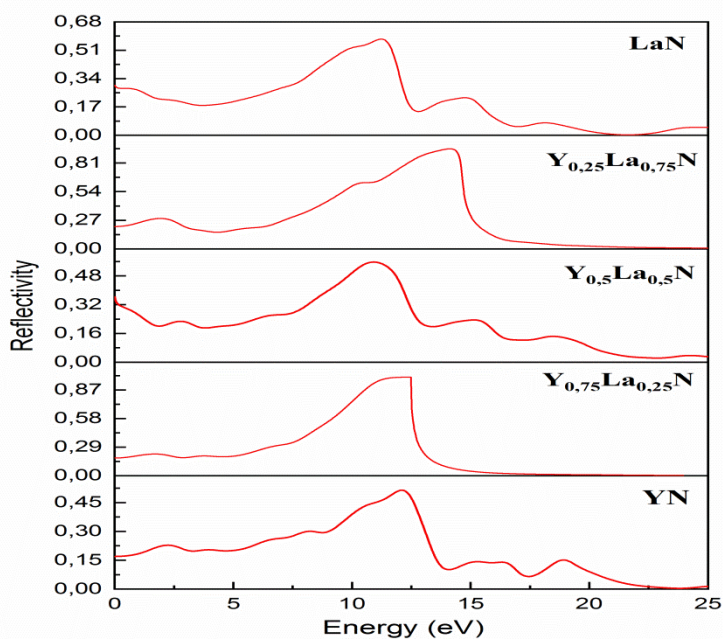


FIGURE ( III-32): Reflectivity for  $Y_{1-x}La_xN$  alloys.

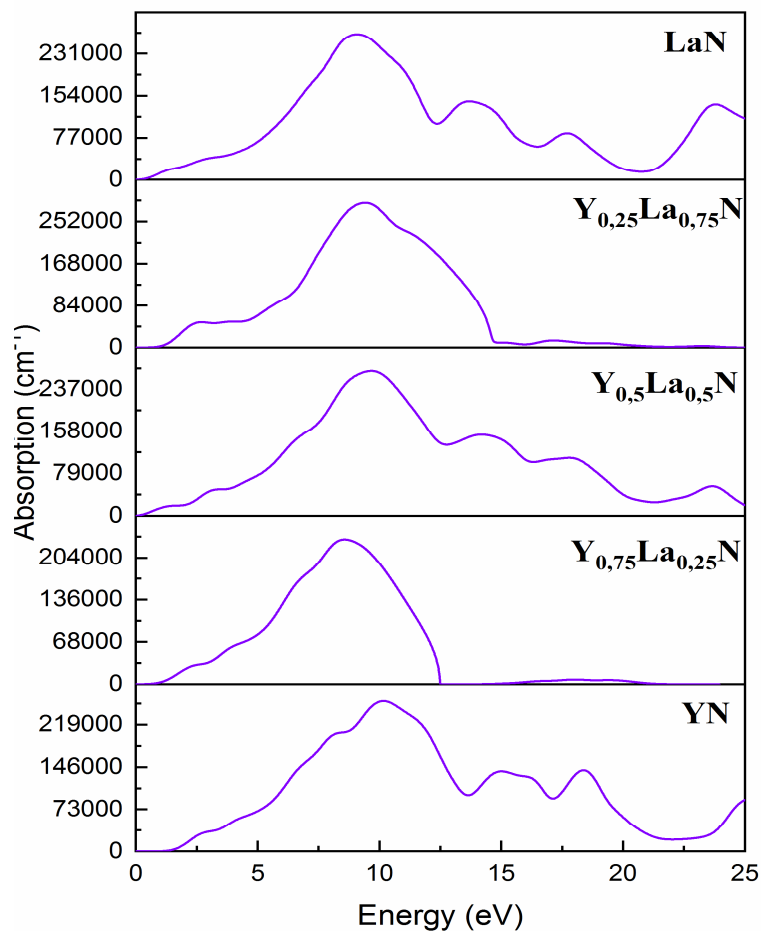


FIGURE ( III-33): Absorption coefficient for  $Y_{1-x}La_xN$  alloys.

**III-6-2. The optical properties of  $YN_{1-x}B_x$  ( $B = P, As$  and  $Sb$ ) alloys:**

FIGURES (III-34) → (III-49) present the calculated optical functions for ternary alloys  $YN_{1-x}P_x$ ,  $YN_{1-x}As_x$ , and  $YN_{1-x}Sb_x$ , and the energy range up to 25 eV.

FIGURE ( III-34), ( III-35), and ( III-36) show the spectra of the reals and imaginary parts  $\epsilon_2(\omega)$  of the dielectric functions of the  $YN_{1-x}P_x$ ,  $YN_{1-x}As_x$ , and  $YN_{1-x}Sb_x$  compounds with different concentrations  $x$ , as a function of the energy of the incident photons.

Analysis of the curve shows that the first critical point of the dielectric function at  $x = 0.0, 0.25, 0.50, 0.75, 1.0$  occurs around 2.55 eV, 1.9 eV, 0.86eV, 2.31 eV 0.22 eV for  $YN_{1-x}P_x$  respectively, and 2.55 eV, 1.95 eV ,0.92eV , 2.42 eV, 2.23 eV for  $YN_{1-x}As_x$ .and 2.55eV ,1.85eV ,1.35 eV, 2.43 eV ,2.26 eV for  $YN_{1-x}Sb_x$ .

Analysis of the  $\epsilon_2(\omega)$  curve shows that the first critical point of the dielectric function at  $x =$

0, 0.25, 0.50, 0.75, 1.0 occurs around 2.55 eV, 1.9 eV, 0.86eV, 2.31 eV 0.22 eV for  $YN_{1-x}P_x$  respectively, and 2.55 eV, 1.95 eV ,0.92eV , 2.42 eV, 2.23 eV for  $YN_{1-x}As_x$ .and 2.55eV ,1.85eV ,1.35 eV, 2.43 eV ,2.26 eV for  $YN_{1-x}Sb_x$ .

The origin of these points is due to the optical transition between the highest valence band and the lowest conduction band. The critical point shifts towards lower energies with increasing concentration in each alloys.

Based on the calculated results of the real part of the dielectric function, we determined the static dielectric constant  $\epsilon_1(\omega)$ , which is a larger quantity and given by the lower limit of  $\epsilon(\omega)$  energy. The values obtained for the static dielectric constant  $\epsilon_1(\omega)$  of  $YN_{1-x}P_x$ ,  $YN_{1-x}As_x$ ,and  $YN_{1-x}Sb_x$  compounds as a function of concentration x are grouped in Table (III-30). It can be observed that the calculated values of the static dielectric constant  $\epsilon_1(0)$ .

**Table (III-30):** dielectric function  $\epsilon_1(0)$  of  $YN_{1-x}B_x$  (B = P ,As and Sb) in approximation HSE06.

compound	$\epsilon_1(0)$				
	0	0.25	0.5	0.75	1
$YN_{1-x}P_x$	5.77	8.80	18.33	9.40	9.42
$YN_{1-x}As_x$	5.77	8.57	29.66	12.91	9.55
$YN_{1-x}Sb_x$	5.77	10.09	27.15	8.74	11.06

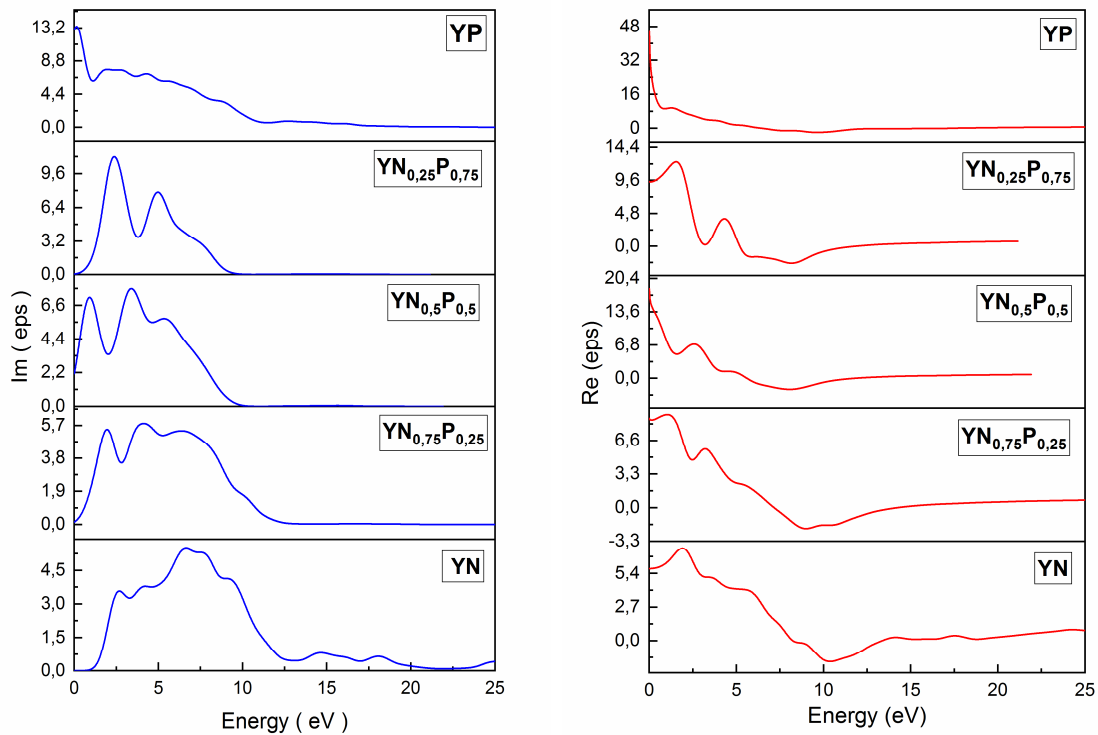


FIGURE ( III-34): Calculated imaginary parts and real parts of the dielectric function for  $YN_{1-x}P_x$  alloys.

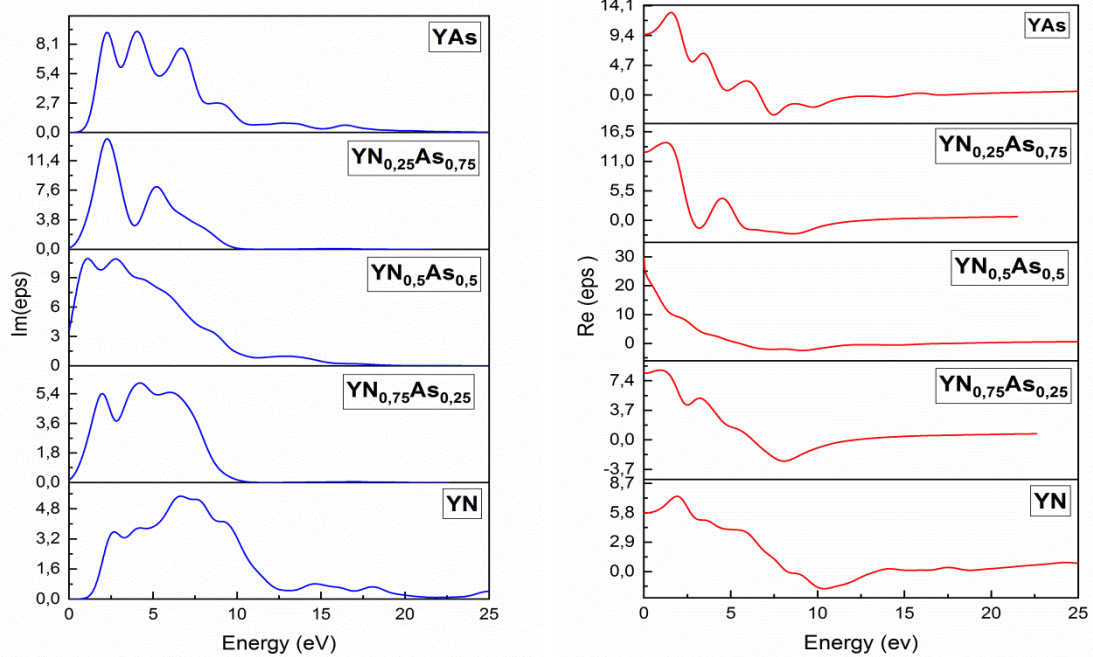
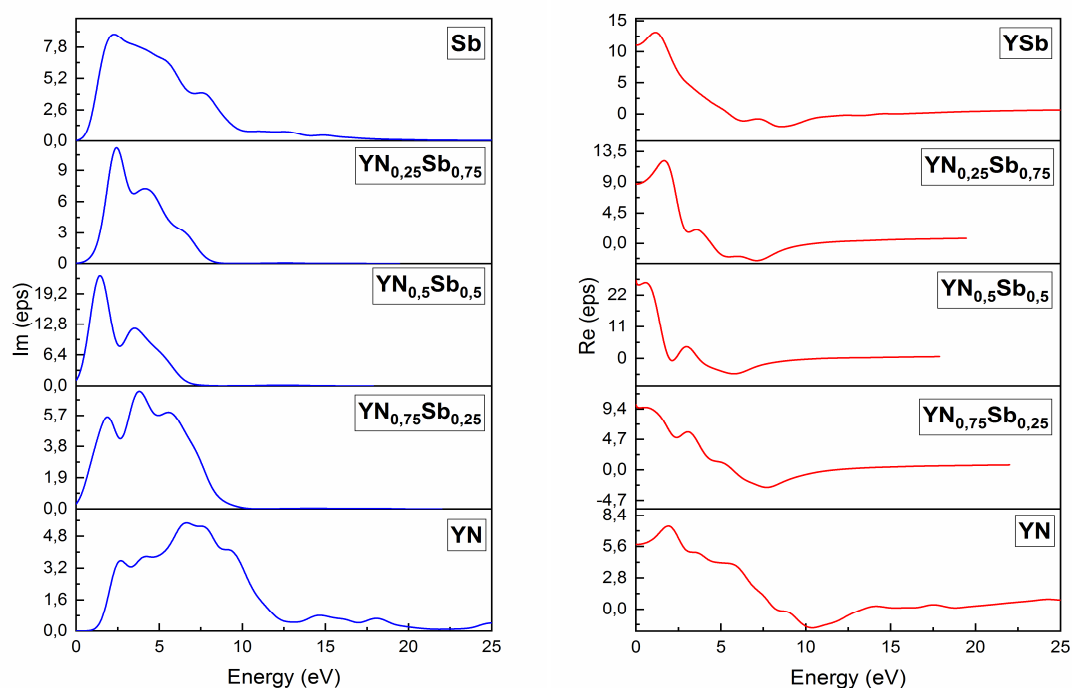


FIGURE ( III-35): Calculated imaginary parts and real parts of the dielectric function for  $YN_{1-x}As_x$  alloys.



**FIGURE ( III-36):** Calculated imaginary parts and real parts of the dielectric function for  $YN_{1-x}Sb_x$  alloys.

FIGURE (III-37), (III-38), and (III-39) show the variation in the refractive index  $n(\omega)$  as a function of energy for the  $YN_{1-x}P_x$ ,  $YN_{1-x}As_x$ , and  $YN_{1-x}Sb_x$  alloy at different concentrations  $x$ . This figure is given the static refractive index  $n(0)$  of each  $x$  composition. We note that the  $n(0)$  values for the  $YN_{1-x}P_x$  alloy are 2.40, 2.96, 4.28, 3.06, and 6.81 eV, and the  $YN_{1-x}As_x$  alloy is 2.40, 2.92, 4.45, 3.59 and 3.09 eV, and the  $YN_{1-x}Sb_x$  alloy is 2.40, 3.17, 5.21, 2.95 and 3.32 eV for concentrations of ( $x= 0, 0.25, 0.5, 0.75$  and 1) respectively, which are in good agreement with the values derived from the Real part of the dielectric function.

For all studied compounds, the refractive index increases and then decreases as the energy increases. The crystal has normal dispersion properties, while the crystal shows abnormal dispersion properties when the refractive index and energy are inversely proportional. On the one hand, the extinction coefficient follows the trend of the imaginary part of the dielectric function. The spectra are similar with small differences in detail. The maximum value of the observed extinction coefficient on the spectra corresponds to energies 10.01, 8.53, 6.64, 2.84, and 7.21 for the  $YN_{1-x}P_x$  alloy. 10.01, 7.71, 6.03, 2.67 and 7.13 for  $YN_{1-x}As_x$  alloy, for  $YN_{1-x}Sb_x$  alloys, is 10.01, 6.80, 1.76, 2.67, and 5.72 for concentrations of ( $x= 0, 0.25, 0.5, 0.75,$

and 1), respectively.

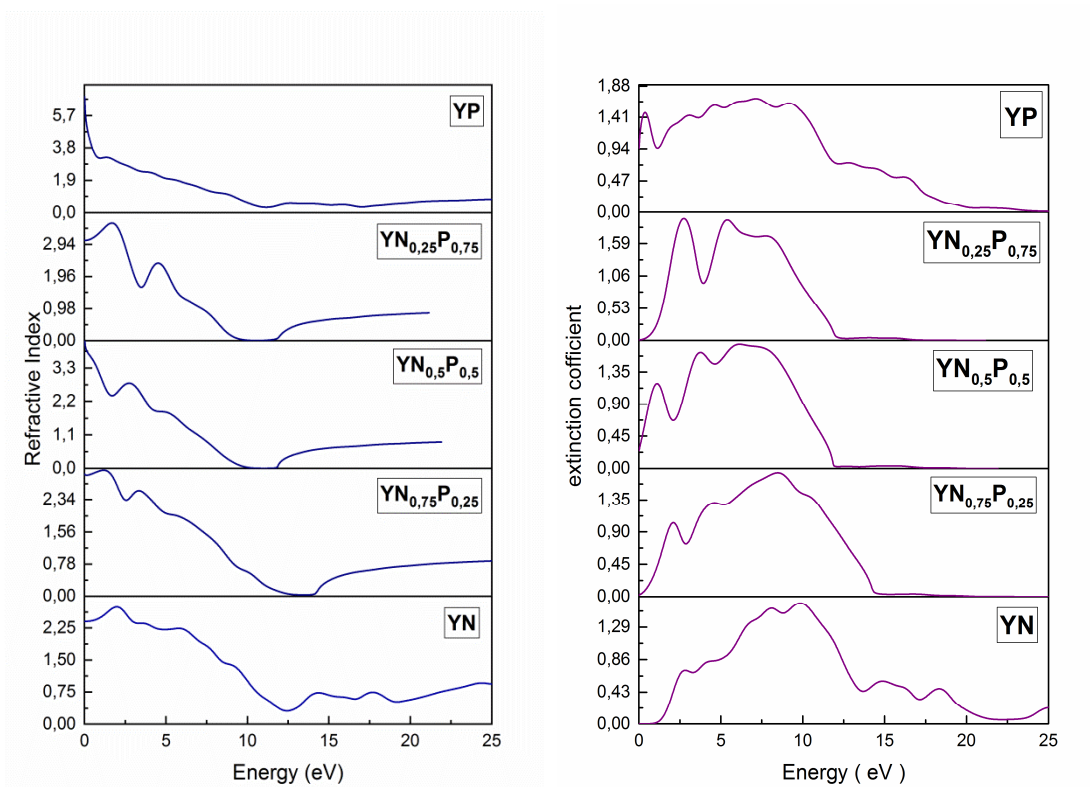


FIGURE (III-37): Variation of refractive index and extinction coefficients for  $YN_{1-x}P_x$  alloys.

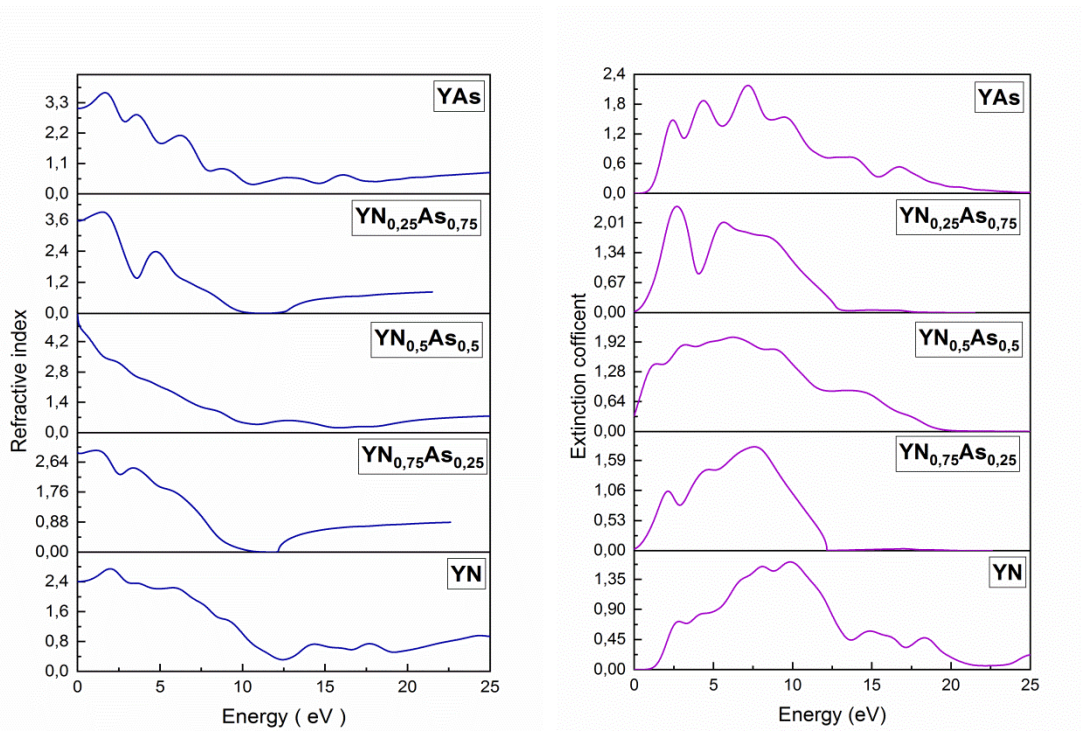
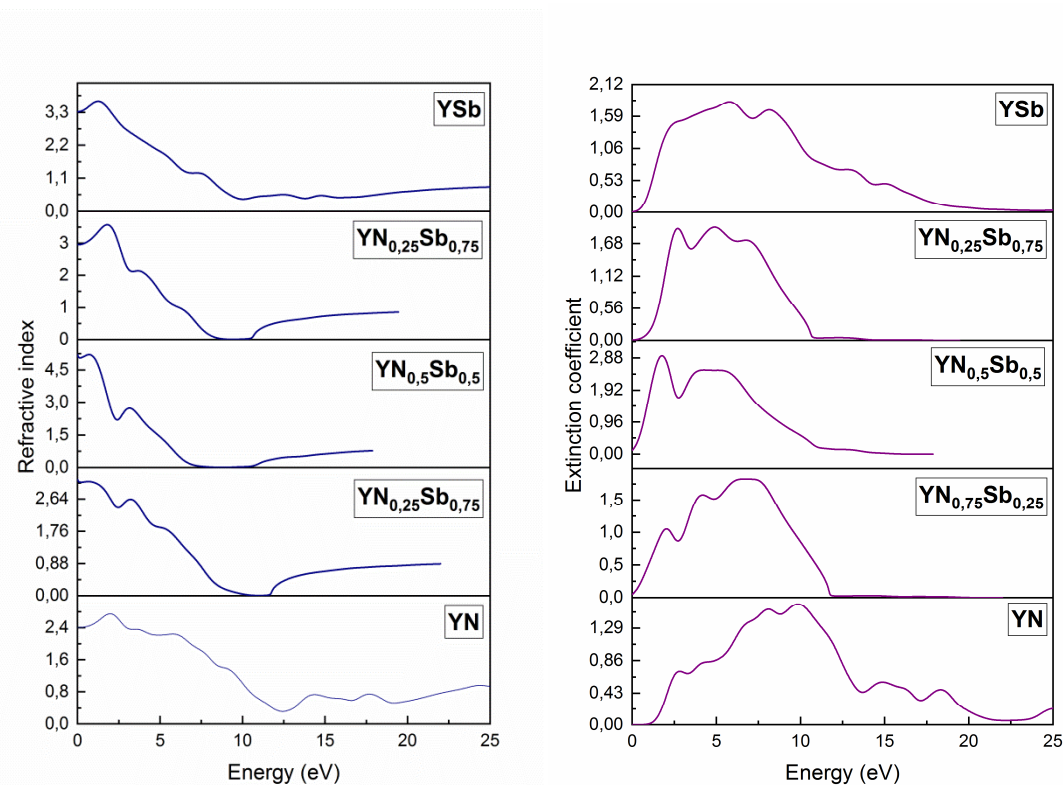
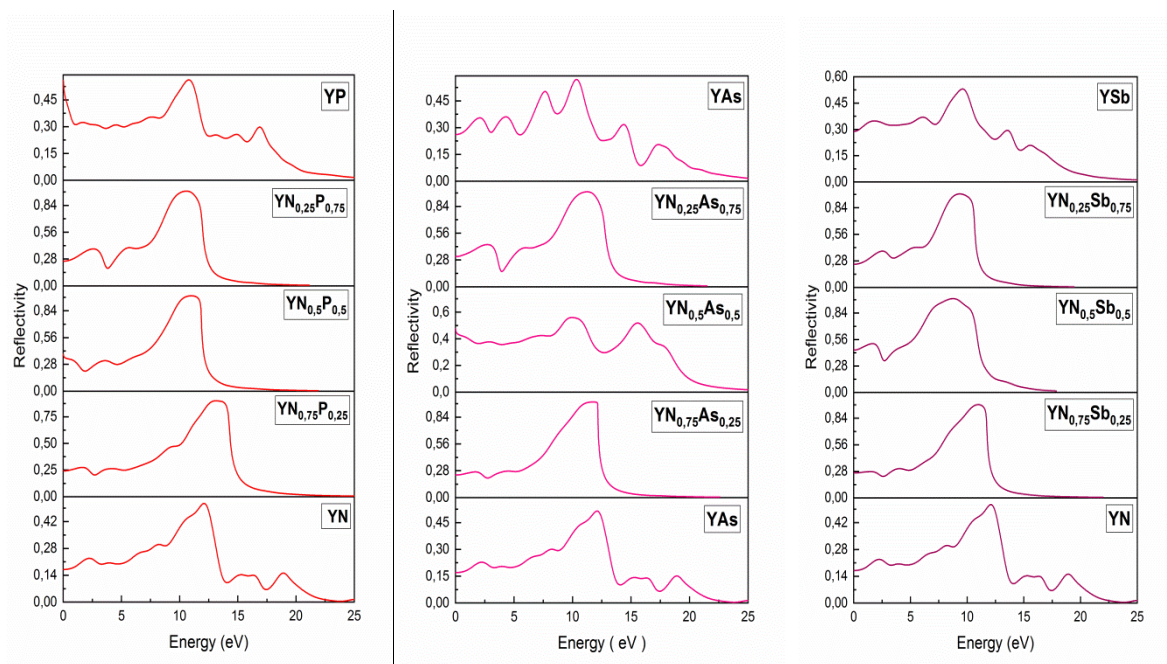


FIGURE (III-39): Variation of refractive index and extinction coefficients for  $YN_{1-x}As_x$  alloys.



**FIGURE (III-39):** Variation of refractive index and extinction coefficients for  $YN_{1-x}Sb_x$  alloys.

The reflectivity of the  $YN_{1-x}P_x$ ,  $YN_{1-x}As_x$ , and  $YN_{1-x}Sb_x$  alloys is shown in FIGURE (III-40). The maximum reflectivity obtained for  $YN_{1-x}P_x$  is 51.83 %, 89.59 %, 98.94 %, 98.44%, and 56.25% in the range [10.8 - 13.4], [12.57 - 14], [9.77-12.24], [9.69-12.08] and [9.6-11.92] respectively. And for  $YN_{1-x}As_x$  equal to 51.83 %, 98.44%, 84 %, 99.65%, and 56,89 % in the range [10.8 - 13.4], [10.35-12.4], [10.01-11.99], [9.93-12.41] and [9.60-12.41], respectively. For  $YN_{1-x}Sb_x$  equal to 51.83 %, 99.34%, 98.73%, 98.22%, 52.71% in the range [10.8 - 13.4], [9.93-11.99], [7.29-10.18], [7.95-10.44] and [8.53-10.76] respectively. But for the energy values above 30 eV, the reflectivity becomes almost non-existent for all compounds. Interestingly, the maximum reflectivity occurs when  $\epsilon_1(\omega)$  becomes negative because in this case, the composite has a metallic behavior in this energy range.



**FIGURE (III-40):** Reflectivity variation for  $YN_{1-x}P_x$ ,  $YN_{1-x}As_x$ , and  $YN_{1-x}Sb_x$  compounds in the HSE06 approximation.

FIGURE (III-41) represents the absorption coefficient for all the compounds studied. There is a gradual change in the absorption edges for the  $YN_{1-x}P_x$ ,  $YN_{1-x}As_x$ , and  $YN_{1-x}Sb_x$  alloys with increased concentration  $x$ . The absorption region of  $YN_{1-x}P_x$ ,  $YN_{1-x}As_x$ , and  $YN_{1-x}Sb_x$  alloys is near-ultraviolet, suggesting that these materials may find applications in different optoelectronic devices. |

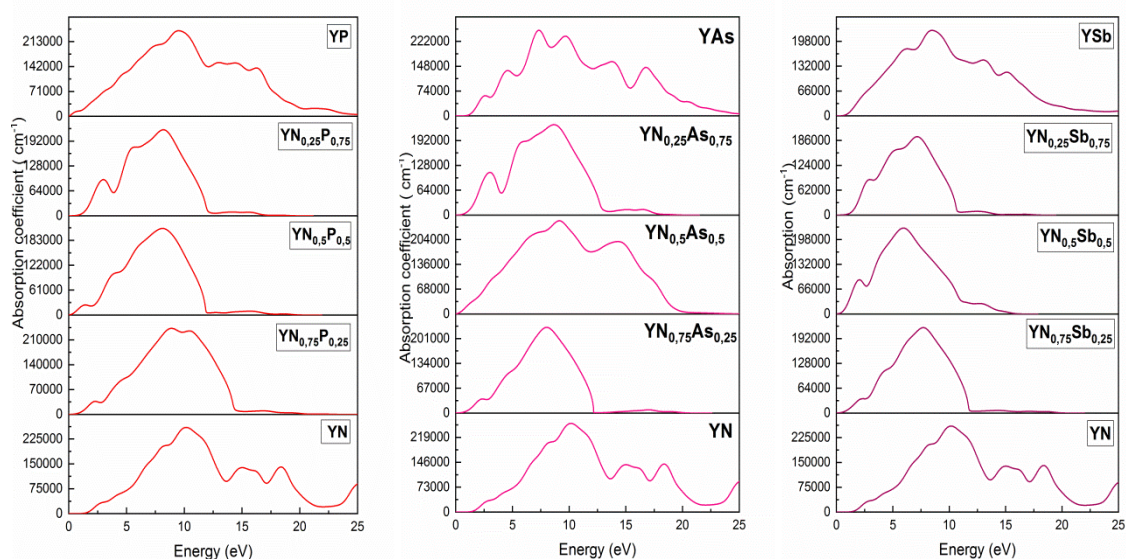


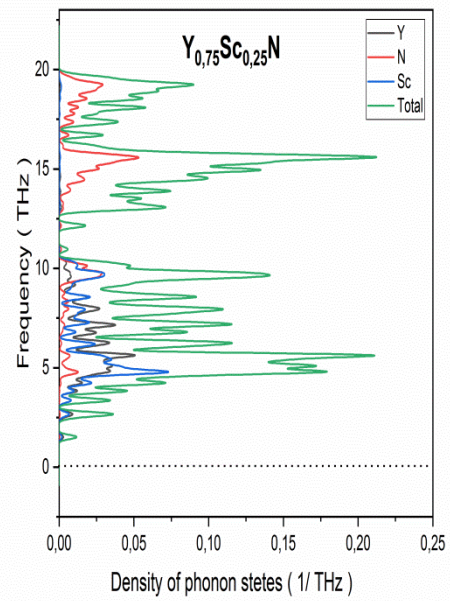
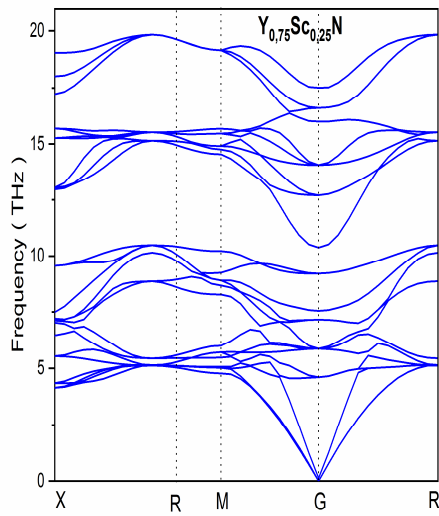
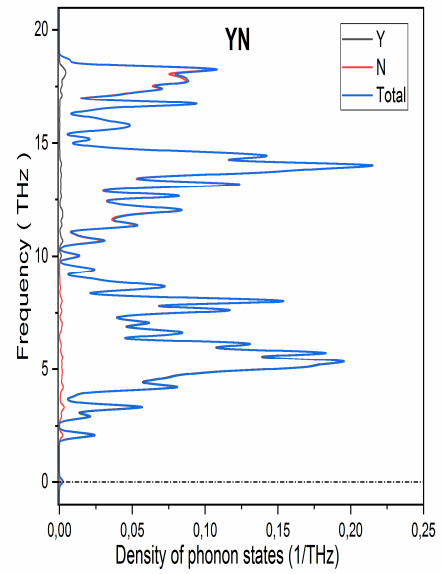
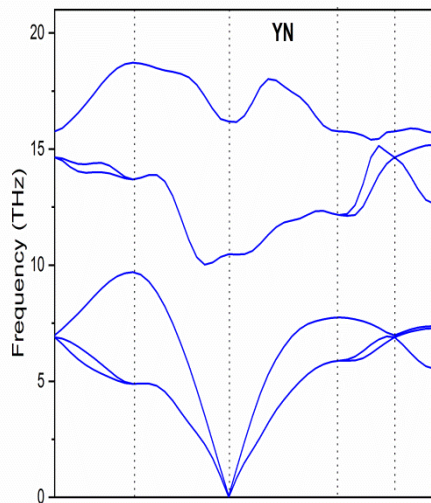
**FIGURE (III-41):** Optical absorption coefficients of the  $YN_{1-x}P_x$ ,  $YN_{1-x}As_x$  and  $YN_{1-x}Sb_x$  alloys calculated using the functional HSE06.

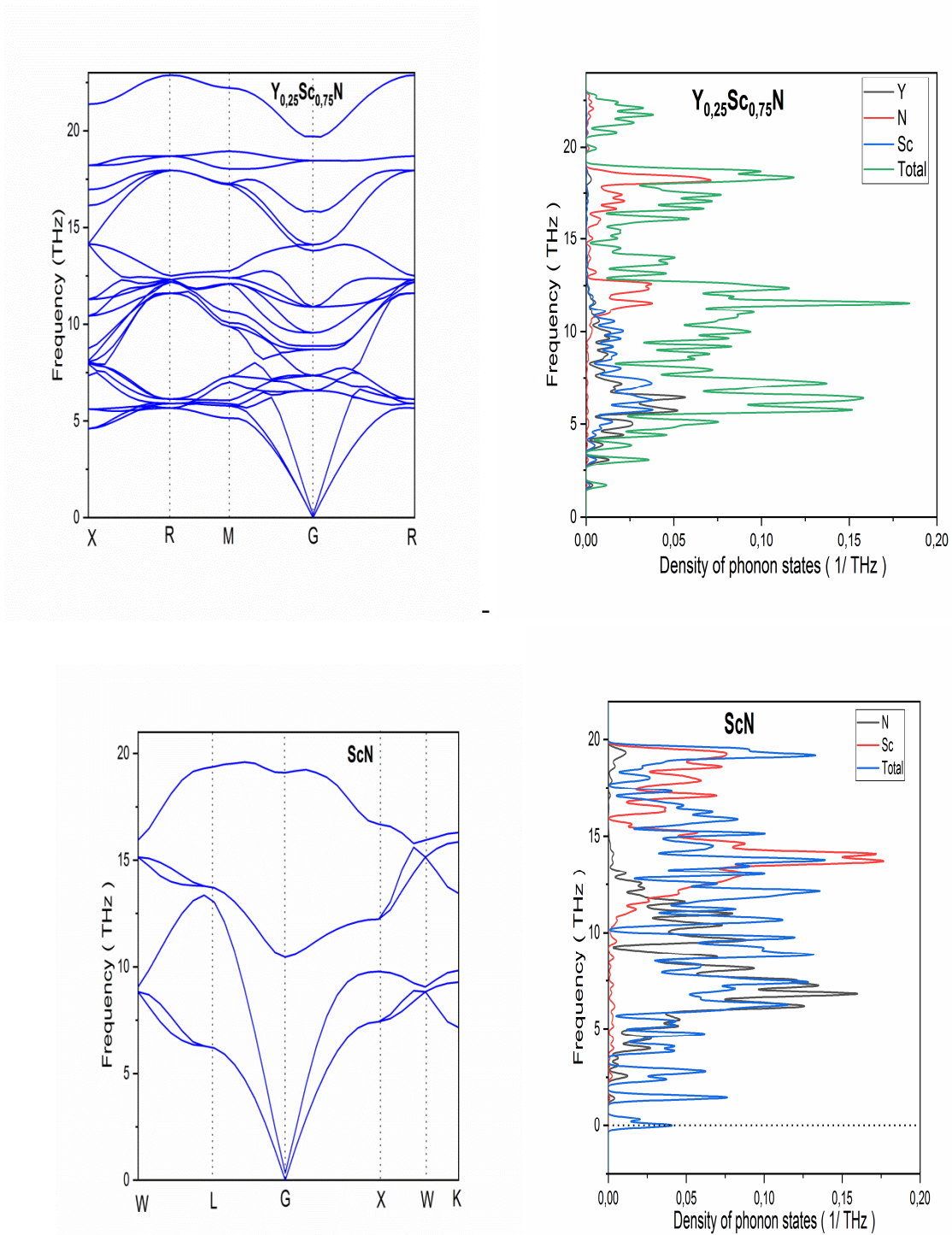
### III-7. Phonon properties of $Y_{1-x}M_xN$ ( $M = Sc$ and $La$ ), $YN_{1-x}B_x$ ( $B = P, As$ and $Sb$ ) alloys:

The study of phonons is an integral part of the physics of condensed matter. Phonons are the proper modes of vibration of a crystalline network and represent waves of vibration characterized by pulsation, wave vector, and polarization. They play a significant role in many physical properties of condensed matter systems, such as thermal and electrical conductivity, as well as in neutron scattering models and related effects. We performed ab initio calculations using the GGA approximation to determine the vibration frequencies of the phonons of the  $Y_{1-x}M_xN$  (  $M = Sc$  and  $La$ ),  $YN_{1-x}B_x$  (  $B = P, As$ , and  $Sb$ ) alloys.

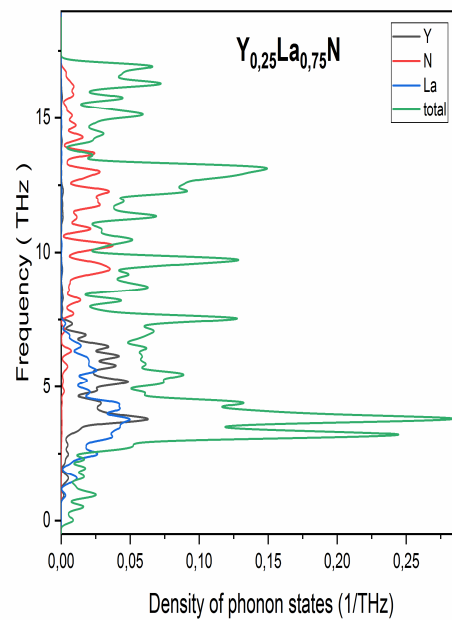
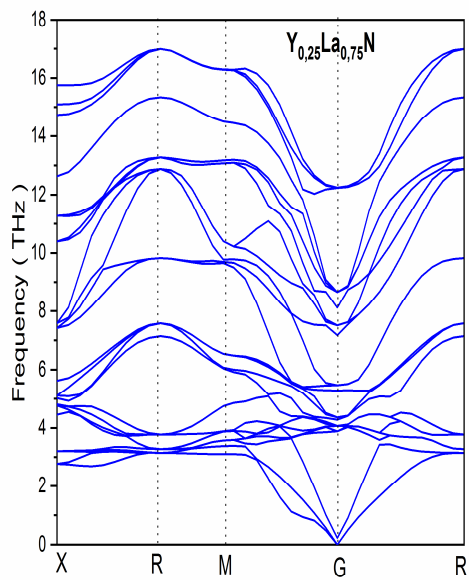
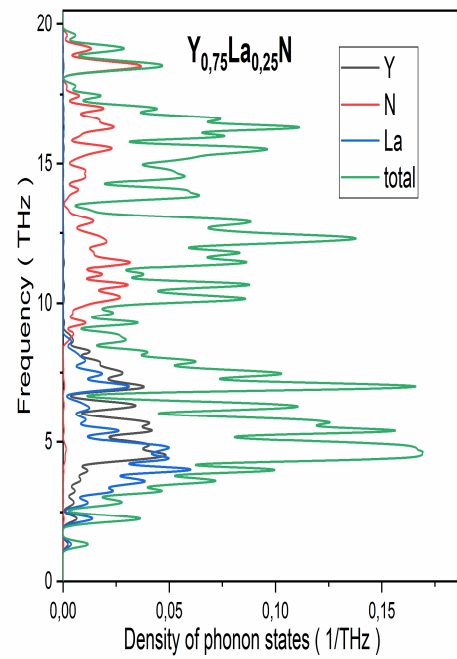
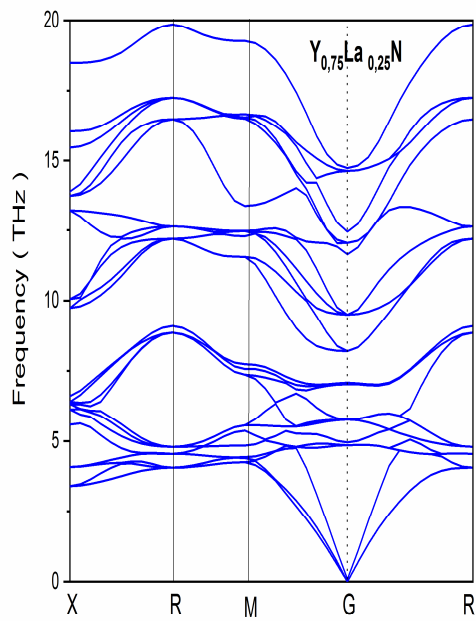
#### III-7-1. Phonon properties of $Y_{1-x}M_xN$ ( $M = Sc$ and $La$ ):

For  $Y_{1-x}Sc_xN$  and  $Y_{1-x}La_xN$  (  $x = 0, 0.25, 0.75$ , and  $1$  ), phonon modes have positive frequencies indicating the dynamic stability of these compounds. In cubic symmetry compounds (  $YN, ScN, LaN$ ), there are two atoms different atoms in the primitive cell, and there are three optical branches and three acoustic branches, two of which correspond to transverse vibrations (TO) and one longitudinal vibration (LO) for each mode type ( see Chapter 2). Our  $Y_{1-x}Sc_xN$  and  $Y_{1-x}La_xN$  alloy results for different concentrations  $x$  (  $x = 0, 0.25, 0.50, 0.75$  and  $1$ ) are shown in FIGURE (III-42) and (III-43) . in phonon DOS, there is no gap between the optical and acoustic phonon branches, as there is considerable overlap between the optical phonon branches. The contribution of the heavier atoms to the total DOS is dominated at low frequencies, and that of the lighter atoms is important at high frequencies. There are no empirical results to compare calculated phonon curves. Our results are predictive and can be valid for theoretical and experimental interpretations in the future.





**FIGURE (III-42):** Calculated phonon dispersion curves phonon DOS for  $Y_{1-x}Sc_xN$  ( $x = 0, 0.25, 0.50, 0.75$  and  $1$ ) alloys along several high symmetry lines in the Brillouin zone.



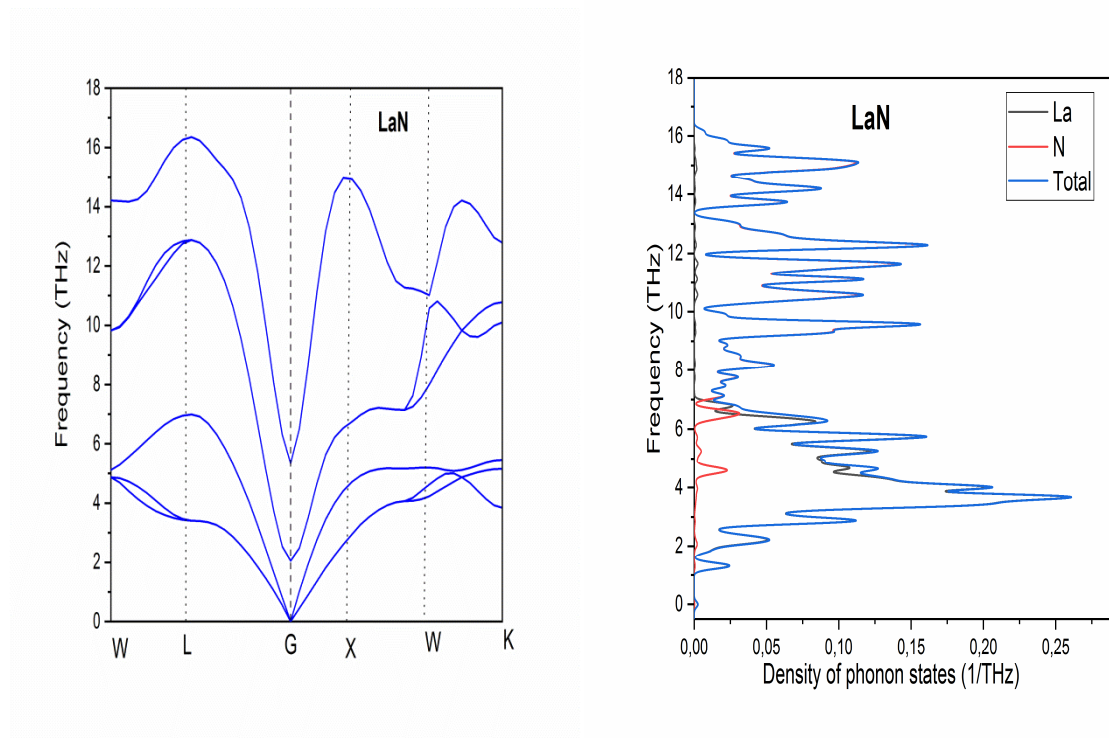


**FIGURE (III-43):** Calculated phonon dispersion curves and phonon DOS for  $Y_{1-x}La_xN$  ( $x = 0, 0.25, 0.50, 0.75$  and  $1$ ) alloys along several high symmetry lines in the Brillouin zone.

### III-7-2. Phonon properties of $YN_{1-x}B_x$ ( $B = P, As$ and $Sb$ ) alloys:

Our computed phonon dispersion curves for  $YN_{1-x}B_x$  ( $B = P, As,$  and  $Sb$ ) alloys along the high-symmetry directions are shown in FIGURE (III-44)  $\rightarrow$  (III-46). We can see  $YN_{1-x}B_x$  ( $B = P$  and  $As$ ) ( $x = 0, 0.25,$  and  $1$ ), indicating the dynamic stability of these materials because the frequencies are positive. For the curve density of phonon states, there is a great interference between acoustic and optical branches. The contribution of lighter atoms is significant at higher frequencies. The obtained phonon frequencies for  $YN, YP, YAs,$  and  $YSb$  are in good agreement with those obtained by Azzi and al [41]. Our results can be considered predictors of other scientific research work.

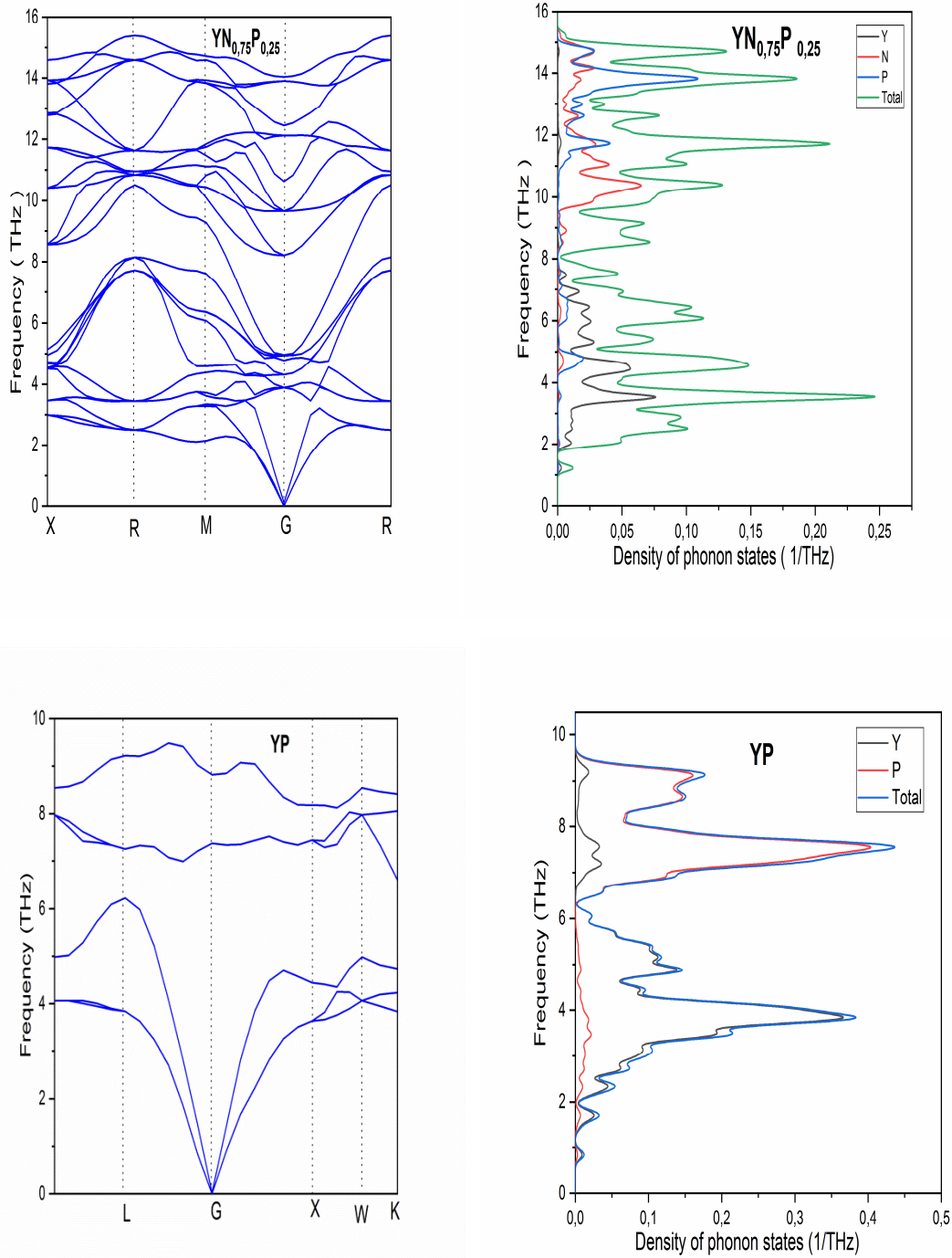


**FIGURE (III-44) :** Calculated phonon dispersion curves phonon DOS for  $YN_{0.75}P_{0.25}$  and YP alloys along several high symmetry lines in the Brillouin zone.

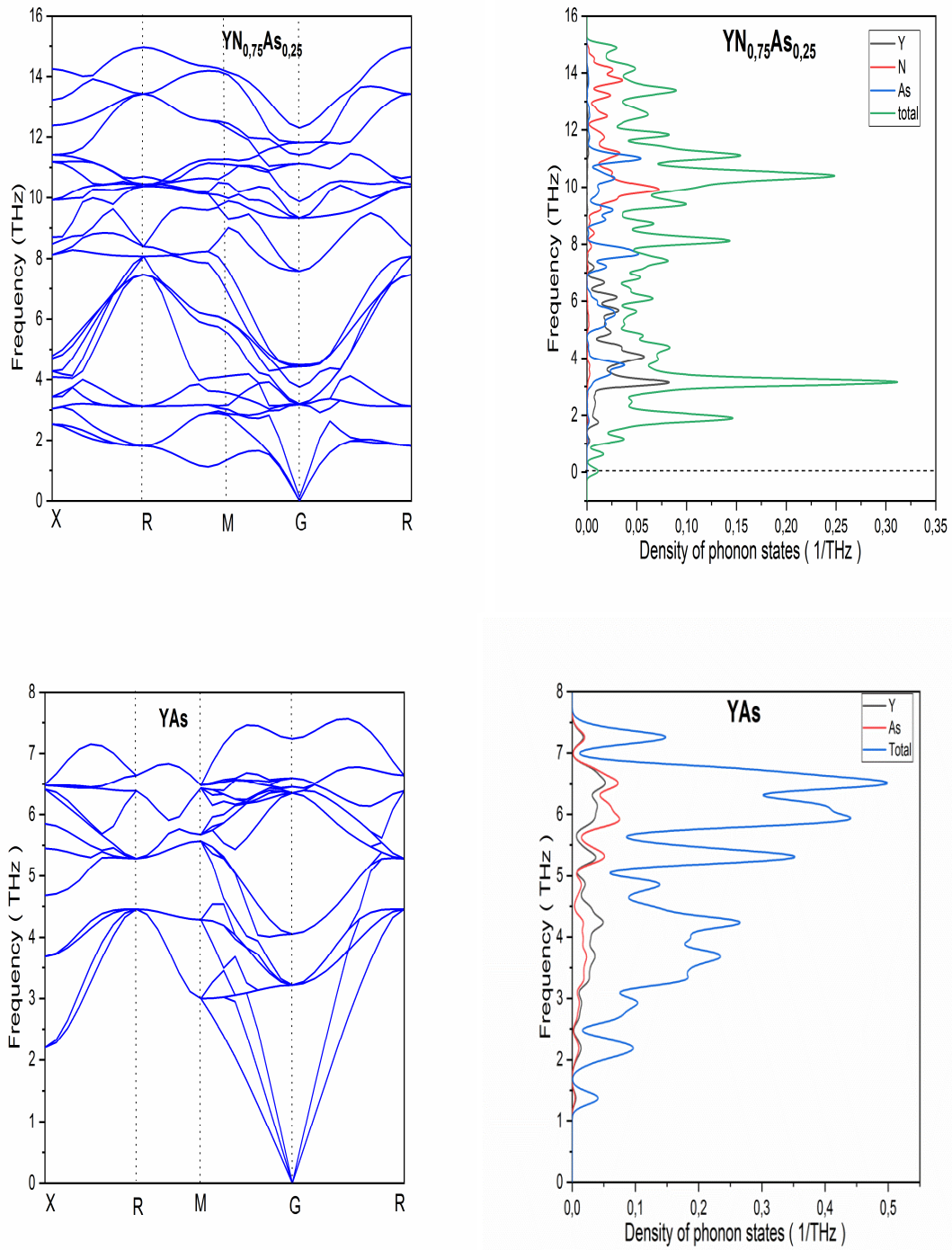


**FIGURE (III-45) :** Calculated phonon dispersion curves and phonon DOS for  $YN_{0.75}As_{0.25}$  and  $YAs$  alloys along several high symmetry lines in the Brillouin zone.

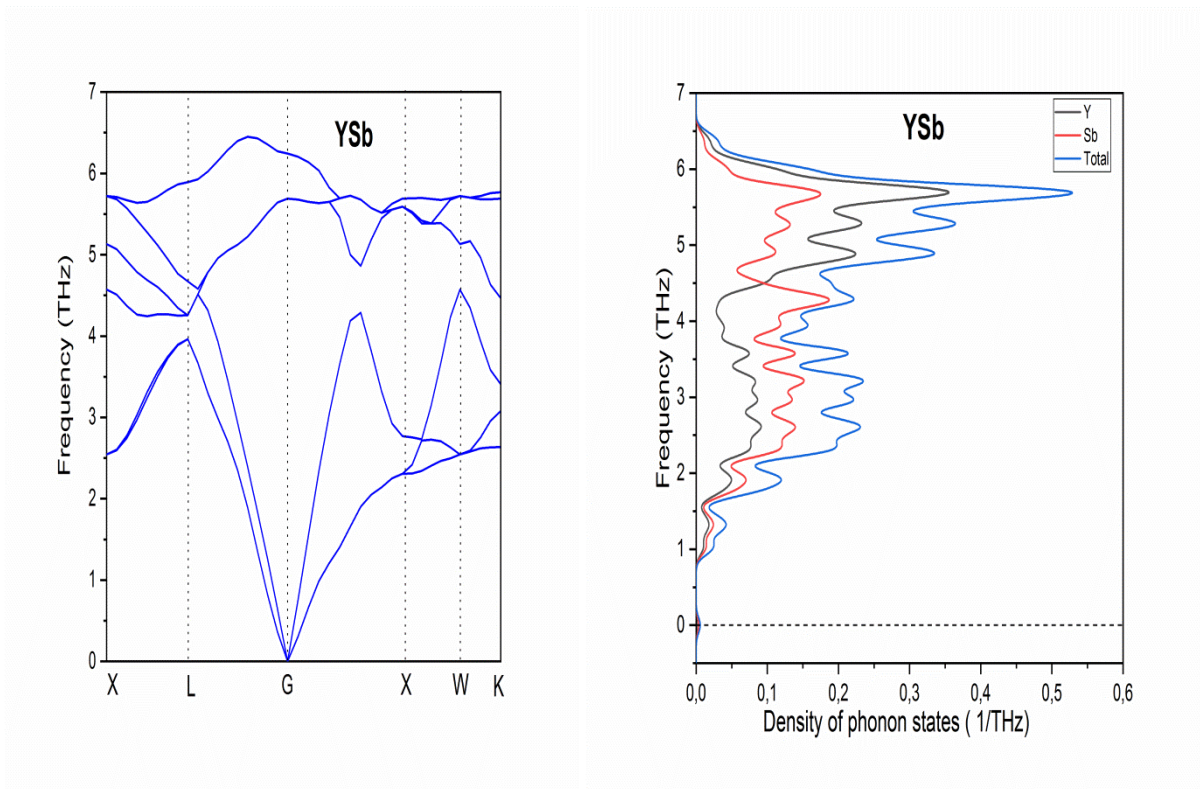


**FIGURE (III-46)** : Calculated phonon dispersion curves and phonon DOS for **YSb** alloys along several high symmetry lines in the Brillouin zone.

---

## Bibliographies

- [1] W. Kohn and L. S. Sham, “One-particle properties of an inhomogeneous interacting electron gas,” *Phys. Rev.* **145** (2), 561–567 (1966).  
<https://doi.org/10.1103/PhysRev.145.561>
- [2] M. Segall, P. J. Lindan, M. Probert, et al., “First-principles simulation: ideas, illustrations and the CASTEP code,” *J. Phys.: Condens. Matter* **14** (11), 2717–2744 (2002).  
<https://doi.org/10.1088/0953-8984/14/11/301>.
- [3] J.P. Perdew, A. Ruzsinszky, G.I. Csonka, O.A. Vydrov, G.E. Scuseria, L.A. Constantin, X. Zhou, K. Burke, Restoring the density-gradient expansion for exchange in solids and surfaces, *Physical Review Letters* **10** (2008)
- [4] H. J. Monkhorst, J. D. Pack, “Special points for Brillouin-zone integrations,” *Phys. Rev. B* **13**, 5188–5192 (1976). <https://doi.org/10.1103/PhysRevB.13.5188>.
- [5] S. L. Shang, Y. Wang, and Z. K. Liu, “First-principles elastic constants of  $\alpha$ - and  $\theta$ -Al<sub>2</sub>O<sub>3</sub>,” *Appl. Phys. Lett.* **90**, 1–3 (2007).  
<https://doi.org/10.1063/1.2711762>
- [6] Jian Liu, Xi-Bo Li, Hui Zhang, et al., “Electronic structures and optical properties of two-dimensional ScN and YN nanosheets,” *J. Appl. Phys.* **115**, 093504 (2014).  
<https://doi.org/10.1063/1.4867515>.
- [7] D.G. Pettifor, *Mater. Sci. Technol.* **8** (1992) 345.
- [8] G. Soto, M.G. Moreno-Armenta, A. Reyes-Serrato, *Comput. Mater. Sci.* **42** (2008)8.
- [9] D. Gall, I. Petrov, N. Hellgren, L. Hulman, J.-E. Sundgren, J.E. Geene, *J. Appl. Phys.* **84** (1998) 6034.
- [10] S.F. Pugh, *Philos. Mag.* **45** (1954) 823.
- [11] N. Kaurav, Y.K. Kuo, G. Joshi, K.K. Choudhary, Dinesh Varshney, *High Press. Res.* **28** (4) (2008) 651–663.
- [12] L. Mancera, J.A. Rodriguez, and N. Takeuchi, First principles calculations of the ground state properties and structural phase transformation in YN, *J. Phys. Condens. Matter.* **15** (2003), pp. 2625–2633.
- [13] J. Hayashi, I. Shirogami, K. Hirano, N. Ishimatsu, O. Shimomura, T. Kikegawa, *Solid State Commun.* **125** (2003) 543.
- [14] L. Mancera, J.A. Rodriguez, and N. Takeuchi, First principles calculations of the ground state properties and structural phase transformation in YN, *J. Phys. Condens.*

- Matter. 15 (2003), pp. 2625–2633.
- [15] S. Duman, S. Bag̃ci, H.M. Tutuncu, G. Ug̃ur, G.P. Srivastava, *Diam. Relat. Mater.* 15 (2006) 1175.
- [16] N. Takeuchi, *Phys. Rev. B* 65 (2002) 045204.
- [17] A. Tebboune, D. Rached, A. Benzair, N. Sekkal, A.H. Belbachir, *Phys. Stat. Solid (b)* 243 (2006) 2788.
- [18] Bakhtiar Ul Haq , A. Afaq , Galila Abdellatif , R. Ahmed , S. Naseem , R. Khenata. *Superlattices and Microstructures* 85 (2015) 24–33.
- [19] A. Bouhemadou, *Comput. Mater. Sci.* 43 (2008) 1112.
- [20] *Computational Materials Science* 79 (2013) 239–246.
- [21] P. Villars, L.D. Calvert, *Pearson’s Handbook of Crystallographic Data for Intermetallic Phases*, American Society for Metals, Metals Park, Ohio, 1985.
- [22] Y.O. Ciftci\*, K. C. olakoglu, E. Deligoz, H. Ozisik, *Materials Chemistry and Physics* 108 (2008) 120–123
- [23] A. Hao, X. Yang, X. Wang, R. Yu, X. Liu, W. Xin, R. Liu, *Comput. Mater. Sci.* 48 (2010) 59.
- [24] M. Shoaib a, G. Murtaza b, R. Khenata c,d, M. Farooq a, Roshan Ali. *Computational Materials Science* 79 (2013) 239–246.
- [25] F. Soyalp, S\_. Ug̃ur, *J. Phys. Chem. Solids* 69 (2008) 791.
- [26] W.D.L. Cruz, J.A. Duaz, L. Mancera, N. Takeuchi, G. Soto, *J. Phys. Chem. Solids* 64 (2003) 2273.
- [27] D. Varshney, N. Kaurav, U. Sharma, R.K. Singh, *J. Alloys Compd.* 448 (2008) 250.
- [28] I. Shirovani, K. Yamanashi, J. Hayashi, N. Ishimatsu, O. Shimomura, T. Kikegawa, *Solid State Commun.* 127 (2003) 573.
- [29] S.J. Clark, M.D. Segall, C.J. Pickard, P.J. Hasnip, M.J. Probert, K. Refson, M.C. Payne, *First principles methods using CASTEP*, *Zeitschrift für Kristallographie*, 220 (2005)567-570.
- [30] J.P. Perdew, A. Ruzsinszky, G.I. Csonka, O.A. Vydrov, G.E. Scuseria, L.A. Constantin, X. Zhou, K. Burke, *Restoring the density-gradient expansion for exchange in solids and surfaces*, *Physical Review Letters*, 10 (2008) 1-4.
- [31] A. Bouhemadou, *Comput. Mater. Sci.* 43 (2008) 1112.
- [32] K.M. Wong, S.M. Alay-e-Abbas, A. Shaukat, Y. Fang, Y. Lei, *J. Appl. Phys.* 113

- (2013) 014304.
- [33] G. Murtaza, B. Amin, S. Arif, M. Maqbool, I. Ahmad, A. Afaq, S. Nazir, M. Imran, M. Haneef, *Comput. Mater. Sci.* 58 (2012) 71.
- [34] W. Feng, S. Cui, H. Hu, Z. Gong, H. Liu, *Comput. Mater. Sci.* 47 (2010) 1060.
- [35] A. Hao, X. Yang, X. Wang, R. Yu, X. Liu, W. Xin, R. Liu, *Comput. Mater. Sci.* 48 (2010) 59.
- [36] S. Saha, T. Sinha, A. Mookerjee, *Phys. Rev. B: Condens. Matter* 62 (2000) 8828.
- [37] Bakhtiar Ul Haq , A. Afaq , Galila Abdellatif , R. Ahmed , S. Naseem , R. Khenata. *Superlattices and Microstructures* 85 (2015) 24–33.
- [38] Aimin Hao. Xiaocui Yang. Xiaoyu Wang Ruomeng Yu. Xin Liu. Wei Xin . Riping Liu. *Compu Mater Sci* 48 (2010) 59–64.
- [39] S. Duman, S. Bağcı, H.M. Tutuncu, G. Uğur, G.P. Srivastava, *Diam. Relat. Mater.* 15 (2006) 1175.
- [40] A. Tebboune, D. Rached, A. Benzair, N. Sekkal, A.H. Belbachir, *Phys. Stat. Solid (b)* 243(2006) 2788.
- [41] S. Azzi, A. Zaoui, H. Boublenza, I.S. Messaoudi, M. Ferhat, *Journal of Alloys and Compounds*, **588**, 133-137 (2014).

### General conclusion

In this work, we studied the structural properties such as the network constant, the compressibility module as well as the total energy of equilibrium, elastic constants: shear module (G), Poisson coefficient ( $\nu$ ), Young module (E), transverse and longitudinal velocities and Debye temperature), Isotropic factor (A), Young modulus, Poisson coefficient and shear modulus and Elastic wave propagation velocities (longitudinal and transverse waves) the direction of the three low-index crystal planes [100], [110] and [111]. the electronic properties (band structure, density of states), optics (dielectric function, absorption coefficient, reflectivity, refractive index, etc.) and phononic (the calculation of phonon frequencies and the dispersion spectra of phonons along the different lines of symmetry) of:

- $Y_{1-x}M_xN$  ( $x = 0, 0.25, 0.5, 0.75, 1$ ) . Where  $\mathbf{M} = \text{Sc}$  and  $\text{La}$ .
- $YN_{1-x}B_x$  ( $x = 0, 0.25, 0.5, 0.75, 1$ ) . Where  $\mathbf{B} = \text{P}, \text{As}$  and  $\text{Sb}$ .

We determined these properties in the rock salt structure.

In this conclusion, we wish to emphasize the following key points:

- First, we studied the structural properties that characterize the fundamental state of systems. The structural study of the alloys showed that the network parameter varies almost linearly with the concentration. There is a good match of these results to previous calculations and experimental data.

In addition, we calculated the elastic constants of  $Y_{1-x}M_xN$  ( Where  $\mathbf{M} = \text{Sc}$  and  $\text{La}$  ) and  $YN_{1-x}B_x$  (Where  $\mathbf{B} = \text{P}, \text{As}$ , and  $\text{Sb}$ ), the elastic constants check well the criteria of mechanical stability in each concentration. This alloy is mechanically stable for all x values in Roksalt phases, elastic constants: shear module (G), Poisson coefficient ( $\nu$ ), Young module (E), transverse and longitudinal velocities, and Debye temperature), Isotropic factor (A). Our results are in very good agreement with those obtained by other theoretical methods.

For  $Y_{1-x}\text{Sc}_x\text{N}$ : bulk modulus B, Young modulus E, and Shear modulus G increase with the increasing concentration of Sc. but for  $Y_{1-x}\text{La}_x\text{N}$  and  $YN_{1-x}B_x$  (Where  $\mathbf{B} = \text{P}, \text{As}$ , and  $\text{Sb}$ ) decreases with the increasing concentration x. The B/G ratio values are below 1.75 for  $Y_{1-x}M_xN$  ( Where  $\mathbf{M} = \text{Sc}$  and  $\text{La}$  ) and  $YN_{1-x}B_x$  (Where  $\mathbf{B} = \text{P}, \text{As}$  and  $\text{Sb}$ )alloy ( $0 < x < 0.75$ ). Therefore, these systems must be classified as fragile materials.

As for our results related to the Young modulus, Poisson coefficient and shear modulus, and Elastic wave propagation velocities (longitudinal and transverse waves) in the direction of the three low-index crystal planes  $\{100\}$ ,  $\{110\}$  and  $\{111\}$ , to date, and our knowledge, there is

no experimental or theoretical data in the literature to compare it with our results, So our results can be considered a prediction.

Then we determined the electronic properties and the DOS, our calculation of the band structure of binary compounds. For YN, ScN, and LaN, the maximum valence lying at the G-point and the minimum of the conduction band lying at the X-point show it is an indirect band gap semiconductor. And concerning the  $Y_{1-x}Sc_xN$ ,  $Y_{1-x}La_xN$  ( 0.25,0.5,0.75 ) and  $YN_{1-x}B_x$  (Where **B** = P, As and Sb) (  $x= 0.25,0.75$  ) are at direct gap because the maximum of the valence band and the minimum of the conduction band is at the same point G. but  $YN_{1-x}B_x$  (Where **B** = P, As and Sb) (  $x= 0.5$  ) and YP YAs, YSb have a semi-metallic character.

The optical properties allow us to determine the dielectric function, reflectivity, absorption coefficient, refractive index, and extinction coefficient of binary-allowed ternary compounds. These results are shown suggest that these materials may find applications in different optoelectronic devices. Finally, the  $Y_{1-x}Sc_xN$ ,  $Y_{1-x}La_xN$  alloy ( $x = 0, 0.25, 0.75, \text{ and } 1$  ) is dynamically stable because all phonon frequencies are positive.